UNIVERSITY OF SOUTHAMPTON

Physical Sciences and Engineering

Optoelectronics Research Centre

Volume 1 of 1

Manufacturing High Purity Chalcogenides

by

Khouler Khan

Thesis for the degree of Doctor of Philosophy

March 2015

UNIVERSITY OF SOUTHAMPTON

ABSTRACT

PHYSICAL SCIENCES AND ENGINEERING

Graduate Research Student

Thesis for the degree of Doctor of Philosophy

MANUFACTURING HIGH PURITY CHALCOGENIDES

Khouler Khan

Interest in infrared fibres has grown immensely as niche applications arise as a replacement for silica based optical fibres, whose properties limit its use in the mid infrared. Some of these applications include laser power delivery, chemical sensing and imaging. Of the many infrared transparent materials, the focus of this thesis in particular, will be on high purity chalcogenide glass. While great strides have been made in reducing optical losses of chalcogenides, further improvements are needed in both synthesis and fibre drawing techniques to attain its theoretically predicted potential.

In this thesis, glass making techniques including sealed ampoule, levitation, chemical vapour deposition and reactive atmosphere processing techniques are developed and evaluated for producing high purity chalcogenide glass. A state of the art reactive atmosphere processing system with high purity gas delivery of five gasses; argon, hydrogen sulphide, hydrogen, oxygen and chlorine is implemented. The system is automated using National Instrument hardware and Labview software which allows monitoring and data logging in real-time. This bespoke automated system to make chalcogenide has led to reduction in losses to less than 1dB per metre in the 3 to 5 μm region in bulk glass. Experiments and improvements to chemical vapour deposition facilities were done with the goals of scaling the method from thin film deposition to producing high purity bulk glass and fibre. Limits to this process have not been overcome and the challenges remaining are detailed within this thesis. However, new concepts have been developed for implementing a CVD to fibre fabrication process and initial results are presented.

The results of this thesis show significant improvement in glass synthesis facilities at the Optoelectronics Research Centre, greatly facilitating production of next generation ultra-low loss chalcogenide glass and fibre.

Table of Contents

List of tables

List of figures

DECLARATION OF AUTHORSHIP

I, KHOULER KHAN declare that this thesis and the work presented in it are my own and has been generated by me as the result of my own original research.

Manufacturing High Purity Chalcogenides

.....

I confirm that:

1. This work was done wholly or mainly while in candidature for a research degree at this University;
2. Where any part of this thesis has previously been submitted for a degree or any other qualification at this University or any other institution, this has been clearly stated;
3. Where I have consulted the published work of others, this is always clearly attributed;
4. Where I have quoted from the work of others, the source is always given. With the exception of such quotations, this thesis is entirely my own work;
5. I have acknowledged all main sources of help;
6. Where the thesis is based on work done by myself jointly with others, I have made clear exactly what was done by others and what I have contributed myself;
7. (a) Parts of this work have been published as:
   Khan K., "***Achieving low loss chalcogenide glasses***", Glass Reflections Glass in the Year of Light, 7th to 9th September 2015 [Abstract]
   Wright P., et al., "***Progress towards Non-Intrusive Optical Measurement of Gas Turbine Exhaust Species Distributions***", Aerospace Conference, 2015 IEEE.
   Bastock P., Khan K., et al., "***Properties of Gallium Lanthanum Sulphide Glass***", CLEO 2015, San Jose, USA, 10 – 15 May 2015
   Mulholland L. and Khan K., "***Chemical Vapour Deposition Powder Capture Apparatus***", FUSION Journal of the American Scientific Glassblowing Society, 2014.
   D.W.Hewak, et al.,"***Preparation of chalcogenide materials for next generation optoelectronic devices***", Advanced Architectures in Photonics '14 Prague, Czech Republic 21-22 Sep 2014

D.W.Hewak, K.C.C.Huang, K.Khan, P.Bastock, C.Craig, E.Weatherby, "***Manufacturing high purity chalcogenide glass***", Society of Glass Technology Annual Meeting (Theme: From Ancient Glass to Modern Techniques) University of Durham, UK 10-12 Sep 2014
K.Khan, Farmer T., "***Fabrication and aero dynamic levitation of chalcogenide glass spheres***", ISNOG 2012 St Malo France 1-5 July 2012 [Abstract]

(b) Contributions made and published apart from this work:

B.Gholipour, P.Bastock, C.Craig, K.Khan, D.Hewak, C.Soci, "***Amorphous Metal-Sulphide Microfibers Enable Photonic Synapses for Brain-Like Computing***", Advanced Optical Materials, 15 Jan 2015
B.Gholipour, V.Nalla, P.Bastock, K.Khan, C.Craig, D.W.Hewak, N.I.Zheludev, C.Soci, "***Plasmonic Nanowire Continuum Light Source***", CLEO '14 San Jose, CA, USA 8-13 Jun 2014
B.Gholipour, D.M.Nguyen, C.Long, V.Nalla, P.Bastock, K.Khan, C.Craig, D.W.Hewak, N.I.Zheludev, C.Soci "***Multimaterial fiber nanomanufacturing: from photodetectors to nonlinear light sources***", SPIE Photonics North Montréal, May 28-30 2014
B.Gholipour, V.Nalla, P.Bastock, K.Khan, C.Craig, D.Hewak, N.I.Zheludev, C.Soci, "***Highly collimated broadband emission from plasmonic nanowire embedded in fiber***", 5th International Conference on Metamaterials, Photonic Crystals and Plasmonics (META 14) Singapore 20 May 2014
B.Gholipour, P.Bastock, K.Khan, C.Craig, D.W.Hewak, N.I.Zheludev, C.Soci, "***Chalcogenide optical axons and photonic synapses***", IPS Meeting 2014 Singapore 26 Feb 2014
B.Gholipour, P.Bastock, C.Craig, K.Khan, W.Zilong, D.Hewak, N.I.Zheludev, C.Soci, "***Photodarkening in chalcogenide fibers: observation and applications***", 4th Asian Spectroscopy Conference (ASC 2013) Singapore 15 Dec 2013
P.Bastock, C.Craig, E.Weatherby, K.Khan, D.W.Hewak, "***Advancing the applications of chalcogenide glass for infrared power transmission***", SPIE Security & Defence (Technologies for Optical Countermeasures) Dresden, Germany 23-26 Sept 2013

P.Bastock, K.Khan, D.Hewak, "***Fabrication of novel glass fibre***", International Conference on Photorefractive Effects, Materials and Devices Winchester, UK 4 Sep 2013 [Poster]

P.Bastock, K.Khan, D.Hewak "***Non-circular glass metal composite fibre***", ISNOG 2012 St Malo France 1-5 July 2012 [Abstract]

Signed:.....

Date: 17th October 2015

Acknowledgements

To my PhD supervisor, Professor Daniel Hewak, it was a great pleasure sharing this experience with you. I would also like to thank other members of Optoelectronics Research Centre, in particular Behrad Gholipour, Paul Bastock, Jonny Butement, Vinita Mittal, Chung- Che Huang, Trevor Austin, Mike Bartlett, Neil Fagan, Iain Anteney, Mark Lessey, Mark Long, Nick White, Mark Light and Ken Frampton, all of whom have contributed to the work in this thesis. I wish to especially thank Edwin Weatherby and Christopher Craig for without their dedication this work would not have been as successful. I would like to thank the Scientific Glass Blowing community, especially Lee Mullholland and Paul Frampton for interpreting and implementing my complicated glassware designs. I would also like to thank Adrian Barnes and Tom Farmer for allowing me the opportunity and assisting with the aero levitation experiments at University of Bristol.

I also wish to acknowledge the expert advice of UK industrial contacts especially, Tony Gibbs (National Instruments), John Mellor (Lenton), Troy Stehr (formerly SAES/Chell). The financial support of EPSRC Centre for Innovative manufacturing in Photonics grant EP/H02607X/1 and other internal ORC sponsors for this work is greatly acknowledged. Finally, I would like to thank my mother, my father, my brother, Sandira and her family for their continuous love and support.

Chapter 1

Definitions and Abbreviations

CCR - Critical Cooling Rate

CVD – Chemical Vapour Deposition

DI – Deionised.

DMO – Domestic Microwave Oven.

GDP – Gross Domestic Product

GDMS – Glow Discharge Mass Spectroscopy

GLS (O) – Gallium Lanthanum Sulphide (with intentional Oxide doping)

HF – Hydrofluoric acid.

HMI – Human Machine Interface

IR – Infrared

FIR – Far Infrared, defined as the wavelength region 30 to 300μm.

FLITES – Fiber-Laser Imaging of Gas Turbine Exhaust Species.

I/O – Input/Output

LD####- Glass number used to log and track samples.

LII, Laser-Induced incandescence.

MFCs – Mass Flow Controllers

MIR – Mid Infrared, defined as the wavelength region 3 to 30μm.

NPT – National Pipe Thread

NI – National Instruments

NIR – Near Infrared, defined as the wavelength region 0.78 to 3μm.

ORC – Optoelectronics Research Centre.

Periodic Table Element abbreviations are used in this thesis, example S for Sulphur, Se for Selenium etc.

PLC – Programmable Logic Controller.

RAP – Reactive Atmosphere Processing.

TFLAS – Tunable Fiber Laser Apsorption Spectroscopy.

UV-Vis-IR – Ultraviolet – Visible – Infrared

VCR – Variable Compression Ratio

xN – x Nines – unit of purity.

Chapter 1: Introduction

Chalcogenide glasses are inorganic materials which contain one or more of the chalcogen elements: S, Se or Te, but not O, in conjunction with more electropositive elements most commonly As and Ge, but also P, Sb, Bi, Si, Sn, Pb, B, Al, Ga, In, Tl, Ag, lanthanides and Na [1]. Chalcogenide glasses transmit light in the infrared (IR) and the transmission cut-off in the IR depends on the mass and strength of the bonds of the various elements forming the material. Unwanted elements introduced in the manufacturing process not only affect the IR cut-off but also the minimum loss that can be achieved experimentally.

An emerging application that benefits from the research in this thesis and which require high purity chalcogenide fibre in both active and passive forms is gas sensing, part of an ongoing collaborative project called fibre-laser imaging of gas turbine exhaust species (FLITES). This consortium was developed to solve the problem of tighter emission regulations moving beyond the capability of current measurement tools in airplane jet engines. Formed by the UK's world-leading academic groups in chemical species tomography (Manchester and Edinburgh), fibre-lasers (Southampton), and gas-detection opto-electronics (Strathclyde), the project marries these academic partners to the countries industrial strengths in aero-engine manufacture (Rolls-Royce) and aviation fuel technology (SHELL) [2]. The consortium aims to underpin a new phase of low-net-carbon turbines by analysis of the exhaust plume by

- Novel fibre lasers adapted for gas sensing, at near – infrared (NIR) and MIR wavelengths;
- Imaging of the spatial distribution of soot, using laser-induced incandescence (LII), in a planar tomographic set-up;
- High-speed tomographic imaging of the spatial distributions of CO_2 and unburned hydrocarbons, using the new gas detection technology of tunable fibre-laser absorption spectroscopy (TFLAS);
- Line-of-sight measurement of NO_x, also using TFLAS;
- Testing on a target engine that employs leading-edge technology, using advanced bio-fuel formulations. [2]

High purity mid infrared (MIR) and far infrared (FIR) transmitting chalcogenides approaching theoretical losses have yet to be achieved and commercialized. In 1965, the first chalcogenide fibre made of As_2S_3 via a double crucible method was presented [3]. At this time losses remained above 10 000 dB/km. Due to the rapid progress at the time in making ultra-low loss fibre using silica-based materials, development of chalcogenide materials suffered when compared financially. Silica fibre easily achieved losses below 1dB/km at telecommunication wavelengths in the near infrared (NIR). However, the unique applications of chalcogenides mentioned above as well as theoretically predicted losses even less than silica in the MIR has aided its continued development. However, no chalcogenide fibre achieving 1dB/km has been realised and commercially available to date which is the goal for the FLITES project.

In [4], a survey of the IR fibre market for 2005 is given. An updated review of the commercial IR fibre market was performed for the FLITES project and the findings showed that most of the products in the 2005 survey are no longer commercially available. The only supply of MIR fibre of reasonable loss is from CorActive who supply fibres based on chalcogenides of arsenic sulphide and selenide. The lowest losses within the transmission range quoted in their brochures are 150 dB/km at 2.7μm for As_2S_3 and 200dB/km at 6 μm for As_2Se_3 and are shown in Appendix A, Figure 81. These chalcogenide compositions are considered toxic due to the element Arsenic and the cost of such a fibre is in excess of £800 per meter.

The FLITES project fits well with the aims of this work and was therefore used as a goal for improvement of the Reactive Atmosphere Processing (RAP) facility described in Chapter 4. The approximate wavelengths of focus for the MIR for FLITES are around 3.6 μm for hydrocarbons and 5 μm for NO_2. The ORC team was commissioned to make the passive fibre for laser delivery to optics around the plume frame and active fibre for fibre lasers. The goal of this project is to show development of bulk glass losses which are less than 1dB/m in the FLITES wavelength region of interest, i.e. 3 to 5 μm. The FLITES project has highlighted the unavailability of ultra-low loss fibres in the MIR available commercially to meet the project needs.

Chalcogenide are made into a glassy state by fast quenching a melt containing the glass forming stoichiometric ratio of chalcogenide elements. Chalcogenide elements are volatile and therefore need to be contained during the melting and homogenizing steps. The main fabrication technique used to make bulk chalcogenides in excess of one kilogram is sealed ampoule [5]. The ampoule is a sealed silica vessel which is placed under high vacuum before sealing. Basic sealed ampoule under high vacuum does not guarantee high purity chalcogenides. The purity of the commercial raw materials and the environment that the materials come into contact from preparation to synthesis are the main factors limiting the development of high purity chalcogenides. Inconsistency of commercial high purity raw material supply is the major restriction to making high purity chalcogenides identified in the literature. The cost of requesting and verifying high purity elements for chalcogenide glass manufacture adds a significant cost and therefore manufacturers of chalcogenides develop their own purification techniques while buying the lower purity and less costly elements.

The main technique to improve the purity which capitalizes on the volatility of chalcogenide elements is distillation. Since many chalcogenides are volatile, they can be heated to form a vapour state which is then transported and deposited in the ampoule leaving behind less volatile components. Sometimes getter materials are added before the distillation step. The role of getter materials is to bond to the impurities elements to form more stable compounds which are then left behind in the distillation step. In addition to distillation, reactive gasses may be used to remove impurities. Chemical vapour deposition has been used to make silica preforms achieving ultra-low loss but this technique has been limited to thin film application for manufacturing chalcogenides. There are many sources of research literature [5-9] on making high purity materials and chalcogenides which cover various designs and techniques for making high purity IR materials. Figure 1 through Figure 3, are schematics of some of the apparatus used to manufacture chalcogenides which incorporate distillation, getter materials and gas atmosphere processing to make chalcogenides. Additional impurities can be introduced during device making steps such as cutting, polishing, fibre drawing, hot pressing and deposition techniques.

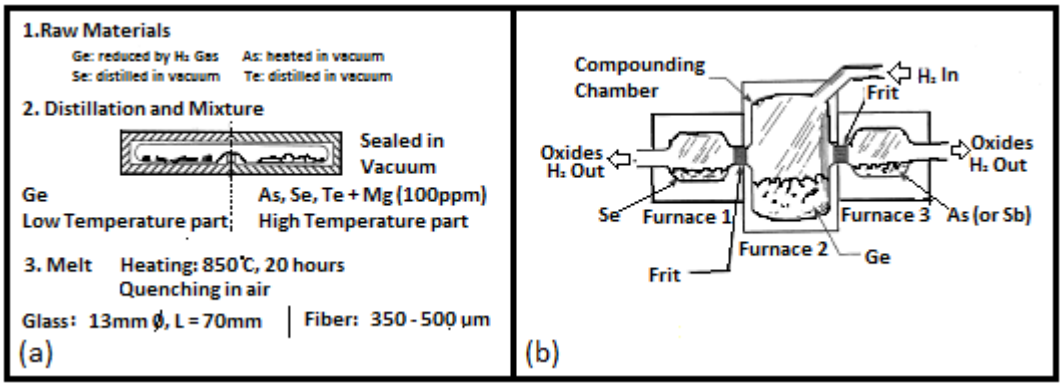

Figure 1 Apparatus used to manufacture chalcogenide glasses, (a) Ge-As-Se-Te (From Inagawa, I. et al., J. Non-Cryst. Solids, 95-96, 810, 1987, [10]. With Permission.) and (b) Ge-Sb-Se (From Hilton, A.R. et al., J.Non-Cryst. Solids, 17, 319, 1975, [11]. With Permission). Both apparatus use distillation and reactive gasses.

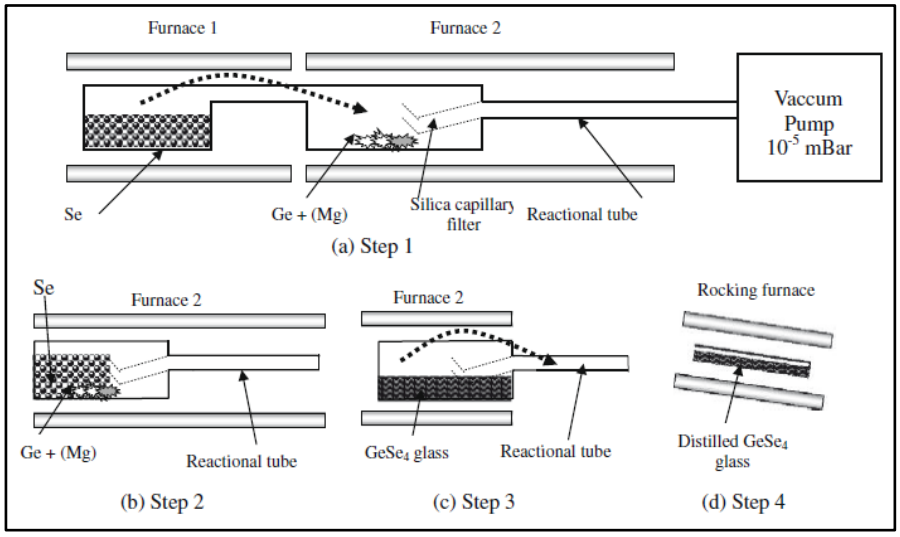

Figure 2 Experimental set-up for the purification and the distillation of the Se. (a) Step 1: purification and distillation of Se, (b) step 2: first synthesis (800–850 ˚C) with or without oxygen getter (Mg), (c) step 3: distillation of the glass and (d) step 4 second synthesis and homogenisation in final silica tube in a rocking furnace (750 ˚C).(From Troles, J., et al., $GeSe_4$ glass fibres with low optical losses in the mid-IR. Optical Materials, 32(1): p. 212-215, 2009, [9]. With Permission)

In summary, chalcogenides have a great potential that have not been realized. Manufacturing processes remain limited and have seen little or no

improvement since the 1970's. Applications requiring high purity chalcogenides are restricted in their development until obstacles can be addressed and overcome. The main challenge is not drawing a fibre, but rather manufacturing a glass with high purity and maintaining high purity until fibre is realised. Varying levels of trace impurities, even at levels of a few parts per million, can alter the spectroscopic behaviour of chalcogenide glass. In optical components such as fibres, impurities not only contribute to the optical loss through absorption and scattering but also serve as nucleation sites for crystallization. Crystallization weakens a fibre and alters its optical and mechanical properties. This thesis aims at developing facilities to fill gaps in manufacturing of high purity chalcogenides that are not considered toxic.

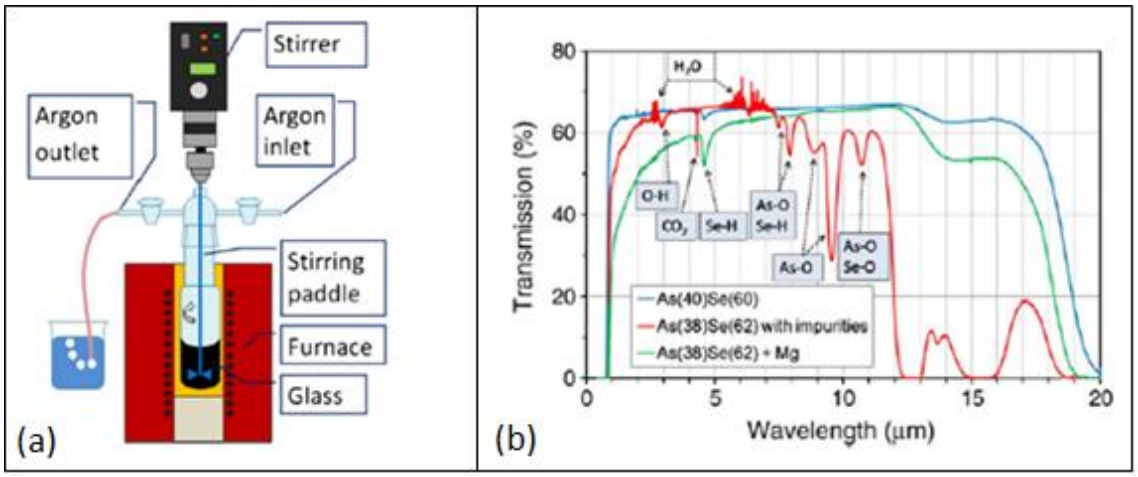

Figure 3 (a) Apparatus used to make arsenic chalcogenides using an Argon atmosphere processing technique and (b) Transmission spectra of various 5 mm-thick glass samples: unpurified $As_{38}Se_{62}$ glass prepared in the open crucible (red curve); $As_{38}Se_{62}$ glass prepared in the open crucible in presence of magnesium as an oxygen getter (green curve). A transmission spectrum of $As_{40}Se_{60}$ glass synthesized in a sealed silica ampoule (blue curve) has been added for comparison. (From Guillevic, E., et al., Fabrication of highly homogeneous As_2Se_3 glass under argon flow. Journal of Non-Crystalline Solids, 357(15): p. 2897-2902, 2011,[8]. With Permission)

1.1 Aims and contributions

In, [12] it is identified that there is a strong need to continue innovating and manufacturing market-worthy fibres, in order to sustain the growth in the fast expanding fibre-based manufacturing sectors. From its inception in the 1960s, the UK has played a major role in shaping the optical fibre industry, and the highly regarded Optoelectronics Research Centre (ORC) at the University of Southampton is at the forefront. The vision is to build upon the rich expertise and extensive facilities that are already in place to create a world-class, industry-led Centre for advanced manufacturing processes for new photonic components and materials that will fuel the growth of UK companies, enabling them to expand their product portfolio, enhance competitiveness and increase their market penetration and overall share. One area identified for exploitation and development is infrared fibres. This is as a result of the market for infrared glass and fibres being sparse [12]. The demand for speciality glass is growing and these advanced materials are of national importance for the United Kingdom (UK). UK businesses that produce and process materials have a turnover of around £170 billion per annum; represent 15% of the country's Gross Domestic Product (GDP) and have exports valued at £50 billion [13]. It is the goal of this thesis to review and assesses the manufacturing processes used to make high purity bulk chalcogenides at the ORC. From this assessment, glass manufacturing systems will be further developed and implemented at the ORC to meet the current and emerging requirements for chalcogenide IR materials. The following outlines the aims and contributions made towards achieving this goal.

The ORC facilities were compromised in 2005 due to a fire which resulted in the loss of facilities developed over 20 years of research. Reconstruction of new facilities was then undertaken after 2005 and provided a unique opportunity to rebuild from the ground up, a new dedicated facility for chalcogenide glass manufacture. This thesis contributes by reviewing various methods for chalcogenide fabrication through experimentation to ascertain the obstacles that prevent achieving ultra-low loss chalcogenide glasses. Through this review, the knowledge base and procedures have significantly increased for chalcogenide glass manufacturing systems at the ORC. Facilities chosen to review, develop and investigate were microwave assisted sealed ampoule,

vacuum distillation sealed ampoule, levitation, reactive atmosphere processing method (RAP) and chemical vapour deposition (CVD).

Before this work, there was no dedicated sealed ampoule facility at the ORC. The aim was therefore to provide a dedicated sealed ampoule setup and procedure. As a result of this work, there are now sealed ampoule facilities and procedures including best practices. This includes a dedicated oxy hydrogen torch sealing station, vacuum sealing setup with connections for high purity gasses for distillation, various silica ampoules (for making small samples and 2 inch sputtering targets) and a basic melt setup. The result of this basic facility is production of chalcogenide glasses for researchers at the ORC. Various chalcogenide glasses were made as part of the work undertaken in this thesis and have been provided to other research groups within the ORC for comparison with commercially bought materials.

Microwave assisted sealed ampoules was investigated to test the scalability of this method for producing bulk glass samples, to determine benefits of reduced glass synthesis times and assess the moisture removal capability claim in the literature [14]. The development of this method at the ORC did not materialise as expected due to explosions when attempting to scale up as well as failure to manufacture glass. The contributions and findings of this method have been detailed in Chapter 3.

Levitation of chalcogenides was investigated to determine its feasibility in chalcogenide glass synthesis as well as to determine the benefits of this method in analysing chalcogenide glasses. In this thesis, the first time levitation, melting and quenching of GLS and GLSO spheres is presented. In addition, spheres have been coated, doped with rare earths, levitated and quenched. Also, laser irradiation for making submicron spheres have been explored as well as a proposed idea of using laser irradiation for device making. The aero levitation technique used in Chapter 3 does not meet high purity specification and was not suited to levitate large samples. Also modifications to accomplish the other proposed studies such as critical cooling rate studies did not materialise. An attempt was made to develop an aero acoustic levitator glass melting system at the ORC but was unsuccessful.

Due to existing infrastructure and knowledge base, the two main fabrication methods focused on in this thesis are RAP and CVD for making high purity

chalcogenides. The first aim was to assess the systems in place and developed in the past prior to the fire. From this assessment, improvements would be made to existing equipment such as the Vertical RAP system and the CVD system while conducting experiments to lead the design of a new Horizontal RAP system. The chalcogenides focused on in these systems are GLS for the Horizontal RAP and GeS/GeSbS for CVD. Added focus was given to reducing losses due to moisture at 2.9μm and also reducing losses in the 3-5μm regions for FLITES. The following are the contributions made.

Gas quality is very important in such systems as impurities in gasses used in synthesis can result in increased losses as well as corrode delivery lines further decreasing the purity of the glasses. As a major contribution, a review of the ORC gas delivery was done and the major flaws identified for delivery of Ar and N_2. This affects all the melt systems and facilities for high purity manufacture at the ORC and was a major focus for improvement. The intermediate improvements through thesis findings due to correction of prior improper installations have brought about significant increase in gas delivery purity and lower moisture absorption losses in the glasses synthesized.

A bespoke horizontal RAP system was designed and implemented completely in-house. The procurement, design and installation of this system is the main focus of the work in this thesis. The horizontal RAP system has been developed with the capability of manufacturing raw materials as well as the final glass. The glass system focused was gallium lanthanum sulphide (GLS) and the gases installed were Ar, H_2, O_2, H_2S and Cl_2. The system is automated using national instruments (NI) and labview allowing for easily integrating instrumentation, control and additional capability completely in-house as the system develops. The existing system has the minimum data logging and safety features incorporated but will be developed in more detail in future work. Mass flow controllers (MFCs), dew point meters, extract flow and gas detection monitors are monitored by the NI controller. This allows for better process monitoring and hence repeatability from melt to melt. The latest glasses produced show a considerable improvement in the 3-5 μm spectral band required by the FLITES project with losses in the bulk glass lower than 1dB/m. Also detailed in Chapter 4, are the improvements to the vertical atmosphere glass processing system which was used to initially investigate the glass forming capability of commercially bought material.

CVD is a high purity method for manufacturing thin films. Several experiments were carried out to ascertain the feasibility of manufacturing chalcogenides in bulk form via CVD to build on the work done in [15]. The contribution again was the improvement of the quality of gas purity. Also the installation and distribution of H_2S from a gas cylinder was done to improve delivery quality and allow longer duration experiments. This replaced the installation which involved generating H_2S from the reaction of FeS and HCl. Scaling CVD to manufacture chalcogenide glasses in bulk was another aim in this thesis. The learnings and development of collection apparatus and various experimental observations leading to these design is shown for the first time. Other experiments were used to highlight the feasibility of integrating CVD and fibre drawing without the need to manufacture a preform or reduce the number of possible contamination steps between deposition and fibre drawing while maintaining the high purity inherent to CVD.

1.2 Thesis layout

Below, the contents of each chapter are summarized.

In Chapter 2, the fundamental losses in optical materials are discussed. Also, the necessary background on intrinsic and extrinsic losses pertaining to chalcogenides is reviewed. Firstly a review of the optical transmission window of chalcogenides is presented. This gives insight into the predicted theoretical losses in these materials based on intrinsic loss mechanisms. This is followed by a discussion of the extrinsic loss mechanisms. At the moment, chalcogenides are limited by extrinsic loss mechanisms and this review is important for identifying the major limitations and steps for improving the purity and thereby lowering the losses. Chapter 2 allows for identifying where the impurity contributions are in the manufacturing process and hopefully identify the main areas to focus development.

In Chapter 3, the sealed ampoule, microwave assisted sealed ampoule and levitation methods for synthesizing chalcogenides are assessed. The experimental results, best practices and difficulties for the development of these methods at the ORC are presented. The limits of these methods to achieving high purity glass are discussed and other areas where they may benefit glass synthesis are outlined.

In Chapter 4, the design of a bespoke horizontal RAP system to manufacture chalcogenides is detailed. In this chapter a brief assessment of commercial raw material quality is undertaken using the existing vertical atmosphere processing system. Also the development and results for the high purity gas delivery infrastructure improvements are detailed. RAP procedures and best practices are developed and presented along with the automation and monitoring that allows full control over future glass development direction. The experimental results are presented which show the capability and limits of the system manufactured and defines the future improvements which are also detailed in this chapter.

In Chapter 5, the development of CVD to make bulk chalcogenides as well as fibre is explored. First a review of CVD systems towards achieving bulk glass is reviewed. The novel collection designs and initial results are presented which aid in outlining the future directions of this technique. Also new ideas of CVD to fibre which minimizes the intermediate steps of manufacturing a preform are presented along with the results and obstacles.

In Chapter 6, conclusions and achievements towards the aims and contributions outlined in Chapter 1 are summarized. The results and learnings from Chapter 3 through Chapter 5 lead to the future system development and research directions which are also detailed.

Chapter 2: Losses in Infrared Materials

In this section, the fundamental concepts needed to understand and evaluate infrared transmitting glasses with focus on high purity (low loss glass) are introduced. Understanding these loss mechanisms allows a manufacturer to focus effort and resources while developing facilities. Using this knowledge, the limits in manufacturing techniques can be better understood.

2.1 Attenuation in optical materials

There are two mechanisms contributing to attenuation of light in an optical glass: the intrinsic and extrinsic. Intrinsic mechanisms refer to theoretical losses that are expected and thus set the predicted minimum level of loss that can be achieved. Extrinsic losses however refer to losses that prevent achievement of the theoretical minimum. Together these two sets of mechanisms have been used to account for the total optical attenuation in an optical material and captured in Equation1 [16].

$$\alpha_T = \frac{A}{\lambda^4} + B_1 e^{\left(\frac{B_2}{\lambda}\right)} + C_1 e^{\left(\frac{-C_2}{\lambda}\right)} + D\lambda^{(1.5-3.5)} + \frac{E}{\lambda^{0-4}} + F(\lambda) + G(\lambda) \quad (1)$$

The first three terms encompass the intrinsic losses from scattering, band gap absorption, and multiphonon absorption respectively. The remaining terms encompass losses such as free carrier absorption, extrinsic scattering, impurity absorption and extrinsic electronic absorption processes. In essence the extrinsic process accounts for impurities and defects that deviate from the ideal glass network whereas the intrinsic considers the ideal pure glass network.

2.2 Review of intrinsic loss mechanisms

Practical losses of chalcogenides still exceed the theoretical losses. In order to assess chalcogenide glass development, practical losses are compared with expected theoretical losses. The following provides a brief review of the intrinsic losses in infrared glasses and fibres.

2.2.1 Intrinsic scattering

The first term ($\frac{A}{\lambda^4}$) in Equation1 is used to capture light scattered through three mechanisms: Rayleigh, Brillouin and Raman scattering. The dominant scattering mechanism [16] of the three is Rayleigh scattering which is an elastic scattering process causing a change in the direction of light other than the incident direction and accounts for 99.9% [3] of intrinsic scatterring. Rayleigh scattering is attributed to either thermally arrested density fluctuation or thermally arrested compositional fluctuations in the glass. Scattering in the Rayleigh regime is prominent when the size of such fluctuation is less than $\frac{\lambda}{4\pi}$ [3]. Brillouin and Raman scattering are inelastic processes involving reradiating of the incident light through interaction with acoustic phonons and optical phonons respectively. It should be noted that scattering losses are λ^{-4} dependent and is therefore substantially deceased at longer wavelengths. The general equations used to capture these losses are:

$$\frac{A_{T\ or\ S}}{\lambda^4} = \frac{8}{3}\frac{\pi^3}{\lambda^4}(n^8p^2)kT(\beta_T\ or\ \beta_S) \approx \frac{8}{3}\frac{\pi^3}{\lambda^4}(n-1)^2kT(\beta_T\ or\ \beta_S) \quad (2)$$

and

$$\frac{A_C}{\lambda^4} = \frac{16}{3}\frac{\pi^3}{\lambda^4}\left(\frac{dn}{dc}\right)^2(\Delta_c)^2\,\delta V \quad (3)$$

Where

$A_{T\ or\ S}$ = attenutation losses due to isothermal or adiabatic fluctuations respectively

λ = wavelength

n = index of refraction

p = photoelastic coefficient

k = Boltzmann constant

T = fictive temperature, T_f

β_T = isothermal compressibility for Rayleigh scattering

β_S = adiabatic compressibility for Brillouin scattering

A_C = attenuation due to compositional fluctuations

Δ_c = mean square concentration fluctuation

δV = volume of fluctuation

Qualitatively, kT can be seen as the driving force for the density fluctuation, β_T is the measure of compliancy of the glass to this driving force and the $n^8 p^2$ term captures density fluctuations into dielectric constant fluctuations [17]. Discussion on the relationships between dielectric properties and optical properties are found in [3].

Glasses can be formed via a melt-quenching process. In this process, the elements forming the glass are mixed together in a glass forming ratio at a temperature where the elements react and combine to form a liquid melt. The mixture is then quickly cooled (quenched) which results in an increase in viscosity which freezes the atoms to form a disordered glass network. The faster the cooling process, the higher the fictive and glass transition temperature T in Equation2 as can be and shown in Figure 4. From Equation2 a higher T leads to a higher loss due to scattering.

A study of the variation in T_f and the effects on the absorption loss in the glass making process and fibre drawing maybe interesting for future research. This will require considerable control and repeatability of the manufacturing processes which does not exist for chalcogenides at the moment. Also there is considerable difficulty to measure temperature of the fibre during fibre drawing processes. At the moment the glass transition temperature, T_g is used as an estimate of the fictive temperature to determine theoretical losses.

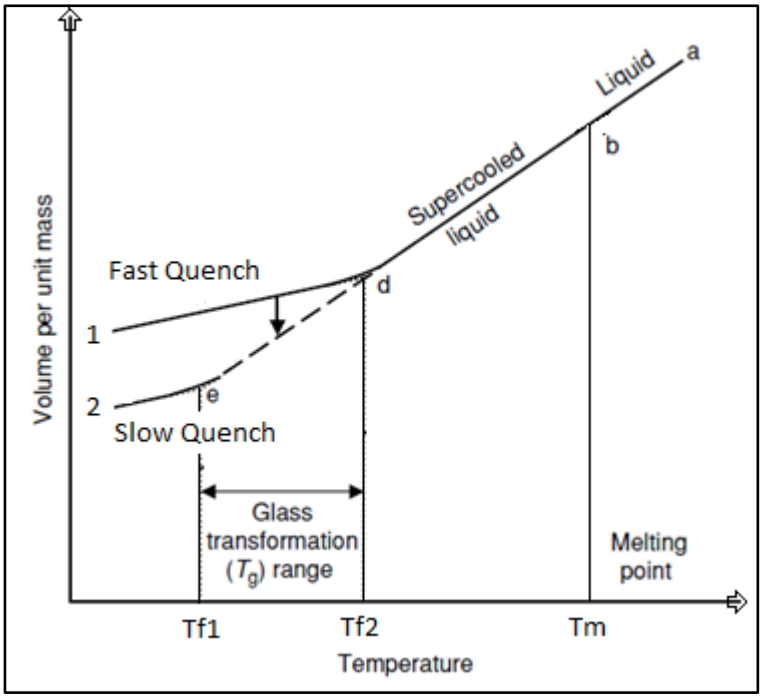

Figure 4 Expected relationship of volume per unit mass vs temperature at constant pressure for different quench rate

2.2.2 Intrinsic electronic absorption – the Urbach tail

The second term, $(B_1 e^{\left(\frac{B_2}{\lambda}\right)})$ in Equation1 captures losses due to intrinsic band-gap absorption. This occurs when the incident light has sufficient energy to promote a valence electron across the forbidden band to the conduction band. Intrinsic electronic absorption rapidly decreases with increasing wavelengths and is generally not considered to significantly affect losses beyond 1μm. Therefore intrinsic electronic absorption determines the cut-off in the short wavelength regime and other intrinsic electronic processes such as the creation of excitons and free-carrier absorptions have lower activation energy and occur at longer wavelengths. The constants $B_1$and $B_2$are usually determined through fitting the exponential equation to the absorption curves from optical spectroscopy.

2.2.3 So-called multiphonon absorption

The third term, $(C_1 e^{\left(\frac{-C_2}{\lambda}\right)})$ in Equation1 captures losses due to the multiphonon edge. This process occurs when the incident light frequency matches the

molecular or lattice vibrations of the bonded atoms of the ideal glass matrix. In addition, absorption not only happens at this fundamental frequency, but also at overtones and combinations. The multiphonon fundamental frequency can be estimated by Equation4.

$$v = \frac{1}{2\pi c}\sqrt{\frac{f}{m}} \tag{4}$$

where,

v = vibrational frequency (cm^{-1})

m = reduced mass of the atoms (kg)

c = is the velocity of light (cm/s)

f = force constant of the bond (dyne/cm)

The multiphonon frequency and harmonics determine the cut-off frequency and attenuation bands in the long wavelength regime. The constants $C_1$and C_2 are determined by fitting the exponential curves to results obtained from optical spectroscopy as outlined in [18]. By having the compositional data of the glass matrix one can determine the major bonds in the glass. Using the force constant and the masses of each atom forming the bonds, the vibrational frequency can be determined using Equation4. The calculated values are shown in Table 1 for some typical bonds and the vibrational wavelengths. The reduced mass is calculated by dividing the product of the mass of each atom forming the bonds by their sum and converting from Atomic Mass Units(amu) to kg using 1.66 $x10^{-27}$ kg/amu. It should be noted that force constants [19] in Table 1 are specific to certain compounds and the associated vibrational wavelength may be slightly different when compared to a specific glass network.

The vibrational frequencies can then be matched to experimental results From IR spectroscopy. For example, vibrational frequency analysis in the IR and matching with Raman spectroscopy is done in [20] for the chalcogenide glass $Ge_{0.17}Se_{0.83-x}Sb_x$. Vibrational frequency data is often more accessible than force constant data therefore the reverse can be done to match data from optical

spectroscopy if the elements of the glass and their possible impurities are known.

Bond (A-B)	Compound	Force Constant, Ncm^{-1})[19]	Amass, amu	Bmass, amu	Reduced Mass, kg	Vibrational Frequency, cm^{-1}	Wavelength, μm
H-H	H_2	5.14	1.008	1.008	8.37E-28	4160	2.4
H-O	H_2O	8.45	1.008	15.999	1.57E-27	3889	2.6
H-O	OH	7.45	1.008	15.999	1.57E-27	3651	2.7
H-S	H_2S	4.29	1.008	32.06	1.62E-27	2729	3.7
H-C	CH_4	5.5	1.008	12.011	1.54E-27	3168	3.2
O-C	CO	18.56	15.999	12.011	1.14E-26	2143	4.7
O-C	CO_2	15.61	15.999	12.011	1.14E-26	1865	5.1
O-S	SO_2	10.01	15.999	32.06	1.77E-26	1262	7.9
O-O	O_2^+	16.49	15.999	15.999	1.33E-26	1870	5.3
O-O	O_2	11.41	15.999	15.999	1.33E-26	1556	6.4
O-O	O_2^-	6.18	15.999	15.999	1.33E-26	1145	8.7
O-O	O_3	5.7	15.999	15.999	1.33E-26	1100	9.1
O-Se	SeO	6.45	15.999	78.971	2.21E-26	907	11.0
O-Te	TeO	5.31	15.999	127.6	2.36E-26	796	12.6
S-S	S_2	4.96	32.06	32.06	2.66E-26	725	13.8
S-S	S_8	2.5	32.06	32.06	2.66E-26	514	19.4
Se-Se	$^{80}Se_2$	3.61	78.971	78.971	6.56E-26	394	25.4
Te-Te	Te_2	2.37	127.6	127.6	1.06E-25	251	39.8

Table 1 Calculated vibrational data using Equation4.

2.2.4 The Intrinsic transmission window

Combining these three intrinsic loss mechanism defines the predicted minimum transmission of IR materials. This is achieved by substituting the wavelength range and parameters $A, B_1, B_2,\ C_1$ and C_2 into equation1. Table 2 shows the parameter values and the predicted minimum loss for some of the more promising chalcogenides. As mentioned, the parameters substituted in the intrinsic terms in Equation1 depend on experimental curve fitting and other parameters determined experimentally. Care must therefore be taken as effects from extrinsic processes are difficult to identify and differentiate. For example, if the curve fitting for the infrared absorption edge was done using 10μm wavelength for determining the parameters C_1 and C_2 for GLS in Table 2, this would lead to a wrong estimation of the minimum loss. This vibrational wavelength of 10μm is more likely associated to O-O bond rather than the S-S

bond as shown in Table 1. Thinner polished samples or ultra-high purity fibre approaching theoretical losses should be used for optical studies as this minimizes the contribution from extrinsic processes on the multiphonon edge.

In [21], a Weak Absorption Tail (WAT) is used to redefine the predicted loss minima near the electronic absorption edge. The authors concluded that the WAT will inhibit transmission loss reduction to levels below 10dB/km in chalcogenide glass fibres. The results in [21] follows from work done in [22] where the WAT in amorphous semiconductor thin films was studied. The authors in [22] associate the WAT to localized states in the band gap caused by defects in the production of thin films. Different production methods led to different energies and shapes of the electronic edge [22]. The authors in [22] conclude that the differences can be overcome by annealing the thin film samples and is also less serious for materials produced in the amorphous state [22].

Glass Material	Rayleigh Scattering or WAT, dB/km	Electronic Absorption, dB/km	Infrared Absorption, dB/km	Projected Minimum, dB/km (wavelength)	Ref
$Ge_{25}S_{75}$	$\frac{3.97}{\lambda^4}$	$5.26 \times 10^{-8} e^{\left(\frac{15.2}{\lambda}\right)}$	$5.63 \times 10^{12} e^{\left(\frac{-164}{\lambda}\right)}$	0.011(4.6μm)	[23]
$As_{40}S_{60}$	$8.4 \times e^{\left(\frac{4.4}{\lambda}\right)}(WAT)$	$1.6 \times 10^{-11} e^{\left(\frac{23}{\lambda}\right)}$	$1.8 \times 10^{9} e^{\left(\frac{-95}{\lambda}\right)}$	23(4.6μm)	[21]
$Ge_{20}S_{80}$	$66 \times e^{\left(\frac{3.2}{\lambda}\right)}(WAT)$	$1.0 \times 10^{-8} e^{\left(\frac{17}{\lambda}\right)}$	$1.1 \times 10^{8} e^{\left(\frac{-59}{\lambda}\right)}$	169(3.6μm)	[21]
$70Ga_2S_3.30La_2S_3$	$\frac{58.9}{\lambda^4}$	$1.81 \times 10^{-4} e^{\left(\frac{12.2}{\lambda}\right)}$	$5.06 \times 10^{9} e^{\left(\frac{-80.1}{\lambda}\right)}$	0.5(3.5μm)	[24]
$72.5Ga_2S_3.27.5 La_2O_3$	$\frac{23.4}{\lambda^4}$	$4.07 \times 10^{-4} e^{\left(\frac{11}{\lambda}\right)}$	$9.72 \times 10^{8} e^{\left(\frac{-65}{\lambda}\right)}$	0.1(2.6μm)	[24]

Table 2 Summary of intrinsic loss and minimum loss prediction data.
(Consolidated from various sources listed in "Ref" column)

In [24, 25], prediction loss studies are carried out for gallium lanthanum sulphide which is the main infrared transmitting material focused on in Chapter 4 and for the FLITES project. The minimum loss from the equations in Table 2 vs experimental fibre curve for GLS is shown in Figure 5[25]. As can be seen the fibre loss is not close to the theoretical minimum loss and it is concluded in [25] to be from extrinsic mechanism. Losses due to extrinsic mechanisms are discussed in the following section.

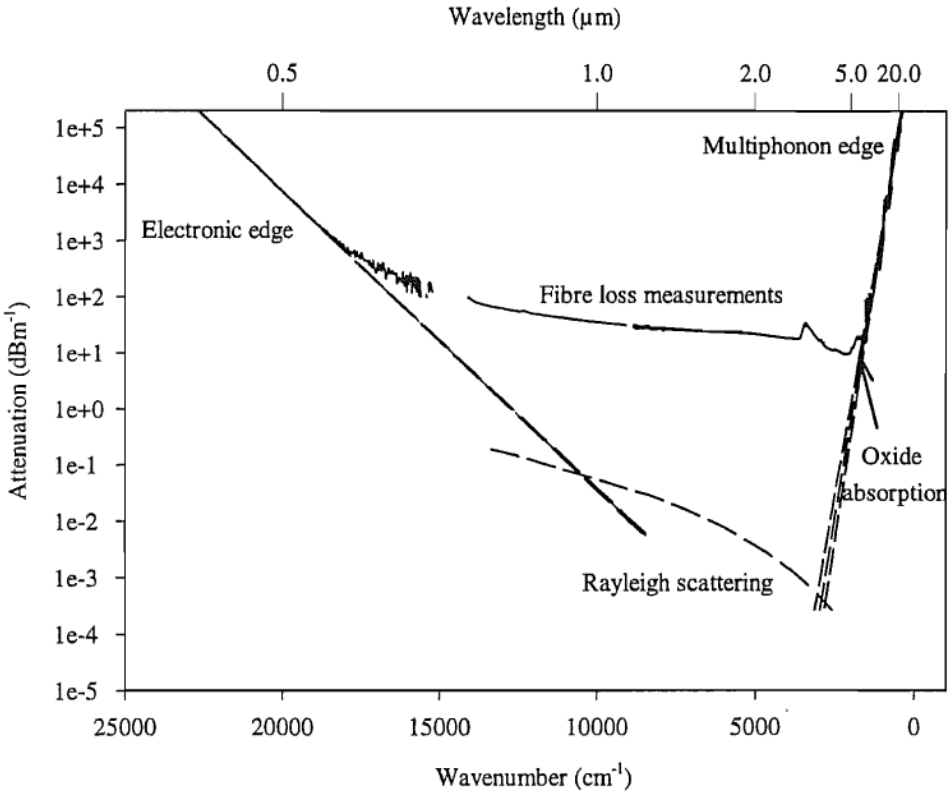

Figure 5 Comparing the theoretically predicted minimum loss and experimentally determined fibre loss for GLS glass. (From Brady D.J., et al., J. Non-Cryst. Solids, 92 -98, 242, 1998. With Permission)

2.3 Review of extrinsic loss mechanisms

The remaining terms in Equation1 capture the losses due to extrinsic scattering and absorption mechanisms. The fourth term, $D\lambda^{(1.5-3.5)}$ is used to capture losses by free carrier absorption. This loss mechanism is as a result of electron or holes in the conduction or valence bands respectively being excited by the incident light and scattered inelastically by phonons and ionized impurities which surrender the energy to the glass lattice [16].

The fifth term, $\frac{E}{\lambda^{0-4}}$ in Equation1 accounts for losses due to extrinsic scattering processes. This is a very important loss mechanism when interpreting loss curves and accounts for the attenuation being far greater than the intrinsic Rayleigh scattering. Extrinsic scattering arise from impurities and imperfections or heterogeneities. The size and difference in properties such as the refractive index from the surrounding materials determine the wavelength power, λ^{0-4} dependency. Mie scattering theory can be used to estimate the losses in fibres as done in [26] for As_2S_3, [25] for GLS and [18] for Fluoride glasses. The Mie equations are developed as follows and taken from [26].

The first assumption is that the impurity, imperfection or heterogeneity is treated as a spherical particles in the dielectric glass medium, so that the light scattered is dependent on three factors, wavelength of light, λ, the particle size, a, and the relative refractive index, m. A scattering efficiency factor Q is introduced and is the ratio of the true scatter cross section to the geometric cross section and is dependent upon particle size, relative refractive index and wavelength. The equations relating these parameters to each other and the loss are defined as

$$m = \frac{n_1}{n_0} \tag{5}$$

where

m is the relative refractive index

n_1 is the refractive index of the particle at a given wavelength

n_0 is the refractive index of the glass at a given wavelength

$$x = \frac{2\pi a n_0}{\lambda} \tag{6}$$

$$p = 2\pi(m-1) \tag{7}$$

Where

x is a measure of the relative size

p characterizes the phase shift of a diametrical ray p

a is the particle radius

λ is wavelength of light in a vacuum

$$E = c\pi a^2 Q \tag{8}$$

where

Q is the scattering efficiency factor

E is the scaterring coefficient (cm^{-1})

c is the number of scattering centers per unit volume

Converting to loss in cm^{-1} to dB gives

$$\alpha_{Extrinsic\ Scattering} = 10 \log_e E \tag{9}$$

Equation 1

Normalize for length, L in meters and total number of particle N gives

$$\alpha_{Extrinsic\ Scattering} = \frac{N}{L} 10 \log_e \left(\frac{a}{r}\right)^2 Q \tag{10}$$

where r is the radius of the fibre.

In summary, using Table 3 and Equations5 through Equation10, relationship between the loss per impurity, imperfection or heterogeneity versus wavelength can be obtained as plotted in [25] for GLS and more comprehensively in [26] for As_2S_3. This can then be used to identify contributions to the experimental losses obtained by optical spectroscopy and supplemented with data from glow discharge mass spectroscopy (GDMS).

The sixth term, $F(\lambda)$in Equation1 accounts for the extrinsic absorption due to impurities whose vibration modes are IR active in wavelengths lower than the intrinsic fundamental vibration frequency of the glass. These absorption peaks present themselves in the results obtained from optical spectroscopy which are then matched using software databases or matching the peaks to those identified in the literature. However one has to account for shifts in the peaks due to differing elements in the glass matrix that surrounds the impurity. Also

a single absorption peak can be as a result of many different impurities existing in the glass matrix. Having many impurities makes isolating and differentiating the effects quantitatively on the absorption data for each impurity increasingly difficult.

Scattering centre	**Scattering efficiency factor, Q**	**Scattering behaviour**
Very small spheres X«1, intermediate index difference	$\frac{8}{3}x^4\frac{(m^2-1)^2}{(m^2+2)^2}$	λ^{-4}Rayleigh
Intermediate size spheres M close to 1, p«1	$2(m-1)^2x^2=\frac{p^2}{2}$	λ^{-2} Rayleigh-Gans
Intermediate size spheres M arbitrary	$2-\frac{4}{p}\sin(p)+\frac{4}{p^2}(1-\cos(p))$	Anomalous diffraction
(a) p > 1	Q → 2	λ^0 wavelength independent
(b) p <1	$Q\rightarrow\frac{p^2}{2}=2(m-1)^2x^2$	λ^{-2} Rayleigh-Gans
Absorbing spheres	$Q_{scatter}+Q_{absorption}$	Complex

Table 3 Scattering behaviour of particles of various sizes and refractive indices. (From Sanghera J.S., et al., J. Appl. Phys., p. 4885 – 4891, 75, 1994. With Permission), [26]

Using the frequencies obtained from optical spectroscopy and the mass of the expected impurity from GDMS can be used to calculate the force constant from Equation4 and match these to known literature data. The difficulty again is that there can be overlapping impurity bonds which are not discernible from one another. The high impurity content of the raw materials and glasses in this

work as shown by the GDMS results in Appendix B Table 10 (column 4 – GWI, column 8 - Testbourne and column 9-Lorad) and Table 11(column 5-8) respectively makes analysis very difficult. Any data from GDMS where an impurity is removed in different melts can assist in the elimination process but again the difficulty increases when there are many impurities which vary between glass samples analysed. The shape of the absorption peak is important as it may give information on the impurity network that surrounds the major impurity. For example if we consider the OH absorption in a chalcogenides glass which has a high concentration of impurities, from the relation mass, force constant and vibrational frequency relationship in Equation4, if the peak is not centred and shifted to higher frequencies, it implies that the OH impurity is surrounded by atoms of smaller mass and weaker bonds. A simple term used to determine the magnitude of loss and effects of the concentration of an impurity is the specific absorption coefficient and is defined as

$$specific\ absorption\ coefficient = \frac{B}{c}, \text{ dB/km/ppm} \qquad (11)$$

Where

B – the attenutation coefficient goal, dB/km

c – the concentration of the impurity, ppm

For example this equation11 can be used as in [16, 27-29], to determine the acceptable concentration of an impurity to achieve a certain loss or estimation of impurity levels from experimental data. For example, if the OH impurity wavelength is required for an application and the specification requires an attenuation coefficient goal, B of less than 1dB/m, since OH has a specific absorption coefficient of 5dB/m/ppm around a specific wavelength, then the concentration, c of OH should be less than 0.2 ppm. This approach requires that the specific absorption coefficient is known and can be estimated by doping the glass with known quantities of impurities and obtaining loss measurements similar to work done in [30] for GLS. Table 4 shows some of the specific absorption coefficients information that can be obtained from the literature while Table 5 shows the impurity content in the most studied and purified arsenic chalcogenide material [29].

Impurity Absorption	Wavelength (um)	Absorption loss (dB/m)	Specific Absorption Coefficient (dB/m/ppm)	Impurity Concentration (ppm)
Sulphide				
H-S	4	10	2.3	4.3
O-H	2.9	0.3	5	0.06
CO_2	4.33		15	
COS	4.95		100	
CS_2	6.68		480	
SO_2	8.63		0.043	
Selenide				
Se-O	10.6		1.03	
S	10.6		0.38	
Telluride				
H-Se	4.5	3	1.1	2.7
Ge-H	5	6		
H_2O	6.3	0.07	34	0.002
Ge-O	7.9	0.16	2.6	0.06
Other information				
Clusters			Up to 50	
Macroscopic imperfections			Up to 50	
Rare-earth ions			Up to.04	
Transition-metal ions			Up to 0.13	

Table 4 Summary and estimation of specific absorption coefficients. (Consolidated from references [16, 27, 28])

The seventh term, $G(\lambda)$ in Equation1 accounts for electronic absorption from extrinsic process such as point defects, structural imperfection and impurity atoms that create electrically active states in the forbidden band so that low energy absorption can take place [16].

Group of Impurities	Impurity in group	Typical content of impurity, ppm at.
Light Elements	H, O, C, N	10-100
Metals	Transition and other metals, Si	0.1-1.0
Analogs of elements-macrocomponents	P, Sb,S,Se	1-100
Embedded into glass network	H, O, N, halogens (OH,SH, SeH NH, AsH-groups)	0.001-10
Dissolved components	CO_2, COS,H_2O,N_2	0.01-10
Heterogenous inclusions	Carbon, SiO_2, Al_2O_3	10^6-10^9 cm^{-3}

Table 5 Impurity groups in vitreous arsenic chalcogenides (From Sonaptin GE., et al., Inorganic Materials, p. 1439-1460, 45, 13, 2009. With Permission) [29]

2.4 Brief review of analysis techniques and limitations

Many analysis techniques were used in analyzing results of this Thesis such as Fourier Transform Infrared (FTIR), Ultraviolet (UV)-Visible (Vis)-NIR, Raman, GDMS, Scanning Electron Microscopy (SEM) and Atomic Force Microscopy (AFM). FTIR is the main technique for studying material transmission, absorption and IR long wavelength cutoff of chalcogenides in the MIR range of 2 – 25 μm. The other techniques were used to supplement FTIR and were utilized to understand where the losses may be attributed. The UV-Vis-NIR is useful in studying the transmission, absorption and short wavelength cutoff of chalcogenides in the region of 400 nm to 3μm. Raman is used to obtain and study the vibrational frequency region (10-100 μm).

GDMS was used to obtain the concentration of impurity elements existing in certain raw materials used and final glass obtained in this thesis. The GDMS data was used to compare to old GDMS data for glasses and raw materials manufactured in-house in the past and is listed in Appendix B Table 10 and Table 11. Also included in Appendix B Table 11 is GDMS for $As_{40}Se_{60}$ which was obtained commercially from SCHOTT. GDMS greatly assist in assessing raw material and purification as well as help in identifying the effects of an impurity on the extrinsic absorption mechanisms discussed previously. These tables will be discussed in more detail in Chapter 4.

The goal is to make low loss MIR glasses in the range 3 – 5 μm for the FLITES project. Bulk glass and not fibre was the main deliverable of this thesis since the majority of the time was focused on building up the infrastructure at the ORC. Therefore, FTIR was chosen as the method to evaluate the improvement in purity of the bulk glass samples produced. FTIR analysis was done on cut and polished bulk glass samples. The FTIR used in this thesis is the Varian 670 model. Sample preparation involves, firstly cutting glass samples from the ingot produced and then polishing two sides parallel to each other. The number of samples obtained for analysis depends on the quantity of glass synthesized. Also the variation in thickness of samples that can be cut and polished from a melt depends on other factors such as bubble size variations which occur between the container and the glass melt. This phenomena is mentioned in [18] as being a problem for oxide and chalcogenides rather than fluoride glasses.

The sample could be further cleaned before placing into the FTIR sample chamber for analysis by rinsing with acetone followed by DI water and drying with an inert gas. If the sample is not dried properly, the acetone and water peaks can be more pronounced on the transmission and absorption curves. The sample chamber is purged by a N_2 gas however purging is limited due to N_2 gas quality and therefore various gas molecules in the chamber are still present; the most notable are moisture and carbon dioxide [16, 31]. These gas molecules absorb and scatter light from the source as shown in Figure 6 by the components I_{a1} and I_{a2}. To reduce this influence on the acquired signal for the sample, a background scan without the sample is conducted.

A background scan is shown in Figure 7 along with the expected wavelength and absorption ranges of the main gas species. Also shown in Figure 7 are responses of the FTIR when different thickness samples are inserted into the sample holder. These samples were made using the RAP process detailed in Chapter 4. The absorption of the gas molecules are seen in the FTIR response and also when the glass samples are in place. Gas molecules in the chamber and not a component of the glass are expected to have narrow bandwidth feature in the FTIR response spectrum varying in order of tens to several hundred nanometers depending on the resolution chosen for sampling. Comparing the background response and the sample response allows for discerning contributions that are from the glass and the FTIR chamber atmosphere. In this example a resolution of $4cm^{-1}$ was chosen to show these feature.

Using the sample response and the background response, the transmission can be obtained for the thin and thick sample is shown in Figure 8. It can be seen that the gas molecule contribution are not completely eliminated in this step as shown by the 4.3μm peak which is attributed to CO_2 which is more pronounced for the thick sample. By manually fanning after positioning the sample in the chamber, the CO_2 feature was sometimes removed as is the case for the thin sample plot in Figure 8. This however was random and not repeatable.

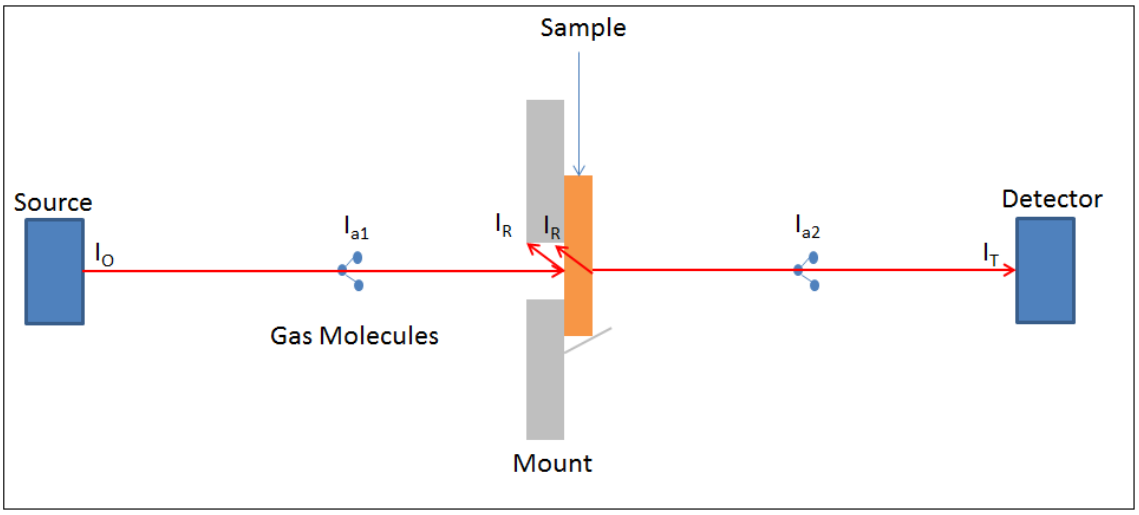

Figure 6 Simple schematic of FTIR chamber showing reflection losses and absorption from gas molecules in the chamber

The transmission curves in Figure 8, does not account for the reflection losses occurring at the sample interfaces when trying to ascertain the loss for the glass alone. The reflection loss components (I_R) are shown in Figure 6 and to account for these reflection losses, FTIRs can be fitted with Attenuated Total Reflectance accessories. Another choice is to use refractive index data if available and Beer-Lambert Equation12.

$$I_t = I_o(1 - R)^2 e^{-\alpha t} \tag{12}$$

where $R \approx \left(\frac{n-1}{n+1}\right)^2$ and

I_t – output intensity, power or transmission

I_o – input intensity, power or transmission

R - Reflectivity

α – absorption coefficient

t - thickness

n – refractive index

Refractive index data to be used in the Beer Lambert equation can be obtained from ellipsometry measurements. However in most cases are limited to measurement up to 1.8 μm. To obtain data for wavelengths further into the IR, sellemier equations as shown in Equation13 can be used to curve fit to experimental data at the shorter wavelengths and extrapolate to the required wavelength in the transmission window of the glass.

Sellemier equation used for refractive index estimation is as follows

$$n^2(\lambda,T) - 1 = \frac{B_1(T)\lambda^2}{\lambda^2 - C_1(T)^2} + \frac{B_2(T)\lambda^2}{\lambda^2 - C_2(T)^2} + \frac{B_3(T)\lambda^2}{\lambda^2 - C_{31}(T)^2} \quad (13)$$

where

λ is wavelength

T is temperature

and $B_1, B_2, B_3, C_1, C_2, C_3$ are parameters determined through curve fitting to experimental data at shorter wavelengths obtained from ellipsometry equipment.

Using the refractive index data and Beer-Lambert equation, the corrected transmission loss can be obtained using the measured sample thickness and is shown in Figure 9. This is one method explored for accounting for reflection losses in this thesis. The disadvantage of this approach is that the compounded errors from the measurement equipment and ellipsometry modelling lead to inaccurate estimates of the loss. Other errors sources can also come from sample surface roughness and compositional variations if using data from measurements of another sample. This method lead to transmission greater than 100% as shown in Figure 9 which is not expected.

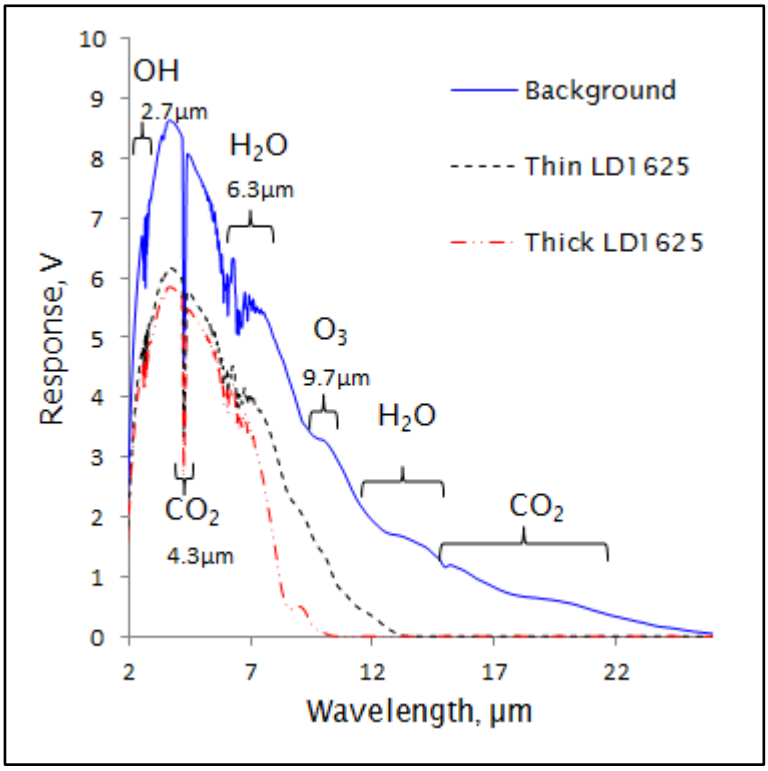

Figure 7 FTIR response signal for background (no sample), thin and thick sample

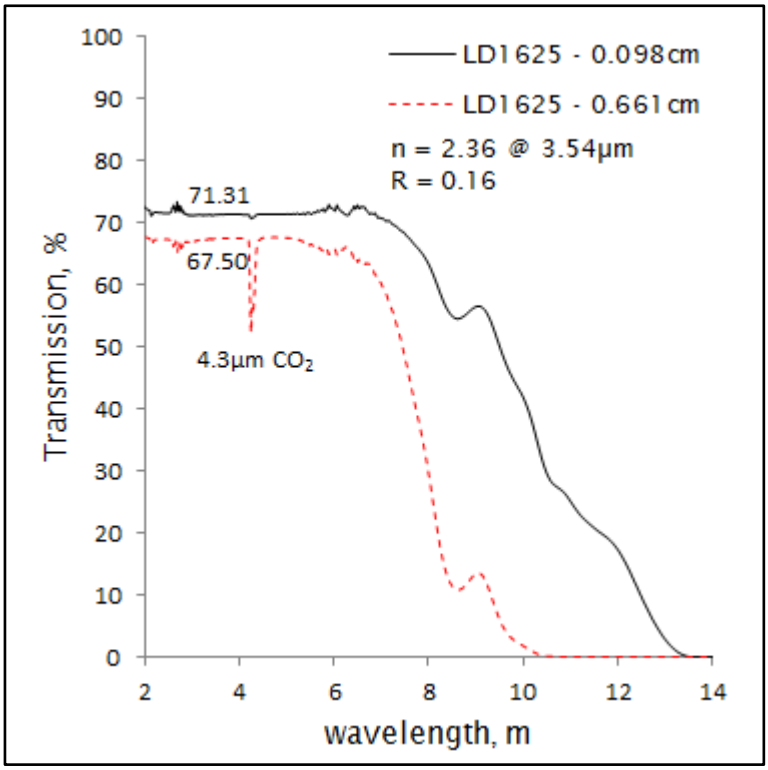

Figure 8 FTIR transmission curve for a thick and thin sample

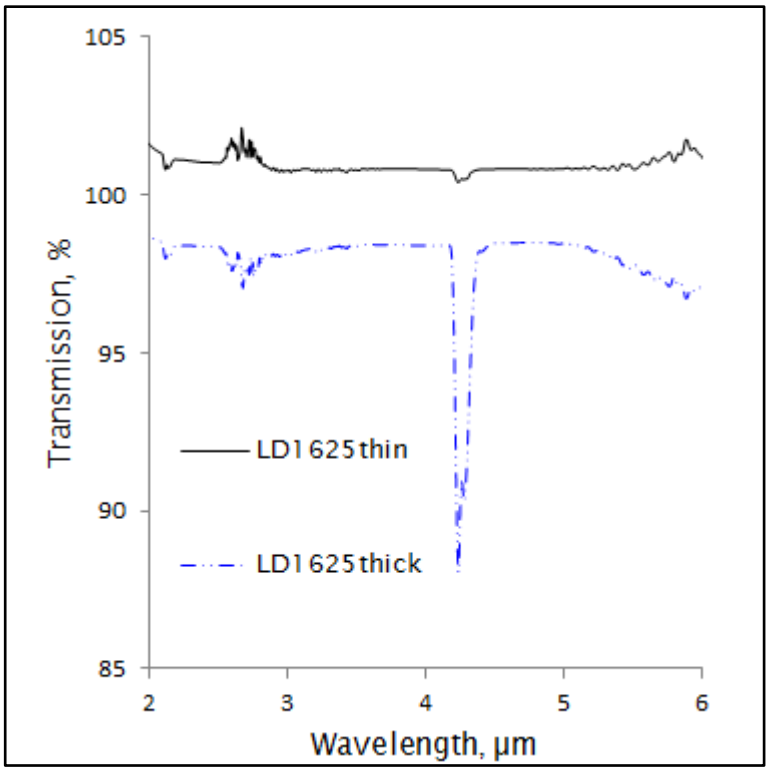

Figure 9 Using Beer-Lambert and sellemier equations ellipsometry results to correct for reflection losses in the thick and thin samples of LD1625

The other method of choice for evaluating the loss in the bulk samples produced by the Horizontal RAP system in Chapter 4 of this thesis involved using a thin and thick sample and the FTIR only. The method involves placing the thin sample into the sample chamber and completing a background scan. The thin sample is then removed and the thick sample is placed in the chamber and an absorption scan completed. The absorption data is then divided by the difference in thickness of the two samples. This method resembles the cutback method used for fibre loss measurement except that two samples are used instead of cleaving the fibre. Therefore the thin sample properties may not exactly exhibit the same properties of its equivalent part of the thick sample. Also there may be slight variations in polishing of the thin and thick samples which can affect the reflection loss component.

The result of correcting reflection loss by use of Beer Lamberts law and Ellipsometry (BLE) as opposed to thin and thick samples method is shown in Figure 10. The BLE method causes an underestimate of the transmission potential of the glass. This is due to the ellipsometry models and sellemier equation used in estimating the real part of the refractive index. The errors in

estimating the refractive index from the BLE method can lead to loss of features such as differences in slope around 3μm. The slope may determine the type of extrinsic scattering behavior as listed in Table 2. Sellemier equations are not intended to be used in absorption regions as the data is fitted to the real part of the ellipsometry data and not the imaginary part. This will lead to loss of features around absorption regions as seen with the moisture peak around 2.9 μm in Figure 10.

Comparing FTIR data in this thesis to those in the literature is difficult as there is a wide variation in format of the presented results. Most published data for bulk glasses are plots of the transmission (%) against wavelength for one sample as shown in Appendix A, Figure 82. Sometimes a value for refractive index (or reflectivity) and the thickness are included allowing the calculation of the loss using Equation12 at that particular wavelength. Comparing to fibre loss data is also difficult as fibre loss measurements are not standardized as discussed in [4]. Fibre measurements results as shown in Appendix A, Figure 81 serve as good indicators for the improvement goals of bulk glass samples made in Chapter 4.

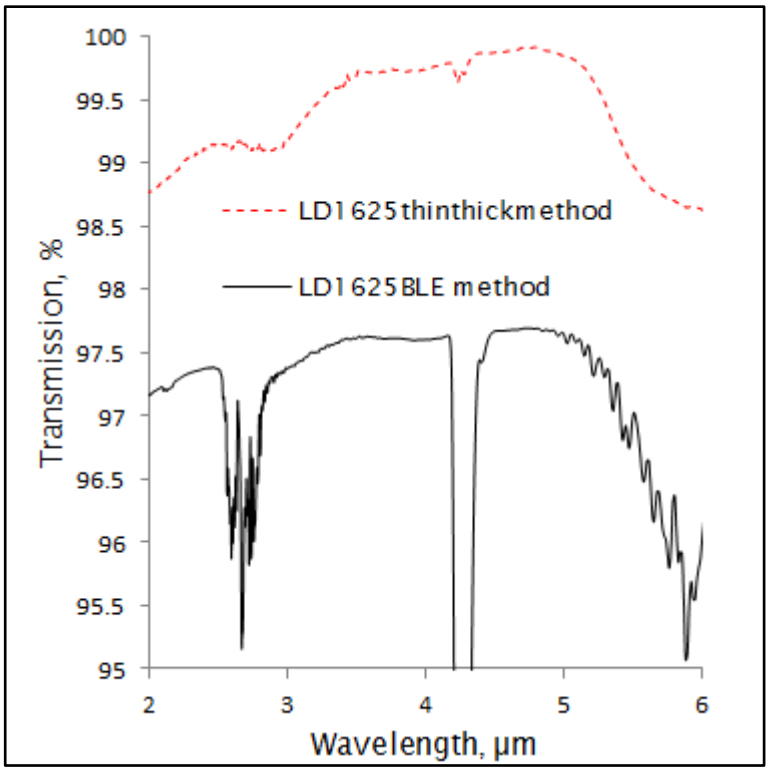

Figure 10 Comparison of the two methods of accounting for reflection losses in bulk glass samples, Method 1 using Beer Lamber and Ellipsometry (BLE) and Method 2 using a thin and thick sample with FTIR only.

2.5 Conclusion

In this chapter the fundamental of losses in optical materials are reviewed and presented. The intrinsic and extrinsic limits are discussed with focus on the main chalcogenide glass compositions in the literature. This information is used to target improvement in facilities and raw materials. The loss contributions within the IR transmission window are definitely due to unwanted bonds to hydrogen, carbon and oxygen with impurity elements or the chalcogenide glass elements. Impurity elements such as transition metal impurities and impurities from the reactor tube such as silica is also a major problem and are easily identified in impurity analysis. Hydrogen, carbon and oxygen can be identified but are difficult to eliminate. The main technique of FTIR used to analyze bulk glass samples is presented and compared to the BLE method. It can be concluded from experimental data that the best and most reliable method is the use of thick and thin samples once samples are properly polished.

Chapter 3: Chalcogenide Synthesis Methods

In Chapter 2, loss mechanisms have been reviewed, in the following Chapters 3, 4 and 5 some of the methods and facilities for making high purity chalcogenides are explored through experimentation. The main methods include basic sealed ampoule, microwave assisted sealed ampoule, levitation methods, RAP and CVD. In this Chapter 3, the work carried out on developing a basic sealed ampoule, replicating microwave assisted sealed ampoules and experiments carried out at the University of Bristol with the aero-levitation method are shown and compared to literature where appropriate.

The sealed ampoule method is by far the most utilized method for making bulk chalcogenide glasses. The sealed ampoule method has the flexibility to be combined with other processing steps such as distillation, CVD and RAP to improve the purity of chalcogenides manufactured. At the ORC glasses have been manufactured mainly by RAP and CVD which are covered in Chapter 5 and 6 respectively. RAP facilities and procedures at the ORC were developed for making GLS from gallium and lanthanum fluoride as detailed in [25]. This RAP does not require incorporation of ampoule sealing. A basic CVD system was developed for making germanium sulphide and germanium antimony sulphide with focus mainly on thin film deposition. Some feasibility work was done on using of CVD to make bulk glass via combination with sealed ampoule and is detailed in [15]. Levitation methods have not received much attention but the ability to melt in a containerless environment is worth investigating. The sealed ampoule, microwave and levitation method have been investigated to evaluate the their limitations and possible benefits.

A dedicated sealed ampoule facility and procedure did not exist at the start of this work and in the next section, the facilities built and procedure developed is detailed with comparison to typical procedural steps in the literature.

3.1 Sealed ampoule

There are many synthesis routes to making bulk chalcogenide glasses with the main technique being sealed ampoules, often combined with vacuum distillation, RAP and CVD to improve purity of raw materials and the final glass. This method is constantly being optimized, for example a recent improvement

was the use of microwave heating to remove water content in [14, 32]. Sealed ampoule synthesis has not received much attention at the ORC with respect to development of infrastructure, procedures and knowledgebase and was chosen for development.

The sealed ampoule method was developed to overcome the high vapour pressure of the raw elements that constitute chalcogenide glass batches and is the method most used in making chalcogenide glasses. By using a sealed container (ampoule) material loss is restricted allowing the volatile components to mix together. Since material is not lost, the sealed ampoule method has good control of the final glass composition. The ampoule is often made of high purity silica with low OH content (typically < 5ppm) to minimize moisture impurities that can diffuse into the batch from the ampoule wall. In cases where the materials can react with silica, often crucibles of non-reactive materials such as vitreous carbon are inserted into the silica ampoule to prevent this reaction. The volatility of the raw elements, especially sulphur and arsenic increases the risk of explosion of the ampoule and is a major health and safety deterrence.

A manufacturing procedure is very important both in terms of safety and achieving high purity. The following section evaluates the sealed ampoule method through development of infrastructure and procedures at the ORC. Lastly recommendations for future developments are given.

3.1.1 Sealed ampoule procedure developed as part of this Thesis

The procedure developed for sealed ampoule is summarized in Figure 11 and the details for each procedural step developed as part of this work are given below.

The first step involves the preparation of the ampoule. This can be a simple rinse with Deionised, DI water followed by drying in an oven above 100˚C. More complicated procedures have been developed in the literature which adds an HF etch step prior to rinsing with DI water. The etching with HF is used to remove defects such as scratches which can occur from improper prior handling or storage. Scratches can weaken the ampoule which increases the risk of explosion of the ampoule during the high temperature melt cycle. It has been observed that scratches are more likely to occur after cleaning the

ampoule rather than before the initial cleaning. Also HF has been known to passivate the dangling bonds at the surface of a material [33]. If true, the HF may result in a decrease reactivity of the ampoule with the melt environment however the converse may be true and in this case may result in an increase in hydrogen impurities within the glass. The HF step also adds additional safety precautions from the hazards associated with using HF.

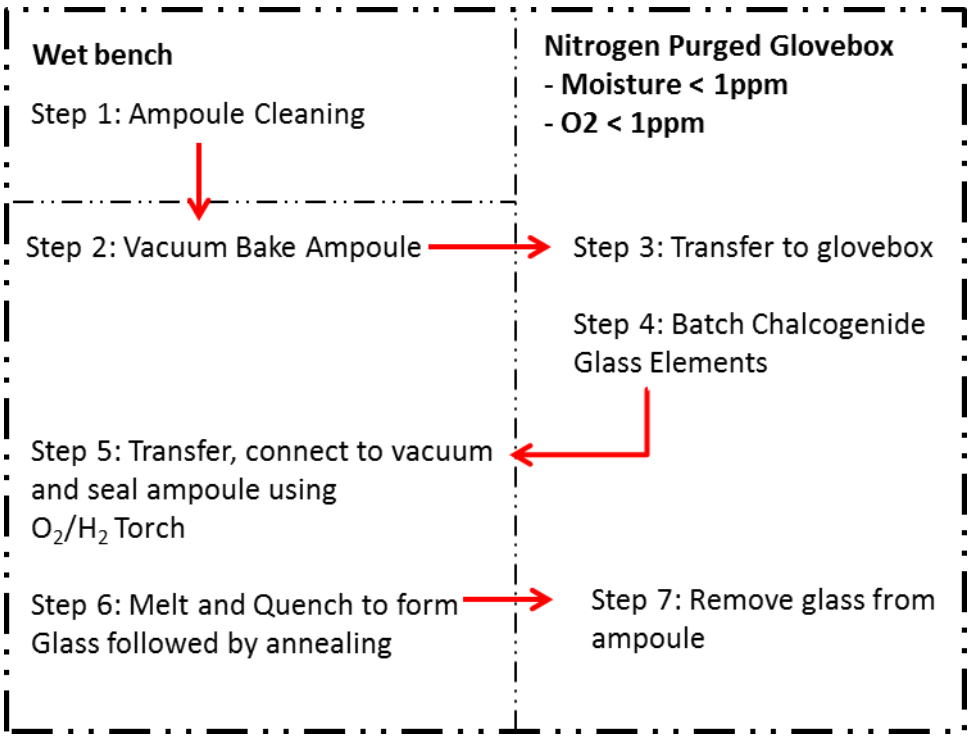

Figure 11 Sealed ampoule steps developed as part of this work and implemented within the class 10K cleanroom at the ORC

The second step involves vacuum drying at a temperature slightly higher than the melt temperature but lower than the softening point of the silica ampoule. Silica has a softening point of 1200 ˚C while most chalcogenide melts are done below 1000 ˚C. This baking process allows removal of moisture and other volatile impurities that would otherwise be trapped when the ampoule is sealed and become incorporated into the final glass. An advantage of this step is that the vacuum sealing system can be tested to achieve high vacuum of greater than 10^{-5} mbar. Through experience, the leak occurs mostly at the vacuum fitting that connects to the ampoule. Since the sealing torch is outside the controlled atmosphere glovebox where the material is stored and batched, the purity of the ampoule can be compromised.

The third step involves closing the vacuum valve, disconnecting without compromising the vacuum in the ampoule and transferring to a high purity glovebox environment where the valve is opened and removed to allow filling the ampoule with the raw materials. Ideally at this stage the purity of the ampoule environment is limited by the purity of the nitrogen or inert gas delivered to the glovebox and the general maintained environment of the glovebox. The glovebox is provided by Innovative Technologies Limited and equipped with oxygen and moisture sensors which are calibrated and maintained to be less than one ppm for both impurities. However the gas to the glovebox may be higher purity therefore the sensor gives an indication of whether the glovebox environment purity is compromised. The work in section 4 of this thesis on improvement of N_2 gas purity supply directly affects the purity achieved within the glovebox and the glasses because the chalcogenide raw materials are stored and batched in this environment.

The fourth step involves filling the ampoule with the raw materials and recording the weights of each component added so that the glass stoichiometry can be determined. Care is taken so that material is not deposited in the section where the ampoule is sealed as this can reduce the integrity of the seal. Depositing material where the ampoule is sealed leads to incorrect compositional determination because of the sealing process. During the sealing process, the high temperature torch raises the temperature of the material above the boiling point becoming vaporized and lost to the vacuum extract. For this reason it is preferable to load materials in shot (3-10mm pellets) form as opposed to powders. Using shots over powders has the advantage of less surface contamination due to smaller surface area being exposed when batching the materials however powders may homogenize more easily and decreases glass melt time. The Klein Flange (KF) compression fitting is the point of failure when establishing a vacuum seal in subsequent steps. The fitting should not be removed when batching the raw elements. This ensures that when the fitting is remade to the vacuum valve, the vacuum sealing capability is not compromised.

Raw materials play a crucial role on the final glass product. Impurities not removed in the synthesis of the raw materials have a high likelihood of being incorporated. In order to make high purity materials consistently, certification from commercial suppliers of the purity of the materials supplied is needed.

This can considerably increase the cost. When purchasing raw materials, the purity is specified in units of nines purity. It is important at this stage to specify to which impurities that this specification is made. For instance, one supplier can have 7 nines purity whereas another has 5 nines purity at a significantly higher cost. The cost difference can be as a result of the number of elements in the periodic table that the purity of the raw materials is specified to. As discussed in Chapter 2 the magnitude of extrinsic impurities is very important to achieving ultra-low loss materials.

The fifth step follows loading the raw materials and is the sealing of the ampoule. The vacuum valve is reconnected and closed in the glovebox to ensure that the ampoule environment is maintained for transport outside the glovebox before sealing. An ampoule loaded with raw material for making a 2 inch sputtering target is shown in Figure 12a. The ampoule is then reconnected to the vacuum pump and the ampoule evacuated to less than 10^{-5} mbar. The higher the vacuum achieved, the lower the impurities in the melt environment. The vacuum ensures that gas molecules are not trapped between the glass component particles. An oxy hydrogen torch is then used to seal the ampoule as show in Figure 12b. Care is needed to ensure that the glass is evenly heated around the seal point. This is achieved by moving the torch around the circumference of the glassware until the glass collapses and seals. If the torch is not moved in this manner and one point on the glassware focused with the torch for too long, failure of the glassware will occur. Failure of the glassware will result in loss of vacuum and high purity will not be achieved.

The sixth step involves transferring to a furnace for melting. Thermal analysis data, melting points data, vapour pressure curves and phase diagrams was used to develop the thermal cycle to be implemented on the furnace. Care must be taken when ramping the furnace to the melt temperature so as to balance mixing and forming the glass while minimizing the vapour pressure within the ampoule. A typical melt cycle is shown in Figure 13. A high vapour pressure will result in an explosion of the ampoule and increases with the volatility of the components of the glass, S > Se > Te. For the more volatile components such as sulphur, it was found that the ampoule wall thickness should be approximately 3mm and typically greater than 1.5 mm in general. Thick wall ampoules are expensive when compared to their thinner wall

counterpart. The ampoules are destroyed during the process of retrieving the glass and therefore increase the cost of manufacturing glass via this method, especially sulphide glass which requires an ampoule with 3mm wall thickness.

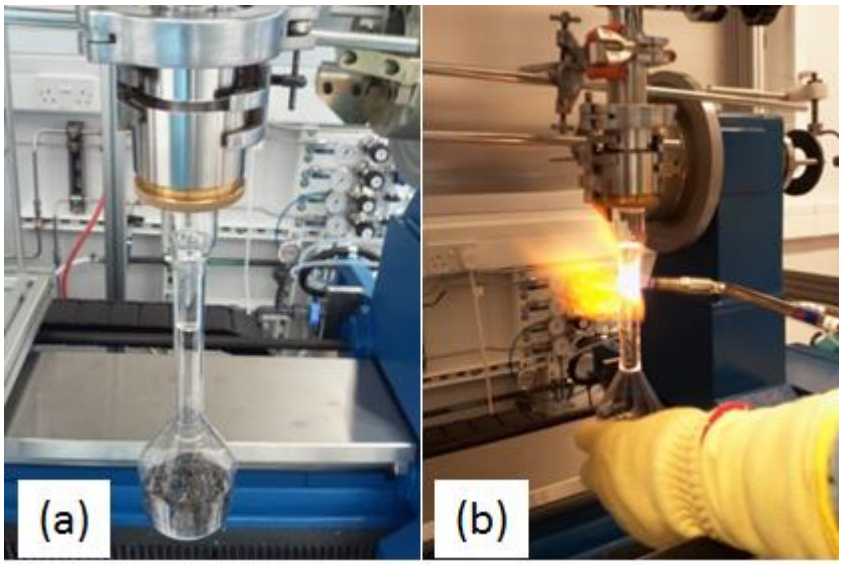

Figure 12 Sealed ampoule (a) ampoule with material within and compression fitting for vacuum to glassware connection (b) sealing using oxy-hydrogen torch

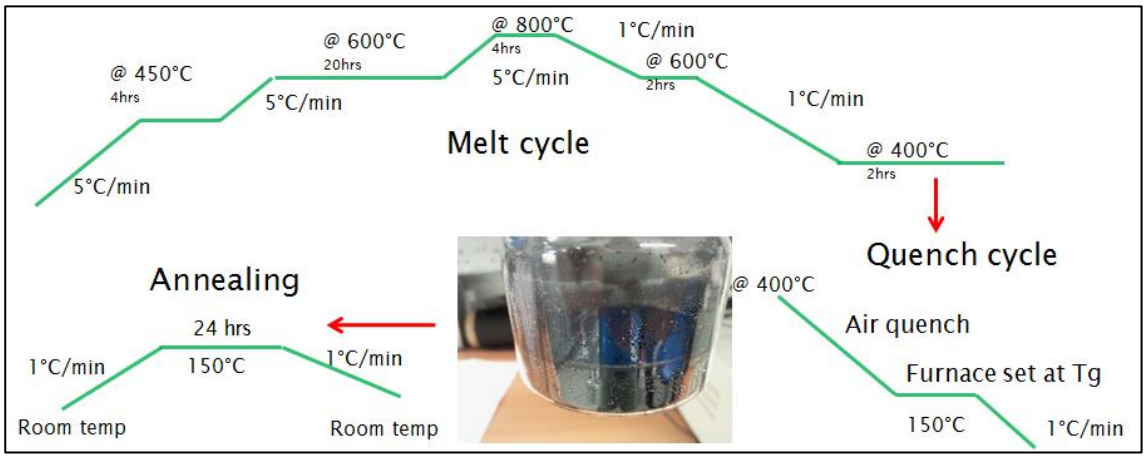

Figure 13 Melt, quench and annealing cycle for $As_2(Se_{80}Te_{20})_3$

During the thermal cycle, the ampoule can be rocked and/or rotated which is believed to improve the homogeneity of the melt, this was not implemented as part of the initial work but will be done as future work. However in [34] the authors experimentally determined results allude to homogeneity being more related to the length of time spent at the melt temperature than rocking the

ampoule. In [34], it can take up to 196 hours to achieve a homogenous melt which can add significant energy costs to the final price of a product. Therefore it is imperative to find a balance between melt duration, rocking and rolling and melt homogeneity. Ampoules were not rock and rolled but left for longer duration for sealed ampoule glasses made within this thesis

At the end of the thermal cycle the ampoule is quenched to form a glass. This involves rapidly cooling the ampoule to a temperature below the glass transition temperature and depends on the stability of the glassware to this thermal shock. A faster quench improves the chances of freezing the random structure of the glass and prevent crystallization. Critical Cooling Rate, CCR studies can be done to determine how fast to quench to avoid/minimize crystallization if it occurs in the glass system [35]. Typically, faster cooling through the crystallization temperature is achieved through the use of gas cooling, cold water or liquid nitrogen. As a melt becomes larger, uniform cooling is increasingly difficult and results in stress related cracks appearing. After cooling, the ampoule is then annealed at or near a temperature close to the glass transition temperature, T_g. Care must be taken as the coefficient of thermal expansion of Silica and the Chalcogenide differ significantly which can lead to cracking of the ampoule and exposure to the environment outside the ampoule. Having the ampoule enclosed by a high purity shield gas was the simplest choice utilized.

The final step is the removal of the glass from the sealed ampoule. There are two methods considered for removing the glass from the sealed vessel. The first method is to chemically etch the ampoule made out of silica by using HF. HF etching of the ampoule has to be done on a wet bench and the etch time needs to be precisely determined unless the glass within is chemically resistive to HF. Since it is not done inside the glovebox the glass is exposed to an uncontrolled environment. The second method is to mechanically break the ampoule within the controlled glovebox environment which should maintain purity. Some researchers in the glass community believe that upon breaking the ampoule, silica glass particles can be impinged into the chalcogenide glass. The mechanical breaking of the ampoule was the chosen method for this work and care was taken while breaking the ampoule. Since high purity ampoules can cost hundreds of pounds depending on size, shape and wall thickness, destruction of the ampoule is not cost effective but necessary.

Figure 14 shows the setup designed for ampoule sealing as well as for future distillation or reactive atmosphere experiments. The design is made up of high vacuum fittings provided by Scanwel. Purified gasses can be connected through the inlet and at the moment two gasses can be connected, Ar and H_2. High purity gasses are used to aid in transport of vapour species in distillation techniques or remove impurities as is the case of using H_2 to reduce oxide impurities. Gas purification is detailed in Chapter 4. A turbo molecular pump and cold trap is used to achieve high vacuum however the vacuum piping and sensor placement was not optimized in this work to achieve the highest vacuum possible. Future work will involve finding ways to incorporate or attain as close to ultra-high vacuum (greater than 10^{-10} mbar, [36]) in the sealed ampoule process to further reduce impurities in the glass synthesis process. At this level of vacuum, only hydrogen gas atoms will be present [36], other impurities such as H_2O and CO would be minimized.

The purpose of distillation and reactive gasses is to overcome the unreliability in purity of commercially available raw materials. The initial setup completely built in-house allows for experimentation on purification steps which is discussed in the following sections. This will help define the future installations and experimental work.

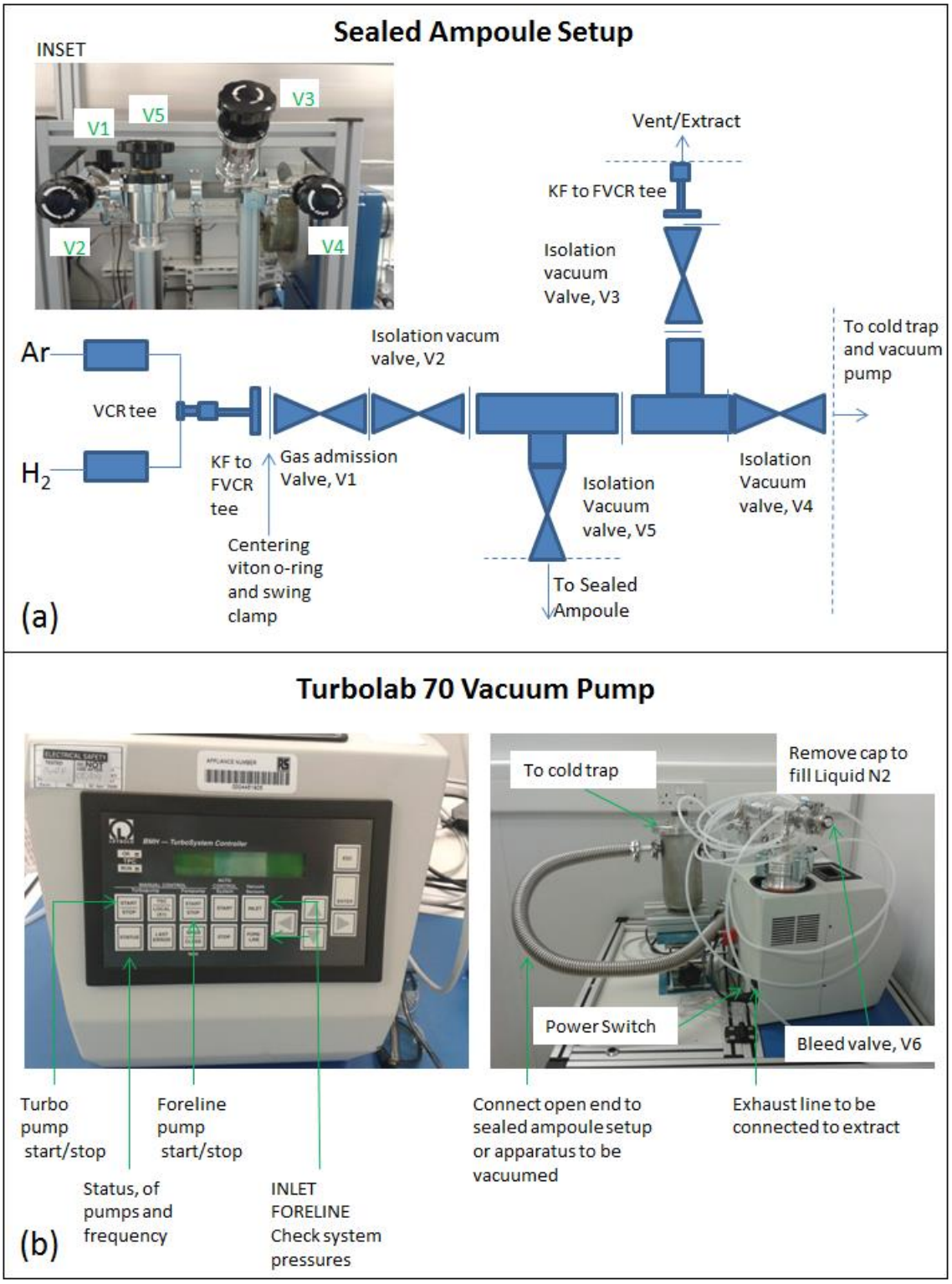

Figure 14 New dedicated sealed ampoule setup developed as part of this work (a) vacuum piping and valves which allow connection of an ampoule to high vacuum as well as allow purging of the ampoule with Ar and H2 gas, Inset shows an actual picture of the vacuum assembly (b) The turbo molecular pump used to attain high vacuum.

3.1.2 Improving sealed ampoule by vacuum distillation, reactive gasses, getters and CVD.

As discussed in Chapter 2, extrinsic scattering and absorption from impurities are a major concern for losses in chalcogenides. The quality control on the purity of the raw materials supplied by commercial suppliers is unreliable and remains a major challenge to researchers trying to show the low loss potential of chalcogenides. The investment into achieving the best raw material quality is usually determined by the importance of the commercial market of the prevailing application for that raw material. For example silica and germanium have benefited largely from the semiconductor and communication industry markets and have resulted in consistent higher purity products being readily available at competitive pricing. Chalcogenides have not received nearly as much attention and reliable quality of supply remains a major obstacle. In addition, commercial supplier's websites state purity greater than 5N purity, however, they do not supply relevant information such as to which impurity element(s) this value pertains to. The price may be used by consumers to infer the purity but can only be certified through impurity analysis. Requests for impurity analysis data increases the cost and is often overlooked by the consumer. To undertake this impurity analysis as a consumer is costly and can be in excess of £400 per sample. The price also depends on the range of impurities specified. Chalcogenide researchers therefore have to undertake impurity analysis cost for themselves in addition to developing purification facilities in-house.

Vacuum distillation, getters, reactive gasses and zone refining are some of the techniques used to further purify raw materials. These methods are usually combined to obtain the highest purity across the periodic table elements. In [37], the purification of the chalcogens, S, Se and Te are discussed and procedures to improve the purity is outlined. Table 6, lists some of the methods for purification of the more common chalcogenide forming materials.

Distillation and zone refining method depends on the thermal properties of the materials and the impurities to be removed. Thermal convection and/or high purity gasses may be used to transport the distilled vapour of the volatile components leaving the less volatile impurities behind. In zone refining, the impurities migrate into the traversing liquefied region gained by heating small

sections of the material to be purified. In the case where gases are used, getter technology can be used for purification of gasses. Getters used in this application of gas purification are usually thin films (example titanium oxide, TiO_2) of materials which have a high affinity to the impurity to be removed from the gas. The thin films are usually deposited in a porous material to increase surface area for reaction. Another method of using getter technology is by adding the getter in element form directly to the ampoule. When added to the ampoule they react with the unwanted impurity forming a less volatile material than the pure chalcogenide elements. The chalcogenide component can then be separated via the distillation method. The most used getters are Mg and Al to remove oxide impurities. It is also possible to use halides, especially chalco-halide powders to remove hydrogen and carbon impurities as detailed in [38].

Material	Purification Method
Ge	Zone melting, chemical etching, reactive gas such as H_2
As	Sublimation in Ar stream or vacuum
S	Distillation in Vacuum or reactive gasses such as S_2Cl_2 stream
Se	Distillation in Vacuum or reactive gasses such as Se_2Cl_2 stream
Te	Zone melting, distillation in vacuum
Chalcogenide glass	Distillation, Zone melting, reactive gasses

Table 6 Various purification methods for chalcogenide materials and glasses [5]

Reactive gases can be combined with glass making techniques to pre/post treat the glass to reduce impurities or react to form the final glass material as in the case of RAP or CVD which will be explored in Chapter 4 and Chapter 5 respectively. A system where RAP is combined with sealed ampoule is shown in [5]. As discussed, getter technologies incorporated into purifiers are used to react and remove the impurities from the gas supply hence increasing the purity of the gas supply and the glass. Combining getter technology as used in purifiers and flowing distilled vapour through is an approach to purification which has not been explored. The specification of conventional purifiers is

discussed in Chapter 4. In Chapter 4 a RAP system used to synthesize the raw materials from raw elements, melt and quench to form bulk glasses while continuously supplying and monitoring high purity process gasses is the goal. The benefit of gas purification technology is therefore discussed further in Chapter 4.

Having control of manufacturing raw materials is beneficial due to the volatile climate of commercial material suppliers. Having such systems allows for making significant improvement to processes and procedures in a cost effective and informed manner. However dependency on supply of raw elements cannot be entirely removed and it is for this reason that the techniques discussed above must be economically incorporated into design of in-house manufacturing equipment. In the following section an emerging method of using microwaves in synthesis of chalcogenides is presented.

3.1.3 Adding microwaves to synthesis

The first reference to using microwave irradiation of chalcogenides was by a group in Oxford in 1992 [39]. In [39], chalcogenides S, Se or Te (5g) were mixed with metal powders Cr, Mn, Sn, Fe and Ta (1-5g) (<100 mesh) and sealed in 10cm outer diameter silica tubes under vacuum. The temperatures of the sample rose rapidly to between 800 and 1000 ˚C with the reactions completing in less than ten minutes. In 2005, a group in India used this method to rapidly synthesize the Se-Te-Sb glass system using a Domestic Microwave Oven, DMO [40].In [40], it took two mins to melt their glass systems which would usually take over 24hrs via conventional melting methods such as resistive furnaces. In 2010, a group in Nottingham published results for microwave synthesis of As_2Se_3 and As_2S_3 chalcogenide glass [14] and proposed that the DMO offered the advantage that it was cheap compared to a resistive furnace and provided energy savings as the time for the glass melt took 35 minutes as opposed to 32 hours using a resistive furnace.

Microwave heating involves two main heating mechanisms. One mechanism depends on the resistivity of the material to be heated. If a material has a suitable resistivity, it will couple with the microwave electromagnetic field producing an alternating electric current leading to ohmic heating. The second

mechanism is dielectric heating whereby the electromagnetic field rotates the dipole moments of the material. As the dipoles of the polar molecules constantly seek to align to the oscillating field, they cause the material to heat up. The authors in [14] conclude that ohmic heating was the main heat source for melting the As_2Se_3 glass due to the element arsenic being a metalloid with sufficient resistivity, orders of magnitude greater than selenium. Figure 15 shows the As_2Se_3 glass produced by this method as well as the difference in the FTIR spectroscopy result for DMO vs conventional furnace. The reduction in the OH peak is quite remarkable and worth incorporation into glass synthesis procedures.

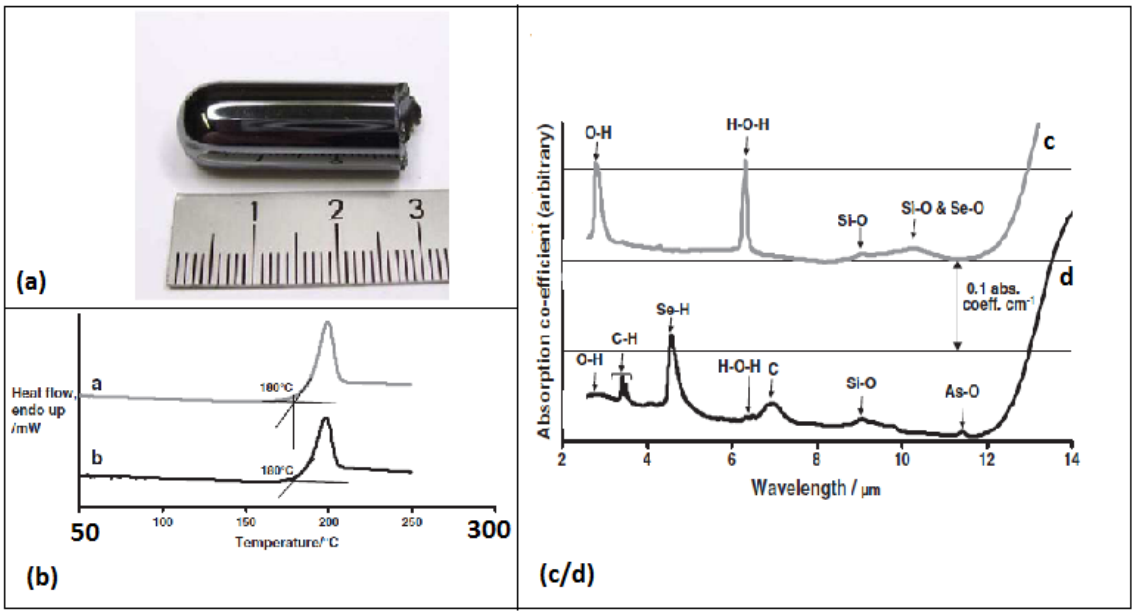

Figure 15 Summary of domestic microwave results. (a) Photograph of the as-annealed As–Se (As40.1Se59.9) glass rod product prepared in the DMO. (b) Top, Differential Scanning Calorimetry (DSC) of the conventionally prepared As–Se (As41.1Se58.9,) glass. (b) Bottom, DSC of the as-annealed As–Se (As40.1Se59.9) product prepared in the DMO. (c) FTIR spectroscopy of the conventionally prepared As–Se (As41.1Se58.9) glass. (d) FTIR spectroscopy of the as annealed As–Se (As40.1Se59.9) product prepared in the DMO. [14] (From Prasad, N., et al., J. of Non-Cryst. Solids, 356(41): p. 2134-2145, 2010. With Permission)

The other composition attempted in [14] was As_2S_3 glass but mixing of the components proved difficult due to the volatility of sulphur. Rapid heating of the arsenic caused the sulphur to become volatile and deposit on cold walls of

the ampoule which prevented mixing. The authors suggested that a mechanism to rock the ampoule would overcome the mixing problem. In [14], microwave assisted melting with variation in the stoichiometry of the chalcogenide glass was not explored. This would provide key information on the limits of using a microwave for producing bulk glass. The authors in [14] identified bulk production as a limitation but provided no possible solutions.

The main advantages of microwave irradiation are the time processing for making a glass, more energy efficient, a cheap heating source and reduction in OH impurities. However, microwave irradiation is not limited to glass making and has a host of other benefits and uses in glass processing as identified in [41]. For example the microwave irradiation has been used and has processing benefits and applications as follows:

1) Microwaves heat from the inside outwards which may be used to minimize undesirable decompositions, oxidation/reduction, loss of volatile materials and other kinetically slow processes that can occur during conventional melting.

2) Rapid heating and capability to heat hot areas of the glass selectively while leaving the cooler areas unaffected is possible. This is particularly helpful in heating chalcogenides that contain sulphur because only the sulphur in contact with the metallic components of the glass making network will be heated and react while the unreacted sulphur will migrate to the cooler walls of the silica ampoule. This is why a silica ampoule can be heated much faster in a microwave than a conventional furnace as the vapour pressure is not allowed to build up.

3) Glass preforms made via the deposition of porous glass on glass rods can be exposed to microwaves and moisture and bubbles are thermally removed [41].

4) Film deposition on glass surfaces and doping of a silica substrate with silver [42].

5) Convert an amorphous glass into a polycrystalline glass-ceramic as done in [43].

A number of attempts was made to replicate microwave synthesis of chalcogenides but has been unsuccessful for the most part. The most successful attempt is shown in Figure 16. Attempts to scale up the mass led to explosion of ampoule and damage to the DMO. It is expected that the microwave would selectively heat the metallic component and not the ampoule and less resistive materials which causes reactions and any volatile components would by thermophoresis, deposit on the cold walls of the ampoule therefore minimizing their contribution to vapour pressure in the ampoule. However, with rapid heating, it was noted that conduction of the heat resulted in the ampoule being very hot.

Also the designs of DMO's are to heat food at significantly lower temperature and as such are inherently cooled so as to protect the chamber from overheating. In some microwave experiments, sufficient temperature could not be achieved. It was also noticed that in [32], that the ampoule was placed in sand and it is believed that the sand acted as an insulating material to trap the heat and allow sufficient temperature for reaction to be achieved however this was not explicitly stated by the authors. The sand can also act to contain explosion of the ampoule. Another restriction is that microwave frequencies are restricted to fixed bands as they can severely compromise electronic devices in its vicinity. If this were not the case then microwave applicator could be used to selectively heat a material through dielectric heating and not only ohmic heating.

Figure 16 Result of a microwave synthesis of As_2Se_3 attempt during this work

For use in distillation experiments, the DMO needs to be modified by making a hole to insert the silica glassware. In this case, safety must be considered for

escape of microwave radiation and is usually achieved by designing a water circuit around the hole to absorb the escaping radiation [44].

3.2 Levitation glass melting

Levitation glass melting has been used in the making of glasses such as fluoride [45] and aluminate glasses [46-48] . Levitation can be accomplished by various methods such as acoustic, aero (use of various gasses), electrostatic, magnetic and optical or a combination of these methods. The choice of levitation methods depend on properties such as size, shape, density, electrical and magnetic properties of the sample. The levitated sample is heated using a laser, resistive furnace or induction coil furnace.

The main benefit of levitation methods is that they are containerless which means that there is no reaction with the crucible walls so that higher melt temperatures are easily achieved. In addition to no container to react with the glass material, the ability to control the environment of the levitator makes levitation methods worth investigating for high purity glass manufacture. Levitation methods allow for studying glass formation in an environment where interaction of crucible walls can induce crystallization or restrict quench rate. For example, faster quench rates as compared to sealed ampoule can be achieved when using laser heating. By turning of the laser the fastest quench rate is achieved however the laser can be modulated to vary the ramp down rate. Another benefit is that the melt process can be done rapidly within one hour including sample and equipment preparation which allows for rapid glass formation studies to be conducted. This is particularly useful when determining glass forming regions with knowledge of the ramp down rate through the use of a pyrometer and laser heating.

Levitation methods have not been used to successfully synthesize chalcogenides from levitated elemental powders to the best of the author's knowledge. This may be due to the variability in volatility of chalcogenide elements which require a sealed ampoule. The sample for levitation is usually created from cold/hot pressing powders which forms a compound of the glass elements that have different thermal properties from the single elements. Other methods proposed are liquid slurry (sol-gel), mechanical dry mixing, laser heating on an appropriately wettable substrate and CVD [49, 50]. Care

must be taken in sample preparation to minimize impurities otherwise it compromises the benefits of containerless melting. Also the size of sample made to date are small and has been limited to less than 5mm.

The first reference to levitation glass melting of chalcogenides was from NASA in [49-51] with proposed benefits to eliminate:

1) optical homogeneities caused by thermal currents and density fluctuations in the 1-g earth environment,

2) contamination from the earth melting crucible by oxygen and other elements deleterious to IR transmission, and

3) heterogeneous nucleation at the earth melting crucible-glass interface.

During this research program in the 1970's, the authors were able to successfully levitate and the $Ge_{28}Sb_{12}Se_{60}$ compositions using acoustic levitation with resistive heating. Resistive heating added design limitations such as choice of materials used in the levitator as well as inducing thermal convection that caused instability in the levitated sample. This Thesis aims at exploring the benefits and limitations of levitation to GLS.

In this thesis GLS and GLSO samples have been successfully levitated using the aero method for the first time. The levitated sample size is limited to a range of diameter between 1.2 - 2mm by the size of the nozzle used to supply the levitation gas. The samples are levitated at a temperature of 975 ˚C using a CO_2 laser. The levitator is an aero levitator and is shown in Figure 17. Beyond this temperature which is measured by a pyrometer, the samples outgas rapidly and levitation cannot be maintained as observed through the viewing port.

The processing steps for making a sample and melting as developed are:

Fusing Steps:

1) Crush previously made glass into suitable sizes for levitation
2) Place glass or powder or combination on a Cu hearth and position in chamber, align laser and pyrometer
3) Pump down chamber using a vacuum pump to 10^{-3} torr
4) Flood with Ar Gas supplied from 7N purity gas cylinders

5) Increase laser power until glass is visibly spherical or powder coalesce and cut the power instantaneously. Repeat as necessary.

Melting Steps:

6) Remove spherical glass piece and Cu hearth and place sample in nozzle within the chamber repeating step 3 and 4.
7) Introduce levitation gas and levitate sample.
8) Balance levitated sample while heating sample

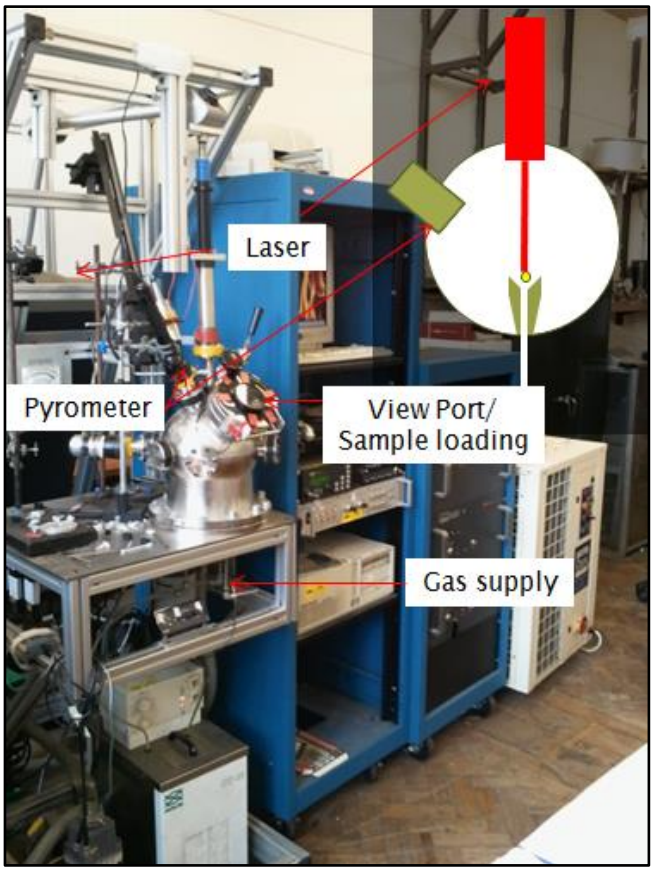

Figure 17 Picture of aero levitator at the University of Bristol, inset is a schematic depicting the inside of the chamber

One experiment explored is the coating of spheres for making core clad fibre. In [52] the authors show a process for making unclad fibre using an acoustic levitator. Once the sample is successfully levitated, a pin is inserted into the melted glass sphere and a fibre drawn by retracting the pin away from the melt. The aero levitator setup in Figure 17 could not be modified to accommodate the fibre drawing capability. A core clad structure has not been

attempted to the author's knowledge and the results of this experiment are detailed next.

Figure 18 shows the results of making a core clad sphere. In Figure 18a, the starting yittria alumina sphere and GLS shard is shown. Figure 18b, shows the core clad structure after the fusing process using the CO_2 laser. Two coated spheres were made and one was levitated while the other was not. Figure 18c and Figure 18d shows SEM and Optical microscope images of the sphere after levitation and quenching rapidly by instantaneously turning off the laser. Figure 18e shows Energy Dispersive X-Rays, EDX of the unlevitated coated Yittria Alumina (AY) sphere showing that the GLS layer was too thick for the EDX beam to penetrate. This is verified by the absence of the Al and Y elements in the EDX spectra in Figure 18e. Figure 18f shows EDX of the levitated sphere showing that the EDX beam was able to penetrate the thickness of the GLS coating and hence the Al and Y peaks appearing in the EDX spectra.

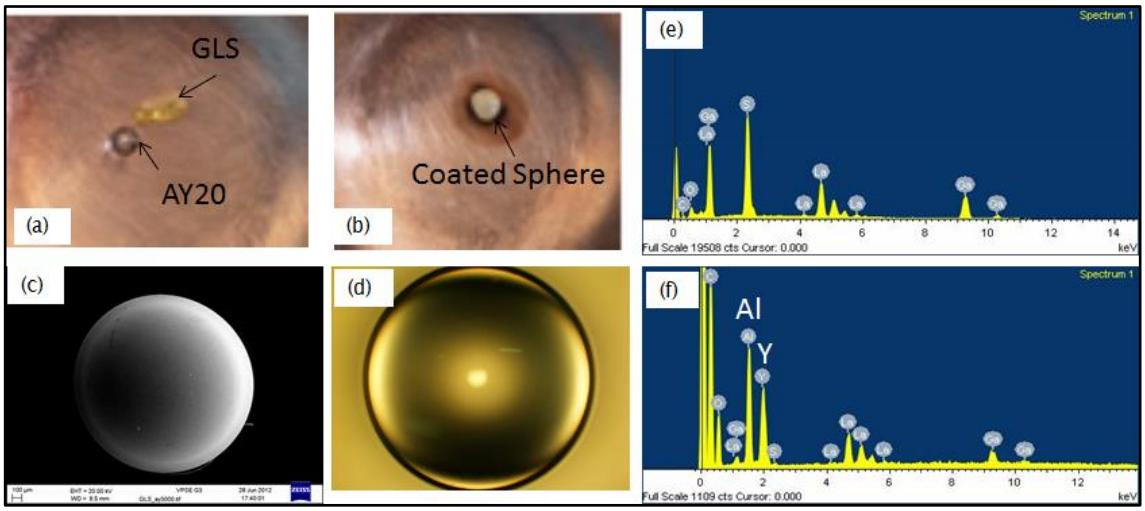

Figure 18 Experimental results for coating spheres (a) the AY20 sphere and GLS shard (b) after fusing in aero-levitator chamber but before levitation melting (c) SEM image of coated sphere after levitation melting (d) Optical microscope image after levitation melting, (e) and (f) EDX spectra of coated sphere before and after aero levitation melting respectively.

Figure 19 shows the temperature vs time measured by the pyrometer for quenching of the coated sphere. A recalescense peak in Figure 19 indicates qualitatively that crystallization occurred. Rescalescence occurs when there is a change in entropy of the system when cooled, in this case an exothermic

reaction such as crystallization of the glass occurs and the energy is emitted as infrared radiation which is detected by the pyrometer. A supercooling study using the recalescense phenomena for AY has been done in [48]. The levitation method has not been used for studying glass forming region of chalcogenides to the best of the author's knowledge and is useful for determining CCR of these materials. The supercooling work could not be carried out for chalcogenides using the equipment in Figure 17 because of the pyrometer having a low limit of 800 ˚C. GLS crystallization occurs below 800˚C and hence a pyrometer with a lower working range is required. This would allow the study of the crystallization spike versus different cooling rates. The absence of a spike would imply that minimal or no detectable crystallization has occurred. This provides CCR studies for materials at higher temperatures that would not otherwise be possible with a Differential Scanning Caliometry, DSC. The laser can be shut off instantly resulting in faster cooling that cannot be achieved with a DSC due to the sample being resistively heated in a DSC sample holder.

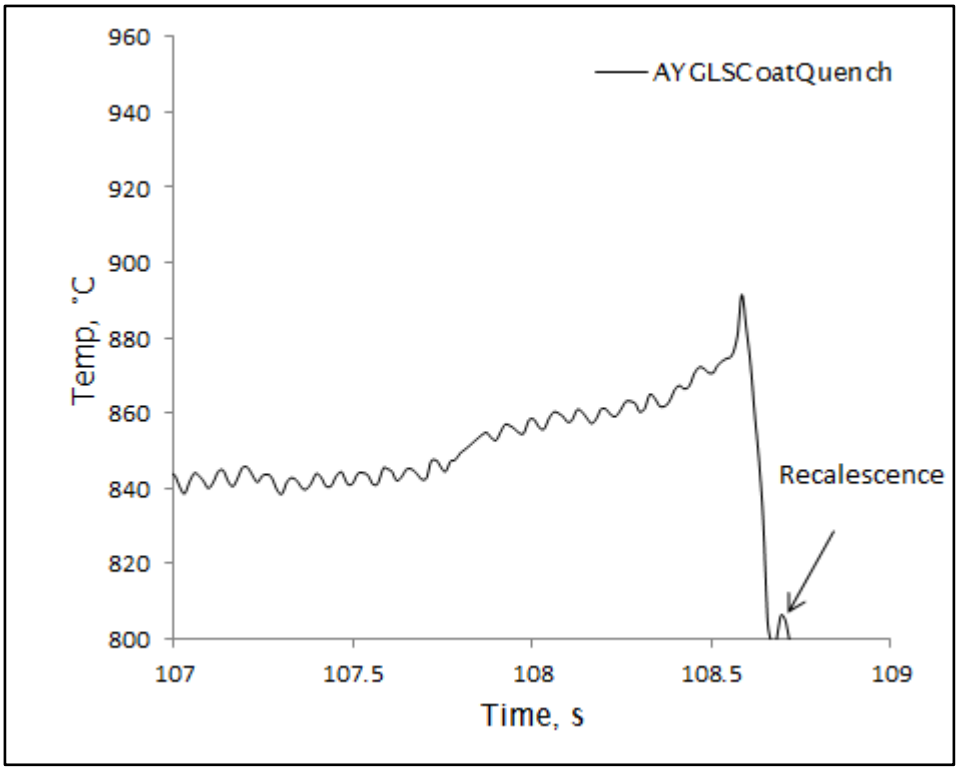

Figure 19 Recalescense effect seen in AY coated GLS sphere levitated and quenched

In Figure 20 experiments were conducted where GLS was doped with Nd. The Nd powder was first made into a small sphere using laser irradiation after

which it was weighed and fused with a weighed GLS sphere. Figure 20a shows the fused sphere while Figure 20b shows an image taken from an optical microscope and Figure 20c shows EDX data confirming the Nd doping. This is a fast method of doping chalcogenides and successful doping of up to 20 mol% was achieved.

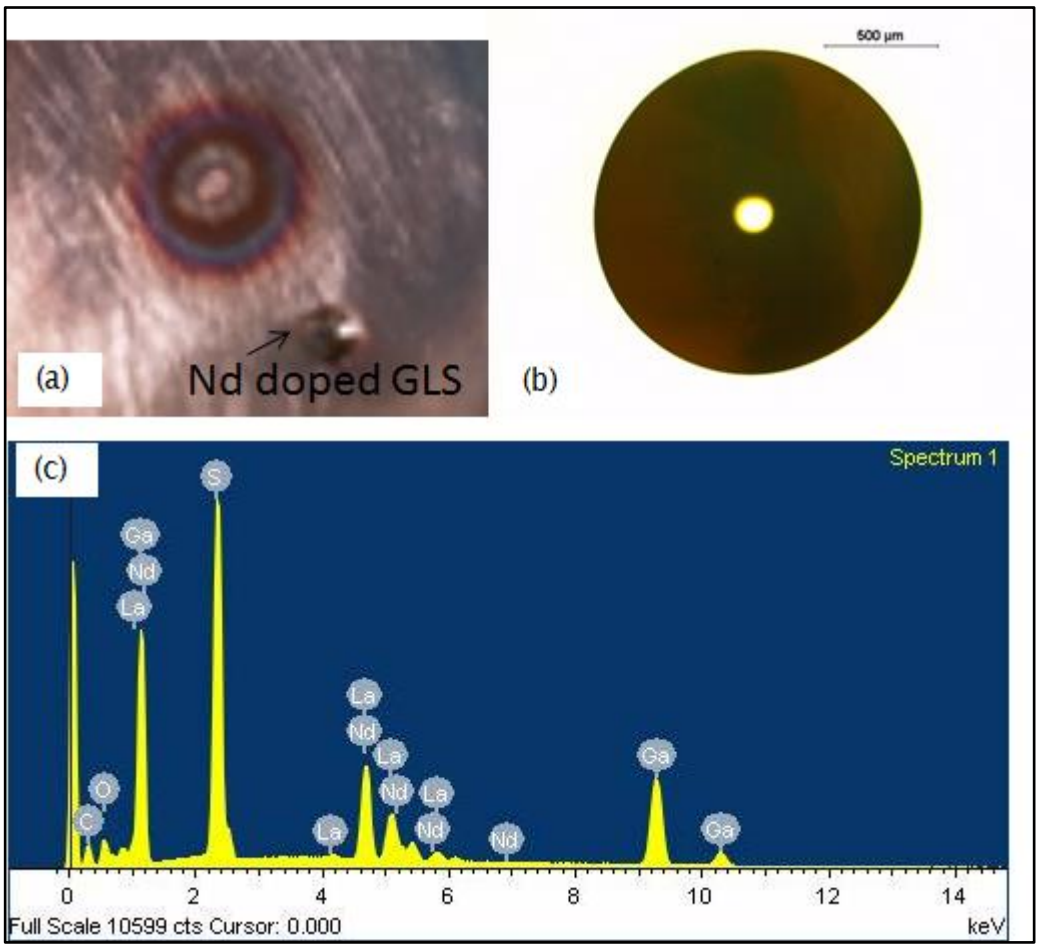

Figure 20 Doping GLS spheres with neodymium (a) doped sphere (b) optical microscope image of doped sphere (c) EDX showing the main element – Ga, La, S and Nd.

The fusing process and wetting principle lead to the development of using smaller particles to create smaller spheres on a much smaller scale for incorporating sub-micron size spheres into devices. The schematic and results shown in Figure 21 summarizes the achievements made. Figure 21a shows a small schematic of the initial setup in which a laser is used to heat the particle under a microscope. In Figure 21b finely crushed and sieved particles are placed on a Cu plate and heated with a laser which resulted in small spheres being formed. In Figure 21b, a Focus Ion Beam, FIB is used to slice a section off

the sphere showing that the sphere was not hollow. In Figure 21d, it was seen that even smaller spheres were being made while Figure 21e shows an attempt to place a sphere close to a waveguide. It may also be possible to deposit via lithography small rectangular patterns of the chalcogenide next to a waveguide or above a buried waveguide and then convert them into a sphere by laser irradiation to make resonating photonic circuits building on the ideas generated in [53].

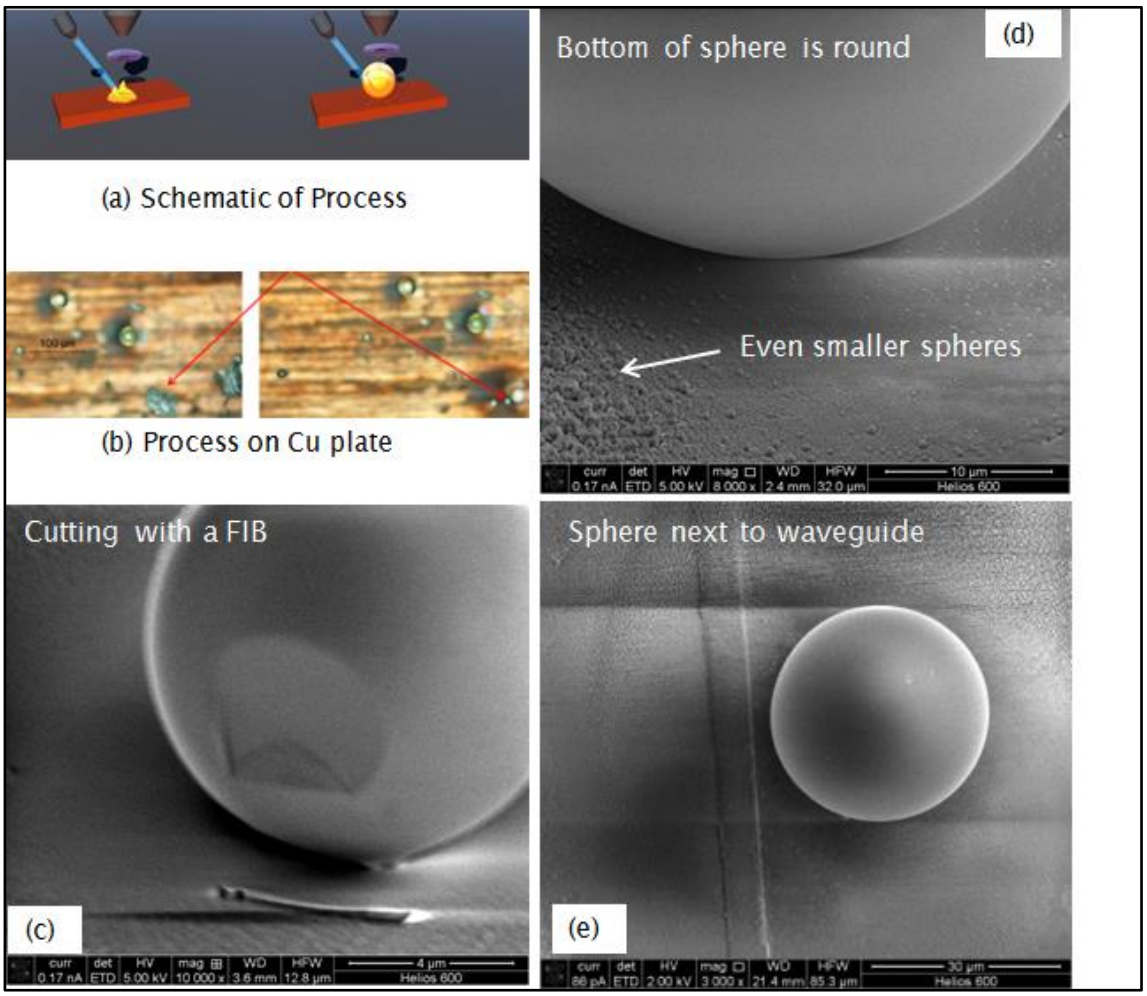

Figure 21 Creating small spheres by laser irradiation (a) Schematic of process (b) experiments result showing the sphere created by laser irradiation (c) cutting sphere with Focus Ion Beam to show that sphere is not hollow (d) Laser irradiation creates even smaller spheres (e) experimental result of manufacturing a sphere next to a waveguide which a possible method to manufacture photonic circuits.

While it may still not be immediately possible to make chalcogenides from raw components via levitation methods, it is still possible to accomplish the following:

1) Trying to draw a fibre from GLS from the levitated melt.
2) CVD coating of spheres.
3) Deforming spheres using aero acoustic levitation.
4) Super cooling of glass melts and observing crystallization at different cooling rates through the process of recalescense.

While the levitation method may not be fully explored to bulk glass synthesis in this work, other benefits of this method are being explored that may enhance the ORC facilities.

3.3 Conclusions

Basic sealed ampoule facilities and procedures have been developed giving the ability to make a wide range of chalcogenide glass composition. The setup has been designed to accommodate high purity gasses to aid in distillation and reactive atmosphere processing in future. The next step is to design and optimize a furnace melt and quench system. At the moment melt facilities lack the ability for rocking and rotating which aids in melt homogeneity. At the moment melt duration is increased which increases energy cost but it is believed to provide good melt homogeneity. However distillation followed by long melt duration via a batch process would not be the ideal commercial solution.

Microwave synthesis has been attempted and successful on a small scale. Attempt to scale and make larger samples was not successful. Sufficiently sized samples were not made for optical studies and the claims of OH removal as done in [14] could not be verified. In future it may be useful for combining microwaves in resistive furnaces which are now commercially available. This may allow for decreasing melt times with the benefits of moisture removal. However the need for high purity powder that increases the surface area which can be contaminated may not be ideal.

Levitation glass melting is limited but may prove useful in analysis by making small samples rapidly. Faster heating and quenching using laser irradiation in a containerless levitated environment can help understand glass formation and crystallization kinetics. Laser irradiation in device formation has been explored briefly and shows some promise. An aero-acoustic levitator has been purchased and is being modified for levitation of glass samples in the future at the ORC.

The basic infrastructure and knowledge base has been developed for sealed ampoule, microwave and levitation methods as part of this thesis. In the next Chapters, RAP and CVD are explored of which facilities existed in the past but were severely compromised due to a fire in 2005.

Chapter 4: Reactive Atmosphere Processing

In Chapter 2 an understanding of the infrared transmission window was developed and in Chapter 3 the methods for making mid infrared materials and the sources of impurities was reviewed. The ORC mainly uses reactive atmosphere systems to manufacture chalcogenides, mainly GLS glass and therefore has considerable infrastructure and research development. RAP has the ability to remove impurities dynamically by using reactive gasses and controlling the temperature and pressure of the reactor chamber. RAP can be combined with other methods as sealed ampoule however at the ORC, GLS is developed without having to seal the reactor tube. While there is some material loss, the ability to form glass in this open system allows reuse of the reactor tube and control the build-up of pressure which are the main deterrents of sealed ampoules.

This chapter focuses on development of reactive atmosphere systems for synthesis of infrared transmitting glasses at the ORC which have the capability to convert raw materials into oxide and sulphide glasses through the use of oxygen and hydrogen sulphide gasses. Other reactive gasses such as hydrogen and chlorine have been installed to further assist in removal of impurities or tailor optical properties. Moreover, high purity argon gas is also included for inert atmosphere glass melts. The system automation, process monitoring and safety monitoring is achieved with NI hardware integrated with Labview software.

4.1 Introduction to RAP at the ORC

In the following sections, RAP facilities developed as part of this work will be reviewed and evaluated. Prior to 2005 the ORC developed horizontal furnace systems to make GLS raw materials and glass. After 2005, another system was developed based on a vertical furnace installation and was the only glass making system existing at the start of this thesis work. As part of this work a new horizontal furnace was design optimized and the vertical furnace system was improved. Next the RAP system design and implementation is presented and the results from glass synthesis are presented and discussed.

4.1.1 Horizontal RAP

Prior to 2005, horizontal furnace systems were developed at the ORC which used H_2S to convert gallium to gallium sulphide (Ga_xS_{1-x}) and lanthanum fluoride to lanthanum sulphide (La_xS_{1-x}). Using the produced Ga_xS_{1-x} and La_xS_{1-x}, or commercially purchased powders, the components were batched, melted and quenched to form GLS glass. The systems were used to make semi cylindrical disks of GLS which were then cut and polished by Crystran Ltd. into 100mm long rods with 10mm outer diameters. Also, smaller vitreous carbon crucibles were used to make disks that were cut, polished and extruded into a core-clad rod as detailed in [25]. These systems were developed and optimized over a period of 20 years and details, functionality and experiments can be found in [25, 30, 54].

In [25, 54] major emphasis is placed on gas purification systems, impurity analysis data, and raw material purification and conversion. The two gasses used were Ar for processing and H_2S for conversion. Detailed drawings showing the purification system and improvements from 2000 to 2005 is included in [25, 54]. However no measurement of the moisture levels in the gases over this period was included in [25, 54] and is therefore identified as an area for further developed which is addressed in this work where the aim is to provide online moisture monitoring capability so that a certain minimum gas quality is maintained from melt to melt. The raw materials used in [25, 54] were 7N purity Ga, 5N purity LaCl and 3-4N purity LaF. In [25], heat treatment studies along with GDMS was used to conclude that LaF is a better starting material to convert to La_xS_y. Another important finding is the need for completely enclosing the melt with vitreous carbon crucibles because the LaF and LaCl attacked the Si liner and incorporate large amounts of Si in the melt which is detrimental to the optical properties in the MIR. In this thesis only the conversion of Ga to Ga_xS_y has been attempted. The focus of this thesis has mainly been to design and optimize a new RAP system for increased capability over past systems. Focus is placed on improving design, detailing procedure and improving repeatability of GLS melts using commercial raw materials initially with making raw materials in-house as the ultimate goal. In the next section the vertical and horizontal RAP work done in this thesis is detailed.

4.1.2 Vertical atmosphere system for manufacturing GLS

After 2005 and before the start of this work, another system was developed by BK automation, which was developed to process GLS using a vertically mounted furnace as shown in Figure 22 and is mainly used for making large disks, sputtering targets and remelting glass cullets.

The system comprises of:

1) A silica tube reduced at the top with ground edges to make a glass to glass seal. The silica tube is pushed into a stainless steel flange at the bottom with o-ring seals.
2) A lenton CSC 12/140/450 split tube furnace rated at 1200°C. The system comes with standard Eurotherm 3216 and 2032 temperature controllers which provide temperature control and over temperature protection respectively. The Lenton system is connected to the input of a Mitsubishi FX1N-40MR-DS Programmable Logic Controller (PLC) which controls and monitors the melt procedure. In addition, the PLC monitors failure of cooling water, door enclosure failure, argon loss and other non Eurotherm temperature points. Procedure and setup was achieved through an EDesigner E100 Human Machine Interface (HMI). The HMI allowed the selection of a manual or automatic mode of operation.
3) Two motors where motor1 is used to move the furnace and cooling coil up or down and motor2 is used to move the crucible stand up or down. When motor2 is moved downwards to allow loading of the sample, the seal system at the bottom of the furnace is broken leading to a break in the controlled atmosphere.
4) An alumina tube with a silica disk which is the platform for placing the sample to be melted.
5) A dual bubbler system for which the main function is to control the back pressure in the Silica tube while melting. Another purpose of the bubbler is to protect the atmosphere in the case of argon supply failure which can cause a flow reversal.

A brief description of the melt procedure is as follows:

1) The raw material of Ga_2S_3 and La_2S_3 in powder form is batched and weighed and then mixed into a PFA bottle and subsequently rolled

outside the glovebox (10K cleanroom environment) to aid in mixing the powders which aid in homogenizing the melt.

2) The mixed contents are then transferred into a vitreous carbon crucible within a nitrogen purged glovebox.
3) The crucible is then removed from the glovebox and placed into the furnace chamber by a motor controlled stand.
4) In the upward position the chamber is sealed but in the load position, the crucible stand is lowered and the seal broken.
5) The crucible and contents is heated to the melt temperature, typically 1150 ˚C under flowing argon and depends on the manual or automatic cycle chosen.
6) When the melt temperature is achieved, a soak timer is used to set the duration, typically 24hours after which the PLC applies the quench cycle (cooled rapidly to room temperature).

The same system can then be used to anneal the glass with slight change to the program parameters such as ramp rate and annealing temperature instead of melt temperature.

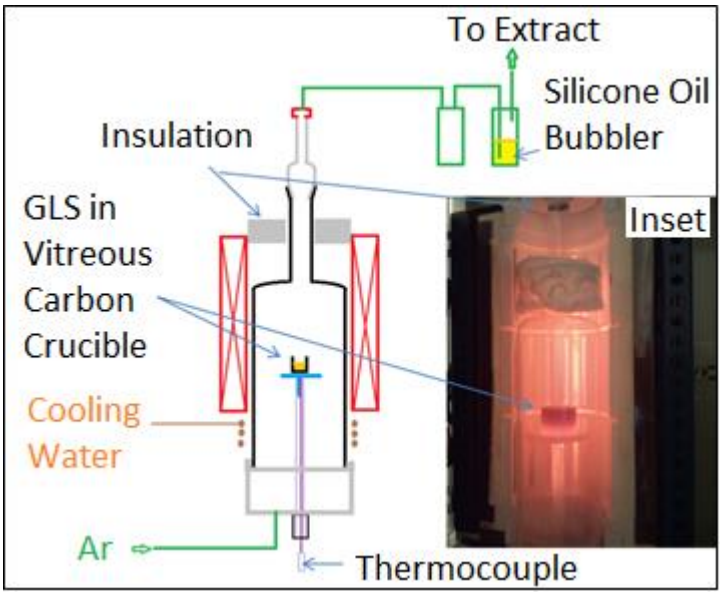

Figure 22 Vertical Furnace schematic, Inset showing an actual glass melt in progress with furnace open.

At the start of this work, the vertical furnace system is used to provide a baseline of the existing glass making facilities. On review, the vertical furnace system did not meet the standards of a high purity installation because:

1) The argon gas supply installation was not a high purity installation as it used non high purity rotameters with NPT fittings. Also a PTFE tube was used to deliver the gas to the furnace flange and was not protected by a high purity shielding gas. Moisture measurement was installed using a dew point meter which recorded readings below -76C.

2) Powder transfer and loading meant that the powder was exposed to the 10K cleanroom environment which can lead to moisture and oxygen contamination. The loading does not allow for a pod to be used for transfer as was done in [54].

3) The glass to glass seal was not an air tight seal which can lead to leaking and back diffusion of impurities.

4) The exhaust is immediately above the melt and on quenching, this configuration can cause back diffusion. It was also observed that exhaust material was dropping back into the melt.

5) The system on recovery of a fault, depending on the failure, would reset to the start position which was reactor seal broken and the stand moved downward automatically via motor 2.

The first goal of this work was to fix and improve the vertical furnace system to make and evaluate glasses from the commercial powder in stock at the ORC. One improvement involved replacement of the E100 display with pushbutton interface and reprograming the Mitsubishi PLC to improve functionality such that the fail position leaves the furnace in the upward position with the furnace reactor still sealed closed to maintain a reliable environment.

4.2 Design and development of RAP systems

As mentioned previously, infrastructure was in place for the vertical RAP system. However minimum infrastructure was in place for development of a horizontal RAP system. In the following the design and development of RAP facilities along with the experimental results that aided the design process and future development are detailed. The main aim was to provide a system for manufacturing high purity mid infrared glasses using RAP techniques. In order to achieve high purity in such a system, an understanding of where the

impurities exist in the system and how they assimilate into the melt is of key importance. Once the impurity is identified, the effect on the transmission window can be analysed via optical studies in the IR. Research into techniques for removing these unwanted impurities can then be undertaken. This is the ideal approach in development of the system and requires having the basic infrastructure developed as part of this work, in place.

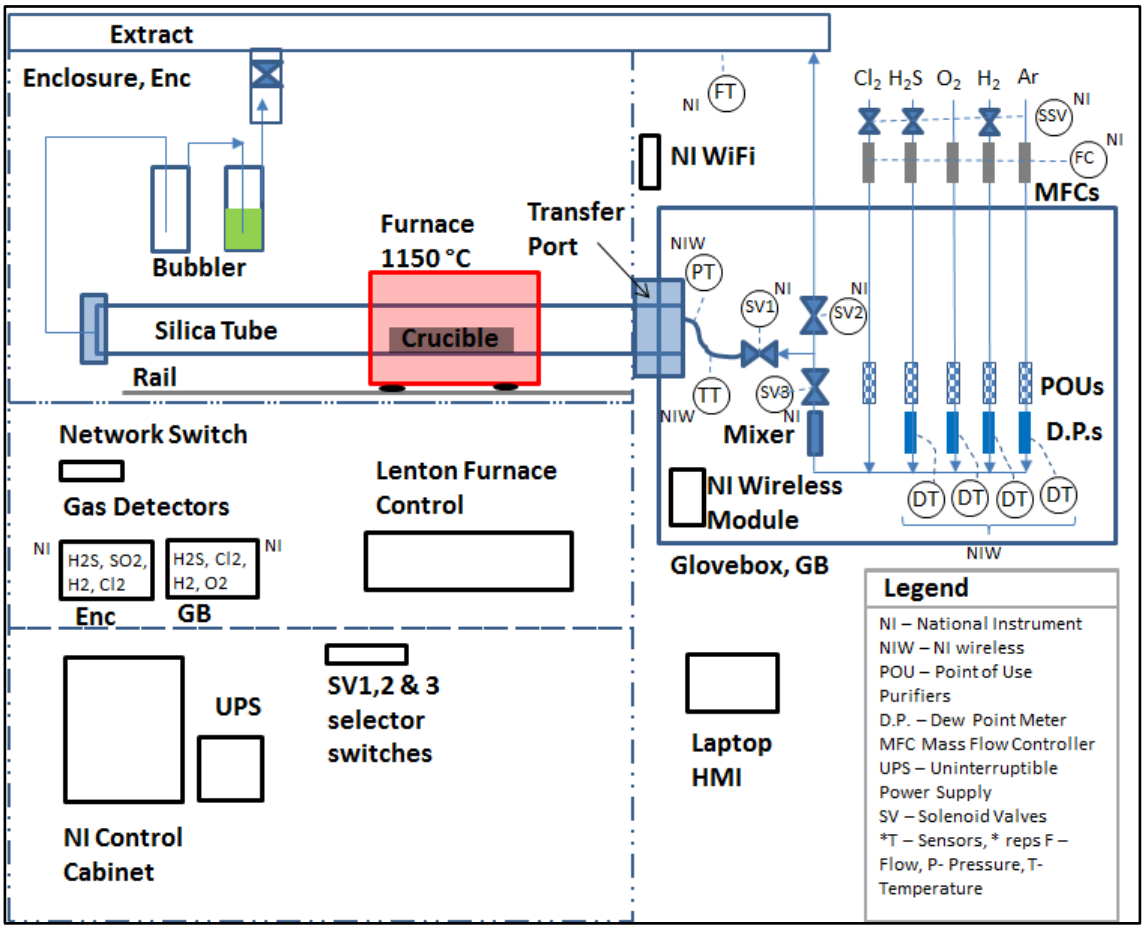

Figure 23 RAP Schematic showing the major components of the system built in this work and their interconnection.

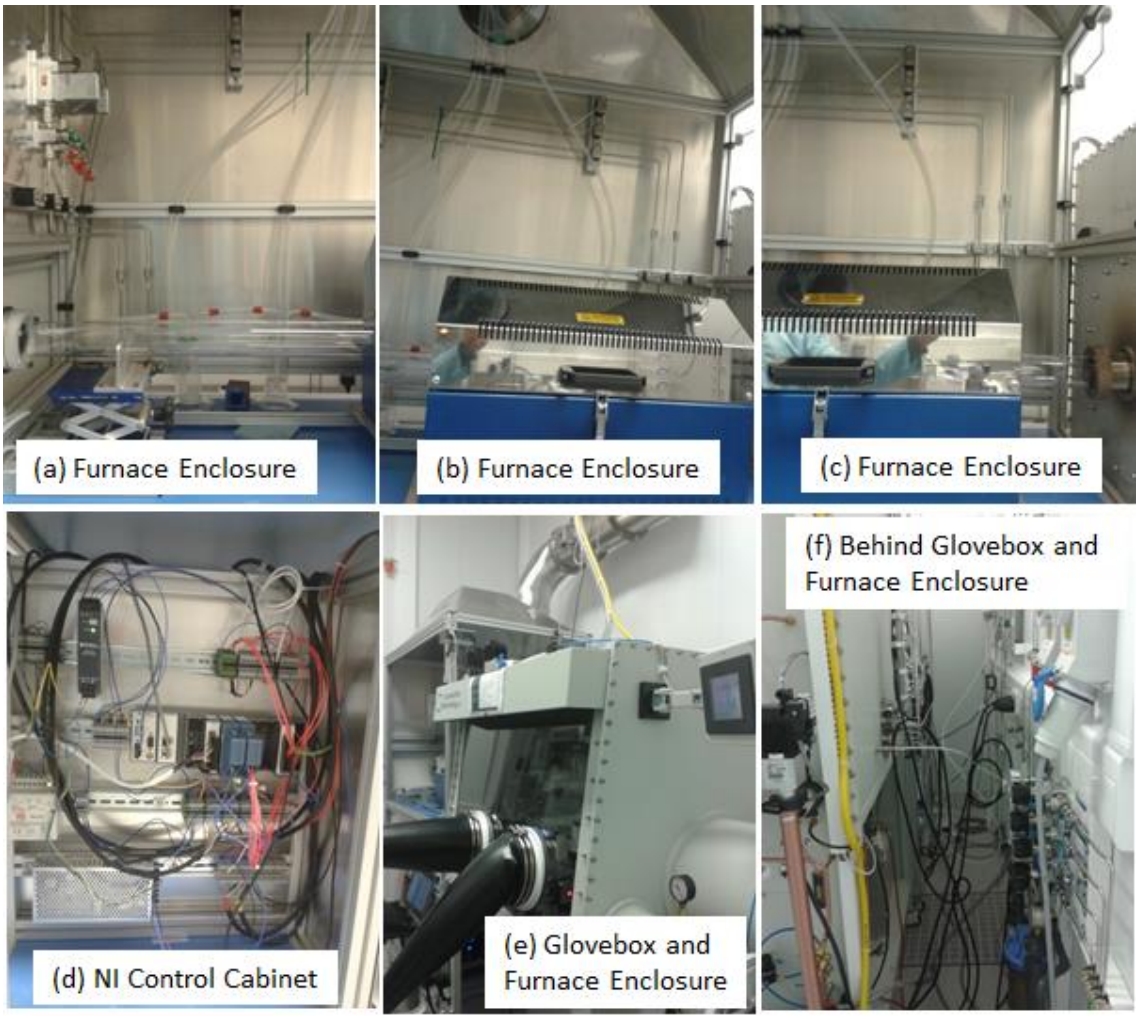

Figure 24 Horizontal RAP (a) shows the outlet of the silica tube, towards the back of the picture is the dual bubbler and the top right are the toxic and flammable gas MFCs, (b) shows the furnace and towards the top of the picture is the extract port where the exhaust tube from the bubbler as well as other exhaust tube from gas detectors are positioned inside, (c) shows the connection of the silica tube to the glovebox using a 60mm internal diameter stainless steel compression fitting, (d) shows the NI control cabinet used to connect to monitoring devices and build operating interface, (e) shows the glovebox used to batch the raw material in a high purity environment, (f) shows the gas delivery and utility supplies to the horizontal RAP.

Figure 23 is a schematic of the basic design of the horizontal RAP system achieved in this project with pictures of the actual system shown in Figure 24. The system is installed in laboratory room 1063 as shown in Appendix D,

Figure 83 which is a class 10K cleanroom environment. The main components are:

1) A glovebox for storing and batching the raw materials in a controlled environment
2) Controlled delivery and purification of selected process gasses.
3) A transfer port to transfer the mixed raw material into the furnace without exposure to a non-controlled atmosphere.
4) A three zone furnace for providing melt/reactive temperatures.
5) The outlet of the tube is connected to an extract system through a bubbler where the gasses are scrubbed to remove toxic components for disposal.

To achieve the high purity horizontal system, the focus of the research was broken down into:

1) Assess the raw material quality
2) Achieving high purity gas delivery
3) Implement automation and safety
4) Develop standard operating procedures and best practices

During the course of this work, over one hundred GLS glass samples have been fabricated using the vertical furnace and horizontal RAP glass melting systems at different stages of development and optimization. In Appendix C, Table 12 the details for the glasses produced that has impacted the development of the high purity horizontal RAP system is summarized.

4.2.1 Raw material quality assessment

High impurity content in the raw material obtained commercially is one of the main problems facing chalcogenide manufacturing. As such, the raw materials used to make GLS that were available in-house were studied to understand what contributions to losses are from raw materials compared to other components of the RAP system. Different La_2S_3 powders supplied commercially were used to prepare glasses simultaneously in an inert Ar atmosphere and using Ga_2S_3 from the same supplier. Figure 25 shows the variability in the

powder and final glasses obtained. Most sources state the colour of La_2S_3 powder as yellow [55] which meant that the color difference may be as a result of impurities, phases differences or the material was not La_2S_3. FTIR was carried out on the three glass samples and the result shown in Figure 26. Raman spectroscopy was carried out on La_2S_3 and Ga_2S_3 powders and the results presented in Figure 27 through Figure 30.

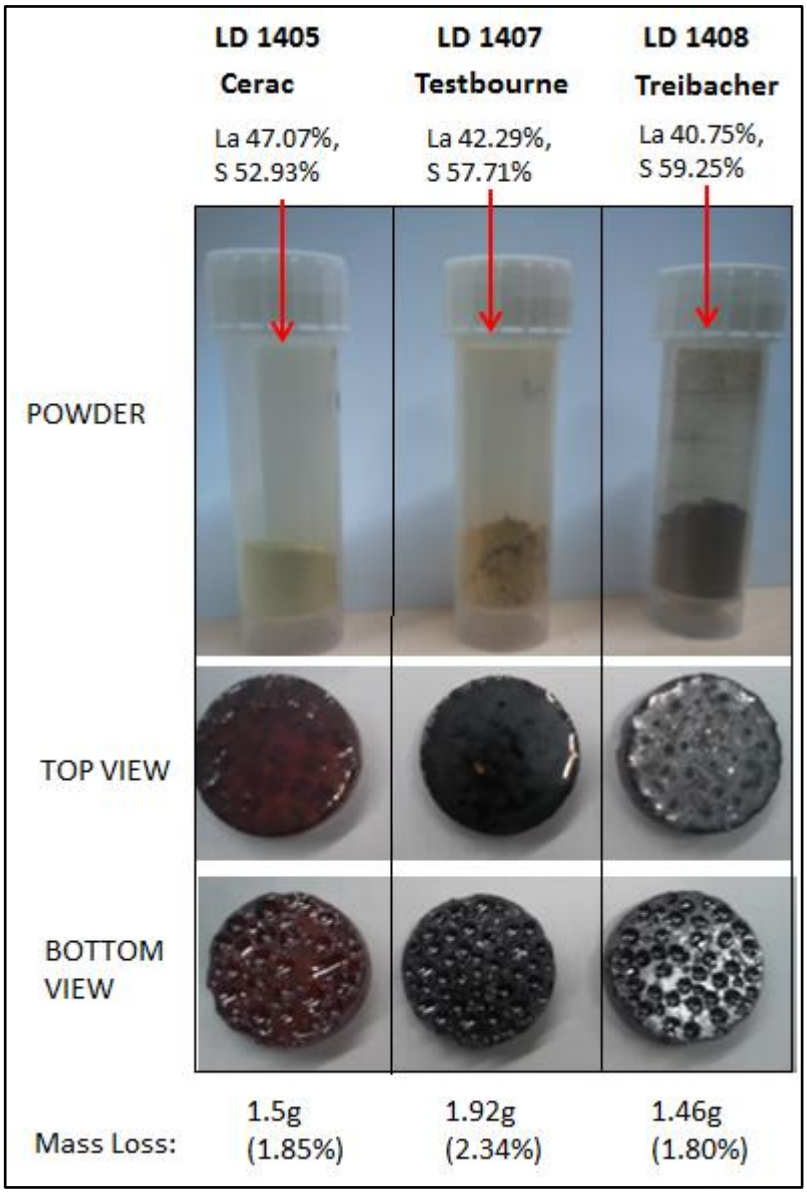

Figure 25 GLS glasses showing the visual difference in La_2S_3 supplied commercially

From Figure 26, the Treibacher glass shows a high loss in the 2 – 6µm region even though it is the thinnest sample. The Treibacher glass shows a general decrease in this region towards the higher wavelength that resembles the

transition metal impurities specific absorption loss versus wavelength in [16]. The OH peak is slightly visible at 2.91µm but much clearer in the Cerac and Testbourne glasses. The peak at 4.67µm could be as a result of Cerium ions as shown in [56] who studied doping GLS with Ce_2S_3. However this peak at 4.65µm is considered as an unidentified band in chalcogenides, [29]. Other chalcogenide peaks identified close to this area are SH at 4.01µm, CO_2 at 4.3 µm, SO_2 at 4.0 and 4.3µm. SO_2 is also identified at 7.34µm and 8.61µm. Therefore SO_2 has to be one contributor to the IR cutoff beyond 7µm. Beyond 7µm, the oxide absorption band appears and each impurity as well as the major glass forming elements can combine with oxygen to form the shape of this band and limit transmission beyond this point. Since the major glass forming components with the lowest mass are sulphur and gallium, we should expect this 8.6µm peak to be as a result of sulphur oxide and gallium oxide bonds.

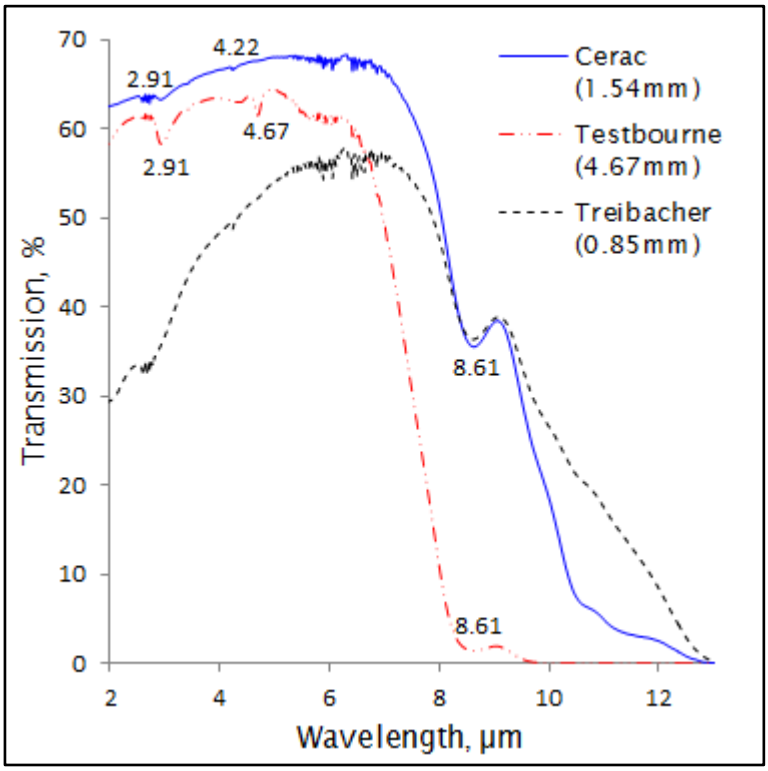

Figure 26 FTIR of three glasses made using different La_2S_3 obtained commercially

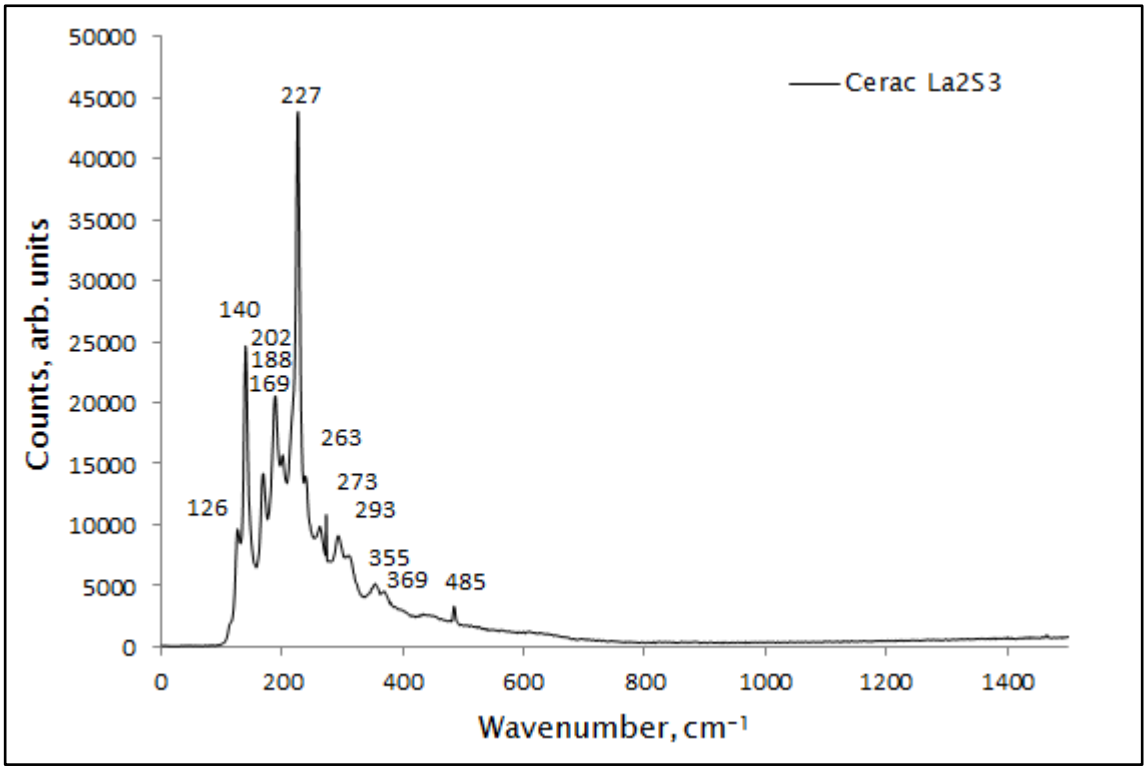

Figure 27 Raman of Cerac supplied La_2S_3 using 532nm laser

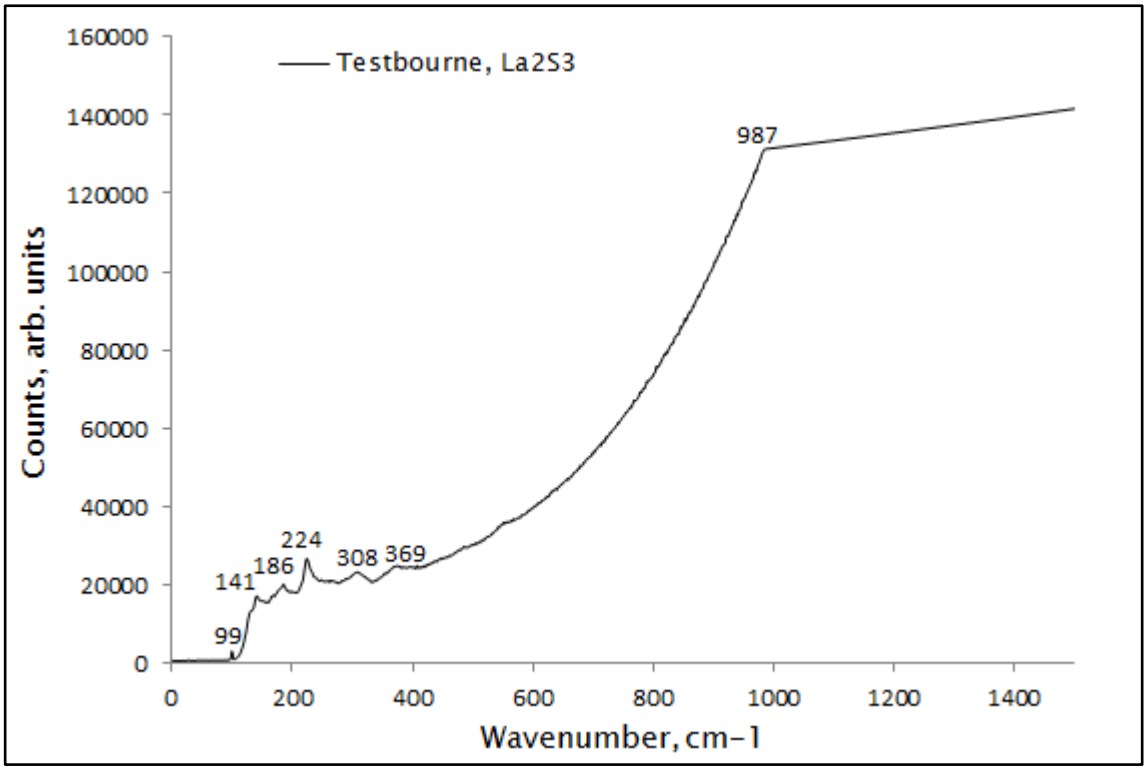

Figure 28 Raman of Testbourne supplied La_2S_3 using 532nm laser

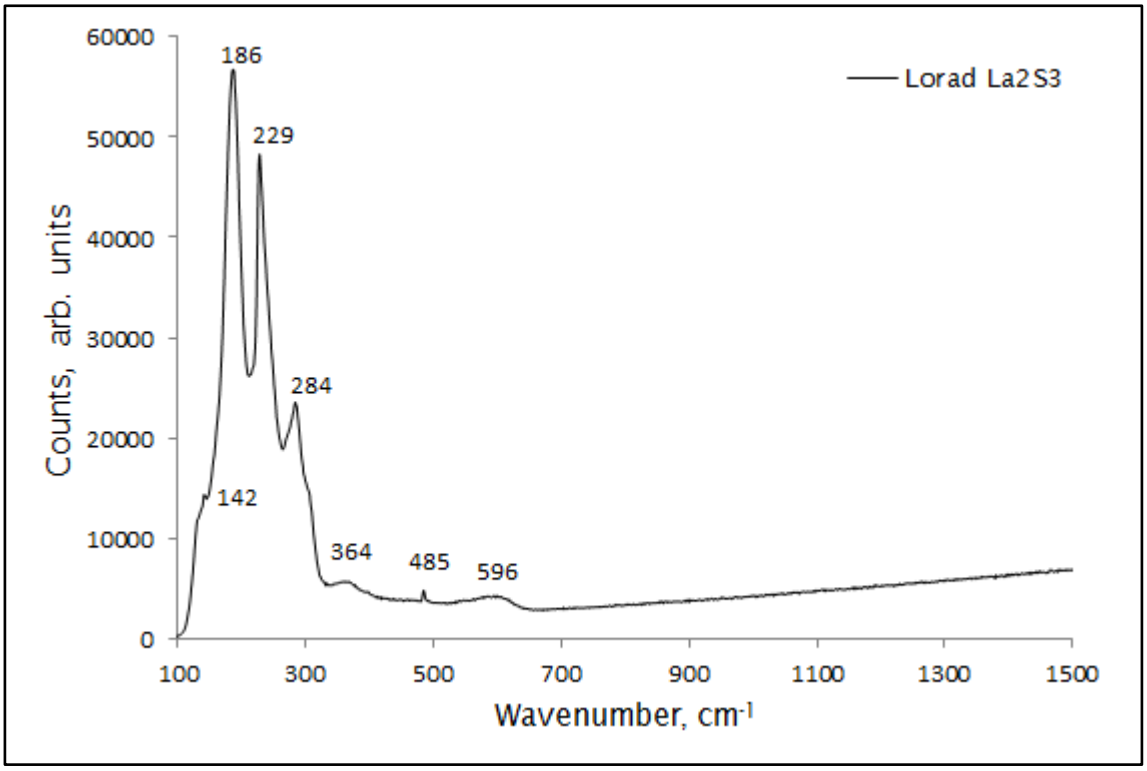

Figure 29 Raman of Lorad supplied La_2S_3 using 532nm laser

Peak, cm-1	**Material/Reference**
Peaks identified in this work	
126,140, 169,188,202,227,263,273,293,355,369,485	Cerac, Figure 27
99,141,186,224,308, 369	Testbourne, Figure 28
142,186,229,284,364,485,596	Lorad, Figure 29
Peaks identified in the Literature	
85,229, 280 other peaks, 125, 186	γLa2S3[57] other peaks
195,230,301	γLa_2S_3, $\beta \rightarrow \gamma$ at 1300℃
91,137,225,283,338,392,447,613	La_2O_3 [58]
Many peaks, see reference as some peaks may be as a result of the slide.	α and β SiO_2 – quartz[59]

Table 7 Raman peaks for La_2S_3 observed in the literature and raw materials

Table 7 tabulates the results from Figure 27 through Figure 29 as well as the main peaks found in the literature for La_2S_3. While all materials exhibit peaks close to the literature peaks, the slight shift may be due to oxidation of the La towards a La_2O_3 bond. The Testbourne powder was found to have clumps of hair as well as reddish coloured particles. The saturation in Figure 28 may be due to the fluorescence of rare earth impurities which maybe the reddish coloured particle. From this information the Lorad powder was selected for high purity work as it had closest relation to the La_2S_3 peaks found in the literature.

Figure 30 shows the Raman analysis of the GWI powder. The peak assignment will be discussed later in Section 4.3 where attempts were made to make Ga_2S_3 in-house. In the next section, the effect of the gas delivery is detailed. This is important as the gas lines could be contaminating the glasses made as will be shown.

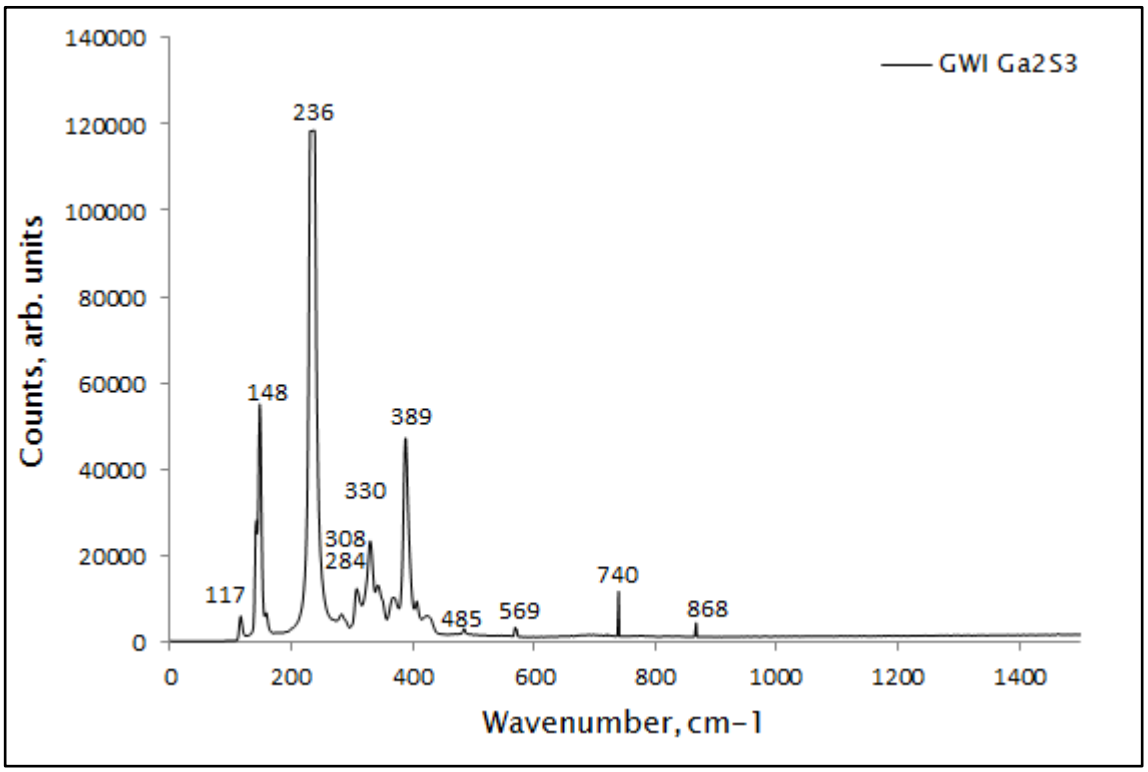

Figure 30 Raman of GWI supplied Ga_2S_3 using 532nm laser

4.2.2 Achieving high purity gas delivery

A basic horizontal melt system was installed using existing components and the setup is shown in Figure 31. Two experiments were undertaken in which glasses were made using an inert argon atmosphere. The difference in the two melts was that no purifier was used for the first melt and a NUPURE PF series POU purifier with a 0.01um particle filter used for the second melt.

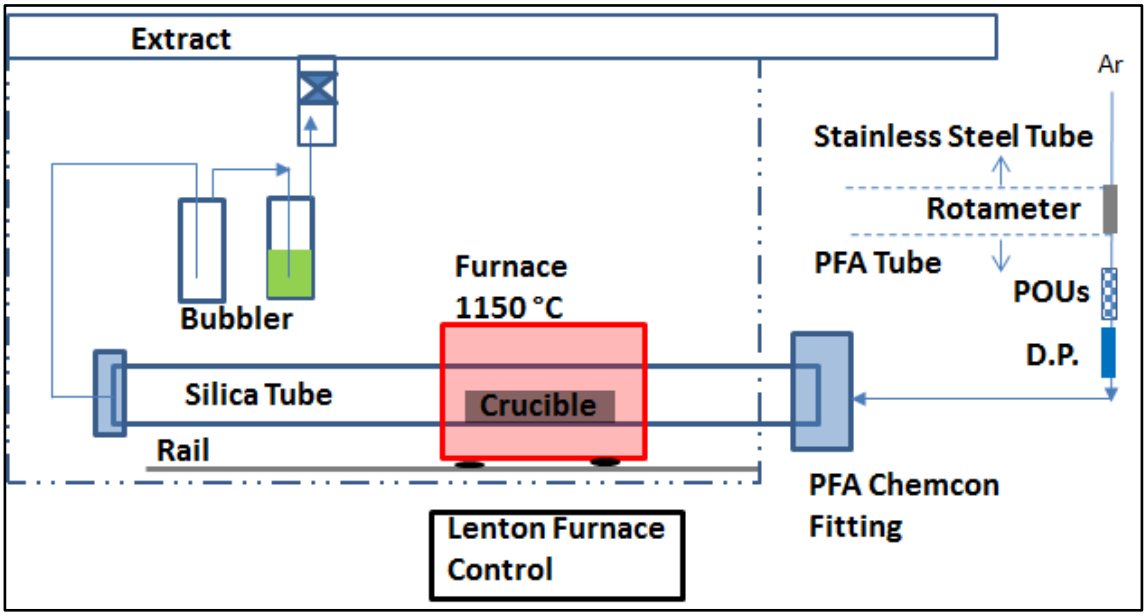

Figure 31 RAP purifier test setup

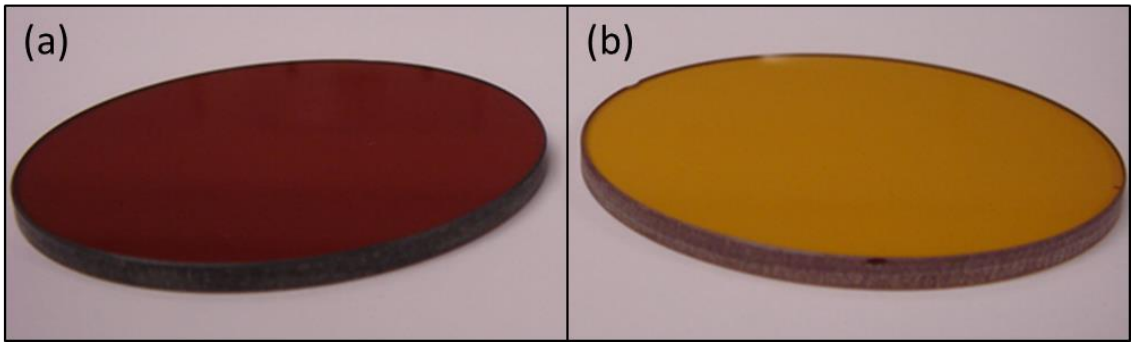

Figure 32 Purifier test results (a) Glass without purifier LD1443 (b) Glass with Purifier LD1447

In Figure 32 a noticeable difference in colour between the two glasses produced can be observed. From the GDMS in Appendix B, Table 11 and UV-Vis spectra in Figure 33, the color difference is attributed to the difference in chromium ions in the glass. In [30], Cr ions possess a strong absorption centred on 0.86 μm in GLS and GLSO attributed to the 5E→5T2 transition in

Cr^{2+} and also causes a red shift of the electronic edge. Since the same raw materials, similar carbon crucible and silica tube reactor was used; it is unlikely that the additional Cr is from these sources. The main source of chromium by elimination can then be attributed to the stainless steel lines before the purifier and therefore the 0.01µm filter in the purifier acts to filter the Cr particulates. On investigation of the stainless steel lines in the processing area, it was noted that there were improperly done welds, as well as no other particle filters after the bulk gas argon purifiers few 100m away. Improper welds provide pockets for moisture to get trapped thereby increasing the potential for leaks and corrosion (especially when using corrosive gasses like H_2S and Cl).

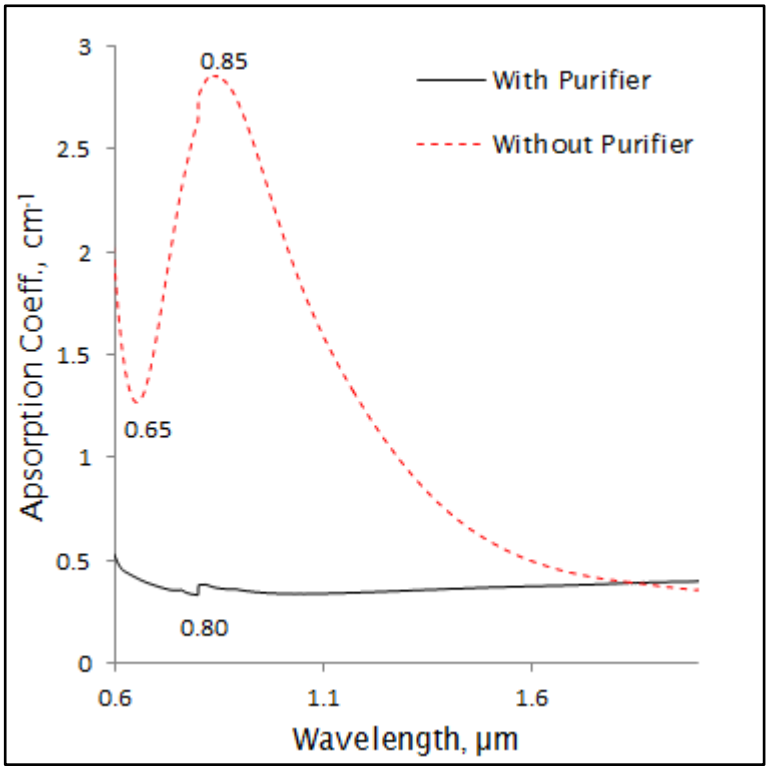

Figure 33 UV-Vis_NIR absorption plot showing the effects of glass without purifier LD1443 and glass with basic purifier LD1447

As the chromium ions are removed from the glasses with the purifier, the effect of Iron ions in the 1.6- 2.5 µm region can be seen in Figure 34 which is supported by the work in [30]. The effect of Nickel ions is noted here for completion as stainless steel is made mainly from a nickel-chromium blend. Nickel ions contribute to absorption at the 2.0µm wavelength and is noticeably stronger in GLSO vs GLS [30].

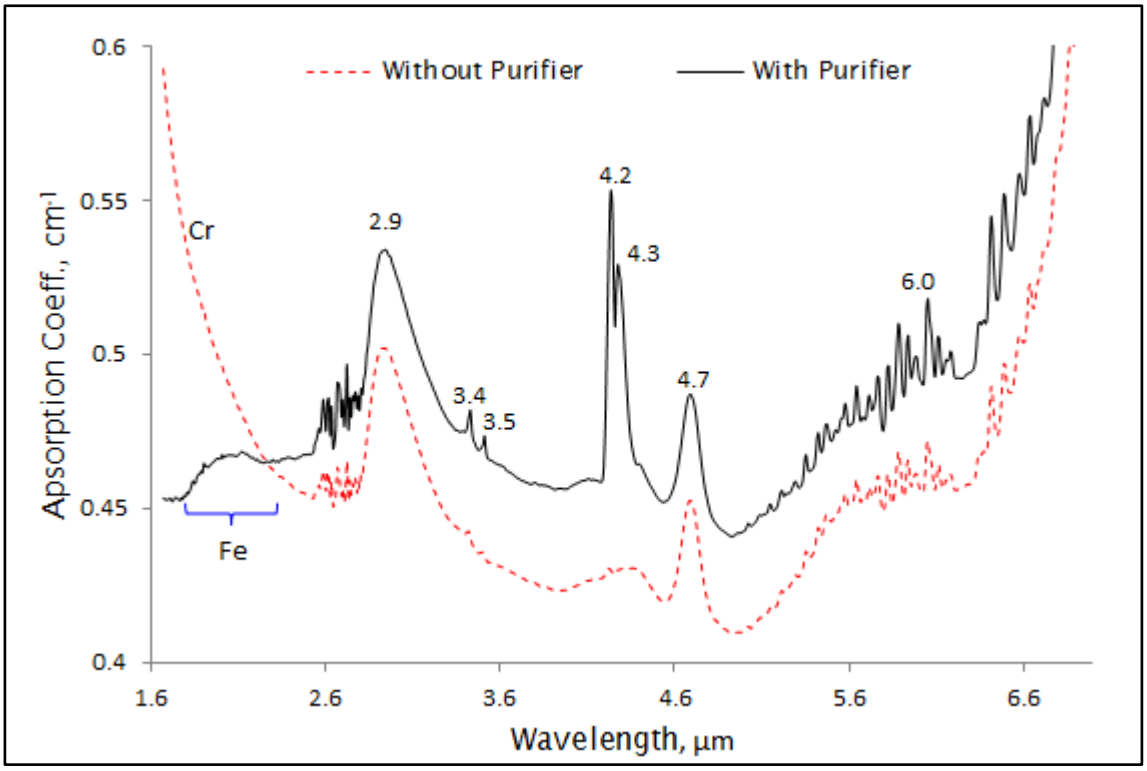

Figure 34 FTIR of GLSO samples without purifier (LD1443) and with purifier (LD 1447)

The result in Figure 34 is corrected for thickness but not refractive index. From equation 12, differences in refractive index as expected with the difference in glass color can result in the sample without the purifier having a lower absorption in the transmission region of 2.6µm and 6.6µm if not corrected for. They exhibit similar absorption peaks where the peak at 2.9µm is due to OH. Using a specific absorption coefficient of 0.0115cm^{-1} per ppm [27] and estimating the height of the peak at 2.9µm from Figure 34 relative to the imaginary line extended at the base of the peak to be 0.05cm^{-1} gives an approximate OH content of 4 to 5 ppm. However if all the absorption is taken to be OH and the contribution for intrinsic contribution subtracted using the equations in Table 2, the OH content is approximately 40 to 50 ppm.

A very rough estimation of the contribution from the input gas can be determined as follows:

$$n = \frac{PV}{RT}, \tag{14}$$

n = number of moles

R = 0.08206 L per atm per mol^{-1} per K^{-1}

T = 25 ˚C = 298 K

P = 1.97 atm

A typical flowrate of 500 sccm gives 720 L in 24 hours, assuming that the system is static, then the process will interact with this volume of gas and all the moisture can be absorbed with the glass, then

n = 1.97 x 720/ 0.08206 x 298

= 58 moles in 24 hours

The dew point reading from the gas at the time of the experiment was -76 C, which implies 0.34 ppmv moisture per mole of Ar. Therefore if it is assumed that all the moisture is absorbed, then approximately 19.7 ppm (0.34 x 58) of moisture is as a result of the gasses during a 24 hours melt cycle.

The peak at 4.7μm is most likely due to Ce^{3+} ions which have been confirmed by intentionally doping with Ce [56]. Although around 4.6μm, the absorption can also have a contribution from Si, Ba and Ca bonding with H. The absorption peak around 6.0μm is due to H_2O and beyond this wavelength, the absorption is dominated by oxide impurities. The peaks at 3.4 and 3.5 μm is due to the CH bond formed by the use of isopropanol to clean the sample prior to mounting in the FTIR and not allowing sufficient time for evaporation. The peaks at 4.2μm and 4.3 μm is due to CO_2 and is likely to be as a result of residual CO_2 in the FTIR chamber and not a feature in the glass, see Figure 7. This can be eliminated with purging the FTIR chamber with a high purity inert gas.

The N_2 purged glovebox as shown in Figure 23 was not commissioned so the glass was batched in another glovebox and transferred to the furnace tube bringing it into contact with the 10K cleanroom environment. Even though the results in Figure 34 does not show a marked reduction in the moisture peak, semiconductor installation requirements, practices and POU results [60] dictate otherwise. Installation and procedural steps can account for the lack of a difference. Impurities can be incorporated at any point in the procedure of glass synthesis and it is often hard to discern the contributors. For example, the glovebox was not connected to the furnace for these experiments and the

material had to be transferred from a glovebox to the furnace exposing it to the 10k clean room environment for duration of no more than 5 minutes. This is enough time for oxidation and hydrolysis of the powders to occur. Another possible contributor is that PTFE tubes used to connect the gas delivery line to the furnace as well as gas flowmeters are not recommended high purity components. PTFE is known to be more susceptible to moisture ingress than PFA and stainless steel. In many cases PTFE or PFA can jacketed with a tube that is purged with a high purity gas. Moisture can also be incorporated into the final melt from the gases used during synthesis, improperly cleaned and baked reaction tube or crucible, leaks in the seals/fittings and the raw materials depending on their history. In the following sections, the improvements made to the infrastructure at the ORC facility towards achieving the system in Figure 23 are detailed.

4.2.3 Gas delivery and purification

Providing high purity gases to the processing tube to create a high purity atmosphere is a key aspect to reduce impurity content of the final product. The impurities in the gas stream can be incorporated into the melt as long as the gas is flowing, however, the gasses can also act to dynamically remove volatile impurities. This is achieved through a high purity gas delivery system.

For a facility of the size of the ORC, a three part purification system as shown in Figure 35 [61] is necessary for high purity gas delivery. The 1st stage of purification is a high throughput purification system placed just after the bulk gas storage indicated by the numbers 1 and 4 in Figure 35. These purifiers typically have a 5 to 10 year lifetime depending on the manufacturer and the quality of gas supplied to the inlet of the purifier. The 2nd stage purifiers are usually used to isolate different processing areas or equipment as shown by the numbers 2, 3 and 5 in Figure 35. Finally for optimum purification a final 3rd stage of purifiers are placed at a minimum distance to the equipment inlet and that closely matches the process input parameters. These purifiers are referred to as Point-Of-Use (POU) purifiers and are essential to maintaining gas purity at this final stage [60]. This design is aimed to prevent deterioration of

purifier lifetimes and risk of cross contamination from improper operation/installations in upstream processing areas.

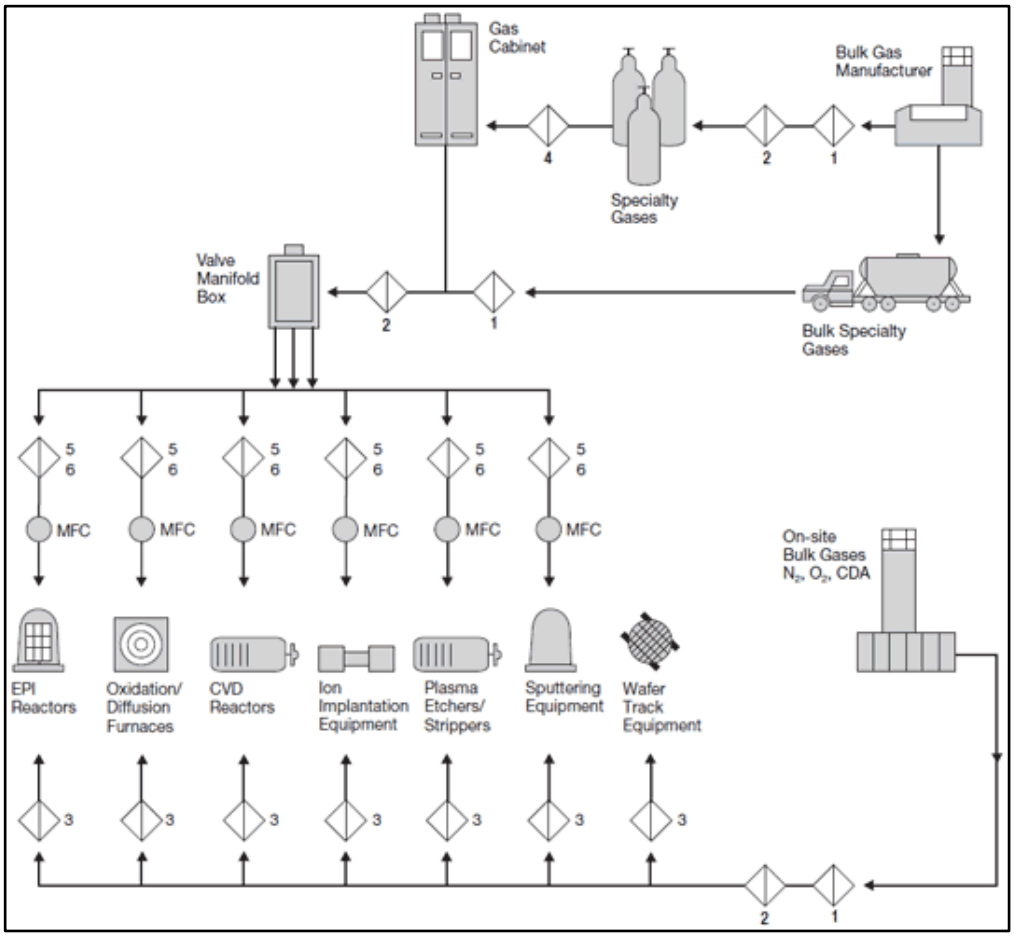

Figure 35 Typical gas purification for high purity facilities, Taken from PALL coorporation webpage, see [61]

A study of the existing ORC facility was performed to determine the quality, layout and components of the purification systems with comparison to the ideal installation in Figure 35. This was done for the five main gases chosen for design of the reactive atmosphere system which are Ar, N_2, O_2, H_2 and Cl_2. The study showed that none of the gases were installed using the ideal installation. For example there was no 2nd stage purification to isolate between process areas. There was also no POU installed. The only purification stage provided was 1st stage purification which had not been maintained since installation in 2005. The existing, installed in this work and future purifier installation are show in Figure 38, Figure 39 and Figure 41 - Figure 44.

A study of commercial POU purifier suppliers was conducted since there was none of these purifiers installed in the existing facility. Four vendors were

reviewed and SAES purifiers met all of the criteria for both installation and outlet purification performance. The impurities and outlet performance is captured in Figure 36 for the various gasses. For ease of installation these purifiers were the most compact in terms of size allowing installation within the glovebox as shown in Figure 37. SAES purifiers were also the most economical with a price range between £500 and £800 depending on the gas to be purified. Integrated into the purifiers are 3nm particulate filters. The particle filters remove particles in the gas line that have sizes greater than 3nm and ensure that these particles are not incorporated into the melt. These particles contribute to absorption loss as well as local changes in the refractive index which increases the scattering losses and the losses increase with the size of these impurity particles as discussed in Chapter 2. The location of these purifiers in the gas delivery process is shown in Figure 38, Figure 39 and Figure 41 - Figure 44.

Media	Gases Purified	Impurities Removed	Outlet Performance
202	Ar, CDA, H_2, He, Kr, N_2, Ne, O_2, Xe, CO_2, N_2O, CO, D_2	H_2O	< 1 ppbV
203	Ar, CDA, H_2, He, Kr, N_2, Ne, O_2, Xe, N_2O, CO, D_2	H_2O, CO_2,	< 100 pptV
		Acids, Organics, Refractory Compounds*	< 1 pptV
		Bases*	< 5 pptV
302	B_2H_6, BCl_3, BF_3, $CClH_3$, Cl_2, CO_2, $GeCl_4$, GeH_4, H_2S, H_2Se, HBr, HCl, N_2O, NF_3, NO, $SiCl_4$, SiF_4, SiH_2Cl_2, $SiHCl_3$, SO_2, $CHClF_2$	H_2O	< 1 ppbV
		Metals Removal	< 1 ppbW
403	Ar, CDA, H_2, He, Kr, N_2, Ne, O_2, Xe, CO_2	Acids, Organics, Refractory Compounds*	< 1 pptV
		Bases*	< 5 pptV
404	Ar, CDA, H_2, He, Kr, N_2, Ne, O_2, Xe, CO_2, C_2H_2, C_3H_6, C_2H_4, NH_3	Organics*	< 1 ppbV
502	PH_3, AsH_3	H_2O, O_2	< 1 ppbV
602	CO	H_2O, O_2, CO_2, Acids, Bases, Organics, Refractories*	< 1 ppbV
702	NH_3, C_2H_7N, $C_2H_8N_2$, C_2H_4, C_3H_6, CH_3SiH_3, GeH_4, H_2-SiH_4 mix, SF_6	H_2O, O_2, CO_2	< 1 ppbV
703	NH_3	H_2O, O_2, CO_2, NMHCs	< 1 ppbV
802	SiH_4	H_2O, O_2, CO, CO_2, NMHCs, Sulphur Compounds	< 1 ppbV
902	Ar, He, Kr, N_2, Ne, Xe	H_2O, O_2, CO, CO_2, H_2	< 100 pptV
		Acids, Organics, Refractory compounds*	< 1 pptV
		Bases*	< 5 pptV
904	H_2, H_2 -Inerts Mix, D_2	H_2O, O_2, CO, CO_2	< 100 pptV
		Acids, Organics, Refractory compounds*	< 1 pptV
		Bases*	< 5 ppbV
905	C_2F_6, C_2H_6, C_3F_8, C_3H_8, $C_2F_4H_2$, C_4F_8, C_4H_{10}, CCl_4, CF_4, CH_4, CHF_3, SF_6	H_2O, O_2, CO, CO_2, H_2 NMHCs	< 1 ppbV
906	CDA, O_2, N_2O	H_2O, CO, CO_2, NMHCs	< 1 ppbV

Figure 36 SAES Point of Use Purifier specifications, Taken from SAES Gas Purification Inc. brochure, see [62]

Figure 37 Pictures showing the purifier and dew point during installation within the glovebox

In addition to the review on purifiers, the other components for high purity installation were checked for compatibility to the process gasses and operating conditions. Stainless steel is used for most of the components in the gas delivery and were checked against [63] which provides best practices for semiconductor applications. This check is a time consuming task for a large facility in which a lot of infrastructure was installed with a large part being underfloor or model numbers hard to read due to installed orientation of the component. Some of the findings were:

1) Fittings at the gas delivery point in the ORC level 1 room 1063 where the Horizontal RAP system is installed were switched from Variable Compression Ratio (VCR) fittings which are standard for high purity installation to National Pipe Thread (NPT) fittings which are not used in high purity installations. These NPT fittings were replaced as part of this work.
2) Some of the VCR fittings seals in the H_2S process used Ag coated O-rings. H_2S reacts with the Ag which compromises the seal and therefore leakage limits[64]. These were replaced as part of this work as H_2S leaks are a major safety concern.
3) Kalrez O-rings were used as opposed to Vitron as suggested in [64]. H_2S can cause Viton O-rings to swell and also harden which can compromise its sealing capability or even crack the silica glass reactor. Even with Kalrez O-rings it is recommended to change these O-rings between glass conversions using H_2S.

4) Check valves were used to ensure that cross contamination of gas lines would not occur.
5) Improper weld as mentioned previously which can trap moisture and increase corrosion as well as contain oxygen from a bad weld process. Good welding practices can be found in [65] and are best practices for critical systems.

In the following sections some of the results of the improvement in OH content of gasses delivered are detailed as well as the gas delivery installation details.

4.2.3.1 Inert gases - Ar and N_2

Ar and N_2 play a very important role in the ORC facilities from purge gasses, carrier gasses and providing high purity inert atmospheres for example in gloveboxes and process equipment. The main 1st stage gas purifiers for Ar and N_2 are located on Level 3 in the Central Utility Building as shown in Appendix D Figure 84. It was found during the review that the dew point meters and purifiers were improperly maintained. The dew point meters had drifted dry and was giving a false indication of moisture purity (-99.9 C). The purifiers were not being regenerated and were approaching their intended lifetime which may be between 5 to 10 years depending on the inlet gas purity and maintenance for such models of bulk purifiers. A study of the Nitrogen delivery with calibrated dew point meters was undertaken to determine the quality of these gasses. A calibrated dew point meter was placed at the outlet of the first stage bulk gas purifiers giving a reading of -93.8C after five months of recording. This study confirmed the false indication of the unmaintained meter. The gas distribution in the novel glass processing area, room 1063, was -76C (0.34 ppm(v) @ 2barg [66] for N_2). This was the maximum reading recorded over a 2 month period and gave an indication for the first time of the increase in moisture levels at the ORC facility between the purified gas and the equipment to be located in Room 1063.

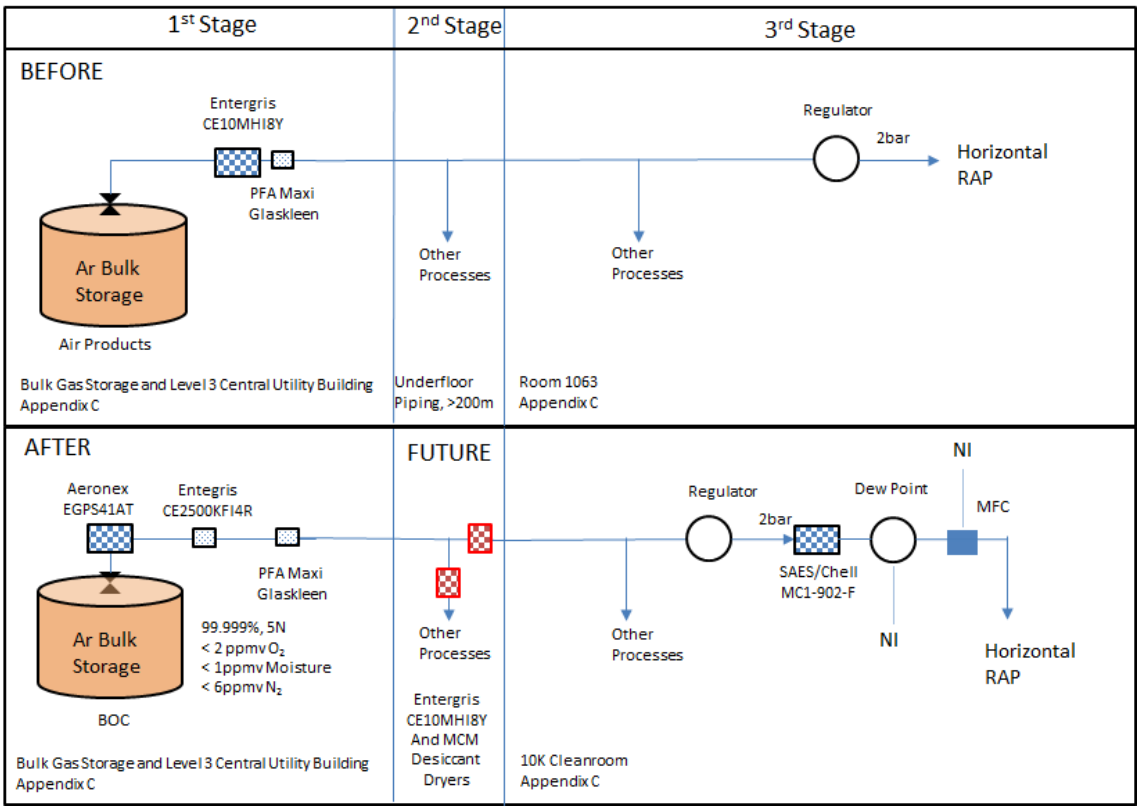

Figure 38 Schematic of Ar gas delivery showing the gas purification upgrades and changes to the gas supplier before and after the completion of this work. Future represents the changes that have been recommended and is scheduled for implemention.

The purification gases to the laboratories did not have 2nd stage and POU purifiers installed which allows for the drop in moisture recorded at the equipment. The location for the RAP system is such that there are a lot of upstream processes which can have an impact on the gas quality being delivered at the RAP system as shown in Figure 38 and Figure 39. Furthermore, troubleshooting and fluctuation of gas purity within this lab if it were not on specification would be very difficult.

The upgraded purifiers and commissioning of the glovebox led to the calibrated dew point meter reading consistently greater than -99C (0.006 ppm(v) @ 2barg for Ar). However to ensure the best lifetime for the purifier, the inlet gas to the purifier should be the best quality to ensure better operational cost to a facility. The analysis from this thesis has led to replacement of 1st stage bulk gas purifiers, newly calibrated dew point meters with better dew point range up to -120C and purchase of intermediate 2nd stage purifiers. The 2nd stage purifiers will be installed in the 2nd quarter of

2015. The bulk 1st stage purifier's replacement for Ar and N_2 has led to increased purity at this point from -93.8C to greater than -118C for Ar and N_2 shown in Figure 40. The inlet dew point meters have not been changed and should be ignored when interpreting Figure 40. After this change the dewpoint sensor after the POUs for the Horizontal RAP system will need to be upgraded from the Easidew model to the PURA model. At the time of writing this thesis the range is -99.9C to -40C and the Easidew model provided by Mitchell Instruments Ltd is used. The PURA model will allow readings up to -120C.

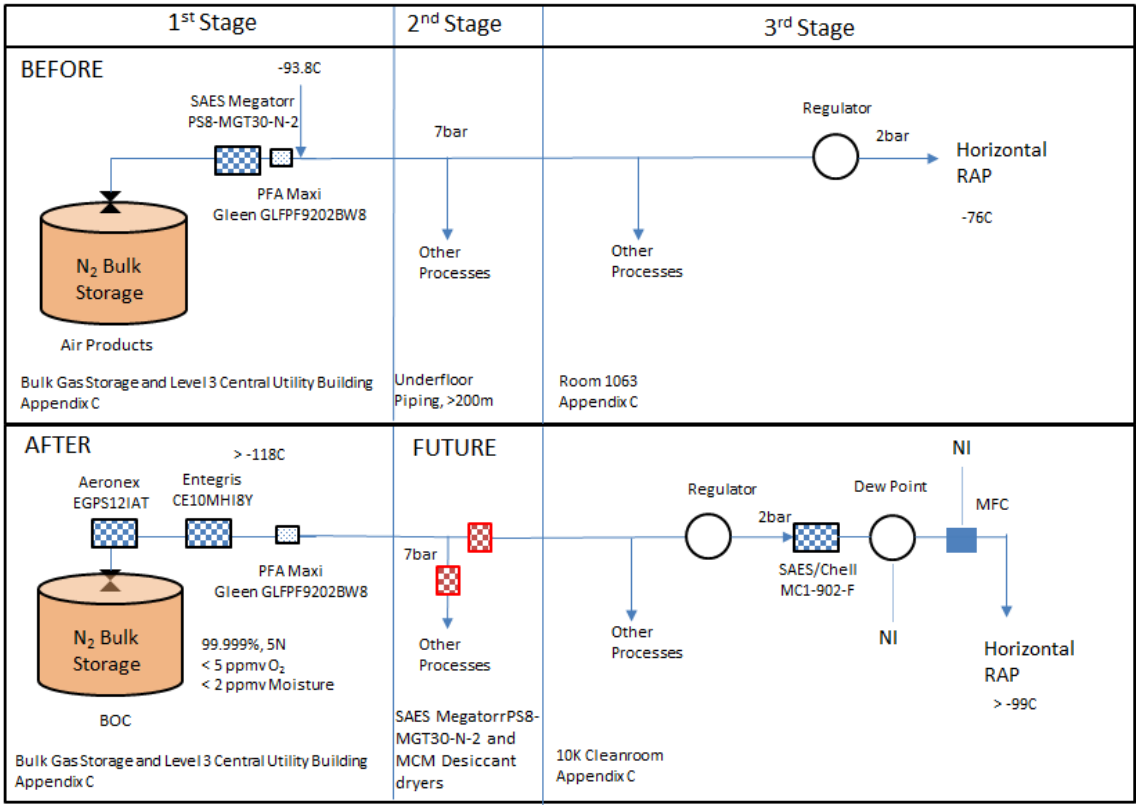

Figure 39 Schematic of N_2 gas delivery showing the gas purification upgrades and changes to the gas supplier before and after the completion of this work. Future represents the changes that have been recommended and is scheduled for implementation.

Figure 40 Picture showing dew point readings at the 1st stage purifiers after upgrade the purifiers.

4.2.3.2 Hydrogen Sulphide

H_2S was installed for the capability of converting raw material into high purity sulphides. The H_2S cabinet in the gas cylinder room located in Appendix D Figure 83 and shown in Appendix D Figure 85 was not commissioned officially and lacked procedures and installation drawings.. These were developed as part of the work in this thesis and some of the schematic and pictures of the final installation is shown in Appendix D Figure 85 through Figure 88. During the development of this, it was found that the N_2 purge gas for purging the moisture in the H_2S lines before turning on the H_2S was connected to the point before the 1st stage purifiers on ORC level 2. Moisture in an H_2S line increases corrosion of the stainless steel lines so a temporary improvement was the addition of a POU purifier to remove moisture in the Nitrogen purge gas. This had the effect of decreasing the dew point from -76C to -90C for commissioning of the H_2S gas delivery.

As mentioned previously the delivery lines in Room 1063 had Ag coated O-ring seals for VCR fittings installation. Ag reacts with H_2S leading to leaks in the fitting and because of the hazardous nature of H_2S it is imperative to avoid incompatible materials as exposure to unacceptable doses of H_2S can lead to death. As such reviews were done on each component in the H_2S circuit to ensure material compatibility. This led to changing Viton O-ring to Kalrez as per the recommendations in [64]. There was considerable installation work especially in Room 1063 and the before and after schematic of these changes is shown in Figure 41. The Dewpoint reading is currently greater than -85C when processing with H_2S. The H_2S is currently being monitored to see the effects as the cylinder is depleted as it is expected that the inlet purity would decrease.

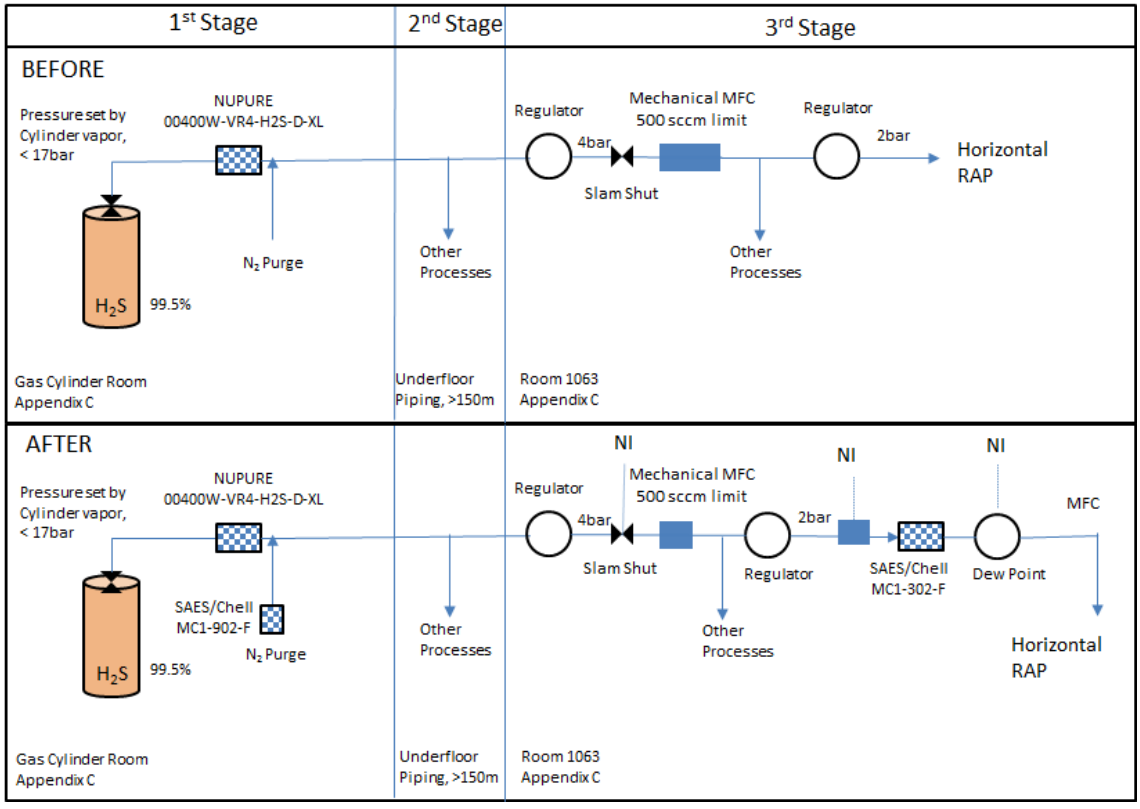

Figure 41 Schematic of H_2S gas delivery showing the gas purification upgrades before and after the completion of this work.

The NI label in Figure 41, Figure 43 and Figure 44 signify the connection to National Instruments. The slam shut valve is linked to Bionics gas detection equipment which closes this valve automatically on detection of H_2S greater than 10ppm which is the limit specified in the Material Safety Datasheet for

H_2S. Mechanical flow meters are used to limit dangerous gasses to 500 sccm in case of an unexpected failure in components in Room 1063.

4.2.3.3 Oxygen

For oxygen the work involved connecting the gas lines from a gas stick already installed in Room 1063. Oxygen was installed for the capability of making heavy metal oxide glasses in the future and the final installation schematic is shown in Figure 42. It can also be used to add small amount of oxygen to a glass which can tailor certain properties such as the case of GLSO.

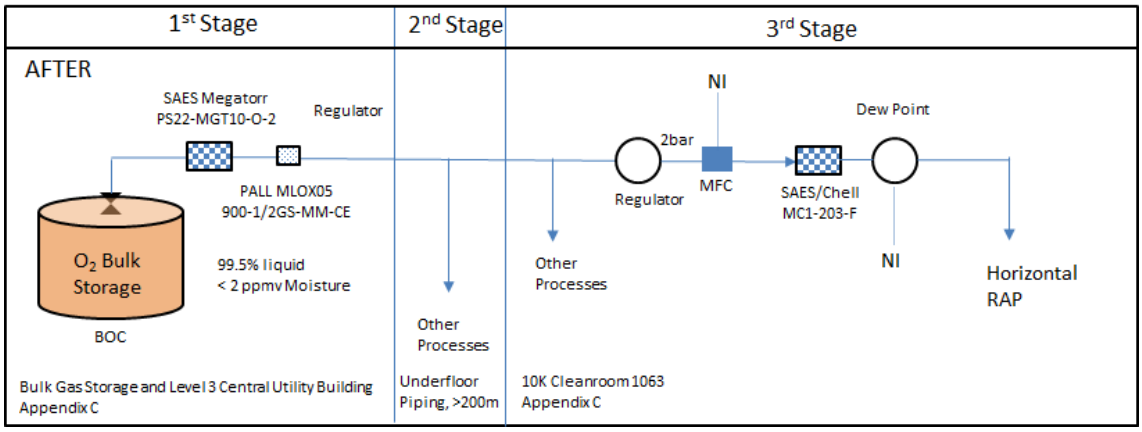

Figure 42 Schematic of O_2 gas delivery, changes made to gas purification are addition of a dew point meter and O_2 3rd stage purifier.

4.2.3.4 Hydrogen

A H_2 gas panel in Room 1063 was modified as part of this work and is shown in Appendix D Figure 89. One modification was to accommodate the Oxy/Hydrogen torch which is used to seal ampoules in Chapter 3 for ampoule sealing. The second modification was to accommodate supply of H_2 to the Horizontal RAP for experiments in reducing oxide and other unwanted components in the glasses. The schematic of the H_2 supply to the Horizontal RAP is shown in Figure 43.

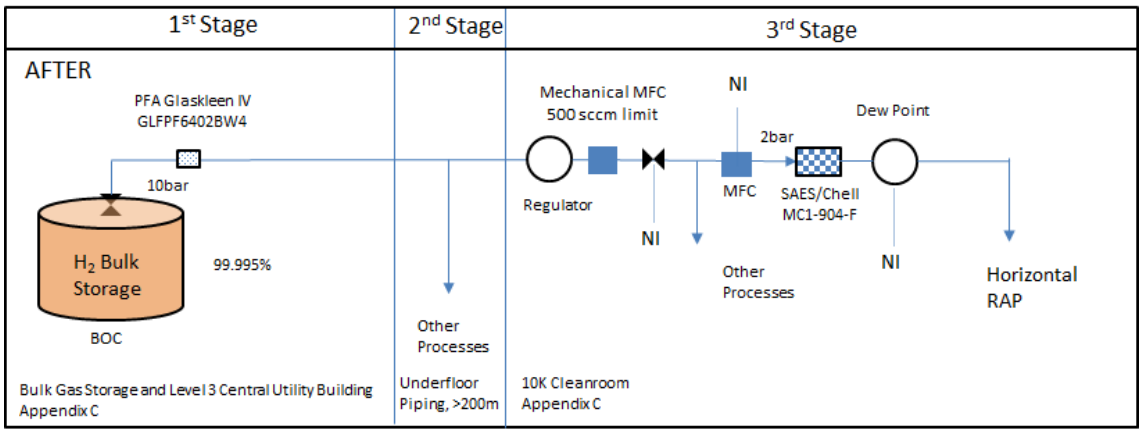

Figure 43 Schematic of H_2 gas delivery, changes made to gas purification are addition of a dew point meter and H_2 3rd stage purifier.

4.2.3.5 Chlorine

Chlorine distribution has not been completely installed. The distribution circuit is shown in Appendix D Figure 90 and the schematic of the future installation in Figure 44. Chlorine was chosen for removing H_2 and other volatile metals that react with Cl. However Cl is a very corrosive gas and requires double jacketed stainless steel tubing.

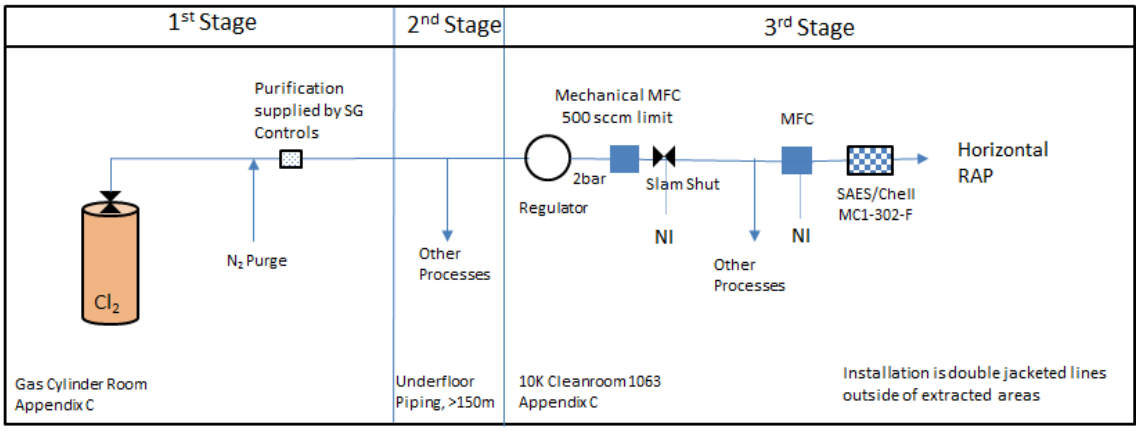

Figure 44 Schematic of Cl_2 gas delivery changes made to gas purification are addition of a Cl_2 3rd stage purifier.

Due to the fire in 2005, cylinders are kept separate and isolated from the processing area as well as due to the size of the ORC and the number of equipment using these gas supplies. Otherwise for smaller installations it may be better for purity and installation cost to have the gas supply cylinders closer to the process equipment.

In the horizontal RAP, there are a lot of components in the gas supply for monitoring, safety and control installed. Using instruments and incorporating them into a control system allows for building recipes and also ensuring consistency between glass melts. In the following section, the design of the automation and controls for the horizontal RAP is covered.

4.2.4 Automation and safety

In this section, the automation and safety systems developed for the RAP is detailed. Automation is important to repeatability and safety of any process. Moreover key process parameters can be monitored and archived automatically aid in analysis of any variations that may occur during the processing steps. Glass synthesis processes at the ORC lack considerably in terms of automation and process monitoring. Because process tasks rely on human interaction, repeatability was compromised. Also with the use of toxic, corrosive and flammable gases used by RAP processes, automatic and safety shutdowns were necessary for this installation. As such, an integrated system was designed for automation and safety shutdown of the RAP developed.

NI control module NI cRIO 9074 was chosen to implement the automation of the Horizontal RAP. The Ni cRIO 9074 is a rugged embedded controller and monitoring system having a 400 MHz industrial real-time processor for control, data logging, and analysis as well as 2M gate, 8-slot FPGA chassis for custom I/O timing, control, and processing. Communication is implemented with two 10/100BASE-T Ethernet ports; RS232 serial port for connection to peripherals. It has a wide range of I/O cards to incorporate many different types of instrumentation signals as was required for this work. The software used to program the cRIO 9074 is Labview and is supported and maintained by the University so no additional licences were required. The automated system implemented to date is a basic, modular system that could be expanded in the future by academic researchers and students for their desired research.

The basic process flow is shown in Figure 45 and Figure 49. The five gases are taken from their respective gas delivery cabinet or gas stick within room 1063 as shown in Figure 45. Each gas is passed through MFCs which are controlled by NI and Labview represented in Figure 45 by FT001 through FT005. A special

design was made using KF fittings and split nuts from Swagelok to deliver the gasses into the glovebox with a tight seal as well as making it easy to remove for maintenance. The gasses are then fed through their respective purifiers, dew point meters and check valves with the exception of Cl_2 which has no dew point meter. Cl_2 condensation can foul sampling lines, harm instruments, and in many cases can dissolve a portion of the very sample being analysed making measurement more costly and unsafe. Cl_2 moisture measurement has been deferred as future work. The body of the dew point meter is the only stainless steel component after the purifier and is difficult to easily isolate from the corrosive gasses such as H_2S. The material used for components after the dew point meter are high purity PFA. The PFA is installed within the N_2 purged glovebox so that is can be shielded by the environment of the N_2 purged glovebox which serves to limit moisture ingress.

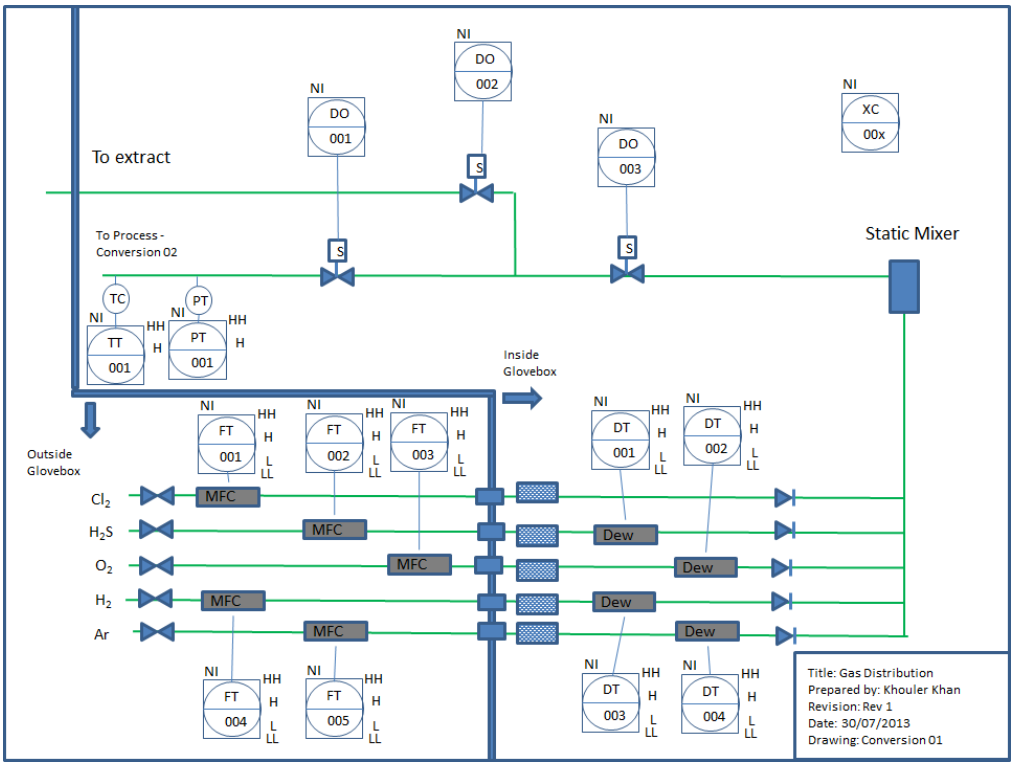

Figure 45 Schematic of gas distribution to the Horizontal RAP

After the check valves which are used such that the gasses are restricted from cross contaminating the other gas lines, the gasses are then passed through a static mixer to help mix the gasses. After the mixer, the gasses are passed through a block and bypass solenoid system. This system allows for bypass of the gas from the reactor or acts as a relief in an overpressure scenario. The open or closed state of these valves are set through a selection switch for

manual control or automatic control via the NI cRIO 9074 control program through DO001 to DO003 in Figure 45. After the valves, the pressure and temperature in the inlet tube to the reactor are monitored through PT001 and TT001 respectively. These are used to protect from over temperature and overpressure scenarios that can develop during processing. Wiring and layout diagrams for the instrumentation and controls in Figure 45 and Figure 49 are shown in Appendix D Figure 91 through Figure 101. Spare I/O has been left for future installation and development.

Basic Human Machine Interface (HMI) screens have been developed and are shown in Figure 46 and Figure 47. The HMI allows for easy monitoring of all the I/O both process and safety. One set of code was developed to run on the cRIO-9074 that would be hidden from the general users of the equipment. Another HMI was developed for installation on a laptop or on remote PCs where users would be able to monitor and set up experiments. In addition, alarm capability was implemented for corrosive and explosive gasses such as H_2S, Cl_2 and H_2. A sample of this code is shown for H_2S with a 10 ppm limit. The gas detection kit is manufactured by Bionics Inc. and supported in the UK by CS Clean Ltd. This kit was interfaced to the NI and Labview for executing safety shutdowns. This was an essential University of Southampton Health and Safety requirement to be satisfied if H_2S was to be used in Room 1063. The wiring diagram for the Gas Detection I/O is shown in Appendix D Figure 100. There are three gas detection boxes installed, two for the Horizontal Rap and one for the CVD. They monitor gasses both outside and inside the respective gloveboxes and general processing areas.

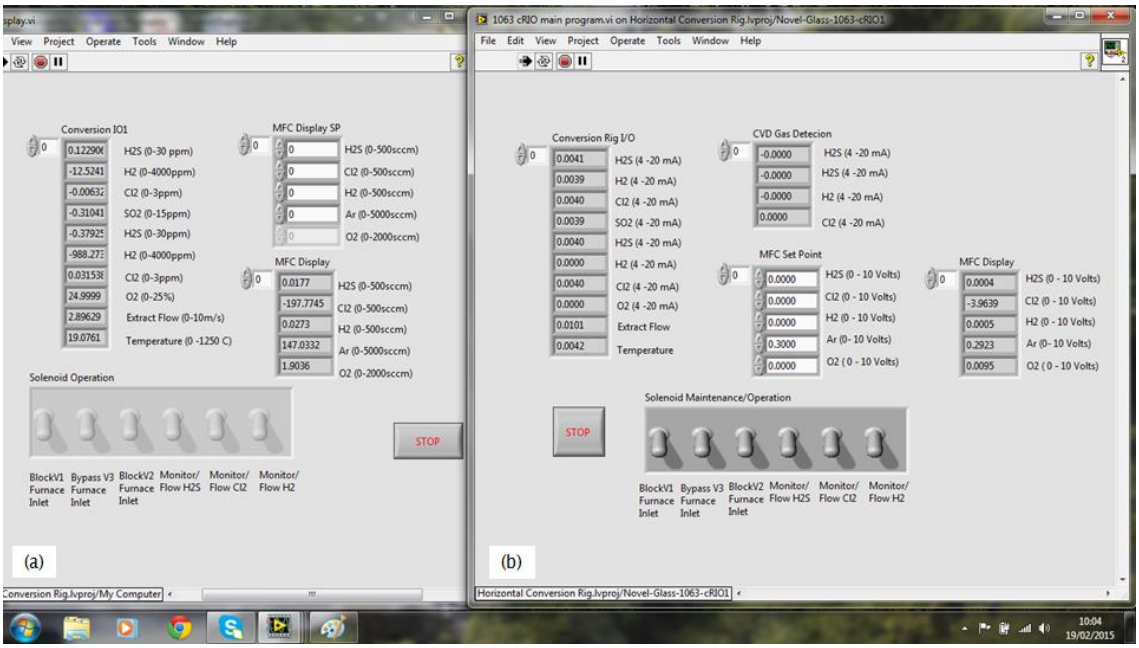

Figure 46 Two basic HMI screens (a) for users for interaction via Laptop or remotely (b) for programmers and experienced users

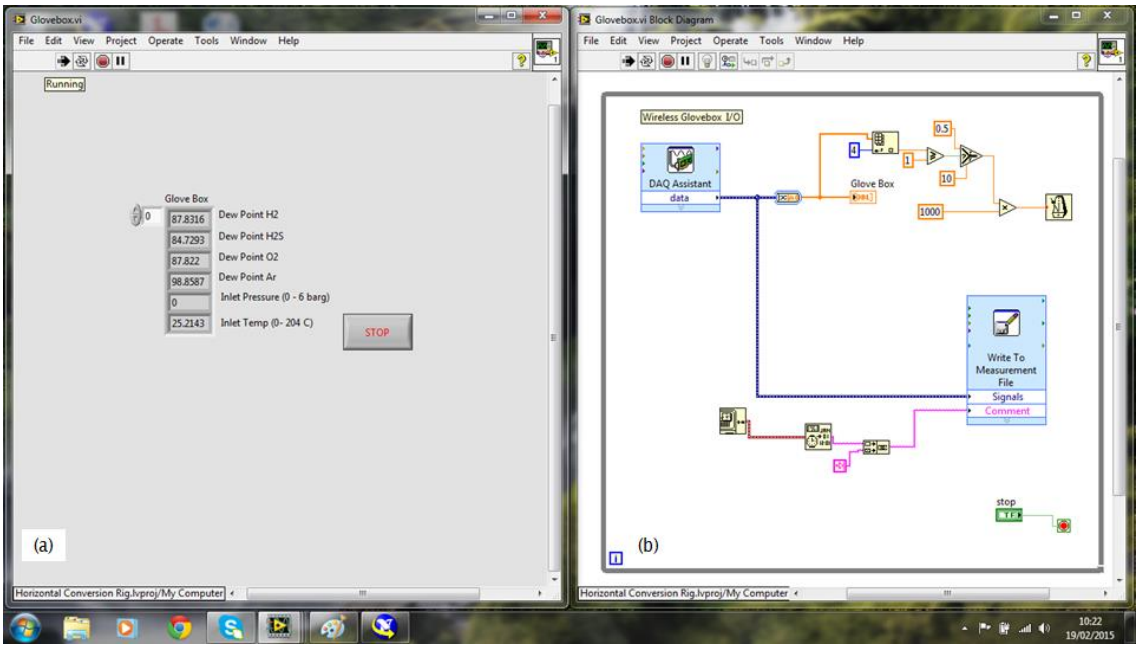

Figure 47 (a) Glovebox HMI and (b) Labview code with basic datalogging

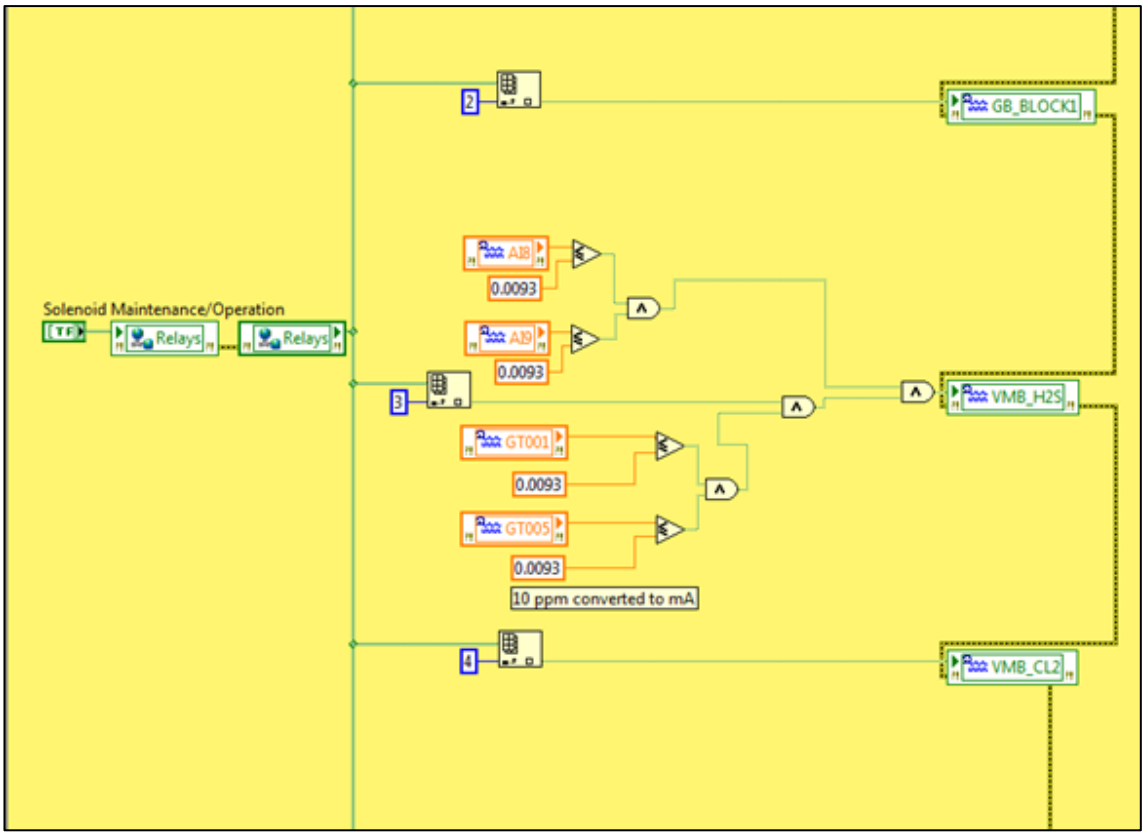

Figure 48 H_2S alarm code

For transfer between the reactor and the glovebox, a connection similar to the design of transfer ports in gloveboxes was manufactured in-house and is shown in Figure 50. The design allowed the crucible to be moved in and out of the glovebox via operation with one hand and without exposure to a non-controlled environment. It ensured that the 60mm tube can be inserted without contamination of the glovebox. The fitting was designed with two feed through inlets to allow for separating gasses or adding another measurement point/pressure relief port. The gas delivery tube can be fed through this fitting and into the reactor tube. At a temperature safe distance, it can be connected to a silica tube that can be inserted further into the silica tube to manipulate gas injection points and flow profile.

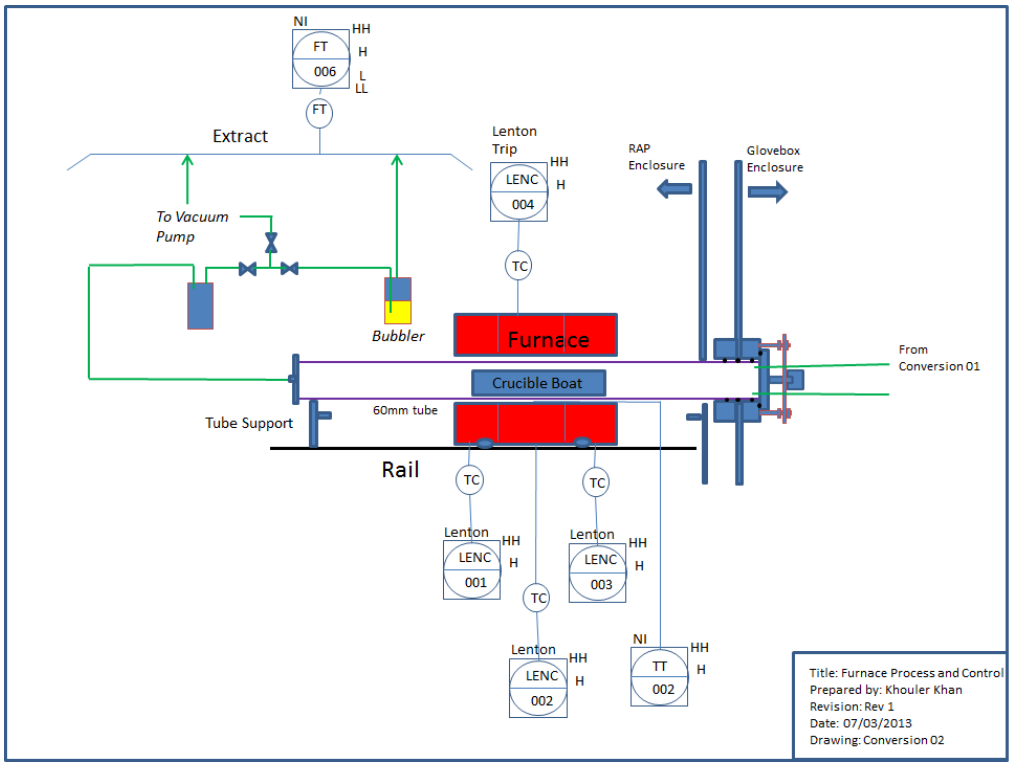

Figure 49 Schematic of the furnace enclosure

Figure 50 Transfer fitting developed as part of this work

Much of the focus in this thesis was the gas purification to the reactor tube. The Furnace was bought before the start of this work and hence automation was not considered. The furnace was bought with standard Eurothem controllers as depicted in Figure 49 by LENC 001 through LENC 003, the communication module was not included which could have been used to

integrate into the NI Hardware and Labview system. Time and budget constraints led to the implementation of a manual rail system which meant that the furnace had to be manually pushed for quenching the glass. In future, these processes will be integrated into the NI and Labview architecture which will allow recipes, complex control strategies and guarantee repeatable experiments that are datalogged.

4.3 System capability and understanding

While it is important to deliver high gas purity, it is also important to reduce the moisture and impurities in the reactor tube to levels where the effects of the purifier can be seen. Each new tube used is washed in a custom built HF tube cleaner supplied by Felcon and shown in Figure 51 of which a typical cleaning cycle is shown in Table 8. This procedure is also done after every use. If the tube is not dried properly, the delivery gas could become saturated with moisture from the reactor tube which will deteriorate the moisture removing capability of the gasses when the raw materials are being processed into the glass. It was found that the silica tube can be flame dried or baked when installed to a temperature above or near the reaction temperature. Baking at such high temperatures ensures that any components which are volatile below the baking temperature are removed including moisture.

Cleaning Step	Time
DI-Pre wash	10 mins
Drain	5 mins
HF wash	10 mins
Drain	10 mins
DI wash	60 mins
Drain	10 mins
N_2 dry	5 hours

Table 8 Tube cleaning procedure

Figure 51 Tube cleaner from Felcon showing a tube cleaning in progress

Not much emphasis was placed on the design of the outlet of the silica reactor tube. Design of RAP systems have evolved from using burners to burn of the outlet gasses to the use of bubblers as more complex gas scrubbing units have been installed. The bubbler acts as a back pressure controller as well as a shield between the process reactor and the extract environment in the case of back diffusion and flow reversal. The back pressure is controlled by a dual bubbler system as shown in Figure 49. The empty bubbler protects against flow reversal due to a loss of extract and the pressure within the furnace tube falling below atmospheric pressure. Care must be taken in selecting the length of the insertion tubes otherwise bubbler liquid can find its way into the reactor.

A simple bubbler calculation was performed to understand the pressure drop the outlet as follows. Density of silicone is 971 kg/m3, extract pressure is 60 Pa however the exhaust tube will be subject to a higher pressure depending on how far it is inserted into the extract tube. The hydrostatic pressure developed by the silicone oil can be calculated as follows:

$$H_p = h \times \rho \times g \quad (15)$$

Where

H_p – Hydrostatic Pressure, Pa

h- height of liquid from the meniscus to the inlet nozzle, m

ρ – density of silicone oil, 971 kg/m^3 @ 25 ˚C

g- gravity, 9.81m/s^2

Therefore if h is 0.03mm, the hydrostatic pressure is 285 Pa which is 2.85 mBar. This implies that the Horizontal RAP runs at a low vacuum which may help in impurity removal as well as no bubbles forming in the glass.

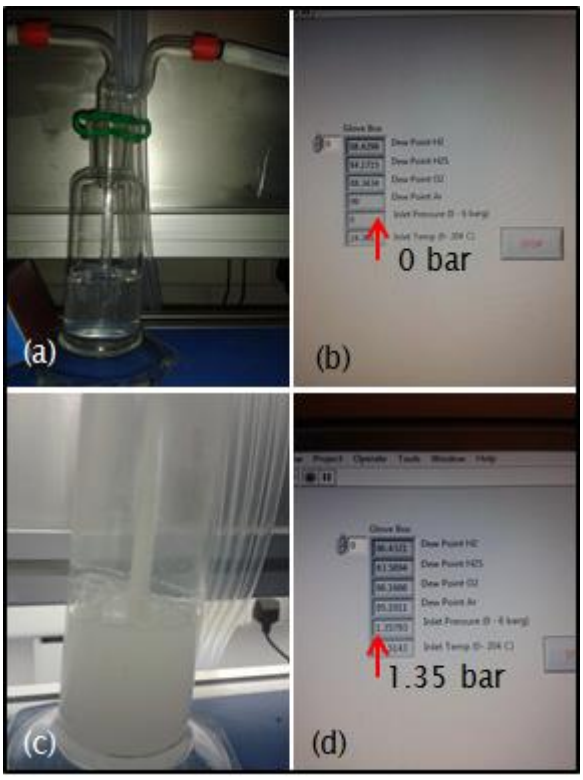

Figure 52 Bubbler and pressure reading during two events (a/b) is a clean bubbler and (c/d) at the end of a conversion of Ga to Ga_xS_y

Figure 52 shows the bubbler before and after a run where Ga is converted to Ga_xS_y. In some cases the bubbler or the outlet tubing can become impeded leading to a pressure increase or the bubbler pressure can change as it becomes contaminated with outgassed or converted material that has been produced as a result of the process. In the particular case in Figure 52 the H_2S

is cracked at high temperature as is the case in the Claus process leading to the deposition of sulphur at the outlet of the furnace which may have resulted in restriction of the outlet tube and hence the pressure build-up. With pressure being monitored, the appropriate safety steps can be taken. For example the block and bypass valves at the inlet to the reactor can be set such that it vents the tube to extract on the inlet side. It is imperative that the height of the bubbler liquid be recorded for each experiment as this can change the operating pressure in the reactor tube which can have an effect on purity as mentioned before.

With the improved purification system in place, a series of experiments was developed to determine the limits of the implemented system and requirements for future development. The experimental process typically involved the following steps:

1) Tube cleaning followed by further drying by flame torch and baking at 1000˚C.
2) Batching Lorad and GWI Raw Materials into a PFA bottle and sealing with a tape in the Inert Gas Glovebox.
3) Removal of the PFA bottle and placing on a roller for 24 hours to mix the powder.
4) Transfer of the mixed powder into the vitreous carbon crucibles.
5) Insertion of the crucible into the silica reactor tube and into the Furnace hotzone.
6) A baking cycle typically greater than 100 ˚C for 24 hours.
7) Increasing temperature to the melt temperature of 1150 ˚C for 24 hours followed by quenching.

The plot of the absorption is shown in Figure 53 for this typical procedure. The baking temperature in this case was 400 ˚C. Using the specific absorption of OH as before, the moisture content was estimated to be 0.608ppm. The moisture content in the gas delivery at -99C was calculated for a 48 hour period as 0.696 ppm which is in good agreement to the OH peak estimation from the FTIR. It suggests that there may be a close correlation to the gas purity delivery and the OH in the glasses however contribution from previous processing of the raw material should not be ignored.

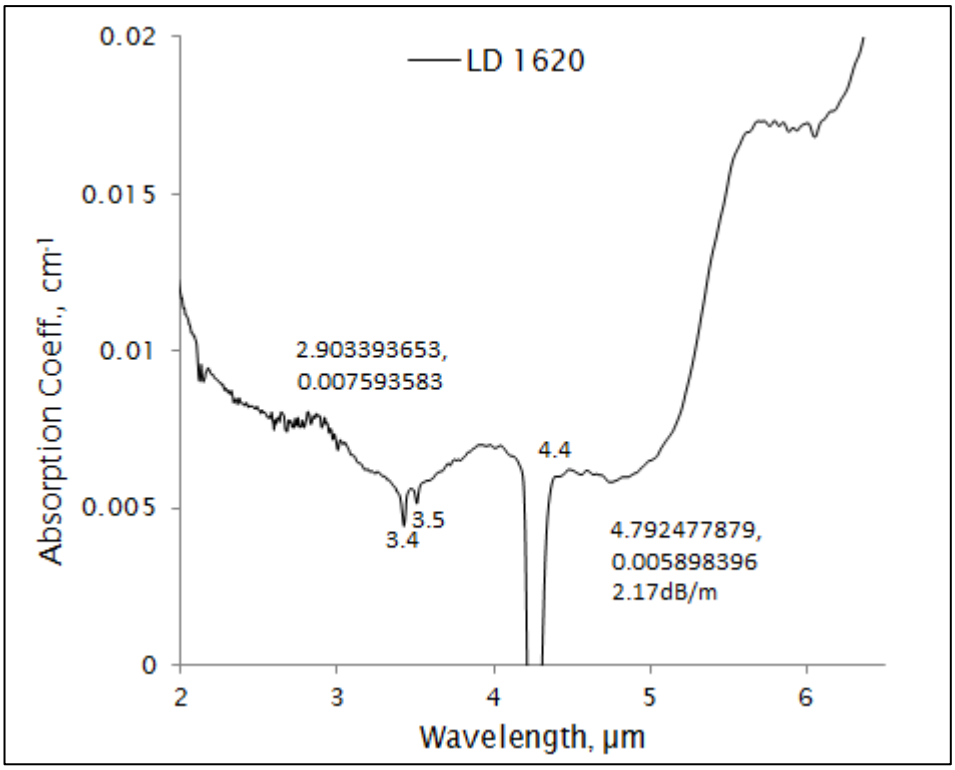

Figure 53 Absorption spectra of LD1620

On observing a melt or conversion, it is observed there is build-up of material on the outlet tube past the furnace and sometimes on the inlet before the furnace as shown in Figure 54. The build-up on the inlet does not always happen and may occur if the tube and o-rings are not securely fitted to the fitting on the glovebox. Pressure and leak testing procedures are being developed to test whether it is as a result of leaks, convection currents due to turbulent flow or due to the position of inlet gas injection. Modelling the reactor in COMSOL would be useful in solving these problem and is a suggestion for future research.

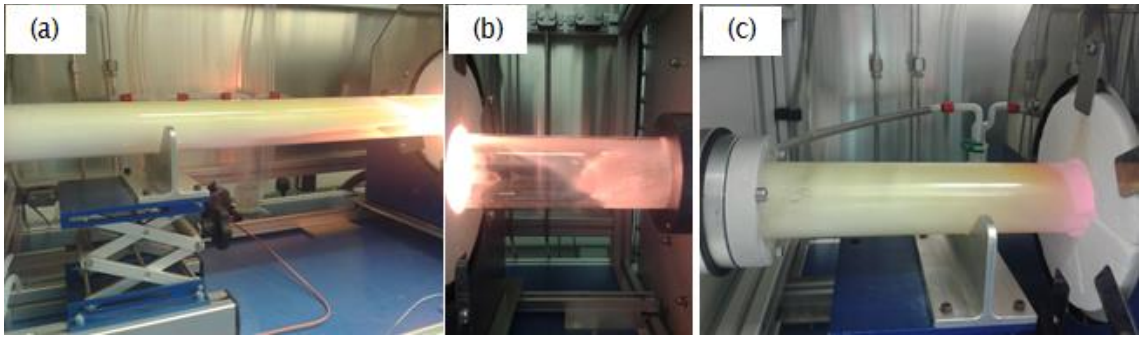

Figure 54 (a) Build-up at the outlet and (b) Inlet build-up of material during a run, also (c) shows the position of the furnace in the quench position

The furnace is moved for quenching and involves shifting the furnace towards the outlet where the material is deposited. This material can be thermally agitated by the hot but rapidly cooling furnace which can cause the material to be deposited into the cooling melt against the inlet flow due to bubbler restrictions. Observing the top of the glass after melting confirmed this as particles of non-glass material could be seen on top of the melt. In the past the furnace was kept in place and a rod inserted to push the crucible out of the hotzone for quenching. Whether or not it was pushed to the inlet or outlet is unclear as this problem was not mentioned in [25]. In an attempt to circumvent this problem a torch was used to remove as much material from the outlet before quenching and the sequence of deposition and cleaning is shown in Figure 57. The absorption curve for this glass is shown in Figure 56. GDMS as recorded in Appendix B, Table 10 confirmed that the glass had slightly more impurities for LD1537 which was quenched to the left while LD1538 was quenched to the right towards the clean inlet. However it was noted that striations in the glass was worse for the quench to the right. Striations are observed in all the glass samples to varying degree but in the quench to the right case it was notably worse. Experiments are being developed to ascertain the source of these striations. Two factors could be the cause, gas flow (turbulent as opposed to laminar) coupled with uneven cooling or vibration while moving the furnace during the quench process. Uneven cooling is as a result of the furnace location to the melt when quenching as shown in Figure 55. LOT-QD has been approached and an agreement is in place for loan of a thermal imaging kit to study cooling effect while quenching as future work. Due to physical space, the cooling furnace is close to either side of the sample depending on the direction of quench movement. As a result this will affect the temperature profile across the glass during quenching which can affect the absorption as discussed in Chapter 2. In the quench to the right experiment, the melt is close to the restricted outlet and hence the flow is expected to be more turbulent which leads to the increased striations. The effect of these striations on the absorption curves have not been studied and are another key area for future research directions.

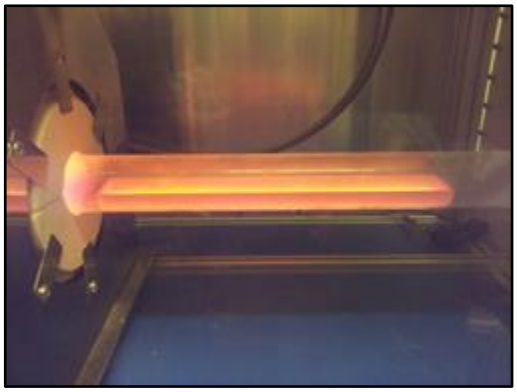

Figure 55 Location of quenching furnace in relation to the melt

In another experiment the tube at the outlet was cleaned multiple times before quenching. This deposition and cleaning cycle process is captured in Figure 57. Figure 57a shows the start of build-up of material at the outlet occurring at 200˚C. Figure 57b shows the outlet tube after cleaning with the high temperature hand torch. The cleaning process became more difficult at the higher temperature and was only carried out for short periods due to the heat as well as safety concerns of damaging the tube or overpressure. The material could be seen moving from the tube surface towards the bubbler so care was taken to not move the torch vigorously to remove too much material at a time which can lead to a blockage of the outlet causing an overpressure. Figure 57 c through Figure 57l show the remaining build-up and cleaning steps as well as the change in colour of the material being deposited in the outlet tube. The moisture level remained the same however there was a significant change in the shape of the absorption curve in the 3-5μm region which benefits the FLITES project. The loss was less than 1dB/m with the minimum loss occurring at 4.7 μm which has not been achieved in the ORC previously in bulk sample to my knowledge.

The observed effect may be that the exhaust material contains extrinsic impurities in this region and was back diffused into the glass during the quench cycle. In future this material will be collected and analysed in an attempt to understand the material being removed.

New furnace design for incorporation with NI control are being reviewed and discussed for future installation. This new furnace should accommodate higher melt temperatures as the current furnace is limited to 1200 ˚C and is therefore being overexerted. This causes failure of thermocouples and the furnace

struggling to reach and control temperature. Higher temperature would mean a larger furnace and space to quench would become an issue. One suggestion is to design the furnace such that it can be moved radially away from the tube which may solve most of the problems described above.

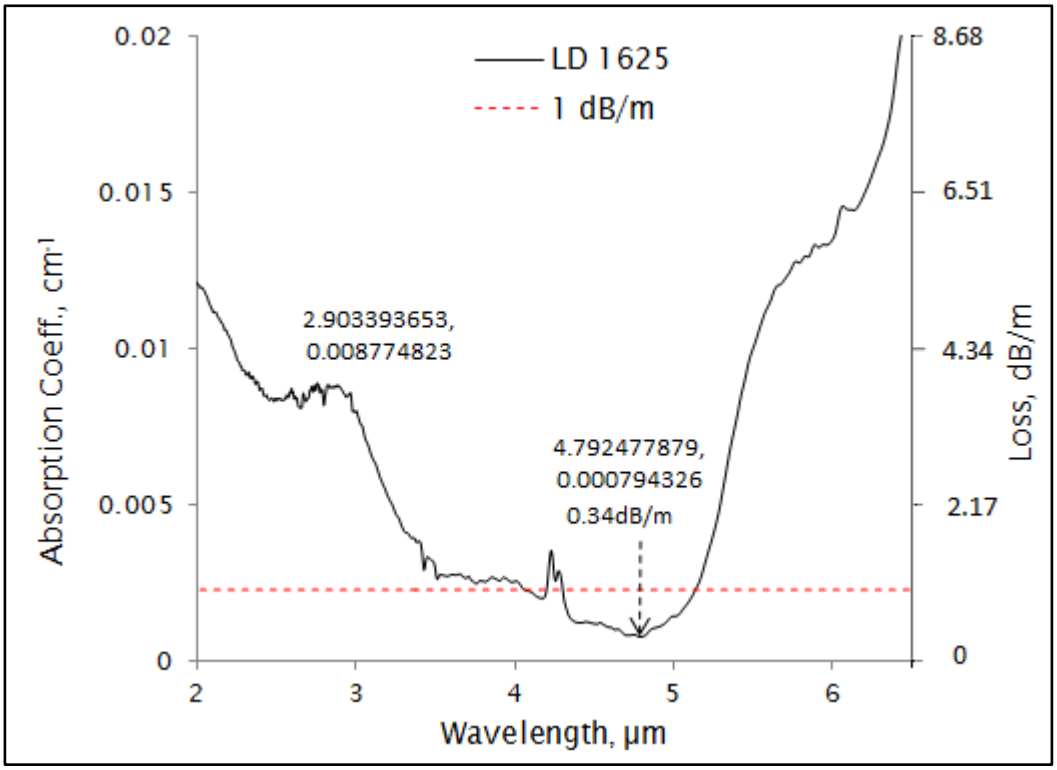

Figure 56 Absorption spectra of LD1625

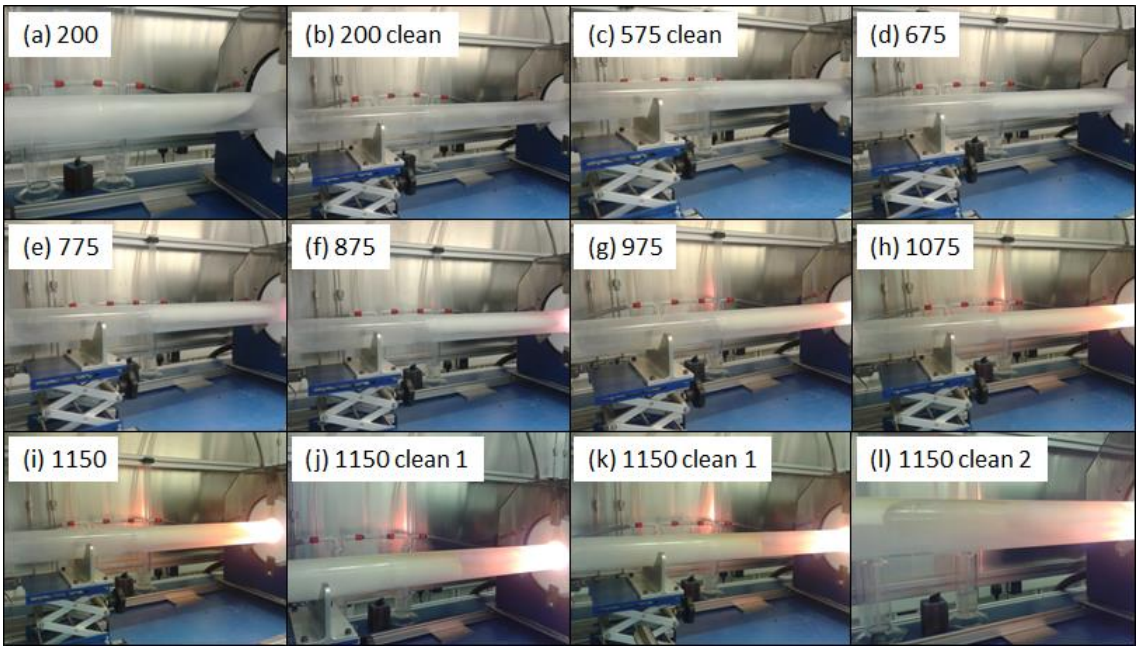

Figure 57 GLS melt cycle with the addition of flame cleaning the outlet tube, (a) through (l) shows the temperature and whether or not the picture is taken after a cleaning with the use of a hand torch.

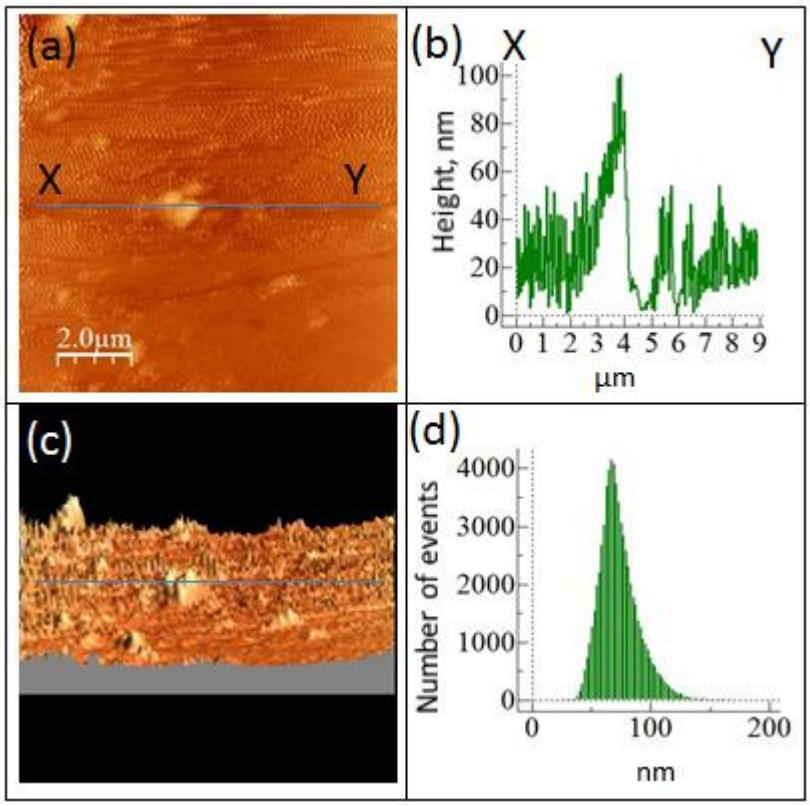

Figure 58 (a) Shows a 2D top view of LD1625's surface, (b) shows the depth profile along the line XY (c) Shows the 3D profile of the surface and (d) shows a

histogram of the height roughness across the surface which is approximately 10μm^2.

In attempts to draw fibre, it was noticed that surface crystallization occurred. On observation the polished rods were seen to have embedded material form on the surface which was not as a result of the melt process. An AFM measurement was done on LD 1625 and another polished GLS sample from before 2005 as shown in Figure 58 and Figure 59 respectively. The varying degree of roughness of the polished is clearly shown. Both samples have been polished by Crystran Ltd. implying that their polishing process has changed since 2005. This is another future research direction to be explored whereby which various polishing specification is performed to determine how they contribute to scattering losses at the surface. Inclusions of particle of this size are detrimental to losses in fibres as studied in [25]. As mentioned in [25], using equations in Chapter 2, "*just 10 particles per metre intersecting the core will give a total loss of > 3dB/m from scattering centres alone.*" For the FLITES project, fibre with loss less than 1dB/m is required and hence the polishing process needs to be improved.

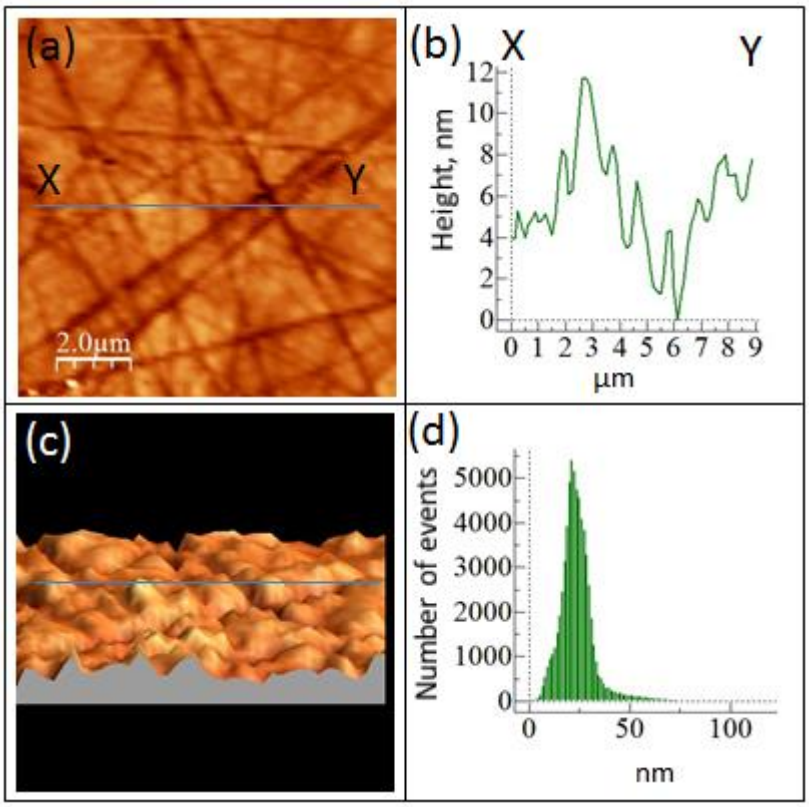

Figure 59 (a) Shows a 2D top view of Old GLS sample surface, (b) shows the depth profile along the line XY (c) Shows the 3D profile of the surface and (d)

shows a histogram of the height roughness across the surface which is approximately 10μm^2.

Some other experiments were carried out using H_2S and H_2 gasses. In these experiments H_2S and H_2 were used to substitute the Ar gas during the 24 hour drying process. The results for H_2S and H_2 are shown in Figure 60 and Figure 61. These gases have higher moisture content and it can be seen in these absorption curves. The H_2 is least purified and it shows in the result. In the future it may be better to use the 6%H_2/Ar lines in the ORC instead of investing into H_2 purification. It should be noted that the sample dried with H_2 was yellow in colour suggesting that hydrogen passivation in the glass network reduced the visible light wavelength cut-off. It was also noted that small particles existed in the glass sample, in which case the H_2 may have reduced certain impurities or glass network elements. While these experiments were just simple experiments done to test the gas supply, the results raise interesting directions for future research especially addressing the difference in the shape of the absorption peak at 6.3 μm.

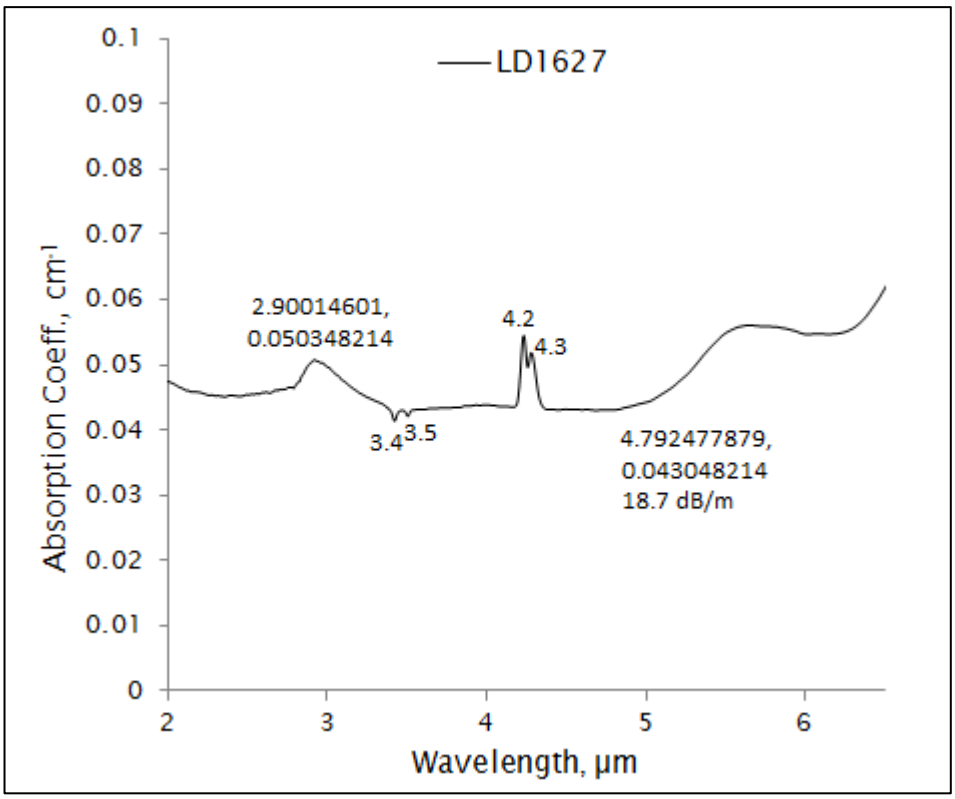

Figure 60 Absorption spectra of LD1627

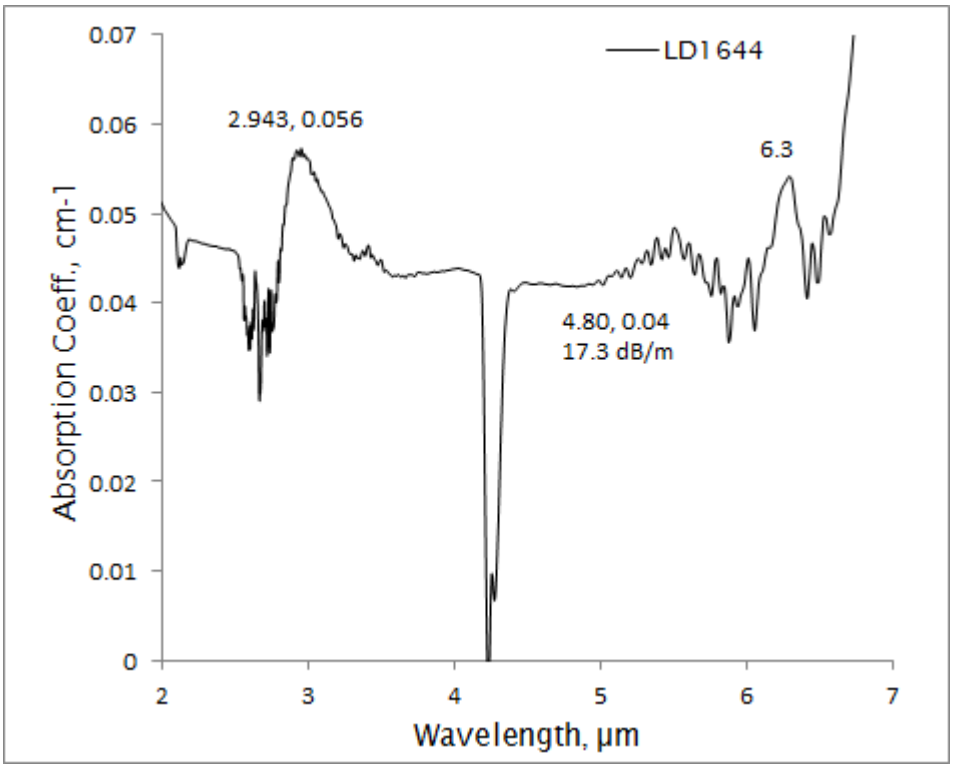

Figure 61 Absorption spectra of LD1644

H_2S was also used to test the systems conversion capability. Using past experimental run sheets, H_2S was reacted with Ga to form Ga_xS_y at 965˚C. The result of this conversion process is shown in Figure 62.

Figure 62 GAC2, conversion of Ga metal to Ga_xS_y

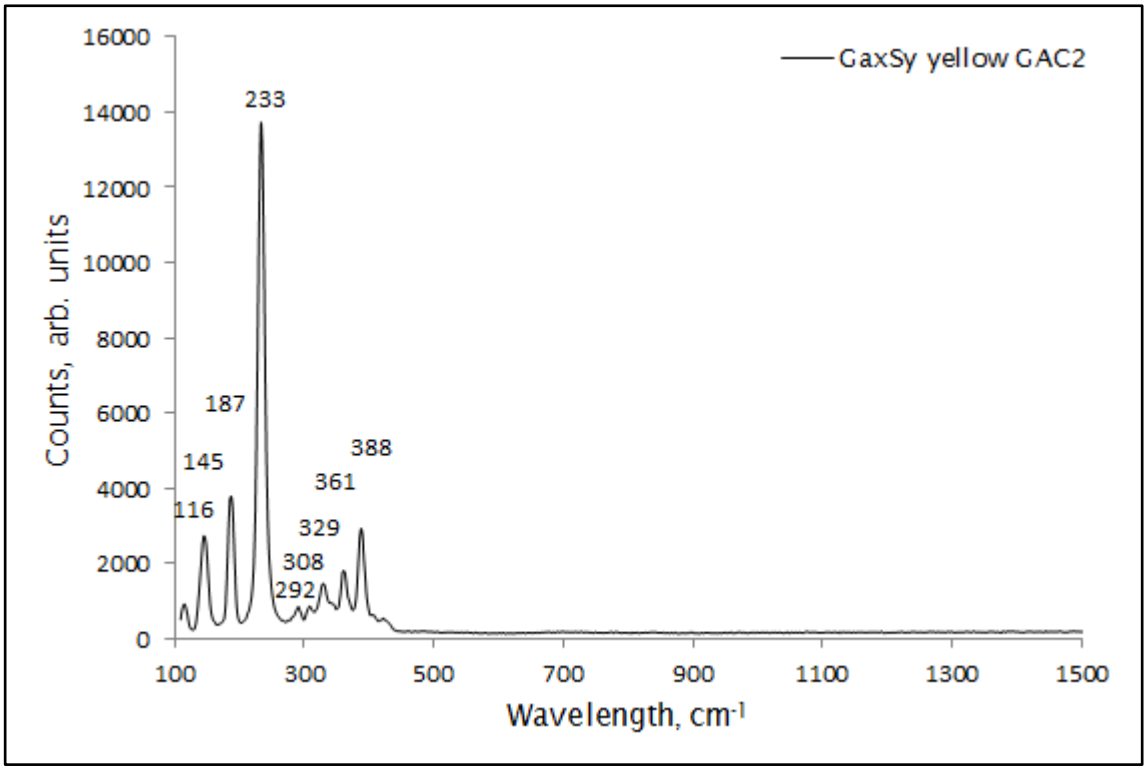

Figure 63 Raman of in-house Ga_xS_y not in contact with crucible wall using 532nm laser

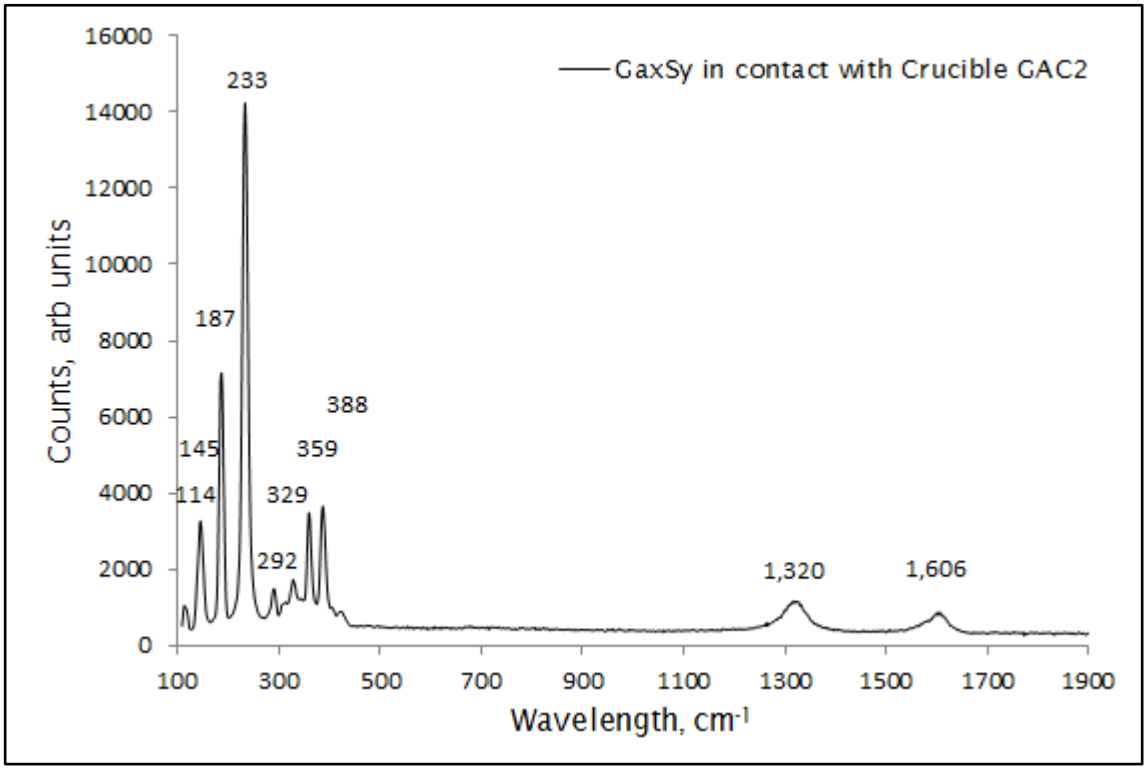

Figure 64 Raman of in- house Ga_xS_y on a sample which was in contact with vitreous coated carbon crucible using 532nm laser

Raman of the GAC2 sample made in-house was used to compare to the Raman od Ga_2S_3 supplied commercially by GWI as well as the literature. The peaks compare favourably and are listed in **Error! Reference source not found.**. It should be noted that in this experiment a vitreous coated crucible was used and the material in contact with the crucible wall contained carbon as per the D and G peak as shown in Figure 64 and listed in **Error! Reference source not found.**.The next step is to optimize the process, as well as get GDMS done to compare to the raw materials produced in the past and also commercially as in Appendix B, Table 10. Future experiments can involve changing the crucible material to silica and vitreous carbon as well as varying, controlling and optimizing experimental conditions such as flow, temperature and duration of conversion. With Silica, reaction of the Ga to form gallium oxide is a major concern. It may be easier to perform post processing to remove carbon as it is more volatile than that of oxide materials.

Peak, cm-1	Material/Reference
117, 143, 148, 236, 284, 308, 330, 343, 369, 389, 407, 424, 485, 569, 740, 868	GWI, Figure 30.
148, 234, 288, 330, 388	α-Ga_2S_3 from [67]
119, 135, 148, 238, 392.4	Ga-S_2, S-Ga_2, Ga-S_2, Ga-S from [68], Authors did not identify peaks around 300cm^{-1}
116,145,187,233,292,308,329,361,388	GAC2 Canary yellow not in contact with crucible wall, Figure 63
114,145,187,233,292,329,359,388,1320,1606	GAC2 black surface in contact with vitreous coated crucible wall, Figure 64
1320, 1606	D and G peak Carbon [69]
145, 171, 200, 345, 417, 768	β-Ga_2O_3 [67]
Many peaks, see reference as some peaks may be as a result of the slide.	α and β SiO_2 – quartz[59]

Table 9 Raman peaks for Ga_2S_3 and observed in the literature and raw materials

4.4 Conclusion

A horizontal RAP system has been designed, built, commissioned and tested. The system is now operational with safety and automation systems in place. Various experiments have been completed to understand and provide a baseline for the system. Focus has been on improving the gas delivery and procedures. Impurity removal within the 3- 5μm region has also been the focus because of the FLITES project. Conversion of raw material has commenced using H_2S.

The lowest loss achieved is 0.34dB/m at 4.79 μm for LD1625, Figure 56 and was as a result of gas purification and improved procedure which involved the cleaning of the outlet tube before quenching. Without the cleaning of the outlet tube, the loss is 2.17 dB/m for LD1620, Figure 53 at the same wavelength. The OH peak is not considerably different between LD1625 and LD1620 with a recorded loss being 3.8 dB/m at 2.9μm. The quantity of OH in the glass is estimated to be 0.6 ppm using the specific absorption coefficient and the FTIR curves. The quantity of OH calculated from the gas delivery is 0.7 ppm using the dew point meter information. While comparable, this minimum may not be solely due to the gas delivery and may still be as a result of procedure in tube cleaning. Additional experiments such as vacuum baking and a dew point with a better measurement range will aid in resolving the OH contributing mechanism.

The use of H_2S in the synthesis of LD 1627, Figure 60 and H_2 for LD1644, Figure 61 increase the hydrogen content in the reactor. This increase is from lower OH removal purifier capability, cracking of H_2S at higher temperatures or flowing hydrogen gas on its own. The increased hydrogen can lead to increase in OH as hydrogen bond with any oxygen in the material or reactor and is shown by the increase in the loss at 2.9μm in Figure 60 and Figure 61 when compared with Figure 53 or Figure 56. The loss is greater than 20dB/m and is comparable to the loss recorded in the past in [24] and shown in Figure 5. Since H_2S is required for conversion and H_2 necessary for O_2 removal, a vacuum baking step pre and post raw material and glass synthesis at a suitably determined temperature may be the best option. Cl_2 may be used to remove hydrogen but the moisture removal from purifiers is still not as good as those for Ar purifiers as shown in Figure 36.

The system will require improvements as theoretical limits have still not been achieved. The GDMS data of the raw materials made in the past compared to the materials used in this thesis have been summarized in Appendix B, Table 10 and Table 11. With the current system capability as well as the improvements in raw materials possible, it is expected that future research will lead to losses closer to the theoretical limits. The possible future directions development of this equipment through various experiments is outlined in Chapter 6.

Chapter 5: Chemical Vapor Deposition

CVD is mainly used for thin film work and involves the formation of a thin film on a substrate material by a chemical reaction of vapour phase precursors. There are many variations to the technique based on the mechanism promoting the reaction. The reactions can be promoted by heat (thermal CVD), higher frequency radiation such as UV (photo-assisted CVD) or plasma (plasma-enhanced CVD (PECVD), each having their own advantages [70]. The CVD process is well established in making high purity bulk silica preforms and was the main impetus in making high purity silica preforms for fibre manufacturing commercially viable. However the technique has not been translated to the manufacturing of high purity chalcogenide preforms to date. In the following we will review literature on CVD and present a CVD method for manufacture of high purity chalcogenides.

5.1 CVD literature review

Limited literature can be found on whether or not scaling of CVD for bulk chalcogenide manufacture is feasible. In one of the few, the authors indicate that CVD of chalocogenides have been unsuccessful [1], but there is no conclusive evidence in [1] or other referenced literature [71] to support this. In the following sections, a review of the existing literature is giving in an attempt to understand the limitations.

5.1.1 Vapor deposition non ORC

In [71] the method explored was a PECVD technique as shown in Figure 65a. This technique was chosen because it was reported to have higher growth rates and high chemical conversion efficiency for silica fiber preforms at the time over modified CVD. The experimental setup used a RF generator (2 Mhz, 1.5kW) to create a plasma of argon ions in a quartz reaction tube evacuated by a rotary pump via a liquid nitrogen trap. The argon also acts as a carrier gas to move the precursors into the reactive plasma zone where they decompose and react to form a glass deposit. The glass deposits on the cooler quartz tube wall as a result of thermophoresis. For design of the system, the effect of the RF operational frequency must be considered as this affects the RF coupling

efficiency and hence the deposition rate. The RF operational frequency also determines the plasma skin depth which determines the diameter of the quartz tube to be used. Optimizing the RF frequency with a laminar flow rate to match the tube diameter, can achieve a more efficient deposition. At the time PECVD was used for growth rates of a few $gmin^{-1}$ with high conversion efficiency of silica. The growth rate (not published in the paper) of their prototype system was limited by the RF generator being a 1.5kW unit. The authors concluded that they could increase the deposition rate appreciably by using a more powerful RF source.

In their follow up work in [72], the authors upgraded to a special 3MHz generator capable of delivering 15 kW designed by Stanelco Products Ltd. In [71] the authors discussed the operation of different pressure regimes, temperature and increasing reaction concentrations on the deposition rate. They also experimented with Helium instead of argon as they expected to have a more laminar gas flow with less natural convection which allowed them to achieve plasma at higher pressures. The author's inferred a deposition rate of 13 μm/min. The authors conclusions are as follows:

Despite the large number of absorption bands in most samples, which can be traced to deficiencies in gas lines and impurities in carrier gas, we believe that PECVD is a promising method for growing thick layers of chalcogenide glasses. Low pressure plasma is a unique way of producing glass directly on the substrate that allows conventional collapsing and fiber drawing if a tube with the correct thermal expansion coefficient is used. High pressure plasma enables higher deposition rates to be reached but requires subsequent remelting of the sooty deposit, and fibers made from this process might use a separate melting stage. The range of compositions and the number of refractive index modifiers that might be incorporated seem less limiting than with a melting process, which suggests that the high pressure plasma route to fibers loses some advantages. We obtained our best results with Ge -S, which readily forms a stable glass.[72]

Figure 65b shows another set-up [73] which uses the CVD process to deposit between two tube restrictions which are then collapsed to form a sealed ampoule. The glass is then melted and annealed in resistive furnaces. Deposition rate was approximately 23mg/min from interpretation of the data

presented. It should be noted that some material was lost at the other end of the evacuated tube. The thickness of the glass samples made were several hundred μm's.

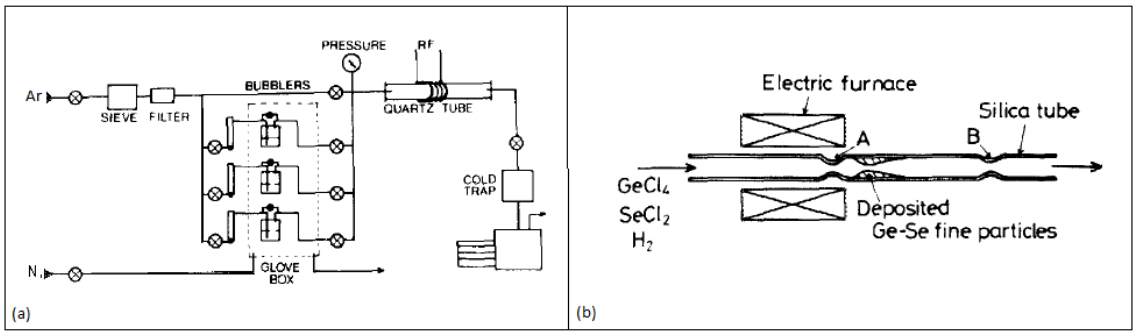

Figure 65 Schematic of apparatus for Si-O and GeSe PECVD (From Blanc, D., et al., J. of Non-Cryst. Solids, 77: p. 1129-1132, 1985. With Permission) [71]. (b) Set-up for chemical vapor deposition. A and B are neck parts used for sealing off and separating (From Katsuyama, T., et al., J. of Applied Physics, 59(5): p. 1446-1449, 1986. With Permission) [73].

It is difficult to determine the current development of the systems above and to my knowledge CVD was not developed further for making bulk chalcogenides via these systems. However at the ORC a CVD system was developed as detailed in [15]. The interest in [15] is the use of CVD to make bulk chalcogenide and the initial experiments in the pursuit of making a bulk preform. In the following section, a review of this system and work in [15] is summarized.

5.1.2 Vapor deposition at ORC

Prior to 2005 work done by Chung Che Huang, Chapter 6 in [15], involved developing a thermal CVD system which was used for deposition of GeS_2 thin films and is shown in Figure 66 [15]. The system consisted of filtered gasses of H_2S (supply purity 99.5%) and Ar (supply purity 99.95%) controlled by MFCs. The Ar is connected to a bubbler containing the precursor (in this case $GeCl_4$ of purity 99.9999%). The Ar is used to transport the precursor to a mixing chamber where it mixes with the H_2S before delivery to a tube furnace which houses a substrate where the film is to be deposited. The exhaust of the system is connected through a series of bubblers to an extract.

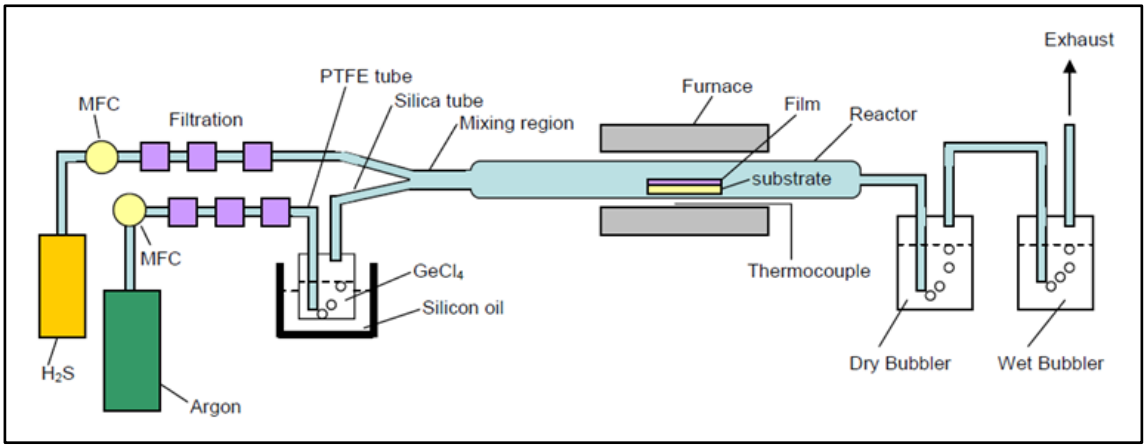

Figure 66 Thermal CVD system (From Huang C., University of Southampton Thesis [15], 2005. With Permission)

Also discussed in [15] are the rate limiting steps to the deposition rate, thermodynamics for feasibility of reaction, hot and cold wall CVD, different precursors and gas purity. However, of greater importance in [15], was the experimental attempts made on achieving CVD of bulk GeS. It was noticed upon removing the substrate, material deposits on the inside of the tube within the furnace and the extract meaning that although the deposition of the film is on the order of tens of μm per hour, there is a lot of uncollected material that is lost in the outlet section.

This material was collected with an estimated 50% efficiency in an apparatus shown in Figure 67 and re-melted in a furnace. The resulting glass was cut and polished by Crystran Ltd and is shown along with the transmission spectrum in Figure 68. The absorption bands at 2.8um, 4 um and 7.5 um are attributed to O-H, S-H and Ge-O respectively.

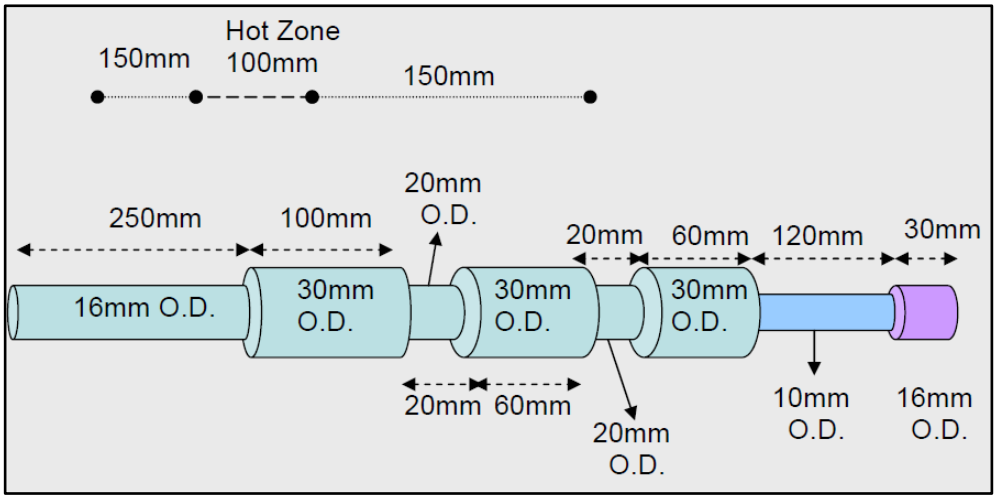

Figure 67 CVD Bulk glass collection apparatus (From Huang C., University of Southampton Thesis [15], 2005. With Permission)

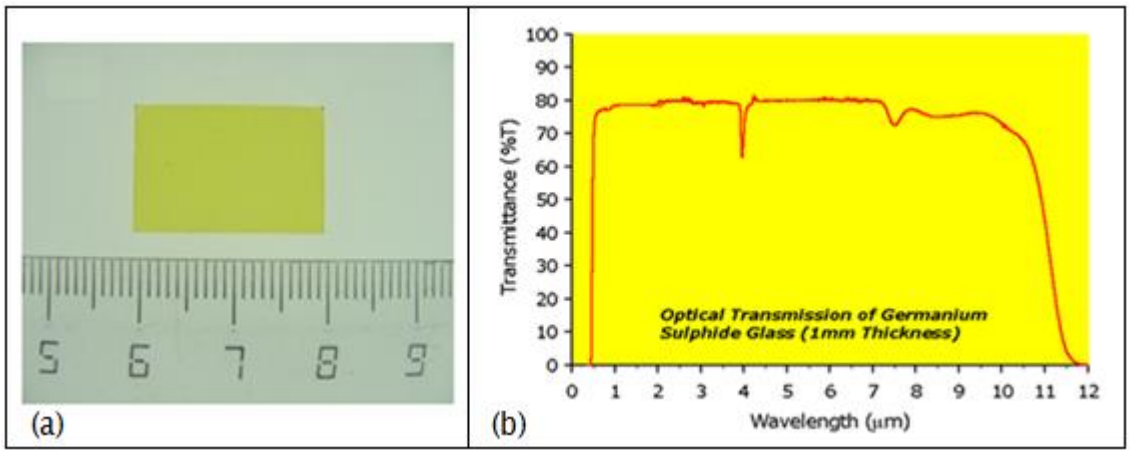

Figure 68(a) GeS bulk glass 20mm x12mmx1mm, (b) transmission spectra (From Huang C., University of Southampton Thesis [15], 2005. With Permission)

The CVD collection apparatus employed was made of silica and had dimensions as shown in Figure 67. The absorption losses are very high and are attributed to ingress of moisture and oxygen from the collection glassware and in [15], the author suggested the use of Heraeus F300 quartz tube with an extremely low OH level, < 1ppm). The absorption results corrected for reflection losses and thickness is shown in Figure 69. The difference in the 430 dB/m loss in the 1mm and the 200dB/m in the 2.7mm is suggested to be as a result of the relative error used in estimating the reflectivity.

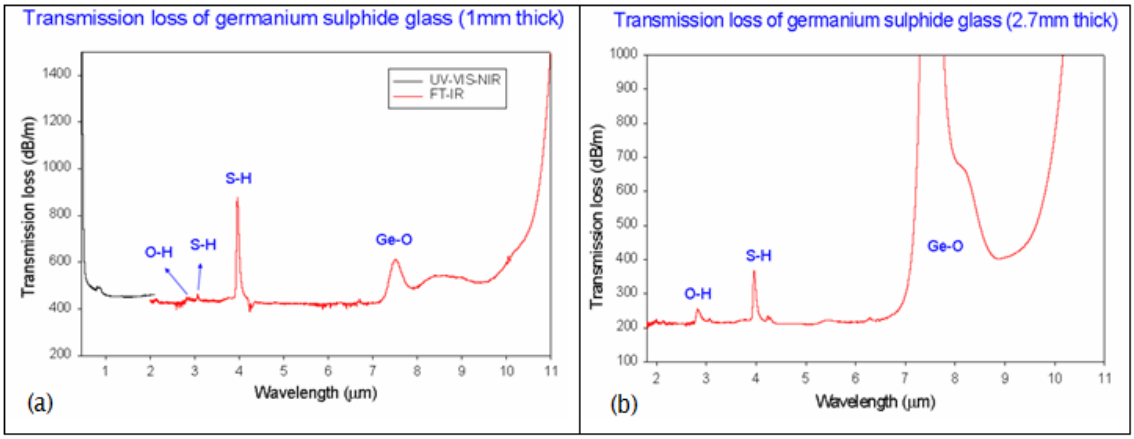

Figure 69 GeS absorption loss for (a) 1mm thick sample and (b) 2.7 mm thick sample (From Huang C., University of Southampton Thesis [15], 2005. With Permission)

With the purification system used as well as the higher purity ampoule, the losses seem to be higher than expected. As the procedure for cleaning, drying and sealing the ampoule was not detailed, it is hard to discern the magnitude of this contribution which is very important from the analysis presented in Chapter 4. Also, the parts of the GDMS detailed in [15] did not show any anomalies however the full sweep of elements was not presented. This system did not exist at the start of this work and therefore the results could not be confirmed. To allow for any reasonable comparison to the result in Chapter 4, a thick and thin sample would be preferable as detailed in Chapter 2.

On review of the current CVD apparatus installed before the start of the work in this thesis, it was decided to initially redevelop the installed system and make improvements to the collection efficiency and purity as is detailed in the following section.

5.2 CVD results and analysis

In this section, the capability of CVD for making bulk glass and fibre is presented.

5.2.1 CVD for bulk Glass

The first set of experiments was designed to understand the deposition characteristics of the CVD system. The system differed from that discussed in [15] as H_2S was generated by a reaction between FeS and HCl. This limits the control of H_2S to the reactor and hence the duration of the experiment. Also there existed no automation and safety systems so the experiments had to be manually observed and could not be left unattended. Figure 70 shows the experimental setup showing the temperature in each zone of the furnace for experiment 1. A porous silica disk with pore sizes of 40 – 100 μm was used in an attempt to increase the collection. The disk cannot be placed in a zone that is close to room temperature as it would be more easily blocked. It was noticed that due to thermophoresis, powder was not deposited in the hotzone of 825˚C and the particles generated was less than 40μm. Deposition occurred at the lower temperature inlet and outlet as show in Figure 70. The deposition at the inlet meant that there could be pressure changes introduced by the porous disk and combination with the temperature profile may have resulted in a counter flow causing back deposition.

Experiment was repeated with the only changes made to the furnace temperature settings as shown in Figure 71. Deposition still occurred at the inlet but this time powder was collected in the chamber.

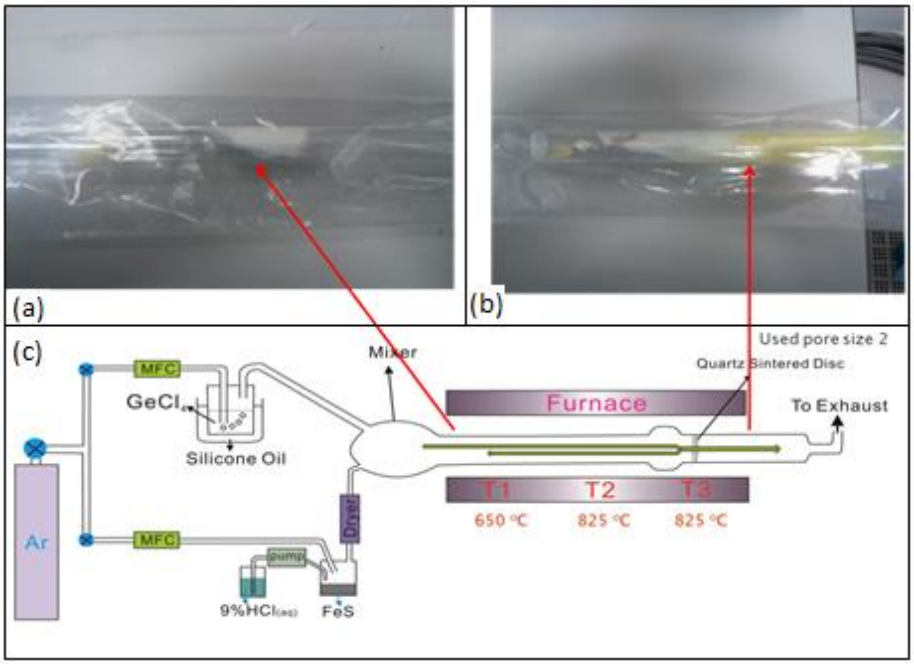

Figure 70 Experiment 1 showing the first attempt at depositing GeS (a) shows that there was a convection flow causing deposit of material at the inlet of the furnace (b) deposition at the outlet of the furnace (c) the experimental setup showing the set temperature in the three zones of the furnace.

It was concluded that the collection method in experiment 1 and 2 was not suitable for further development as the amount of powder collected was too small a quantity to make bulk glass. Also the risk of plugging and overpressure was a major concern as well as sealing the chamber for melting into a glass.

In experiment 3 a crucible was inserted into the tube instead of the expanded bubble. A change of the inlet temperature was chosen to maximize powder generation using previous run sheets as well as changing the temperature in the middle zone in an attempt to decrease convection currents. The results and experiment setup is shown in Figure 72. The result showed that there was still deposition at the inlet. The crucible was not fixed into the outer silica as it was thought that it could be removed and used as a crucible for fibre drawing. However the glass seal did not stop deposition occurring on the outside of the crucible. Safety concerns meant that fibre drawing via the crucible method was not possible.

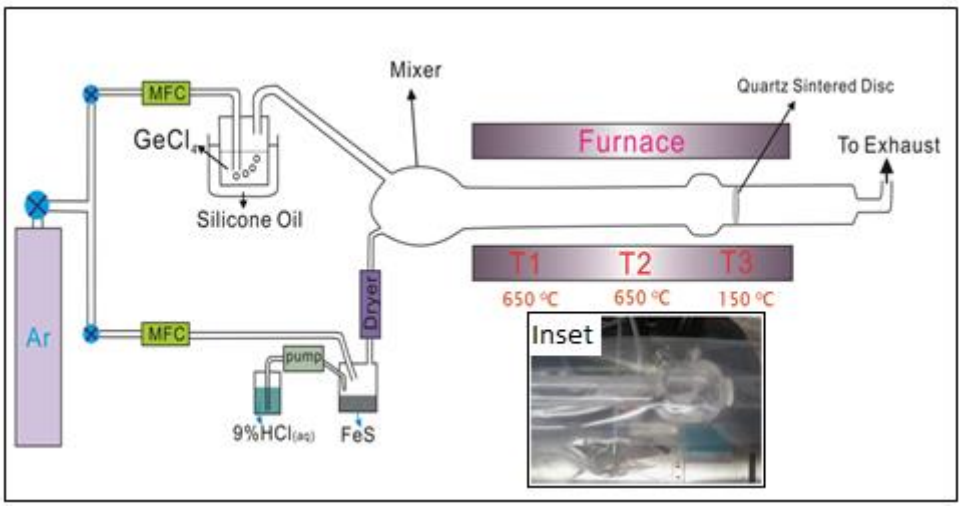

Figure 71 Experiment 2 showing the second attempt at depositing GeS with a different furnace temperature profile in the three zones. The Inset shows the deposition is within the specified collection bubble.

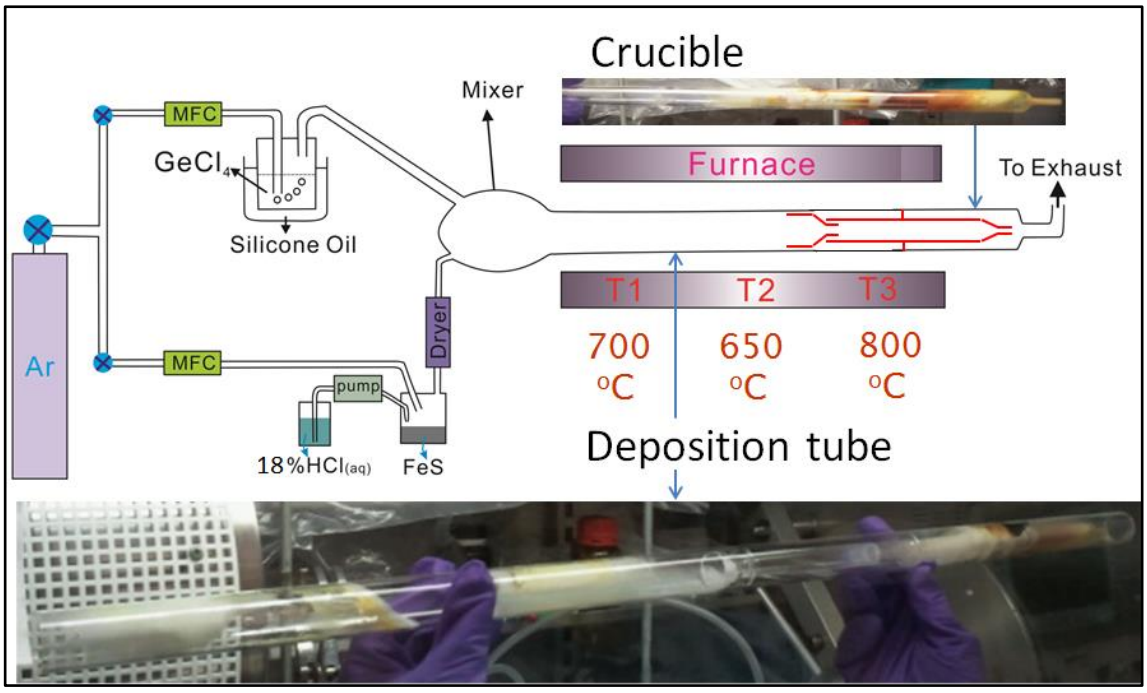

Figure 72 Experiment 3 Inserting a inner tube as a collection apparatus

The outlet of the silica tube is connected to extract via a PFA tube and various fittings. It was observed during these experiments that the PFA tubes had a lot of powder build-up meaning that a lot of the powder was still not being collected optimally. This build-up of powder can cause variations in the pressures between experiments and lead to different deposition conditions.

However since more powder was deposited in the outlet area than in the silica tube, it was decided to leave the temperature of the three zones consistent at or around 700˚C and make a collection apparatus at the outlet of the furnace.

The first attempt involved the modification of a commercially bought PFA bottle which acted like a gravity separator [74]. The results of this experiment 4 shown in Figure 73. The outlet tube beyond the collection apparatus had visibly less build-up of powder. The powder proved difficult to remove from the bottle as well as weigh accurately due to the depth of the bottle as well as the buoyancy of the powder in the glovebox inert gas atmosphere. Since transfer of the powder at this stage would add a step where purity is compromised as well as a heating step required after collection to form the final glass, the PFA bottle was not a viable collection apparatus.

The use of a silica glassware design instead of the PFA bottle was chosen which would allow for sealing and melting of the powder that require higher temperatures than the PFA could withstand. The apparatus for this experiment 5 is shown in Figure 74. Figure 74b shows the powder buildup on the wall of the silica glassware. In the bottom section of the glassware as shown in Figure 74c, the powder can be seen to grow upwards across a gap of 1cm. Powder was still depositing at the outlet tube beyond the glass apparatus and some of it could be shaken back into the collection section of the glass apparatus. It was concluded that all of the powder was still not being collected. The change in the glassware weight was recorded indicating that approximately 1.5g of powder was collected in a 2 hour run.

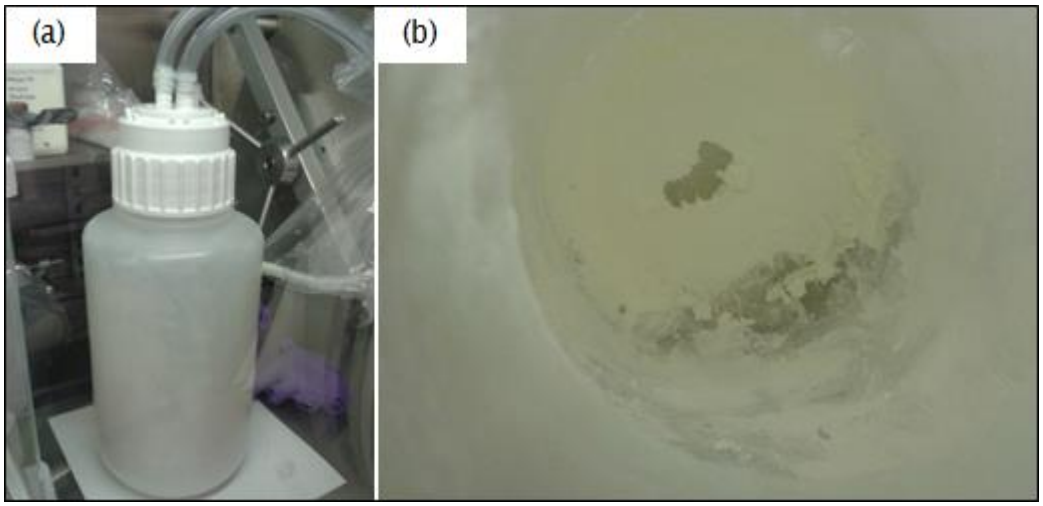

Figure 73 Experiment 4 Modified PFA bottle connected at the outlet of the CVD reactor tube.

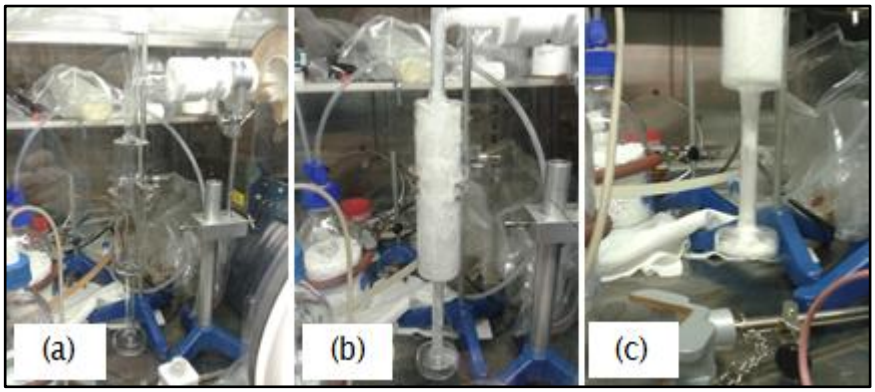

Figure 74 Experiment 5 Silica glassware connected to the outlet of the CVD reactor tube (a) before experiment (b) during experiment (c) showing the growth

The powder was still getting past the porous disc and gravity separation apparatus in experiment 4 and experiment 5. Also it was able to get past a bubbler by being transported in the bubbles generated by the bubbler. The powder generated was analysed to determine its size and therefore a suitable separation mechanism. If it was less than 0.1μm, the upward forces from the gas flow will make separation difficult and collection apparatus design more complicated. An SEM image was taken of some of the collected powder and is shown in Figure 75. This shows that the powder generated is sub 0.1 μm size.

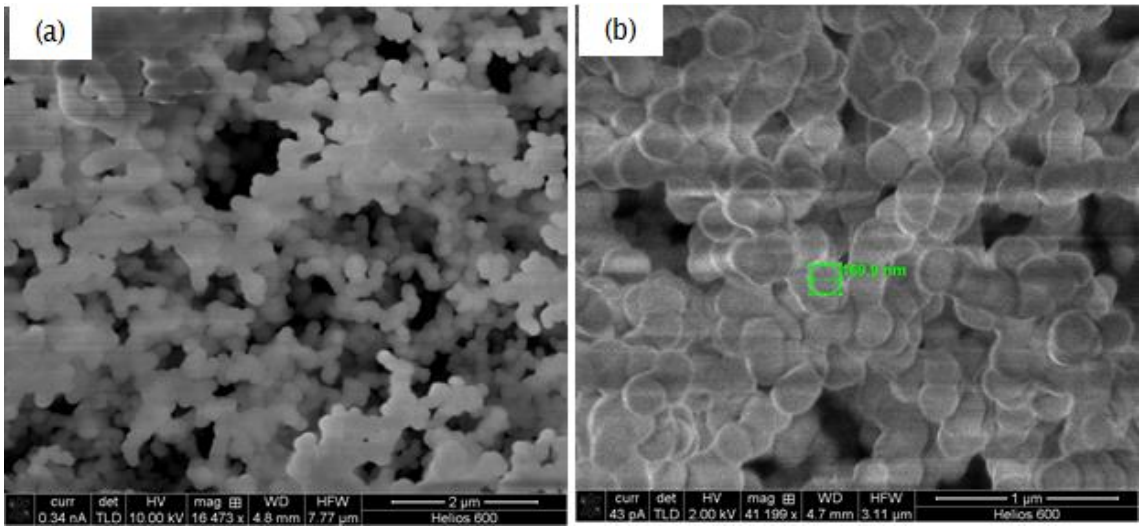

Figure 75 (a) and (b), SEM images of GeS powder at different magnifications, in (b) show a size marker on the order of 169.9nm.

Raman spectroscopy has been carried on the powder samples and is shown in Figure 76. The peaks are confirmed in [75, 76] which study the composition relationship of these peaks. The peaks at 340cm^{-1} and 367 cm^{-1} are attributed to the GeS_4 tetrahedra bond stretching. The peak at 430cm^{-1} is attributed to the S-S chains between the GeS_4 tetrahedra. The small peak at 256cm^{-1} is attributed to ethanelike S_3Ge-Ge-S_3 units. The peaks below 210cm-1 can be attributed to vibrations in the S_8 rings. From the literature of Ge_xS_{1-x} glasses and thin films, the composition with the raman alludes to powder composition very close to GeS_2.

From the initial results, the following approach was taken:

1) Change from generating H_2S from FeS by upgrading and installing H_2S to room 1063 as done in Chapter 4. This allowed longer experiment durations but also required automatic and safety systems to be implemented.

2) Improve Ar gas supply purity to the CVD reactor as described in Chapter 4. The Ar is used as a carrier gas and hence its purity will directly affect the deposited material purity. This could be one of the factors leading to the high losses in Figure 69.

3) Design a collection apparatus based on the learnings from experiments in Figure 70 through Figure 74.

4) Injection tubes designed to keep gasses separated only until with the reaction temperature zone. This ensures that reaction and mixing is taken at a known temperature and hence variation in powder composition should be minimized.

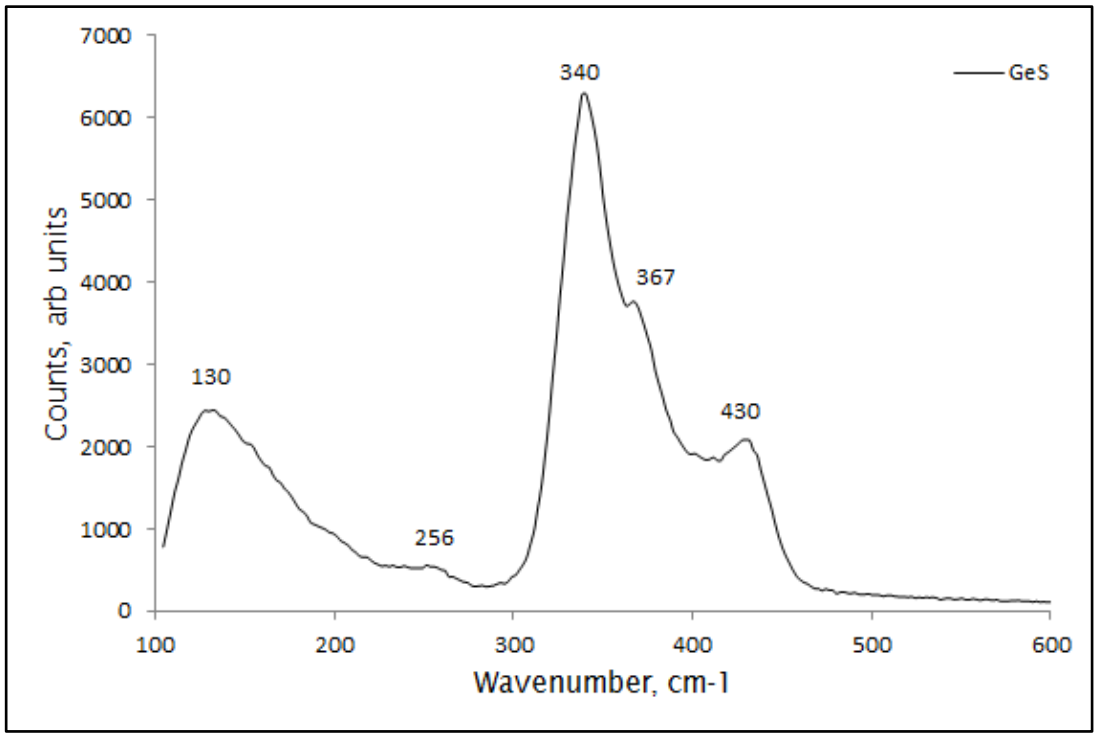

Figure 76 Typical GeS raman spectra obtained using 532nm laser

It is believed that the key to collection design apparatus should utilize the following:

1) Surface area for deposition.
2) Build-up of powder between the 1cm gap.
3) Gravity separation while inducing agglomeration of particle.
4) That the powder does not stick easily to PFA.
5) A collection chamber that allows for sealing and melting and also some form of centrifugal separation.
6) The apparatus should also not have any sections that could be easily be blocked by the powder causing overpressure. Causing restriction can

cause increases in pressure and hence a decrease in flow rate of precursors and hence variability in deposition rate.

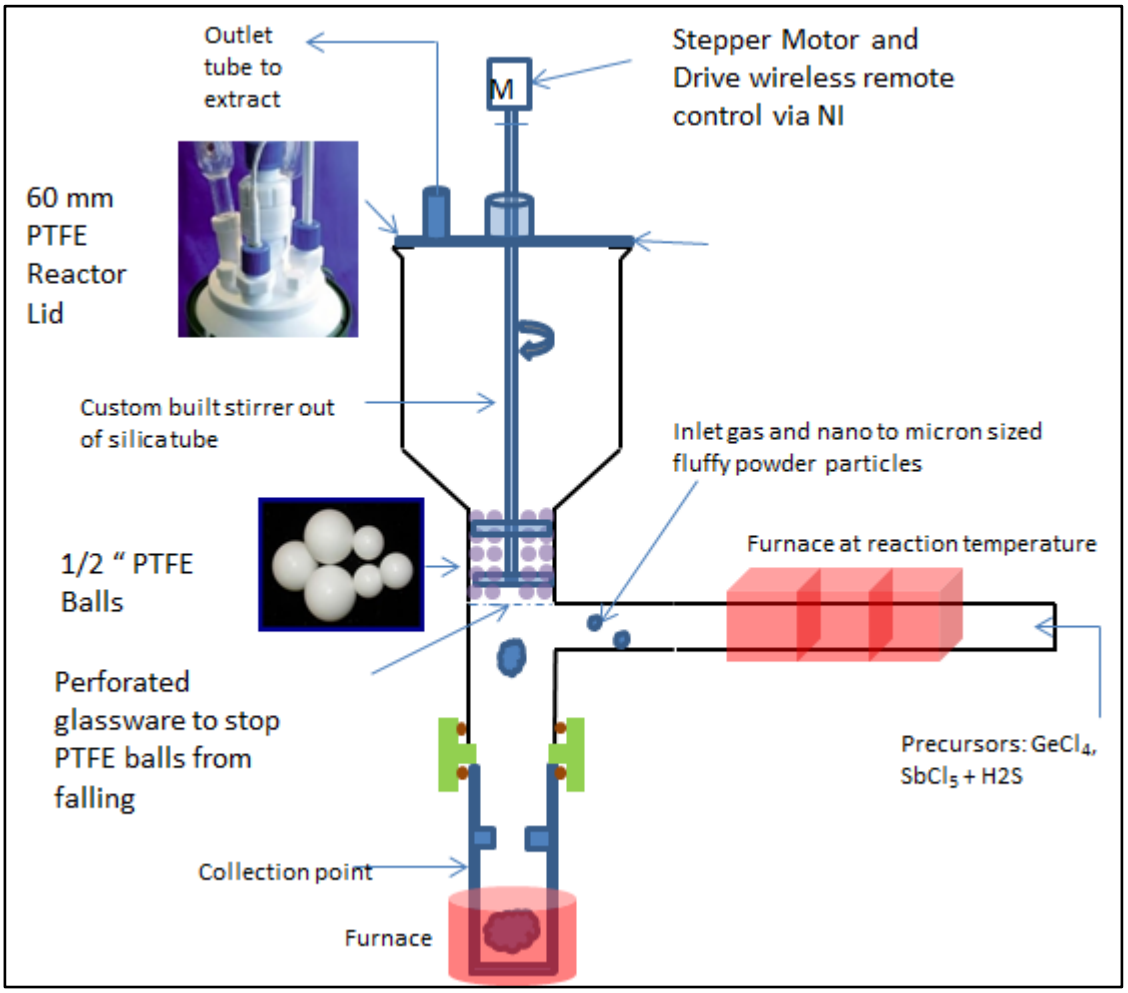

Figure 77 CVD bulk glass collection apparatus version 1

Two variations of the design apparatus from utilizing the learnings above are shown in Figure 77 and Figure 78. Figure 78 inset shows the constructed apparatus which has to be installed. The proposed operation is such that the powder can be deposited on the cage structure or the surface of the PFA balls. The stirrer will either break the powder growing on the cage structure or PFA balls. It is believed that constant rotating of the PFA balls will ensure that blockage at this section does not occur. The bottom section where the powder collects can be designed as an ampoule which can later be sealed and melted. In another scenario, the collection chamber can be designed such that it acts as a crucible for crucible fibre drawing. The motor controls have been implemented and all that is left is for connection and commissioning within the CVD glovebox in Room 1063.

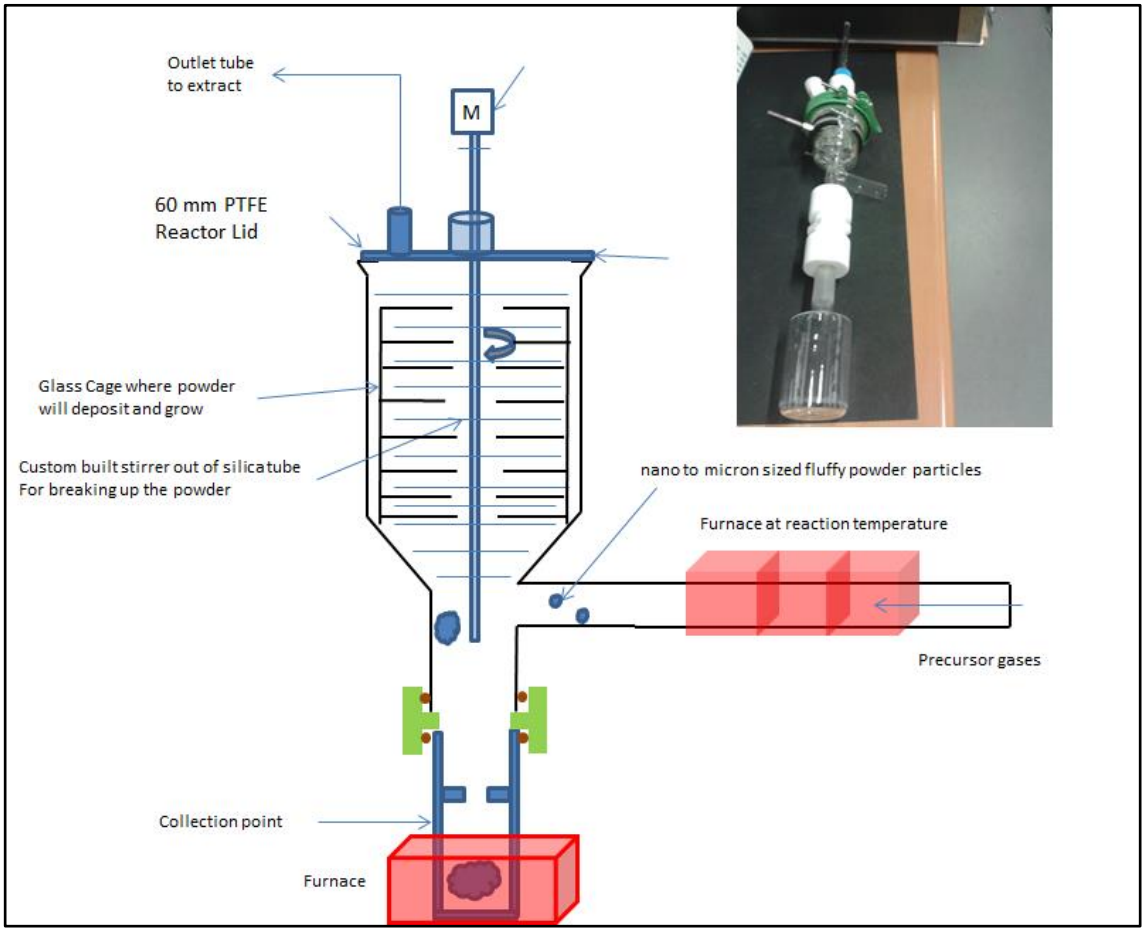

Figure 78 CVD bulk glass apparatus version 2, Inset showing the actual apparatus constructed.

At the time of writing this thesis, the apparatus was built with the glasswork done by the scientific glass blowers at the Chemistry department in the University of Southampton. The details of making the apparatus is covered in [77]. It is to be commissioned and installed in the second half of 2015 for experimentation.

Other areas for improvement identified for the CVD system is the installation of MFCs that integrate bubbler technology which provide continuous flow of precursor gasses. Other automation and controls need to be implemented before longer runs can be made safe. This at least includes pressure control and pressure relief devices. Gas detection and shutoff on detection of H_2S leaks have been implemented.

5.2.2 CVD for fibre

Collection of powder to be melted into glass is one option. It still suffers from the need for many additional steps before it can be formed into a fibre. These additional steps such as cutting and polishing as well as extrusion can lead to additional contamination. Applying techniques similar to the fabrication of silica preform was evaluated for application to a chalcogenide version within the existing facility. The existing facility is not ideal as the furnace is a large three zone furnace as opposed to a silica preform installation where a burner is traversed along a rotating tube changing the deposition zone while building up layer by layer of soot. To achieve such a setup, one would require a suitable tube with thermal and mechanical properties as the deposited material. In silica preform fabrication, the reactor tube is silica which can be obtained in high purity and bulk tube form. For chalcogenides a hollow tube of such dimensions is not readily available. Also the tube in the silica system does not require installation in an inert atmosphere which would be the case for a chalcogenide system. A traversing RF coil may be the best solution to be implemented. Other experiments have been adapted to the current CVD setup which has provided some initial results which show promise for this idea. At first it was thought that a small layer can be built up and then the tube collapsed under vacuum and drawn into a fibre. However suitable cladding glassware was not readily available and therefore experiments for developing the best coating conditions was done.

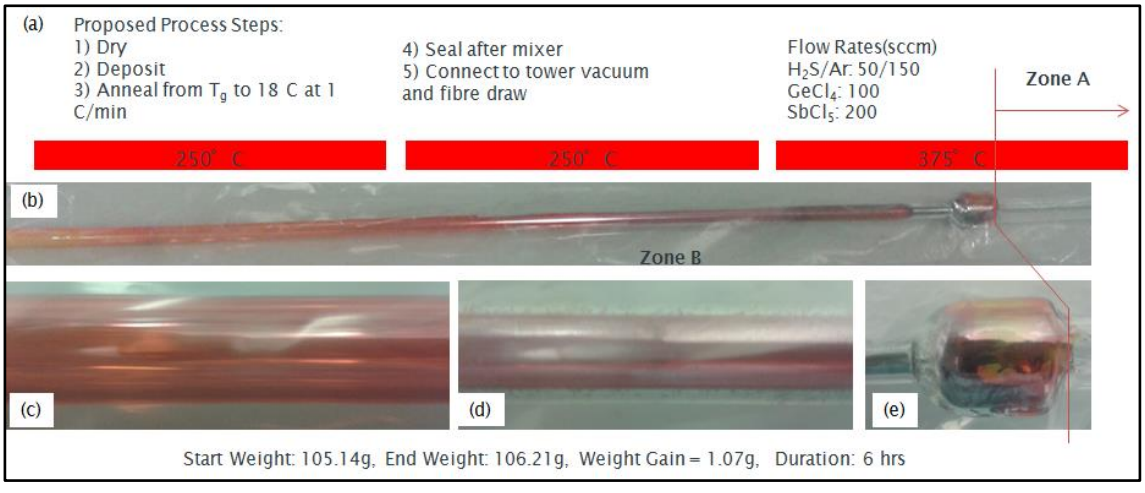

Figure 79 CVD fibre drawing depostion stage result showing (a) depsotion steps and process conditions (b) deposition apparatus (c) deposition at the

outlet of the apparatus (d) deposition at centre of the apparatus and (e) deposition at the inlet mixing area

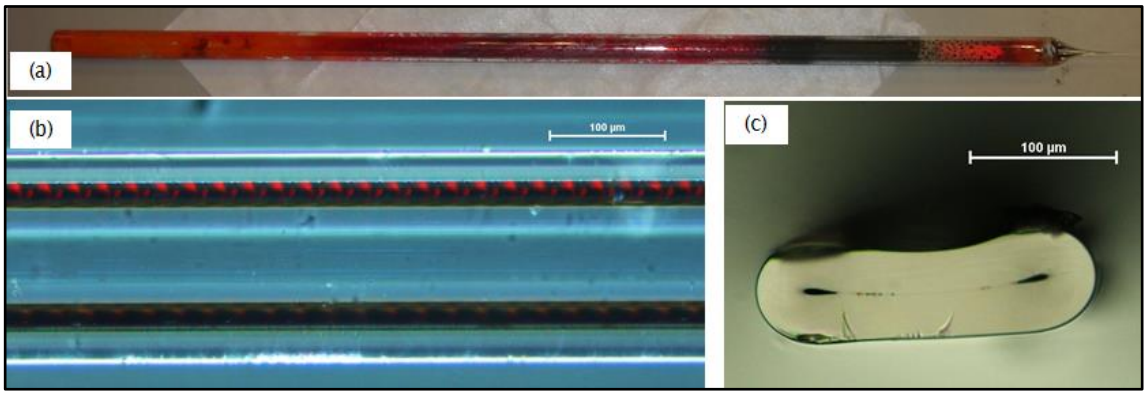

Figure 80 CVD fibre drawing fibre drawing result (a) Tube after collapsing and drawing on the fiber tower (b) Optical microscope image of the drawn fiber showing the dual core (c) optical microscope of the cross section of the fiber after cleaving

Figure 79 shows the experimental conditions and results for coating a borosilicate tube with GeSbS. The setup involved a tube with three separate inlets which are kept separate until they reach into the hotzone where they are mixed in a small chamber and accelerated through a small restriction towards the deposition zone. This experiment has also been repeated with sodalime glass instead of the borosilicate glass. While the glassware is mismatched for fibre drawing, an attempt was still made to draw into a fibre of which the results are shown in Figure 80. From these experiments, an idea has been developed in which the tube can be high purity silica which can then be used as a crucible for fibre drawing after deposition. After depositing the material, the inlet restriction can be sealed and with the tube held vertically under vacuum, the glass can be melted towards the sealed section. The silica glassware can then be cut and polished to form a nozzle and with the application of pressure at the top of the tube, crucible drawing can be accomplished. To increase the surface area in the deposited zones, cut tubes of smaller diameters can be inserted to increase surface area for depositing material. The results are promising and future work can involve either method as follows;

1) Developing a cladding glass tube through extrusion or rotational casting followed by CVD deposition and collapsing the tube into a fibre

2) CVD into a high purity tube and using crucible drawing as described above.

With method 2, further design and infrastructure development may allow incorporating the collection device on the fibre tower to realise a continuous fibre drawing tower.

5.3 Conclusions

In this Chapter, CVD for use in making chalcogenide bulk glass and fibre is reviewed. The review showed that CVD for bulk glass was promising but under developed when compared to its use in making chalcogenide thin films. Also maintaining the inherent high purity of CVD as well as collecting the deposited material remained a problem.

In this work the different mechanisms are experimented with to increase collection of deposited material for making bulk chalcogenide glass. The most promising mechanisms have been listed and incorporated into novel collecting apparatus to be tested in future work. Also initial results for CVD to fibre are shown. A method to making chalcogenide fibre by combining CVD and crucible drawing is introduced.

Gas purity has been improved in the CVD apparatus as a result of the work done in Chapter 4. However automation is still at its infancy and will need improvement in the future for a more repeatable process. With increased gas purity, increased automation and novel apparatus as detailed high purity bulk glass and low loss chalcogenide fibre can be envisaged in the near future.

Chapter 6: Conclusions and Future Work

6.1 Summary

In this thesis facilities for high purity chalcogenides at the ORC have been developed. Many techniques for synthesis and exploration of chalcogenides such as sealed ampoule, microwave assisted sealed ampoules, levitation methods, reactive atmosphere processing and CVD have been attempted. In-house facilities have been developed for sealed ampoule, levitation and reactive atmosphere processing methods. The major accomplishments are described below..

A dedicated sealed ampoule setup has been developed. A standard operating procedure and best practices document has been developed and is also detailed in Chapter3. Glasses have been successfully made and passed to various research groups for making devices and characterization. Safety is still a major obstacle to overcome as explosive ampoules can occur randomly. GLS and GLSO have been levitated for the first time and have not been reported previously. Coating and doping of spheres has been accomplished for the first time which has also not been reported to the best of the author's knowledge. Laser irradiation from a device fabrication standpoint has been introduced. An aero acoustic levitator has been acquired and purchased. This will allows for in-house experiments on levitated glass melting in the future.

All the glass melting methods require the use of high purity gasses as part of their manufacture. A review and upgrade of the gases facilities at the ORC was done. Considerable improvement to the gas purity and delivery to the ORC chalcogenide facilities have been made. The changes involved the replacement of unmaintained 1st stage purifiers at the bulk gas source and point of use purification. For the first time at the ORC, the dew point of gasses at the equipment is being monitored and logged to ascertain there effects on glasses made from melt to melt. The dew point has increased from -76C at the start of this project to greater than -99C and has led to a considerable decrease in the moisture in the glasses as detailed in Chapter 4. A minimum loss has been achieved of 0.34dB/m at 4.8 μm and close to or less than 1dB/m within the 3-5 μm range, see Figure 56 which was the goal for the FLITES project. Procedure

and understanding of the system has increased exponentially in a short period recapturing and improving facilities that took over 20 years to develop. The system has now has the hardware and software in place form monitoring, safety and data logging which is a major improvement over past designs.

CVD techniques for producing bulk glass have been explored. Results indicate that bulk powder collection for making bulk glass is feasible. However the final designed apparatus for collection has yet to be tested. Innovative ideas for CVD into fibre drawing have been presented with initial results showing great promise.

6.2 Future research directions

The work presented in this thesis has led to securing grant EP/M015130/1. This grant will further the development of facilities at the ORC. The aims of the proposed research are as follows:

- To establish the UK as a world-leading speciality glass research and manufacturing facility
- To discover new glass compositions and optimize existing ones, particularly in glasses made with sulphur
- To develop links with UK industry and help them to exploit these new glass materials
- To demonstrate important new electronic, telecommunication, switching devices from these glasses
- To partner other UK Universities to explore new and emerging applications of speciality glass

There are many areas that need further development and the following is an attempt to capture some of the possible research directions, some of which have already been mentioned in various sections of this thesis. The glass melting systems chosen for development are sealed ampoule, RAP and CVD. With sealed ampoule there is considerable room for improvement such as distillation and incorporation of getter technology. Working with getter research and development companies directly may lead to more unconventional methods of purification. For example by integrating the thin film getter technology in the path of the vapour, this can increase the surface area for reaction and impurity removal as opposed to adding the getter directly

to the melt as larger particles. Other areas requiring development are in melting and quenching facilities such as rock and rotating furnaces as well as increasing batch size.

The horizontal RAP system has a lot of room for improvement. Research into improving the procedures, equipment specifications, automation and safety are required. The following is a list of some of the future research activities identified.

1) Conversion of raw materials example Ga to Ga_2S_3 and LaF to La_2S_3 as done in the past. Other sulphide such as Ge to GeS_2 will be explored for comparison with CVD bulk glass methods.
2) Automation safety and data logging improvements, furnace upgrade to allow NI control, additional instrumentation for outlet pressure, vibration monitoring and automatic quenching which will allow development of automated glass recipes to be developed and implemented.
3) Automatic quench control/monitoring with high temperature thermal imaging camera from LOT-QD. Other variation may be to raise the crucible that is in contact with the silica glass tube allowing gas to flow under the crucible. This may allow more uniform cooling of the vitreous carbon crucible. If the furnace can be removed radially and shielded, the inlet gas can be lowered and a cooling gas applied to the outside of the silica tube. This may help eliminate striations in the glass.
4) Transfer port upgrade to allow larger melts and easier more reliable glassware sealing. Also add overpressure relief.
5) Vitreous carbon liner in the hotzone of the furnace to protect against Silica and oxide inclusions from the reactor walls. The idea is that carbon is more volatile and easier to remove than these other impurities.
6) Improve outlet design, for example, add pressure relief and automatic bypass to vent valves, a parallel bubbler and/or vacuum pressure control system. Control of the vacuum pressure can allow tailoring of volatile impurity removal as well as vacuum baking the tube for more efficient and shorter processing steps.

7) Experiment with other gases, for example using O_2 to make high purity heavy metal oxide glasses, H_2 and Cl_2 for impurity removal and modifying the transmission window cut-off.
8) The 2nd stage purification is set to be installed in the 2nd quarter of 2015. This would be the final stage of the gas purification upgrade at the ORC and a study to determine the final limits to the reduction of the moisture levels in the glasses would be the next research objective. SAES Getter R&D has been approached as part of the new grant to help identify further areas to improve purification.

Future work focus in the CVD area shall continue on the improving bulk powder collection and CVD to fibre ideas. Automation and safety in the CVD equipment is also required for better control of the experiments.

In conclusion, it is hoped that the ideas and results generated from this work would lead to ultra-high purity glass and devices made of chalcogenides being realized in the near future.

Appendices

Appendix A - Commercial chalcogenides

CorActive
Specialty Optical Fiber Manufacturer

Mid-IR Fiber Products

PRODUCT DESCRIPTION

CorActive delivers a full range of Infrared Transmission (IRT) optical fibers to address beam delivery requirements in the mid-IR region. CorActive's IRT series of infrared fiber solutions have been specifically designed to provide ultra low loss optical transmission while offering excellent mechanical properties. CorActive's mid-IR fibers enable significant performance improvements in many applications that have relied on free space optics, low quality fiber or other beam delivery methods.

CorActive mid-IR transmission fiber is manufactured under an exclusive license agreement with the U.S. Naval Research Laboratory (NRL). NRL holds several key patents on infrared fiber manufacturing technologies and processes.

Two chalcogenide glass compositions are offered:

IRT-SU: Sulphide glass (As_2S_3) series offer the lowest absorption in the 2-6μm region.

IRT-SE: Selenide glass (As_2Se_3) series features the broadest transmission range from 2μm up to 9μm.

ADVANTAGES

- Lowest optical losses on the market
- High power handling
- Wide operating range (up to 9μm)
- Outstanding flexibility and strength
- Proof tested for increased long-term reliability
- Highly reliable and consistent manufacturing process allowing production runs in the km range

APPLICATIONS

- IR Countermeasures
- FT-IR Spectroscopy
- Mid-IR Laser Beam Delivery
- Sensing and Environmental
- Non-Linear Applications

SPECIFICATIONS

Optical	IRT-SU	IRT-SE
Transmission Range (μm)	2 to 6	2 to 9
Typical Core Refractive Index	2.4	2.7
Typical Attenuation (dB/m)	0.15 @ 2.7μm	0.20 @ 6μm
Typical Attenuation (dB/m)	0.7 @ 4.0μm	0.5 @ 4.55μm
Geometrical&Mechanical		
Core Non-Circularity (%)	< 1	< 1
Core/Clad Concentricity Error (μm)	< 5	< 5
Protective Coating Material	Single Coat Acrylate	Single Coat Acrylate
Tensile Proof Test (kpsi)	> 15	> 15
Environmental		
Chemical Resistance	Insoluble in water, concentrated hydrochloric acid, non-oxidizing acids, gasoline, toluol, alcohol and acetone	

TYPICAL TRANSMISSION SPECTRA

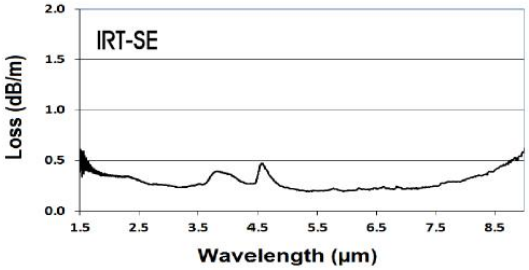

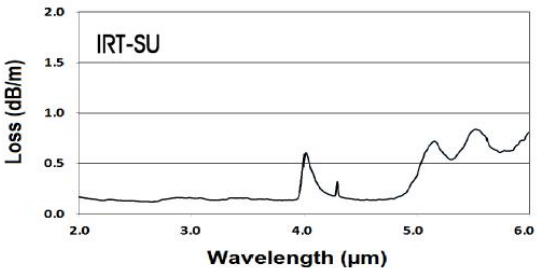

Note: IRT-SU transmission spectrum valid for 100/170 fiber only

Figure 81 CorActive IR As_2S_3 and As_2Se_3 fibre data

Infrared Chalcogenide Glass IRG 26

Transmission of Infrared Glass IRG 26 with Thickness 10.0 mm (Typical Values)

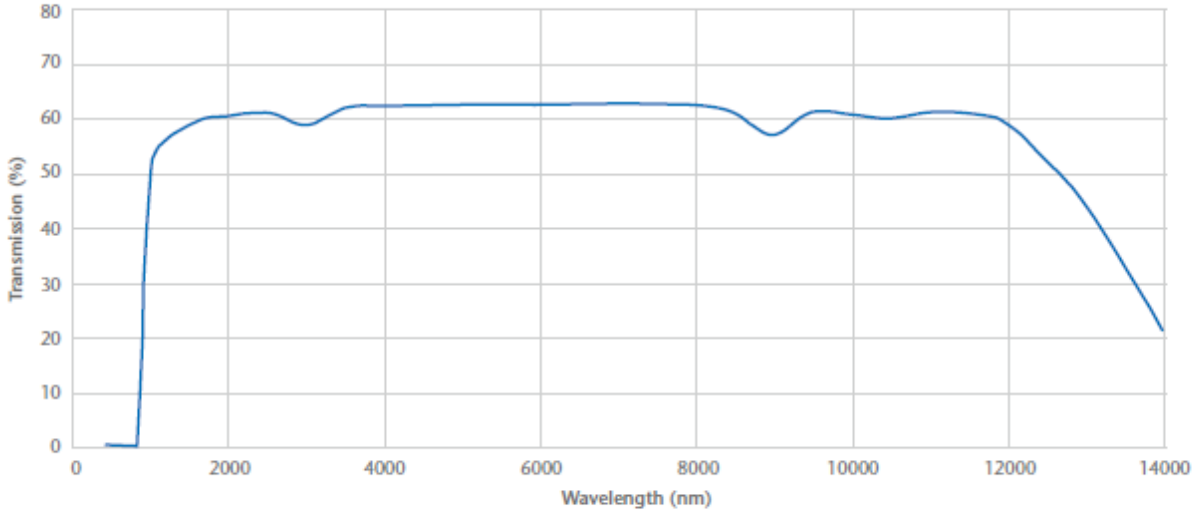

NIR: 750 – 1400 nm	
Wavelength (nm)	Transmission T(%)
750	0.00
800	0.00
850	11.18
900	40.95
950	49.80
1000	52.51
1100	55.22
1200	56.87
1300	57.94
1400	58.64

SWIR: 1400 – 3000 nm	
Wavelength (nm)	Transmission T(%)
1400	58.64
1450	58.99
1550	59.48
1650	60.17
1750	60.43
1850	60.52
1950	60.78
2050	60.89
2150	61.01
2250	60.97
2350	61.23
2450	61.24
2500	61.29
3000	59.19

MWIR: 3000 – 5000 nm	
Wavelength (nm)	Transmission T(%)
3000	59.19
3500	62.27
4000	62.64
4500	62.79
5000	62.84

LWIR: 8000 – 14000 nm	
Wavelength (nm)	Transmission T(%)
8000	62.80
8500	61.45
9000	57.30
9500	61.38
10000	61.11
10500	60.28
11000	61.43
11500	61.33
12000	59.69
12500	53.12
13000	45.37
13500	34.29
14000	22.37

Advanced Optics
SCHOTT AG
Hattenbergstrasse 10
55122 Mainz
Germany
Phone +49 (0)6131/66-1812
Fax +49 (0)3641/2888-9047
info.optics@schott.com

www.schott.com/advanced_optics

SCHOTT
glass made of ideas

Figure 82 Schott glass IR As_2Se_3 chalcogenide

Appendix B - GDMS

Table 10 GDMS samples raw data

Date	01-Aug-00	23-Mar-04	04-Apr-13	22-Aug-00	06-Sep-00	23-Mar-04	04-Apr-13	13-Jun-13
Composition	GaC 23 - Surface	Ga_xS_y	Ga_2S_3	La_2S_3	La_2S_3	La_2S_3	La_2S_3	La_2S_3
Supplier	ORC	ORC	GWI	ORC	ORC	ORC	Testbourne	Lorad
Notes	GAC23 - Surface	GAC 75		LAC26	LAC 27	LAC36		
~~H~~								
Li	0.27	<0.05	<0.1	0.03	< 0.01	<0.01	0.76	0.55
Be			<0.1			<0.1	<0.1	<0.1
B			<0.1			<0.1	0.95	1.0
~~C~~	5800	<= 10		<= 11	<= 20			
~~N~~								
~~O~~	2700	<= 110		<=190	<=70			
F		<0.1	<5	<0.1	1600	<5	200	<5
Na	7	0.04	8.9	0.13	0.7	8.9	720	~2%
Mg	320	0.02	0.45	0.04	0.8	0.45	11	2.5
Al	230	0.3	2.7	0.06	0.92	2.7	13	4.3
Si	2100	7.8	50	5.8	10	50	575	60
P	4		0.55	<0.01	0.4	0.55	7.2	4.6
S	Major	Major	Major	Major	Major	Major	Major	Major
Cl	150		0.95	0.16	1.2		35 *	20
K		<0.1	1.7			<0.05	14	1.5
Ca	21	0.3	4.5	1.3	2.1	19	800	15
Sc		<0.005	<0.1			<0.005	<0.1	<0.1
Ti	11	0.02	0.2	0.02	0.2	0.05	1.3	0.37
V	0.09	<0.01	<0.1	0.11	0.06	<0.01	0.1	0.013
Cr	3.4	<0.01	1.2	0.75	1	<0.01	1.5	0.72
Mn	0.27	<0.01	0.44	<0.005	<0.005	<0.005	11	0.21
Fe	30	0.1	6.5	0.9	0.71	0.02	24	2.7
Co	0.12	<0.01	0.2	<0.01	0.11	<0.01	<0.1	<0.1
Ni	2.4	0.02	2.1	0.63	0.92	0.02	0.6	0.20
Cu	35	0.04	0.2	<0.05	0.09	0.14	1	0.40
Zn	30	<0.1	2.2	<0.5	<0.05	<0.5	$\underline{<}$10	<10
Ga	Major	Major	Major	0.02	0.85		10	15
Ge		<1	<5			<1	<5	<5
As		<0.05	<0.5			<0.5	<0.5	<0.5
Se		<0.1	<1			<0.1	<1	<1
Br	<0.5		<1	<0.5	<0.5		<1	<1
Rb			<0.5				<0.5	<0.5
Sr		<0.05	<0.1			<0.05	30	0.44

Y			<0.1				0.2	3.2
Zr			0.078				0.05	0.29
Nb			<0.5				<0.5	<0.5
Mo			0.1				0.25	0.12
Ru			<1				<0.1	<0.1
Rh			<5				<1	<1
Pd			<1				<1	<1
Ag	_		≤5			_	<5	<1
Cd			<1				<1	<1
In	Binder	Binder	<1	Binder	Binder	Binder	<1	<0.5
Sn		<0.05	<0.5		3500	<0.05	3500	<0.5
Sb		<0.05	<0.5		1.2	<0.05	1.2	<0.5
Te			<1		_		≤1	<0.5
I			<0.5				1.7	<0.1
Cs	<0.5		<0.1	<0.5	<0.5		<0.1	<0.1
Ba			<0.5				450	0.80
La			<0.5	Major	Major	Major	Major	Major
Ce	15	<0.01	<0.1	0.52	0.53	0.64	550	0.70
Pr			<0.1				34	0.12
Nd			<0.1				100	0.20
Sm			<0.5				0.85	0.53
Eu			<0.1				0.6	0.45
Gd			<0.5				<5	<0.5
Tb			<0.1				0.15	<0.1
Dy			<0.5				0.45	<0.5
Ho			<0.1				0.15	<0.1
Er			<0.5				0.2	<0.1
Tm			<0.1				0.12	<0.1
Yb	_		<0.5				<0.5	<0.5
Lu			0.23				<0.2	<0.2
Hf			<0.5				<0.5	<0.5
Ta			<10				<10	<10
W			<1				<1	<1
Re			<0.1				<0.1	<0.1
Os			<0.1				<0.1	<0.1
Ir			<0.1				<0.1	<0.1
Pt		<0.05	<1			<0.05	<1	<1
Au			<1				<1	<1
Hg			<1				<1	<1
Tl			<0.1				<0.1	<0.1
Pb		<0.05	<0.1			<0.05	3.7	0.25
Bi		<0.01	<0.1			<0.01	0.17	<0.1
Th			<0.05				<0.05	0.40
U			<0.05				<0.05	<0.05

Table 11 GDMS samples raw data continued

Date	02-Aug-00	18-Feb-00	24-Oct-13	04-Apr-13	04-Apr-13	13-Jun-13	13-Jun-13
Composition	GLS	GLSF	$As_{40}Se_{60}$	GLSO	GLSO	GLS	GLS
Supplier	ORC	ORC	Schott	ORC	ORC	ORC	ORC
Notes	LD953	LD1004-4, 25 % LaF3	Vitron IGR 26	LD1443	LD1447	LD1537	LD1538
~~H~~							
Li	0.33	0.16	<0.05	0.31	0.15	0.48	0.10
Be			<0.05	<0.1	<0.1	<0.1	<0.1
B			<0.05	0.7	0.43	1.2	0.90
~~C~~	15	330					
~~N~~							
~~O~~	8600	350					
F			<1	<5	<5	<5	<5
Na	2	3.5	0.81	110	130	6500 *	2650
Mg	0.12	0.2	0.10	8.6	9	2	1.3
Al	3.2	0.14	2.4 *	20	11	6.9	6.5
Si	340	1	25 *	370	200	72	55
P	1	0.06	0.29	5.8	4.4	2.6	2.4
S	Major	Major	6.0	Major	Major	Major	Major
Cl	0.08	0.15	1.0	12	13	50 *	44
K			<0.5	10	12	4.5	1.4
Ca	1.7	6.8	0.90	500	450	14	15
Sc			<0.05	<0.1	<0.1	<0.1	<0.1
Ti	0.17	0.27	0.045	5.4	0.78	0.77	0.53
V	<0.05	0.12	<0.01	0.1	<0.1	0.020	0.26
Cr	0.4	0.12	0.13	250	4	1.0	0.85
Mn	0.08	0.59	$\underline{\leq}$0.1	7.3	13	0.35	0.10
Fe	1600	2.4	0.38	25	25	6.5	9.0
Co	0.03	0.05	<0.01	0.15	0.2	0.10	0.10
Ni	0.73	0.21	0.035	1.3	2	2.2	1.2
Cu	0.66	0.65	$\underline{\leq}$0.1	1.5	2.2	0.60	1.2
Zn	<0.5	<0.5	$\underline{\leq}$0.2	25	20	4.0	3.5
Ga	Major	Major	<0.05	Major	Major	Major	Major
Ge			<0.5	<5	<5	<5	<5
As			Major	<0.5	<0.5	<0.5	<0.5
Se			Major	<1	<1	<1	<1
Br	<0.5	<0.5	<0.5	<1	<1	<1	<1
Rb			<0.01	<0.5	<0.5	<0.5	<0.5
Sr			<0.1	15	15	0.30	0.16
Y			<0.1	0.32	0.15	2.0	2.0
Zr			<0.1	0.4	0.17	0.36	0.46
Nb			<0.1	<0.5	<0.5	<0.5	<0.5
Mo			$\underline{\leq}$0.1	0.6	0.15	0.15	0.25

Ru			<0.1	<1	<1	<1	<1
Rh			<0.1	<5	<5	<5	<5
Pd			<0.5	<5	<5	<5	<5
Ag			<0.1	≤5	≤5	<5	<5
Cd			≤1	<1	<1	<1	<1
In	Binder	Binder	<10	≤1	≤1	<0.5	<0.5
Sn			0.45	20	2.7	<1	<1
Sb			≤0.1	0.9	0.3	<1	<1
Te			0.35	<1	<1	<1	<1
I			<0.1	<1	<1	<0.5	<0.5
Cs	<1	<1	<0.05	<0.1	<0.1	<0.1	<0.1
Ba			<0.05	280	285	0.75	0.50
La	Major	Major	<0.01	Major	Major	Major	Major
Ce	0.46	1	<0.05	200	170	0.50	0.32
Pr			<0.05	20	12	0.16	0.30
Nd			<0.05	75	40	0.15	0.60
Sm			<0.05	0.35	0.5	<0.5	<0.5
Eu			<0.05	0.2	0.2	<0.1	<0.1
Gd			<0.05	<5	<5	<1	<1
Tb			<0.05	<0.1	<0.1	<0.1	<0.1
Dy			<0.05	<0.5	<0.5	<0.5	<0.5
Ho			<0.05	<0.1	<0.1	<0.1	<0.1
Er			<0.05	<0.5	<0.5	<0.5	<0.5
Tm			<0.05	<0.1	<0.1	<0.1	<0.1
Yb			<0.05	≤0.5	≤0.5	<0.5	<0.5
Lu			<0.05	0.2	<0.	<0.1	<0.1
Hf			<0.05	<0.5	<0.5	<0.5	<0.5
Ta			≤1	<10	<10	<10	<10
W			<0.05	<1	<1	<1	<1
Re			<0.05	<0.5	<0.5	<0.5	<0.5
Os			<0.05	<0.1	<0.1	<0.1	<0.1
Ir			<0.05	<0.1	<0.1	<0.1	<0.1
Pt			<0.1	<1	<1	<1	<1
Au			<0.5	<1	<1	<1	<1
Hg			<0.5	<1	<1	<1	<1
Tl			<0.1	<0.1	<0.1	<0.1	<0.1
Pb			0.028	0.8	0.6	<0.1	<0.1
Bi			<0.05	<0.1	<0.1	<0.1	<0.1
Th			<0.01	<0.05	<0.05	0.12	0.14
U			<0.01	<0.05	<0.05	<0.05	<0.05

Note: All GDMS values are quoted in parts per million weight units.

Appendix C - Glass Summary

Table 12 Summary of GLS glasses

Glass	Raw material*	Processing	Analysis
LD 1405 Molar ratio - 65:32:3 Vertical furnace (no additional gas purification)	Ga2S3, GWI – Batch# DTM110308 (99.99) La2S3, Cerac – Batch # L_1019 (99.9) La2O3, Testbourne – Batch # L1-10017-P (99.9)	Ar: 5L/min D.P. unknown Temp: 1094 °C 24 hr melt followed by quench and annealing at 500 °C for 24 hrs	FTIR
LD 1407 Molar ratio -65:32:3 Vertical furnace (no additional gas purification)	Ga2S3, GWI – Batch# DTM110308 (99.99) La2S3, Testbourne – Batch # L1-10020-P (99.9) La2O3, Testbourne – Batch # L1-10017-P (99.9)	Ar: 5L/min D.P. unknown Temp: 1098 °C 24 hr melt followed by quench and annealing at 500 °C for 24 hrs	FTIR
LD 1408 Molar ratio - 65:32:3 Vertical Furnace (no additional gas purification)	Ga2S3, GWI – Batch# DTM110308 (99.99) La2S3, Treibacher – Batch # 26-4822 (99.9) La2O3, Testbourne – Batch # L1-10017-P (99.9)	Ar: 5L/min D.P. unknown Temp: 1097 °C 24 hr melt followed by quench and annealing at 500 °C for 24 hrs	FTIR
LD 1443 Molar ratio - 65:32:3 Horizontal RAP (no additional gas purification)	Ga2S3, GWI – Batch# DTM092208 (99.999) La2S3, Testbourne – Batch # 1654-2 (99.99) La2O3, Testbourne – Batch # 1651-4 (99.99)	Ar: 0.5L/min, D.P. was -76C Temp: 1150 °C 24 hr melt followed by quench and annealing at 500 °C for 24 hrs	UV-Vis-NIR FTIR GDMS
LD 1447 Molar ratio - 65:32:3 Horizontal RAP (0.1µm NUPURE purifier)	Ga2S3, GWI – Batch# DTM092208 (99.999) La2S3, Testbourne – Batch # 1654-2 (99.99) La2O3, Testbourne – Batch # 1651-4 (99.99)	Ar: 0.5L/min, D.P. was -86C Temp: 1150 °C 24 hr melt followed by quench and annealing at 500 °C for 24 hrs	UV-Vis-NIR FTIR GDMS
LD 1537 Molar Ratio - 65:35 Horizontal RAP (0.1µm NUPURE purifier)	Ga2S3, GWI – Batch# DTM101908 (99.999) La2S3, Lorad Lot 25 (99.9)	Ar: 0.5L/min , D.P. was -98C Temp: 1150 °C 24 hr melt followed by quench and annealing at 500 °C for 24 hrs	FTIR GDMS

LD 1538 Molar ratio - 65:35 Horizontal RAP (0.1µm NUPURE purifier)	Ga2S3, GWI – Batch# DTM101908 (99.999) La2S3, Lorad Lot 25 (99.9)	Ar: 0.5L/min, D.P. was -98C Temp: 1150 °C 24 hr melt followed by quench and annealing at 500 °C for 24 hrs	FTIR GDMS
LD 1620 (65:35) Horizontal RAP (3nm SAES purifier) Upgraded building purification	Ga2S3, GWI – Batch# DTM101908 (99.999) La2S3, Lorad- Lot 25 (99.9)	Ar: 0.5L/min pre melt bake at 500°C, D.P. was > -99C Temp: 1150 °C 24 hr melt followed by quench and annealing at 490 °C for 24 hrs	FTIR Thick and thin sample
LD 1625 (65:35) Horizontal RAP(3nm SAES purifier) Upgraded building purification	Ga2S3, GWI – Batch# DTM101908 (99.999) La2S3, Lorad - Lot 25 (99.9)	Flame treat tube with hand torch after removing from tube washer Ar: 0.5L/min pre melt bake at 500°C, D.P. was > -99C Multiple tube outlet cleaning with hand torch Ar: 0.5L/min ,D.P. was > -99C Temp: 1150 °C 24 hr melt followed by quench and annealing at 490 °C for 24 hrs	FTIR Thick and thin sample
LD 1627 (65:35) Horizontal RAP (3nm SAES purifier) Upgraded building purification	Ga2S3, GWI – Batch# DTM101908 (99.999) La2S3, Lorad - Lot 25 (99.9)	Flame treat tube with hand torch after removing from tube washer H2S: 0.5L/min pre melt bake at 500°C, D.P. was -85 C Ar: 0.5L/min, D.P. was > -99C Temp: 1150 °C 24 hr melt followed by quench and annealing at 490 °C for 24 hrs	FTIR Thick and thin sample FTIR
LD 1644 (65:35) Horizontal RAP (3nm SAES purifier) Upgraded building purification	Ga2S3, GWI – Batch# DTM101908 (99.999) La2S3, Lorad- Lot 25 (99.9)	Flame treat tube with hand torch after removing from tube washer H2: 0.5L/min pre melt bake at 500°, D.P. was -86 C Ar: 0.5L/min, D.P. was > -99C Temp: 1150 °C 24 hr melt followed by quench and annealing at 490 °C for 24 hrs	Thick and thin sample

Appendix D - Installation drawings and pictures

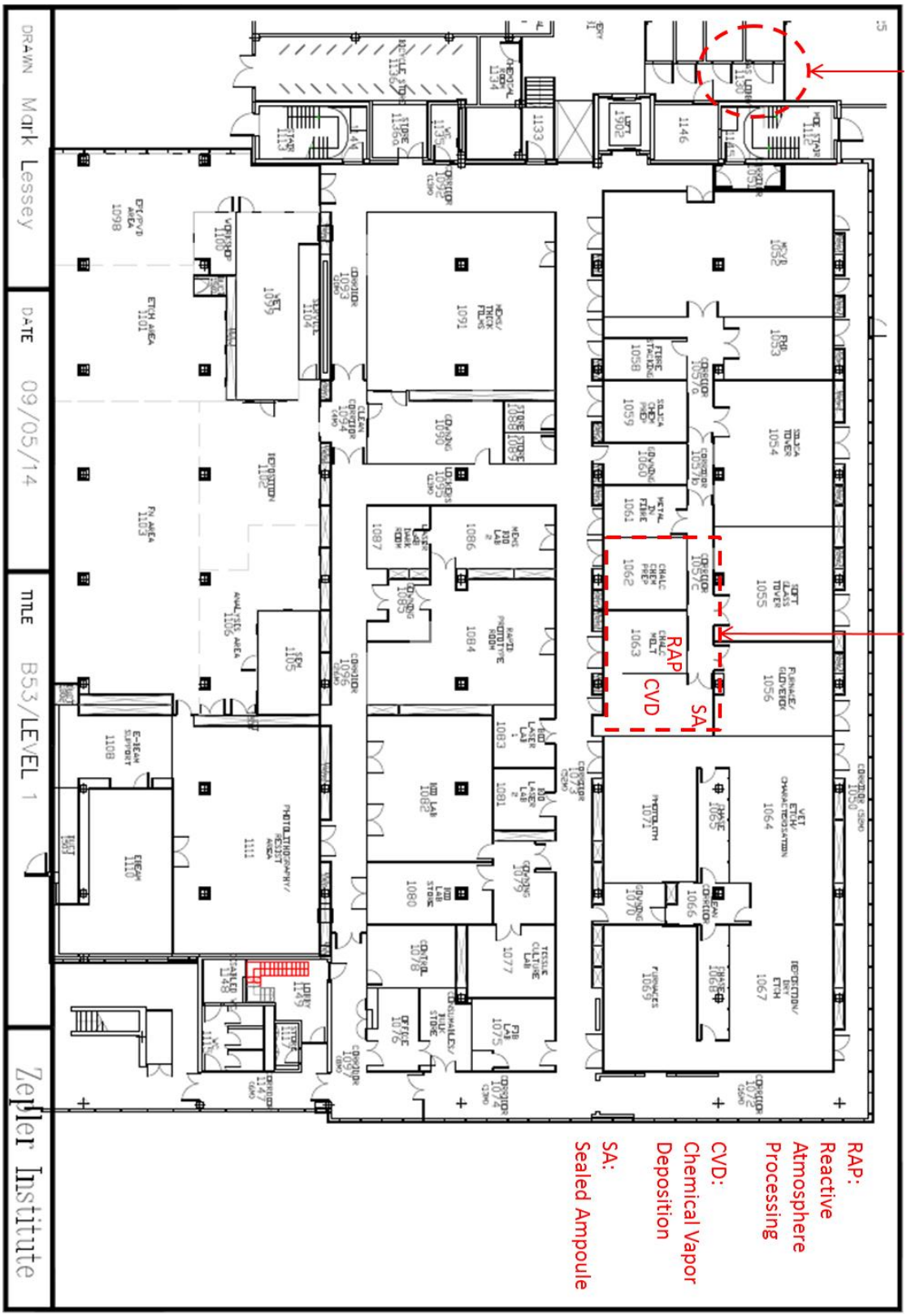

Figure 83 ORC level 1 facilities schematic

Appendix D

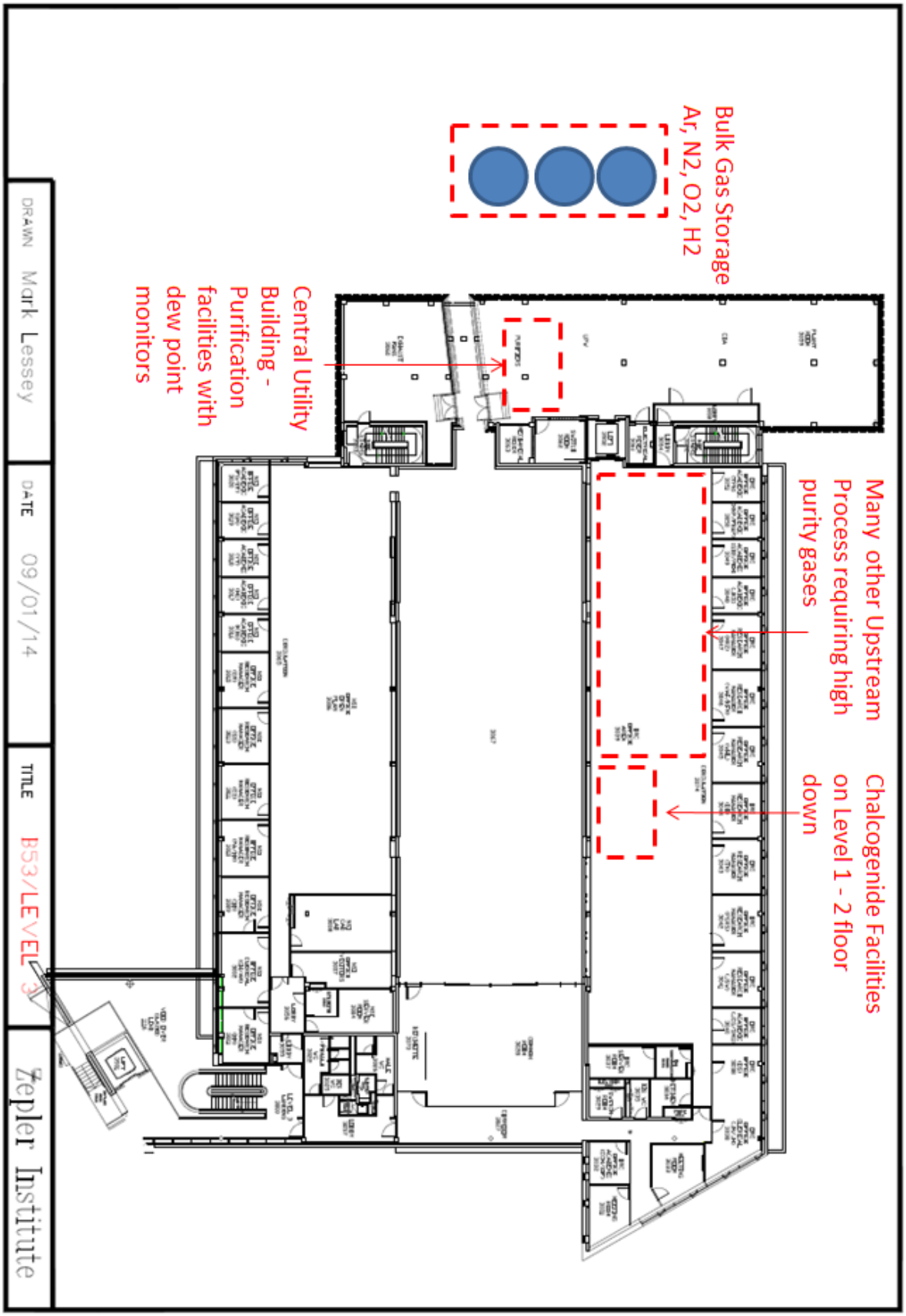

Figure 84 ORC level 3 facilities schematic

Figure 85 H_2S gas cyclinder panel (a) H_2S distribution circuit (b) auto changeover controls (c) N_2 Purge gas

Appendix D

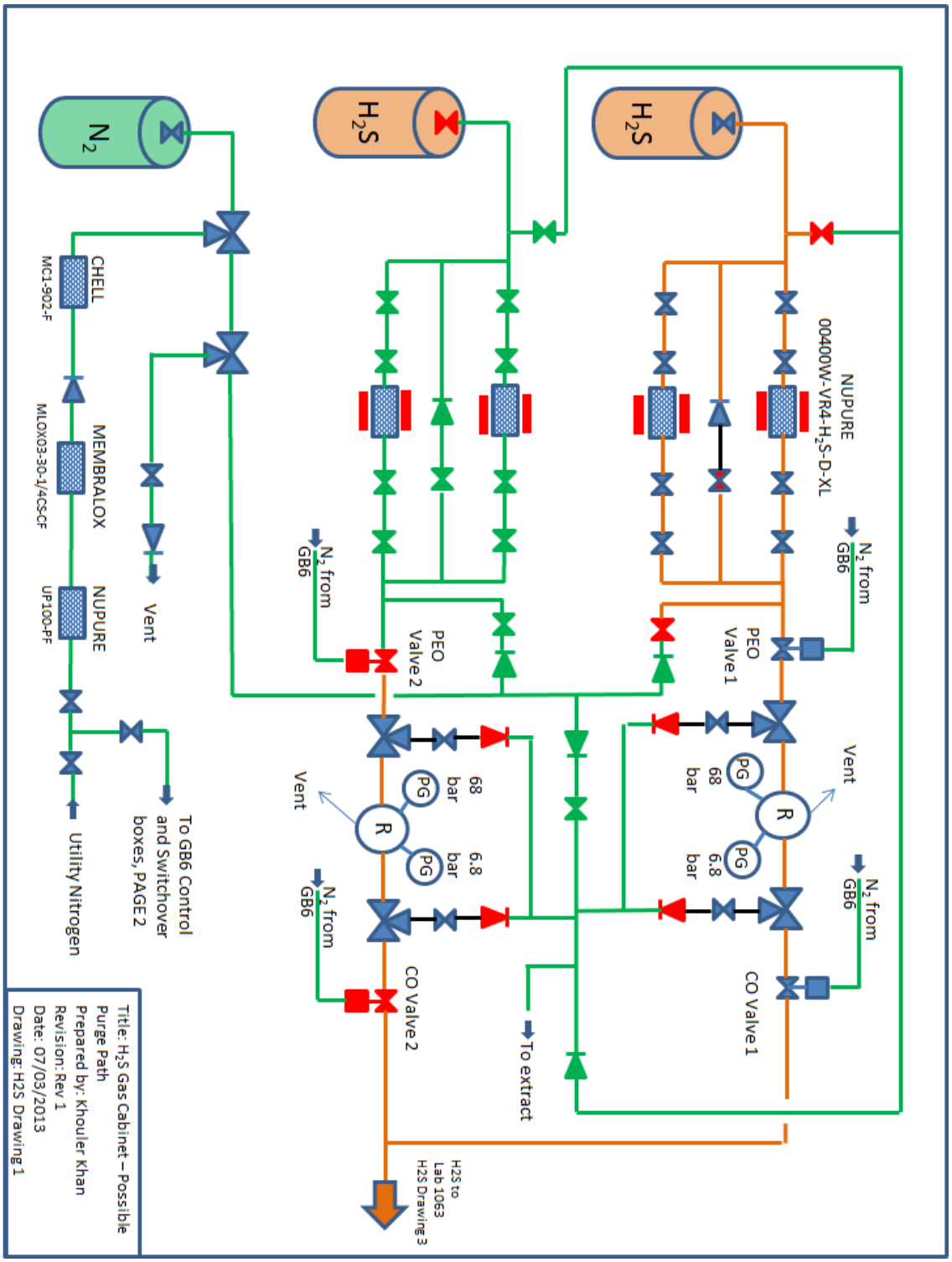

Figure 86 Schematic of H_2S distribution circuit and N_2 purge in gas cylinder room

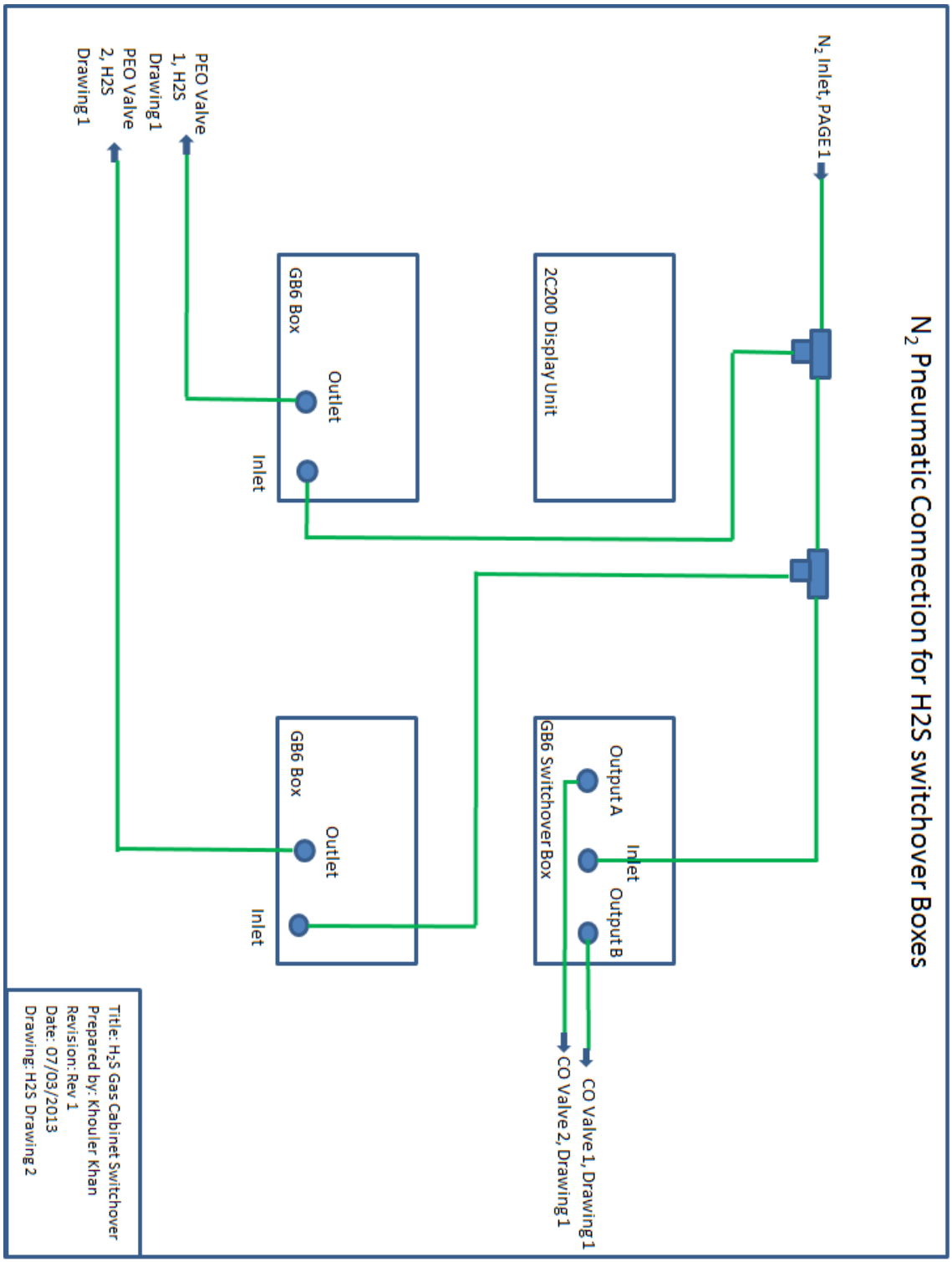

Figure 87 Schematic of auto changeover circuit gas connections

Appendix D

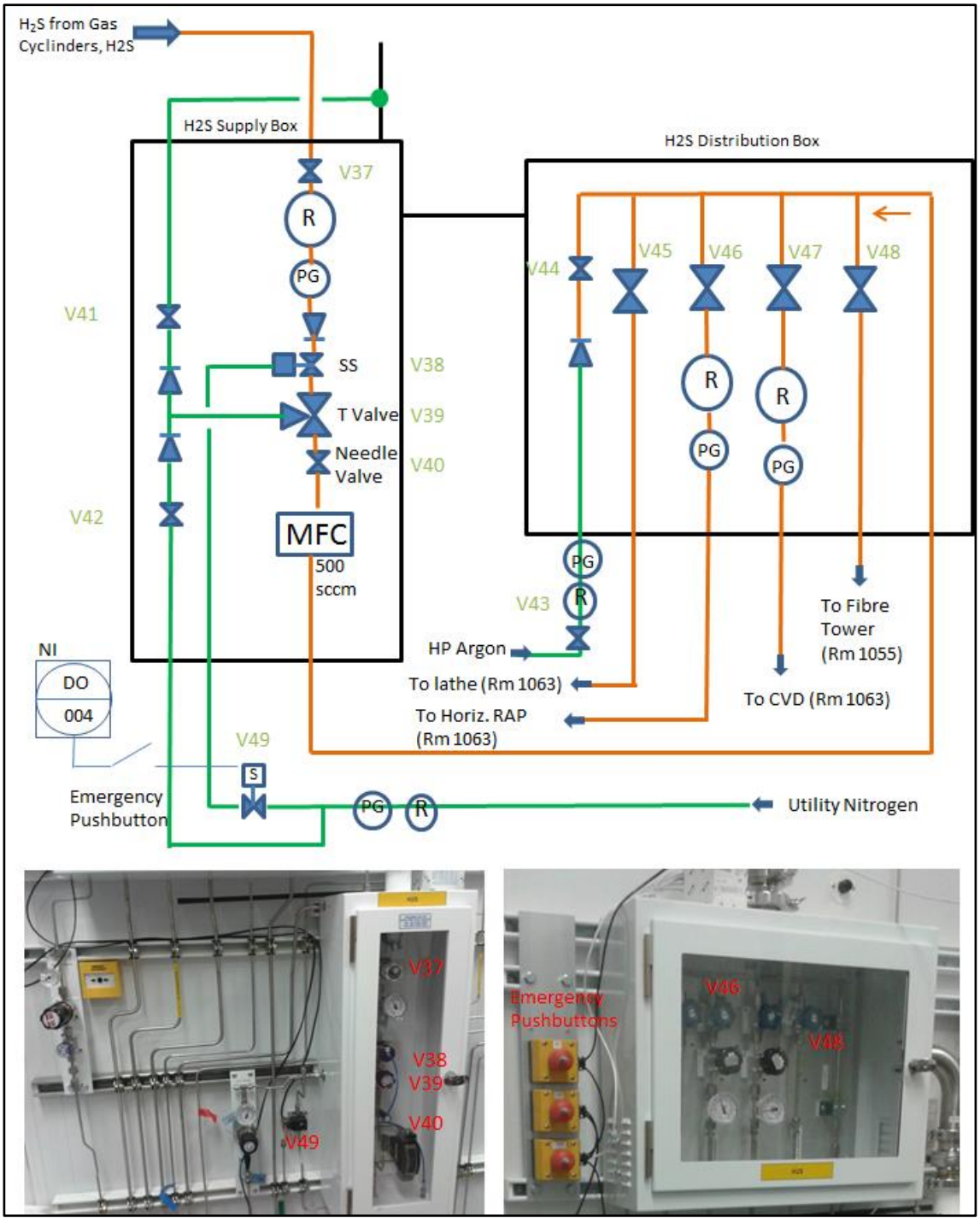

Figure 88 Picture and schematic of the H_2S gas delivery in room 1063

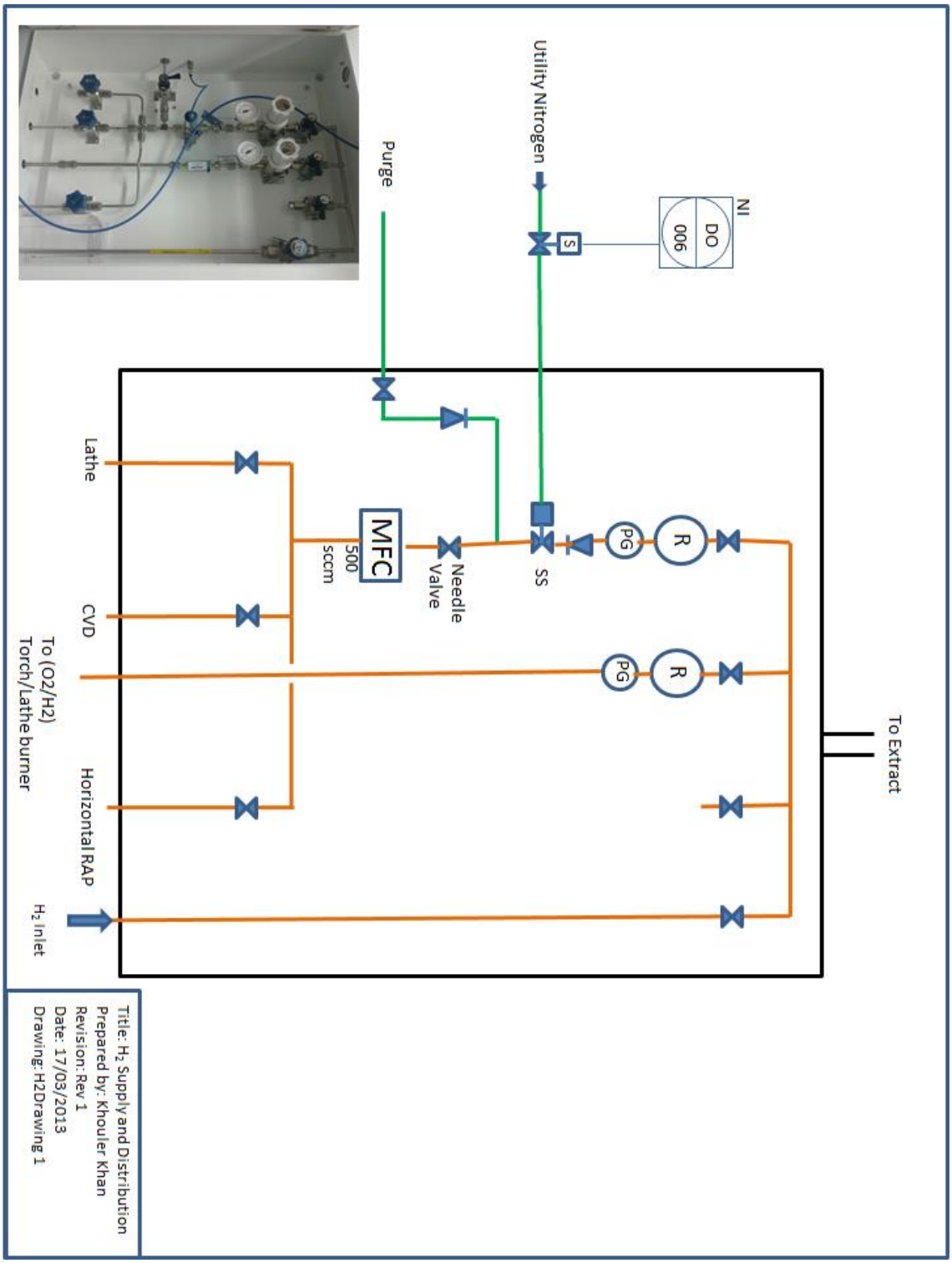

Figure 89 Picture and schematic for H_2 gas delivery in room 1063

Appendix D

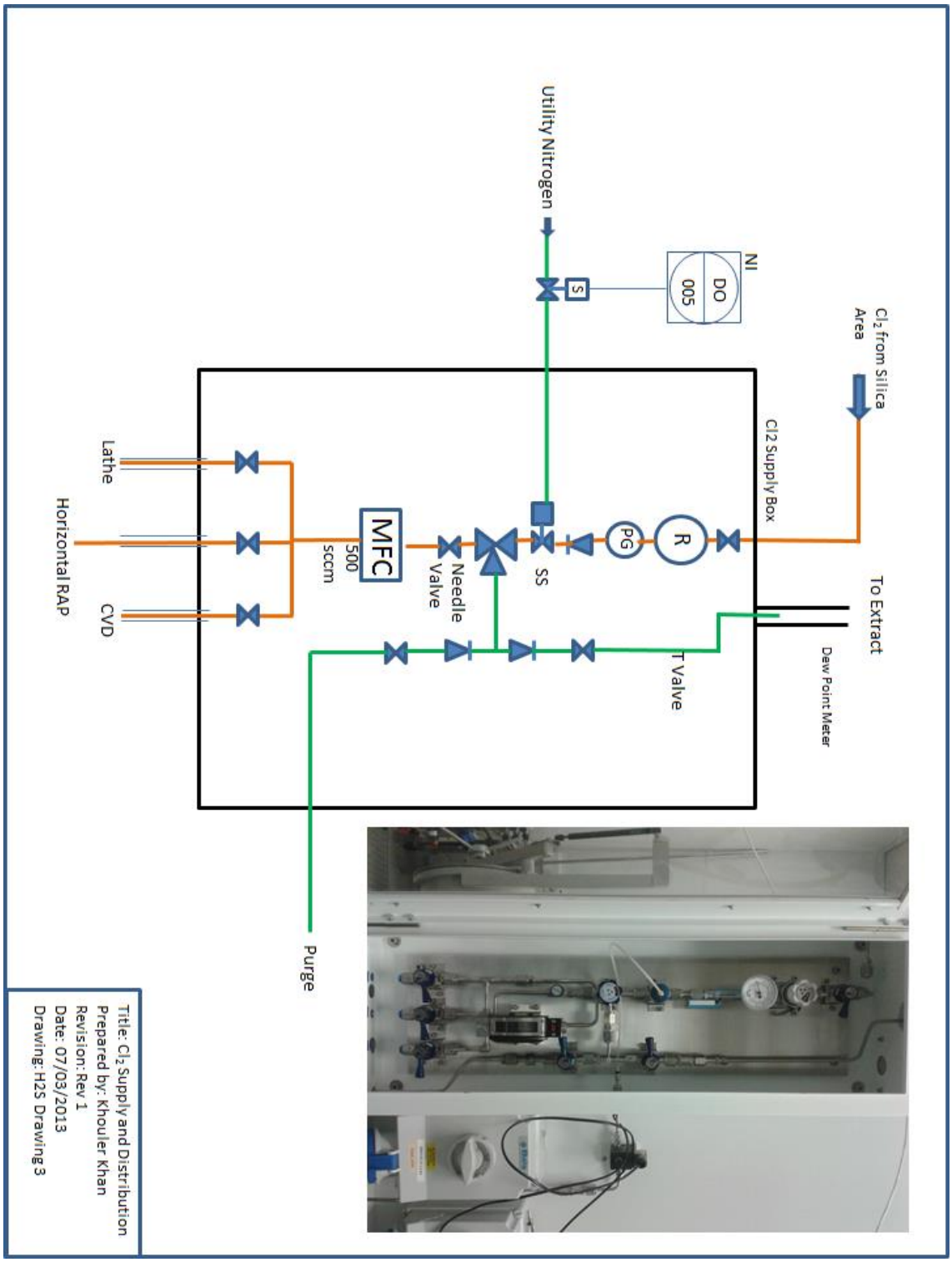

Figure 90 Picture and schematic for Cl_2 gas delivery in room 1063

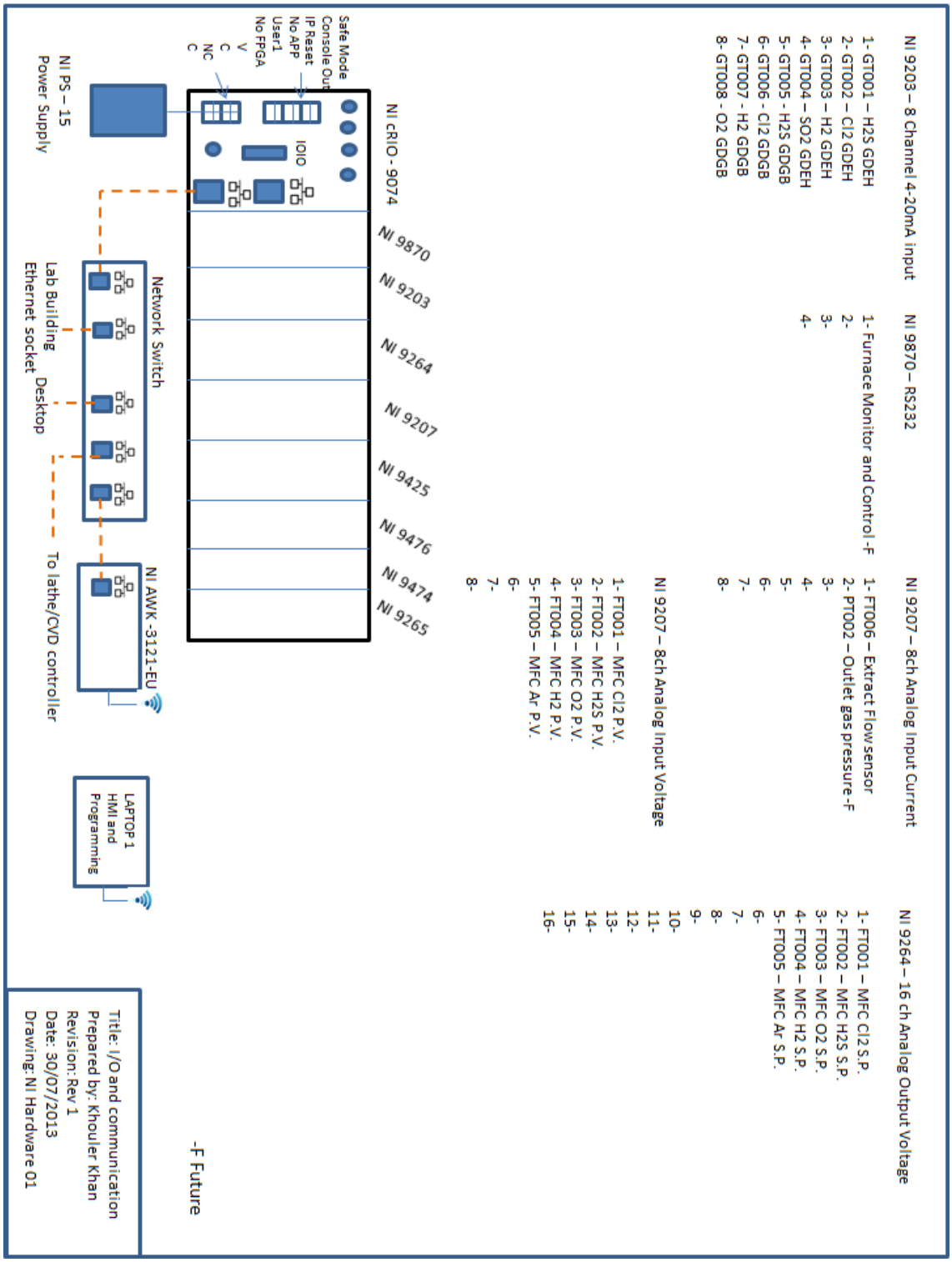

Figure 91 NI I/O and communication schematic 1

Appendix D

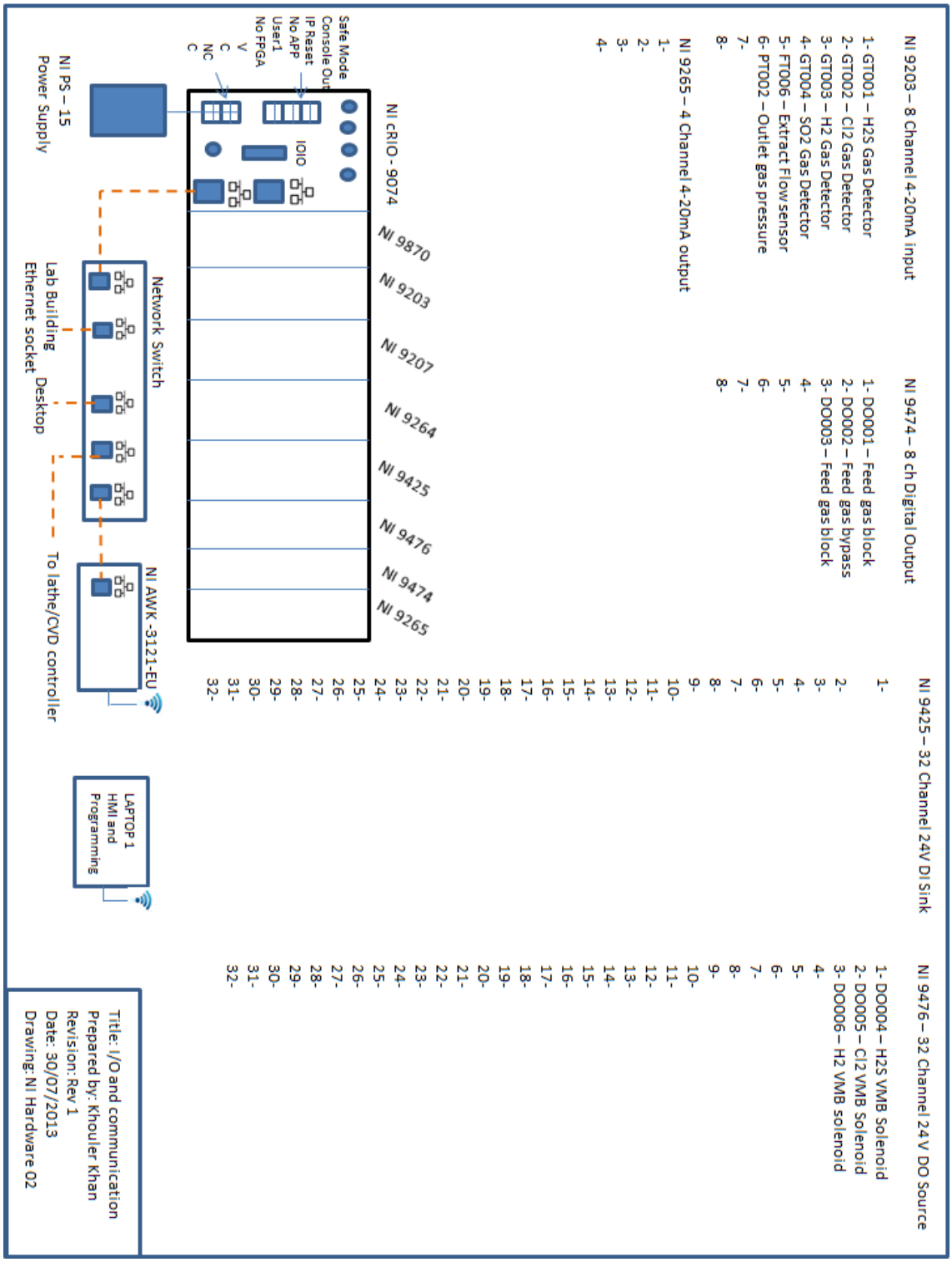

Figure 92 NI I/O and communication schematic 2

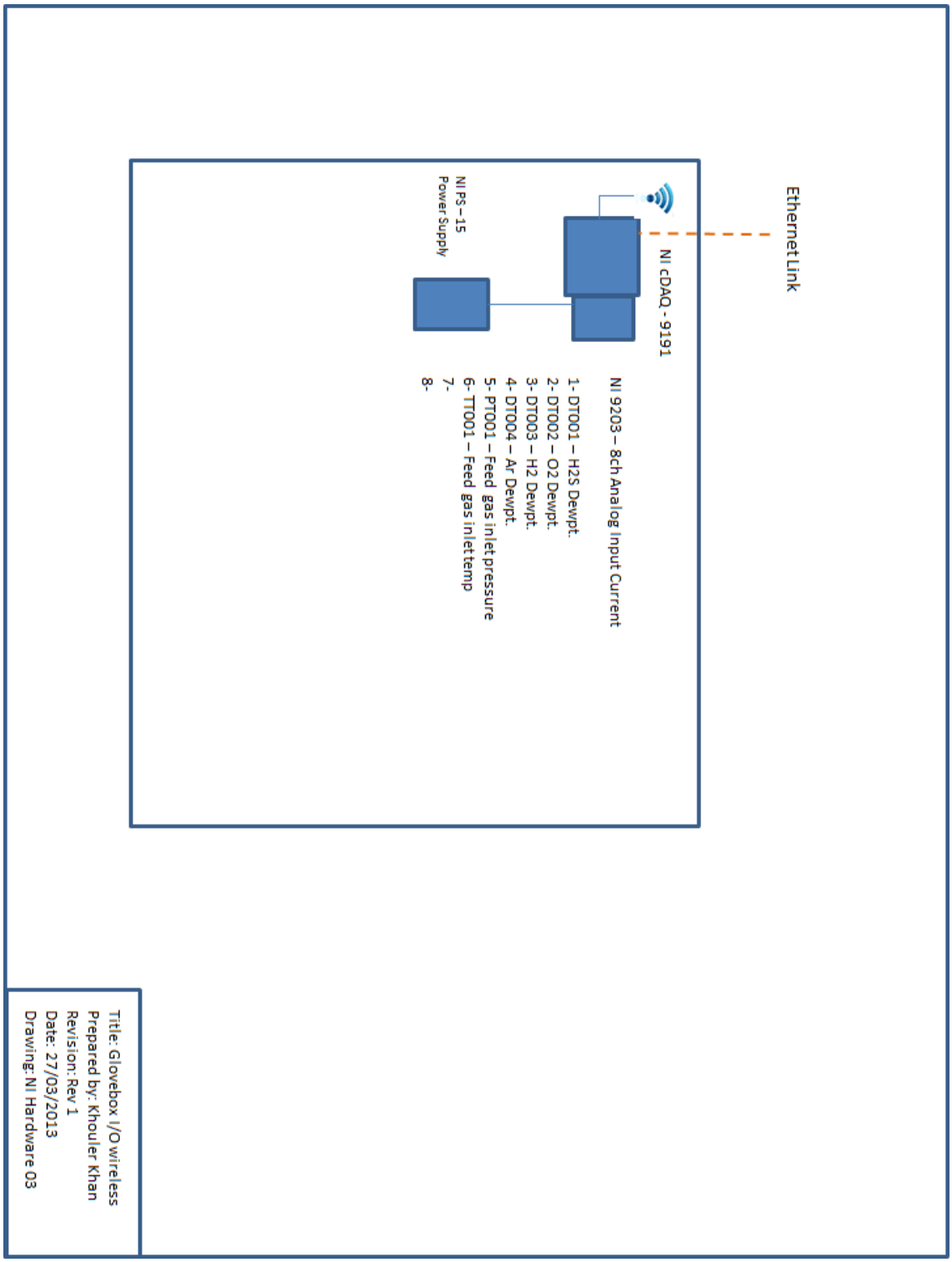

Figure 93 NI I/O and communication schematic 3

Appendix D

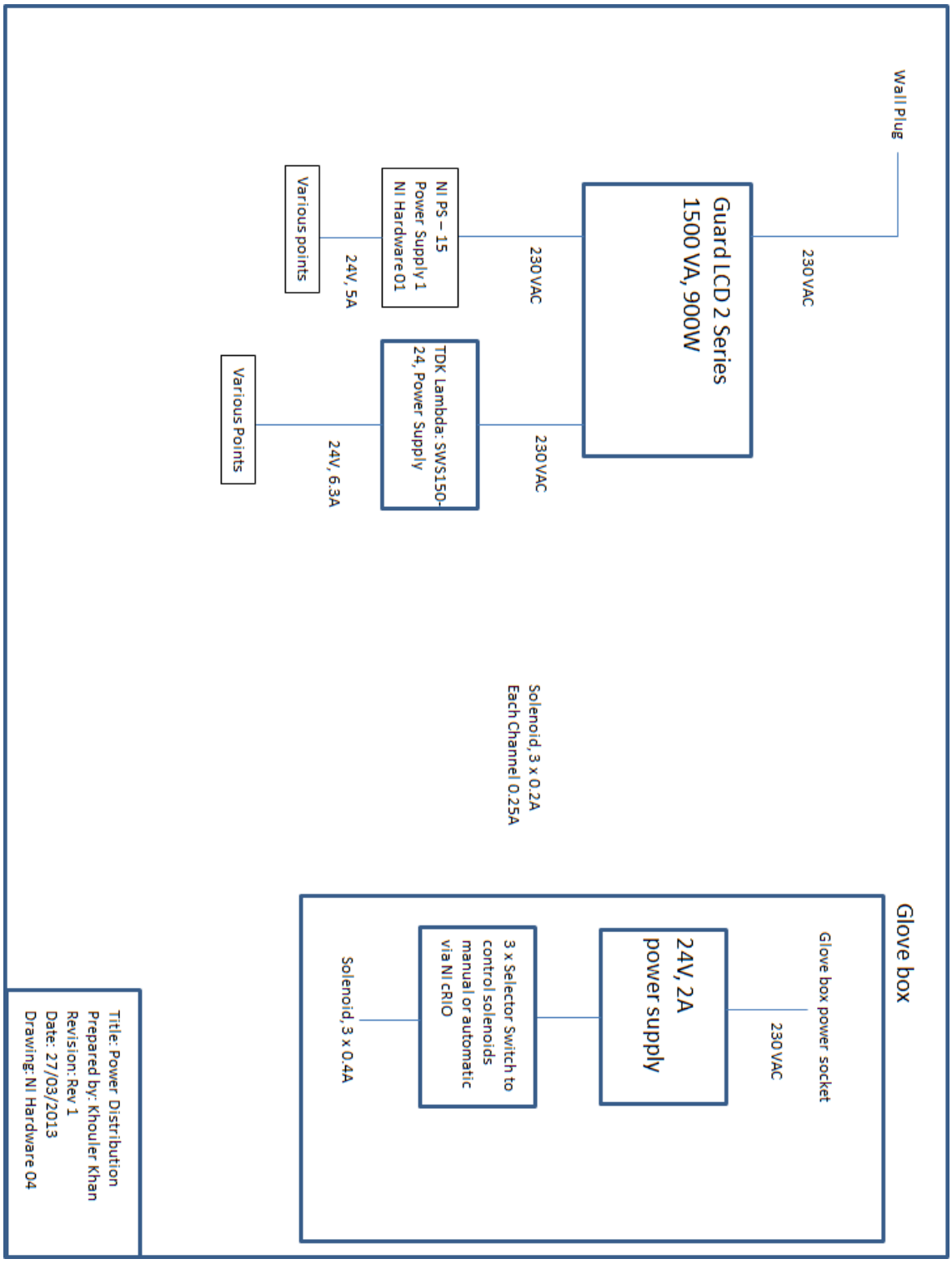

Figure 94 Horizontal RAP power distribution to instruments and control

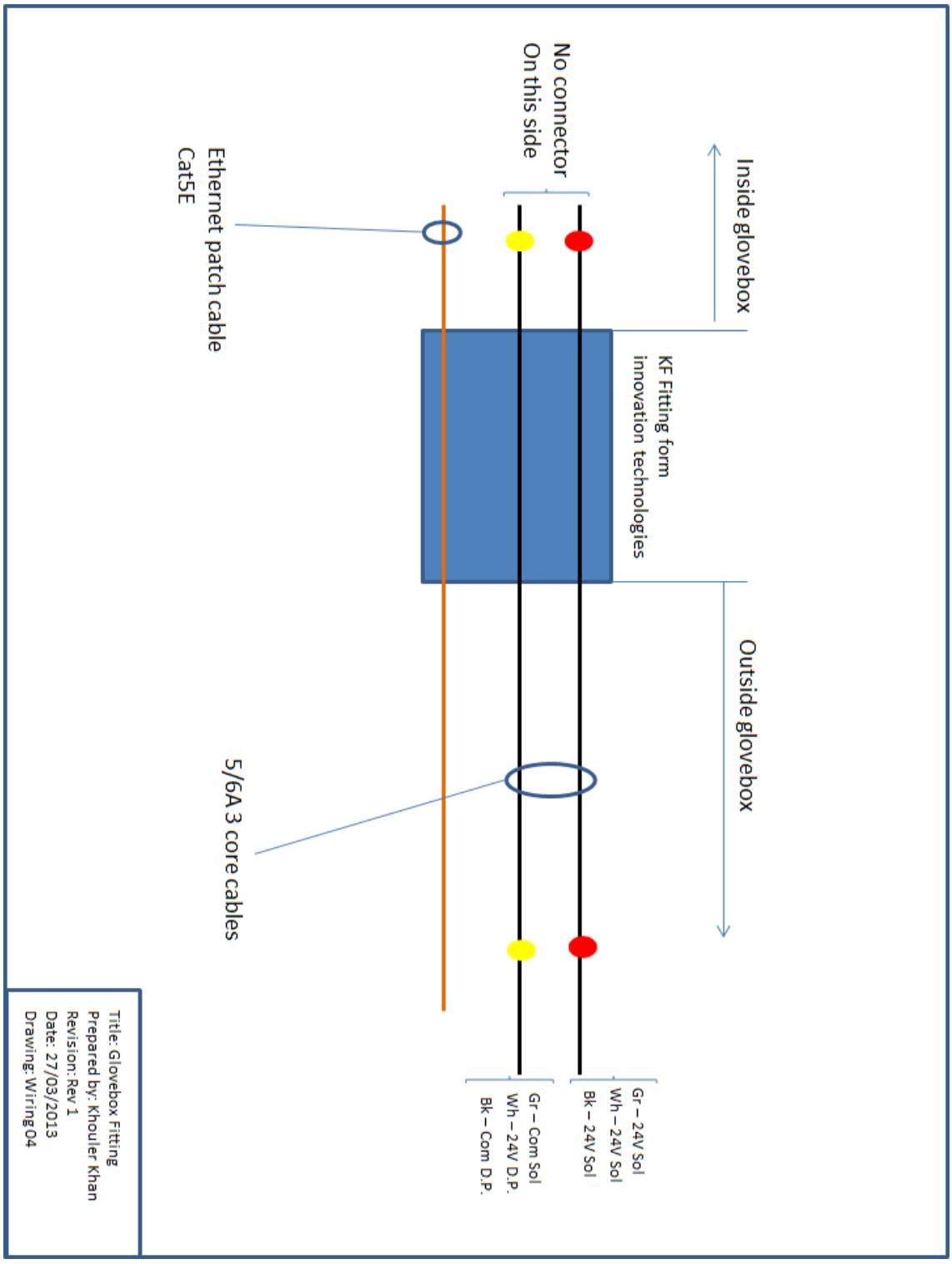

Figure 95 Glovebox electrical and communication feedthrough fitting schematic

Appendix D

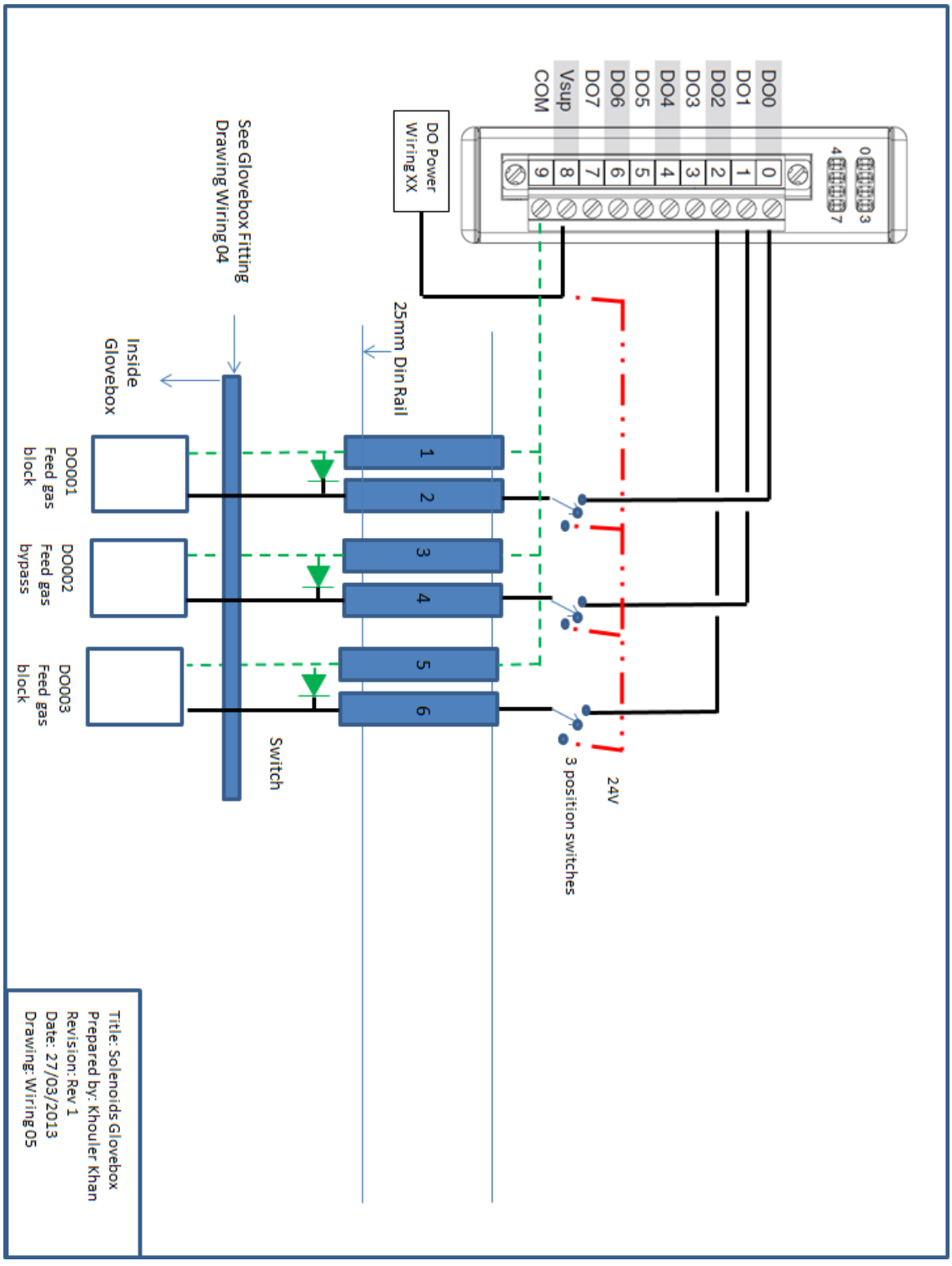

Figure 96Block and bypass wiring diagram

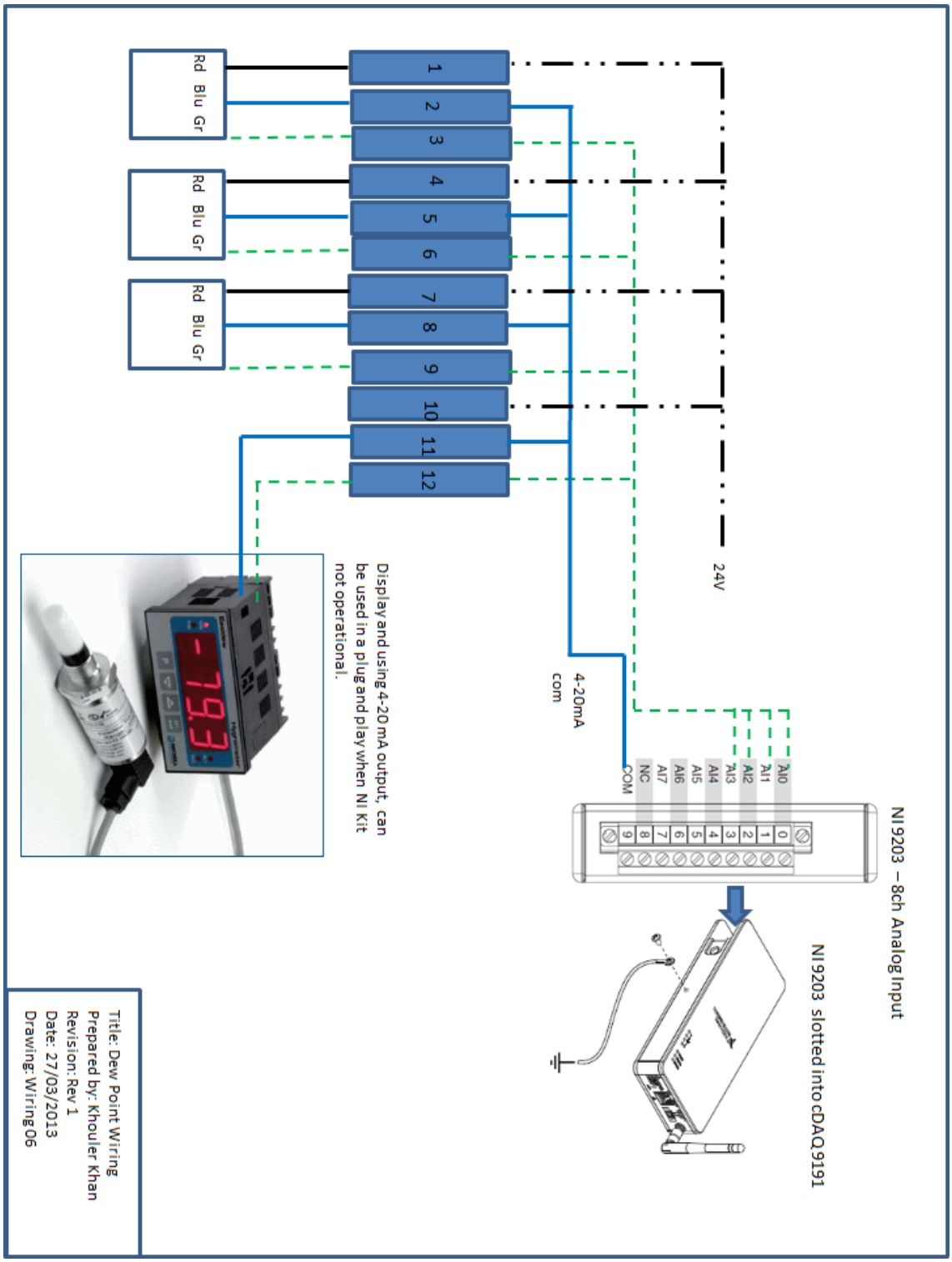

Figure 97 Dew point meter wiring diagram

Appendix D

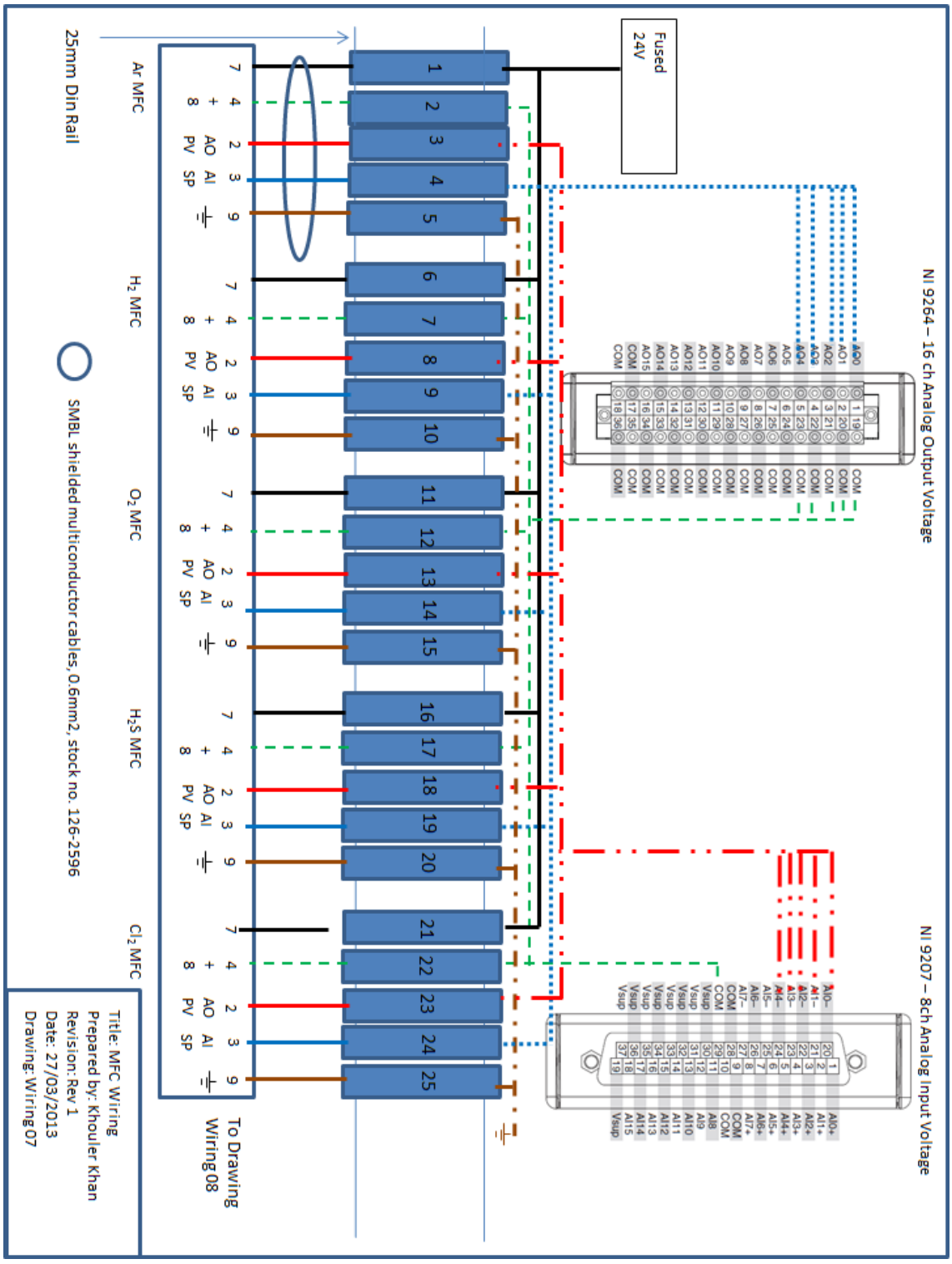

Figure 98 MFC wiring diagram 1

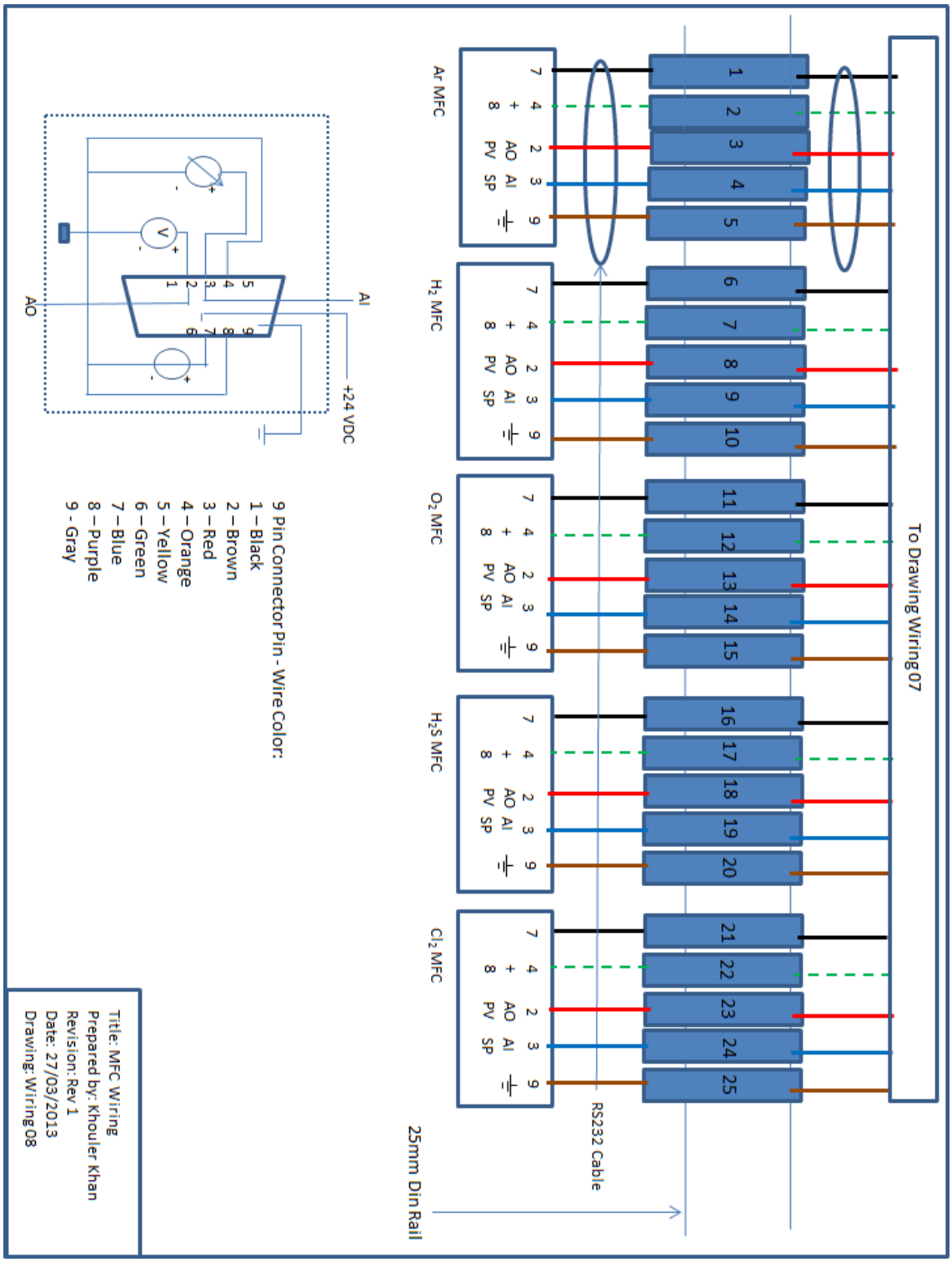

Figure 99 MFC wiring diagram 2

Appendix D

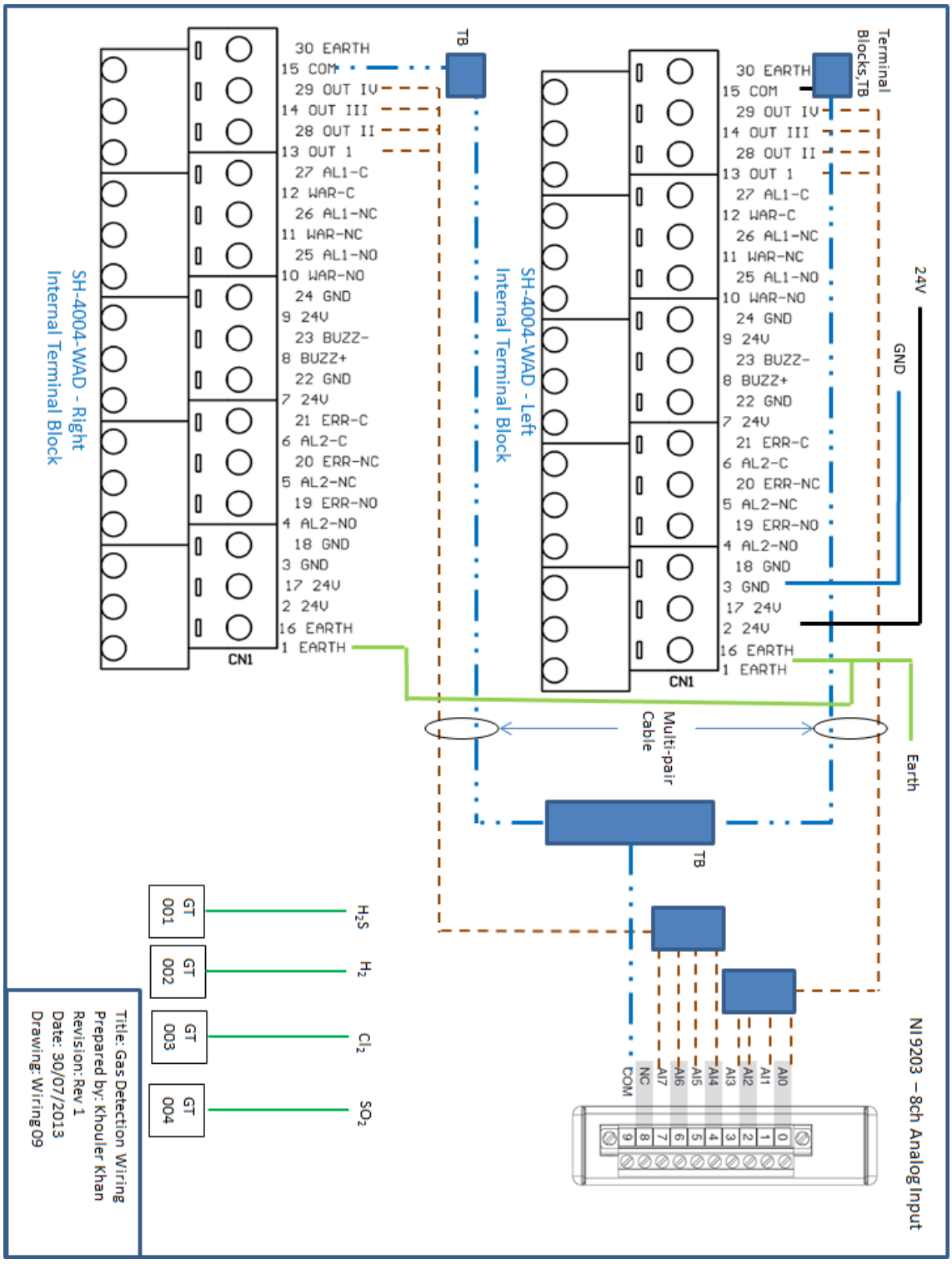

Figure 100 Gas detection wiring diagram 1

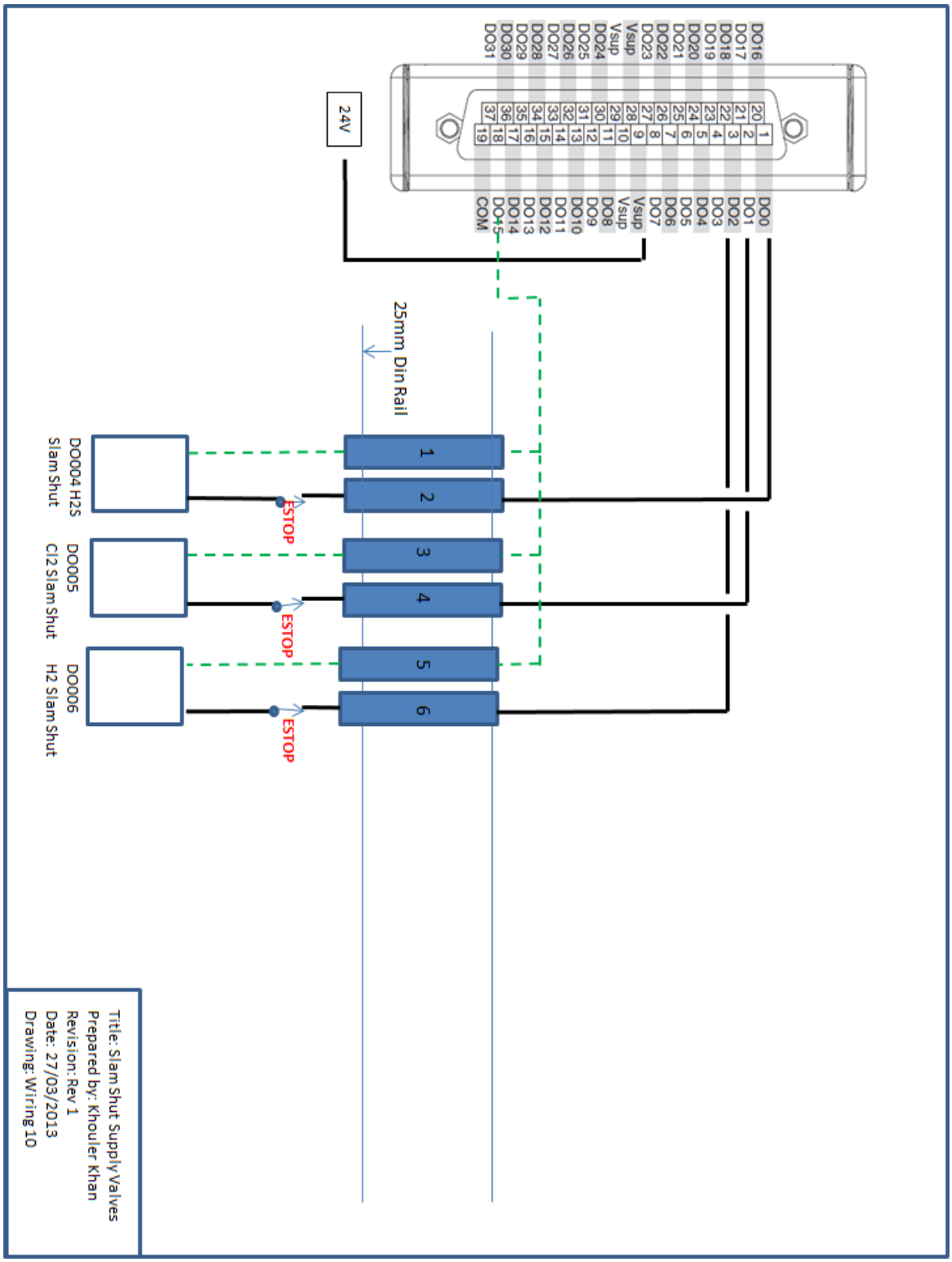

Figure 101 Emergency stop pushbuttons wiring diagram

References

1. Seddon, A., *Chalcogenide glasses: a review of their preparation, properties and applications.* Journal of Non-Crystalline Solids, 1995. **184**: p. 44-50.
2. Mc Cann H., e.a. *Fibre-Laser Imaging of Gas Turbine Exhaust Species*. 2012 [cited 2015 02 Jan]; Available from: http://www.flites.eu/.
3. Varshneya, A.K., *Fundamentals of Inorganic Glasses*. 2006: Society of Glass Technology.
4. M., D., *Characterization of Optical Fibers in the Mid-Infrared*. 2005.
5. Sanghera, J. and I.D. Aggarwal, *Infrared Fiber Optics*. 1998: Taylor & Francis.
6. Miles, P., *High Transparency Infrared MaterialsÃ Â¢ Ã Â.* Optical Engineering, 1976. **15**(5): p. 155451-155451-.
7. Pastor, R.C. and L.E. Gorre, *Preparation of high purity compounds of sulfur, selenium, and tellurium*. 1989, Google Patents.
8. Guillevic, E., et al., *Fabrication of highly homogeneous As 2 Se 3 glass under argon flow.* Journal of Non-Crystalline Solids, 2011. **357**(15): p. 2897-2902.
9. Troles, J., et al., *GeSe 4 glass fibres with low optical losses in the mid-IR.* Optical Materials, 2009. **32**(1): p. 212-215.
10. Inagawa, I., et al., *Optical and thermal properties of chalcogenide Ge-As-Se-Te glasses for IR fibers.* Journal of Non-Crystalline Solids, 1987. **95**: p. 801-808.
11. Hilton, A., D. Hayes, and M. Rechtin, *Infrared absorption of some high-purity chalcogenide glasses.* Journal of Non-Crystalline Solids, 1975. **17**(3): p. 319-338.
12. Payne D., e.a. *EP/H02607X/1 - EPSRC Centre for Innovative Manufacturing in Photonics*. 2010 [cited 2015 09/10/2015]; Available from: http://gow.epsrc.ac.uk/NGBOViewGrant.aspx?GrantRef=EP/H02607X/1.
13. Hewak, D. *EP/M015130/1 - Manufacturing and Application of Next Generation Chalcogenides*. 2014 09/10/2015]; Available from: http://gow.epsrc.ac.uk/NGBOViewGrant.aspx?GrantRef=EP/M015130/1.
14. Prasad, N., et al., *First time microwave synthesis of As< sub> 40</sub> Se< sub> 60</sub> chalcogenide glass.* Journal of Non-Crystalline Solids, 2010. **356**(41): p. 2134-2145.
15. Huang, C., *Development of germanium based sulphide glass by chemical vapour deposition (CVD)*, in *Optoelectronic Research Centre*. 2005, University of Southampton. p. 212.
16. Klocek, P., *Infrared fiber optics / Paul Klocek, George H. Sigel, Jr.* Tutorial texts in optical engineering ; v. TT 2, ed. G.H. Sigel. 1989, Bellingham, Wash., USA: SPIE Optical Engineering Press.
17. Pinnow, D., et al., *Fundamental optical attenuation limits in the liquid and glassy state with application to fiber optical waveguide materials.* Applied Physics Letters, 1973. **22**(10): p. 527-529.
18. France, P.W., *Fluoride Glass Optical Fibres*. 2012: Springer Netherlands.
19. Optics, B., *Guide for Infrared Spectroscopy*. 2011, Bruker Optics.
20. Sharma, P., et al., *Far-infrared study of amorphous Ge< sub> 0.17</sub> Se< sub> 0.83− x</sub> Sb< sub> x</sub> chalcogenide glasses.* Journal of Alloys and Compounds, 2009. **480**(2): p. 934-937.

21. Kanamori, T., Y. Terunuma, and T. Miyashita, *Preparation of chalcogenide optical fiber.* Review of the electrical communication laboratories, 1984. **32**(3): p. 469-477.
22. Wood, D. and J. Tauc, *Weak absorption tails in amorphous semiconductors.* Physical Review B, 1972. **5**(8): p. 3144.
23. Shibata, S., et al., *Prediction of loss minima in infra-red optical fibres.* Electronics Letters, 1981. **17**(21): p. 775-777.
24. Brady, D., et al., *Minimum loss predictions and measurements in gallium lanthanum sulphide based glasses and fibre.* Journal of non-crystalline solids, 1998. **242**(2): p. 92-98.
25. Brady, D.J., *Gallium lanthanum sulphide based glasses for mid-infrared optical fibres*, in *Optoelectronics Research Centre*. 1999, University of Southampton. p. 166.
26. Sanghera, J., L. Busse, and I. Aggarwal, *Effect of scattering centers on the optical loss of As2S3 glass fibers in the infrared.* Journal of applied physics, 1994. **75**(10): p. 4885-4891.
27. Sanghera, J.S., L.B. Shaw, and I.D. Aggarwal, *Applications of chalcogenide glass optical fibers.* Comptes Rendus Chimie, 2002. **5**(12): p. 873-883.
28. Sanghera, J.S. and I.D. Aggarwal, *Development of chalcogenide glass fiber optics at NRL.* Journal of non-crystalline solids, 1997. **213**: p. 63-67.
29. Snopatin, G., et al., *High-purity chalcogenide glasses for fiber optics.* Inorganic Materials, 2009. **45**(13): p. 1439-1460.
30. Petrovich, M., *Gallium lanthanum sulphide glasses for near-infrared photonic applications*, in *Electronics and Computer Science*. 2003, University of Southampton. p. 253.
31. Hubert M., *CHALCOGENIDE GLASSES FOR INFRARED APPLICATIONS: NEW SYNTHESIS ROUTES AND RARE EARTH DOPING*, in *DEPARTMENT OF MATERIALS SCIENCE AND ENGINEERING*. 2012, THE UNIVERSITY OF ARIZONA. p. 248.
32. Thompson, D., et al., *Microwave assisted synthesis of high purity As 2 Se 3 chalcogenide glasses.* Physics and Chemistry of Glasses-European Journal of Glass Science and Technology Part B, 2013. **54**(1): p. 27-34.
33. Hull, R. and INSPEC, *Properties of Crystalline Silicon*. 1999: INSPEC, the Institution of Electrical Engineers.
34. Bhosle, S., et al., *Melt Homogenization and Self-Organization in Chalcogenides-Part I.* International Journal of Applied Glass Science, 2012. **3**(3): p. 189-204.
35. Gabbott, P., *Principles and applications of thermal analysis*. 2008: Blackwell Pub.
36. Agilent Technologies, I., *HIGH AND ULTRA-HIGH VACUUM FOR SCIENCE RESEARCH*, I. Agilent Technologies, Editor. 2011.
37. Chulzhanov, Y., et al., *Preparation of high-purity chalcogens.* Chemistry for Sustainable Development, 2000. **8**: p. 29-31.
38. Sanghera, J.S., V.Q. Nguyen, and I.D. Aggarwal, *Placing chalcogenides or chalcohalide batch containing hydrogen impurities in a reaction chamber, adding tellurium halide, heating to melt the batch and forming hydrogen chloride, distilling the melt*. 1998, Google Patents.
39. GavináWhittaker, A., *Microwave-assisted solid-state reactions involving metal powders.* Journal of the Chemical Society, Dalton Transactions, 1992(18): p. 2751-2752.

40. Sivakumaran, K. and C.S. Nair, *Rapid synthesis of chalcogenide glasses of Se–Te–Sb system by microwave irradiation.* Journal of Physics D: Applied Physics, 2005. **38**(14): p. 2476.
41. Kharissova, O.V., B.I. Kharisov, and J.J.R.z. Valdés, *Review: the use of microwave irradiation in the processing of glasses and their composites.* Industrial & Engineering Chemistry Research, 2010. **49**(4): p. 1457-1466.
42. Livshits, P., et al., *Local doping of silicon by a point-contact microwave applicator.* Microelectronic engineering, 2011. **88**(9): p. 2831-2836.
43. Clark, D.E., D.C. Folz, and J.K. West, *Processing materials with microwave energy.* Materials Science and Engineering: A, 2000. **287**(2): p. 153-158.
44. Arai, S., *Activated gas generator*. 1980, Google Patents.
45. Baniel, P. and C. Belouet, *Gas film levitation: a unique containerless technique for the preparation of fluoride glass rods.* Journal of non-crystalline solids, 1993. **161**: p. 1-6.
46. Weber, J., *The Containerless Synthesis of Glass.* International Journal of Applied Glass Science, 2010. **1**(3): p. 248-256.
47. Watanabe, Y., A. Masuno, and H. Inoue, *Glass formation of rare earth aluminates by containerless processing.* Journal of Non-Crystalline Solids, 2012. **358**(24): p. 3563-3566.
48. Skinner, L.B., et al., *Phase separation, crystallization and polyamorphism in the Y2O3–Al2O3 system.* Journal of Physics: Condensed Matter, 2008. **20**(20): p. 205103.
49. LARSEN, D. and M. ALI, *Space processing of chalcogenide glass[Final Report, 22 Feb. 1974- 30 Sep. 1976].* 1977.
50. Firestone, R. and S. Schramm, *Space processing of chalcogenide glass.* 1978.
51. ALI, M. and D. LARSEN, *Space processing of chalcogenide glass[Annual Summary Report, 22 Feb. 1975- 21 Feb. 1976].* 1976.
52. Weber, J.R., et al., *Glass fibres of pure and erbium-or neodymium-doped yttria–alumina compositions.* Nature, 1998. **393**(6687): p. 769-771.
53. Kieu, Q. and V.P. Veiko. *Laser fabrication of optical microspheres*. in *Laser-Assisted Micro-and Nanotechnologies 2003*. 2004. International Society for Optics and Photonics.
54. Mairaj, A., *Optical waveguides and lasers in improved gallium lanthanum sulphide glass* in *Electronics and Computer Science*. 2003, University of Southampton. p. 150.
55. Forster, C.M. and W.B. White, *Optical absorption edge in rare earth sesquisulfides.* Materials research bulletin, 2006. **41**(2): p. 448-454.
56. Schweizer, T., *Rare-earth-doped gallium lanthanum sulphide glasses for mid-infrared fibre lasers*, in *Electronics and Computer Science*. 2000, University of Southampton. p. 154.
57. Knight, D.S. and W.B. White, *Raman spectroscopic study of the rare earth sesquisulfides*. 1989, DTIC Document.
58. Sotnikov, A., et al., *Lanthanum oxide sulfurization in ammonium rhodanide vapor.* Inorganic Materials, 2014. **50**(10): p. 1024-1029.
59. Etchepare, J., M. Merian, and L. Smetankine, *Vibrational normal modes of SiO2. I. α and β quartz.* The Journal of Chemical Physics, 1974. **60**(5): p. 1873-1876.
60. Chakraborty, R., K. Brown, and M. Horikoshi, *Comprehensive Performance Testing and Characterization of Various Point-of-use (POU)*

Inert Gas Purification Technologies Used in Microelectronics Fabrication Processes. Gases and Technology, 2004.
61. Corporation, P. *Gas Flow Schematic and General Gas Purifier Recommendations*. 2015 [cited 2015 19/03/2015]; Available from: http://www.pall.com/main/microelectronics/gas-purification-for-semiconductor-manuf-54168.page.
62. SAES Pure Gas, I. *MicroTorr Specification MC1*. Gas Purification 2015 [cited 2015 10/10/2015]; Available from: http://www.saespuregas.com/Library/specifications-brochures/MC1_spec.PDF.
63. Collins, S.R. *Stainless steel for semiconductor applications*. in *Mechanical working and steel processing conference proceedings*. 1997. IRON AND STEEL SOCIETY OF AIME.
64. Dasgupta, N.P., et al., *Design of an atomic layer deposition reactor for hydrogen sulfide compatibility.* Review of Scientific Instruments, 2010. **81**(4): p. 044102.
65. Wolf, E. *Orbital welding in critical systems*. in *5 th International Conference: Trends in Welding Research*. 1998.
66. Systems, A.M. *Dewpoint Equivalents Calculator*. 2015 [cited 2015 19/03/2015]; Available from: http://www.dew-point.com/equivalents.asp.
67. Rao, R., et al., *Synthesis of low-melting metal oxide and sulfide nanowires and nanobelts.* Journal of electronic materials, 2006. **35**(5): p. 941-946.
68. Ahamad, T. and S.M. Alshehri, *Green Synthesis and Characterization of Gallium (III) Sulphide (α-Ga2S3) Nanoparicles at Room Temperature.* Nano Hybrids, 2014. **6**: p. 37-46.
69. Ferrari, A. and J. Robertson, *Interpretation of Raman spectra of disordered and amorphous carbon.* Physical review B, 2000. **61**(20): p. 14095.
70. Jones, A.C. and M.L. Hitchman, *Chemical vapour deposition: precursors, processes and applications*. 2009: Royal Society of Chemistry.
71. Blanc, D. and J. Wilson, *Plasma deposition of chalcogenide glass.* Journal of Non-Crystalline Solids, 1985. **77**: p. 1129-1132.
72. Blanc, D. and J. Wilson, *Plasma-enhanced chemical vapor deposition of Ge-Se and Ge-S compounds.* Optical Engineering, 1988. **27**(10): p. 271017-271017-.
73. Katsuyama, T., S. Satoh, and H. Matsumura, *Fabrication of high-purity chalcogenide glasses by chemical vapor deposition.* Journal of applied physics, 1986. **59**(5): p. 1446-1449.
74. F, M. *Fundamentals of gas solids/liquids separation*. **2015**.
75. Kotsalas, I. and C. Raptis, *High-temperature structural phase transitions of Ge x S 1-x alloys studied by Raman spectroscopy.* Physical Review B, 2001. **64**(12): p. 125210.
76. Yamaguchi, M., T. Shibata, and K. Tanaka, *A resonance Raman scattering study of localized states in Ge–S glasses.* Journal of non-crystalline solids, 1998. **232**: p. 715-720.
77. Mulholand, L. and K. Khan, *Chemical Vapour Deposition Powder Capture Apparatus.* American Scientific Glassblowers society, 2014. **LXII**(4): p. 19-22.